N° d'ordre : 40415 Année 2010

UNIVERSITÉ DES SCIENCES ET TECHNOLOGIES DE LILLE
UNIVERSITÉ DE LILLE 1
ÉCOLE DOCTORALE SCIENCES POUR L'INGÉNIEUR

THÈSE

Présentée pour l'obtention du grade de

DOCTEUR DE L'UNIVERSITÉ DE LILLE 1

DISCIPLINE : MÉCANIQUE

par

MOUSAB HADAD

Ingénieur diplômé en Suisse

ÉVALUATION DE L'ADHÉRENCE ET DES CONTRAINTES RÉSIDUELLES DE REVÊTEMENTS OBTENUS PAR PROJECTION THERMIQUE

ADHESION AND RESIDUAL STRESS EVALUATION OF THERMALLY SPRAYED COATINGS

Thèse soutenue le 19 Novembre 2010 devant le jury composé de :

Directeur de thèse :	Professeur JACKY LESAGE	Université de Lille 1, France
Rapporteurs:	Professeur MARIANA STAIA	Université Centrale de Caracas, Venezuela
	Professeur GERARD MAUVOISIN	Université de Renne, France
Examinateurs:	Dr. STEPHAN SIEGMANN	Directeur de division. Nova Werke AG, Suisse
	Professeur ANNE LERICHE	Université de Valenciennes, France

ACKNOWLEDGEMENT

I would like to express my gratitude to my supervisor Professor Jacky Lesage vice-president of the University of Science and Technologies of Lille, head of the mechanical failure analysis laboratory, for his guidance and for giving me the opportunity to carry out this research under his supervision. I would like to acknowledge Professor Didier Chicot for his advises and his support on the indentation measurements.

I would like to acknowledge Professor Mariana Staia, Professor Gérard Mauvoisin, Dr. Stephan Siegmann, and Professor Anne Anne Leriche for their kind agreement in examining my thesis and their kind acceptance being part of the jury.

I would like also to acknowledge, Prof. Louis Schlapbach, Prof. Lukas Rohr, Dr. Stephan Siegmann and Prof. Patrik Hoffmann to offer me the opportunity to undertake my thesis during my work in the Swiss Federal Laboratories for Materials Science and Technology. The pleasant working environment of this institute has encouraged me to successfully complete my research work.

I wish also to express my sincere thanks to Dr. Johann Michler for his help and fruitful scientific discussion on the mechanical testing part included in this thesis.

My deepest thanks to Prof. P.P. Bandyopadhyay (IIT Kharagpur- India) for his valuable time spent in English correction and also would like to acknowledge my colleague in EMPA, Dr. Jamil Elias for the French correction.

I am also deeply grateful to Dr. Sven Stauss for his support for the finite element simulations. I would like to acknowledge Prof. Jacques Forchelet and Prof. Luc Espic from the University of Applied Sciences in Canton de Vaud (Switzerland) for their support and their encouragement.

I also gratefully acknowledge Dr. Séverine Bellayer from “École Nationale Supérieure de Chimie de Lille” for the EPMA measurements.

I take this opportunity to thank my colleague in EMPA Dr. Christoph Niederberger for his patience and help for the HRSEM measurements.

I would like to dress to Mr. Reinhard Hitzek (Stellba Schweisstechnik AG) for allowing me to use the HVOF facility to coat my samples.

My grateful appreciation goes to Bernhard Von Gunten for his help in spraying samples using VPS and FS, to my office colleague Hans Peter Feuz for helping in profilometry measurements, to Gehard Bürki for helping in the microscopy, and to all my colleagues in EMPA and my friends.

I would like dress my grateful acknowledgement to Armasuisse in Thun-(Switzerland) for providing funding for this research project.

My deepest acknowledge to my closest friend Chantal Béroud for being a constant source of inspiration, her kindness and her encouragement. I would like to be grateful to my closest friend Dhirar Osman for being one of the sublime sources of ambitions.

Lastly, my heartfelt respect and special thanks go to my beloved parents for their encouragement and patience throughout my life. I express a very special and heart felt thankfulness to my wife for her patience during the week-ends when I was writing my thesis. Our beloved twin (Nour and Rayan) came to our life on June 2010 when I started writing the thesis and their arrival added a new charm to our life. I express my beloved uncle Ziad Elmawal for his great support and inspirations.

TABLE OF CONTENTS

SYMBOLS AND ACRONYMS

f	*Deflection of beam, [mm]*
r	*Arc radius of deflected beam, [m]*
k	*Curvature of beam, [1/m]*
T_d	*Deposition temperature, [K]*
T_a	*Room temperature, [K]*
α_s, α_c	*Coefficients of thermal expansion (CTE) of substrate and coating, resp, [K^{-1}]*
μ	*Shear modulus, [MPa]*
M	*Balanced moment in beam, [N.m]*
E_s, E_c	*Young modulus of substrate and coating resp, [GPa]*
K_{ca}	*Apparent interfacial toughness, [MPa. $m^{0.5}$]*
K_{ca0}	*Extrapolated interfacial toughness with infinite coating thickness, [MPa. $m^{0.5}$]*
K_I, K_{II}	*Stress intensity factors, [MPa. $m^{0.5}$]*
G_c	*Energy release rate, [J/m^2]*
(P_c, a_c)	*Critical load, critical crack length, [N], [μm]*
K_1, K_2	*Non-dimensional calibration factors of incremental hole drilling*
K_{IC}	*Interfacial toughness [MPa. $m^{0.5}$]*
$g(\alpha,\beta)$	*Non-dimensional mismatch Dundurs parameters*
D/d, R/a	*Delamination ratio of coating to substrate deformation imprint*
Ra	*Interfacial roughness, [μm]*
τ	*Interfacial shear strength, [MPa]*
$\sigma_{max,c}$	*Coating strength, [MPa]*
σ_{res}	*Residual stress, [MPa]*
i	*Crack number*
σ_{ind}	*Residual stress calculated by interfacial indentation method, [MPa]*
σ_{IHD}	*Residual stress by incremental hole drilling, [MPa]*
σ_{Godoy}	*Residual stress based on Godoy approach, [MPa]*
ε	*Strain deformation*
$S.D$	*Standard deviation*
φ	*Angle of between the principle direction and the strain gauges*
$\tilde{l}$	*Mean crack spacing [μm]*
l_c	*Critical crack spacing [μm]*
H_V	*Vickers Hardness, [GPa]*
$AISS$	*Apparent interfacial shear strength, [MPa]*
$IISS$	*Intrinsic interfacial shear strength, [MPa]*
$LEFM$	*Linear elastic fracture mechanics*
$U.T.S$	*Ultimate tensile strength, [MPa]*
$Y.S$	*Yield strength, [MPa]*
SEM	*Scanning Electron Microscope*
$EPMA$	*Electron Probe Micro Analyser*
EDS	*Energy-Dispersive X-Ray Spectroscopy*
XRD	*X-Ray diffraction*
VPS, APS	*Vacuum plasma spray, Atmospheric plasma spray*
FS	*Flame spray*
$HVOF, HVAF$	*High-velocity oxygen/fuel, air/fuel*
$HVIF$	*High-velocity impact forging*
$CGSM$	*Cold Gas Spray Method*
$DGUN$	*Detonation- Gun spraying*

LIST OF TABLES

LIST OF FIGURES

ABSTRACT

Coating adhesion and residual stress are the principal parameters determining the reliability and performance of coated components in service. While many techniques were employed for adhesion evaluation, none of them possesses universal suitability. Therefore, it is unfortunately not always possible to compare measurements obtained by different methods, because of experimentally determined adhesion values are not free from effects assignable to the measurement conditions, e.g., loading and geometrical conditions. Therefore, reliable methods are in high demand for practical adhesion measurements. Several parameters can influence practical adhesion quantification, e.g., coating thickness, interface roughness and, in particular, residual stress. Very often, a single constant value of residual stress is wrongly attributed to coating system in the engineering application field. Therefore, it is primordial to increase the fundamental knowledge on residual stress, state, intensity and gradient in coating and especially, its influence on adhesion to optimize coating performance in service.

The lack of wide investigations of practical adhesion and the effect of residual stress, both conducted by various approaches, was the main motivation to undertake this study. Therefore, the research work presented in this thesis focused on practical adhesion and residual stress of thermally sprayed coatings with the following objectives:

1. enhancement of knowledge of adhesion and on the main influencing parameters: e.g. coating thickness, interface roughness and, in particular, residual stresses intensity and gradient,
2. conducting an analytical and experimental study on residual stress and on the practical adhesion of thermally sprayed coatings, as well as, to express

these practical adhesion and residual stress in an accurate physical order using reliable methods and, if possible, to correlate between adhesion measurement methods,

3. studying the annealing effect on the residual stress and on adhesion.

Three representative types of coatings of practical interest were selected to cover wide range of materials: metallic (NiCr 80-20), ceramic (Al_2O_3) and composite (WC-Co-Cr) coatings having mainly two levels of thickness and interfacial roughness. These coatings were obtained using different processes; flame spray, vacuum plasma and high velocity oxy fuel processes on different substrate materials having different thermal expansion coefficients, mechanical properties and application field; e.g., structural steel St 52-3, austenitic chromium-Nickel steel AISI 304, stainless steel X3CrNiMo13-4, and titanium alloy TiAl-16V4.
The practical adhesion evaluation is often influenced by: loading conditions, coating thickness, interfacial roughness and residual stresses state and gradient. Therefore, four methods were selected to measure adhesion:

i. tensile adhesion test (pull-off) according to EN 582
ii. interfacial indentation
iii. in-plane tensile test
iv. Rockwell-C indentation assisted by finite elements simulation

The selection of these methods was based on the following approaches:

1. loading method:
    i. loading perpendicularly to the interface, in tensile (e.g. pull-off) and in compression (e.g. Rockwell-C indentation),
    ii. parallel to the interface: in tensile (in-plane tensile test) or in compression (interfacial indentation).

    Furthermore, the way of stressing the coating or the interface is also a very important issue to investigate the residual stress influence on adhesion and the degree of adhesion method sensitivity to the residual stress induced.
2. The additional approach of selecting these methods; was to cover a wide range of test application; e.g. the pull-off and Rockwell-C indentation tests

are widely used in industries, whereas, the in-plane tensile and interfacial indentation tests are still under development in laboratories.

To evaluate residual stresses, the experimental and theoretical studies were conducted using different methods to provide a good insight to residual stress state, intensity and gradient through coating/substrate system. The testing methods are hereunder:

i. curvature bending test based on the beam theory to express the state and intensity of the overall residual stress in the whole sample,
ii. incremental hole drilling to locally provide the gradient of residual stress through the coating-substrate,
iii. interfacial indentation methods based on a extrapolating mathematical model to provide residual stress state and intensity at and near the interface.

The conclusion of this study can briefly summarized as follows:

1. The origin of residual stress of thermally sprayed coating was identified; the state of residual stress measured was in coherence with the physical properties of materials and deposition process. All methods were in agreement, giving general trend in state and intensity of stress state. The difference in the measured order of magnitude of residual stress intensity was attributed to two factors:
   i. the difference in physical models of residual stress calculation which contain certain limits and assumptions,
   ii. the difference in volume of the investigated zone. For example, in the interface indentation model the resulted residual stress was restricted to the investigated zone along the interface, the incremental hole drilling provides a through thickness stress gradient in a volume of ~1 mm^3, whereas, the bending curvature provides strain measurements of tenth of millimeters over few cm of length.

However, the residual stress measurements performed by these three methods provide a large insight to its gradient, intensity and state, and hence, they are complementary to each other.

2. The results of tensile adhesion test (EN 582) did not yield a physical value to quantify the adhesion, and gave very poor fracture information on the interfacial properties. Subsequently, it could not be correlated to other tests.
3. In spite of the good agreement found between the experimental results and finite elements simulation of Rockwell-C indentation, this method is still restricted to brittle coatings where a large coating delamination occurs to fit the theoretical model.
4. The performed adhesion methods measured mainly what is termed the "practical adhesion". From the results, it appears that interface indentation and in-plane tensile tests provided the best prospects of relating practical levels of adhesion to the performance of real engineering components in service. Moreover, a perfect accordance was found in the in-plane tensile results, since the adhesion values were found to increase with both increasing coating thickness and interface roughness. However, metallic coating showed quasi-linear correlation between results obtained by interfacial indentation and in-plane tensile tests. This is a novel and important finding recorded in this thesis. It may be noted that this is the first attempt to compare the results of the two tests. The fact that the two tests gave perfectly coherent and reliable results demonstrates their pertinence to evaluate adhesion since they are based on very different geometric and loading conditions.
5. Coating annealing helped to decrease residual stress intensity in the coating and at the interface. Consequently, adhesion was observed to be decreased. However, the quantified magnitude order of stress relief was found to be dependent on the coating thickness and interface roughness.

RÉSUMÉ

Pour les revêtements obtenus par projection thermique, c'est-à-dire entrant dans la catégorie des revêtements épais, l'adhérence sur le support et les contraintes résiduelles sont les paramètres principaux déterminant leur fonctionnalité et leur performance en service. Bien que de nombreuses méthodes aient été essayées pour évaluer l'adhérence, il n'existe pas, à ce jour, de test satisfaisant toutes les exigences tant techniques que théoriques nécessaires pour représenter valablement l'adhérence d'un revêtement sur son substrat. Les tests utilisés cherchent généralement à provoquer le décollement du revêtement, cependant, ceux qui peuvent s'appliquer à un système et une configuration géométrique donnée ne s'appliquent pas nécessairement à un autre système et une autre géométrie. Dans ces conditions, il est rarement possible de comparer les mesures obtenues par les différentes méthodes car les valeurs expérimentales sont directement en fonction de la méthode utilisée.

Les paramètres qui peuvent influencer la quantification de l'adhérence sont l'épaisseur du revêtement, la rugosité d'interface et, en particulier, les contraintes résiduelles toujours présentes après la projection thermique. Dans le domaine industriel, quand elle est estimée ou mesurée, c'est bien souvent la valeur de la contrainte résiduelle moyenne dans le revêtement qui est utilisée comme paramètre de conception. Cependant l'intensité et la répartition des contraintes peuvent être extrêmement différentes d'un revêtement à un autre. C'est pourquoi la donnée de la contrainte moyenne présente certes un intérêt mais est très insuffisante pour prévoir et comprendre le comportement d'un revêtement. Il est donc de très grande importance d'approfondir la connaissance fondamentale sur l'état des contraintes résiduelles et de leurs effets sur l'adhérence afin d'optimiser la performance de revêtement en service.

Même s'il existe de nombreuses méthodes d'essai, il n'y a pas eu encore d'étude complète traitant de la validité des approches expérimentales et analytiques mises

en œuvre pour évaluer l'adhérence en terme de propriété intrinsèque. De plus, l'absence de mesures systématiques et la difficulté de décrire l'état des contraintes résiduelles par un ou des paramètres pertinents susceptibles d'être introduits dans une formulation analytique rend impossible, pour le moment, la prise en compte des contraintes résiduelles dans un modèle prédictif du comportement. Ces deux aspects ont motivé la présente étude avec, à la base, l'idée essentielle de comparer plusieurs méthodes d'essais capables d'aboutir à une ténacité d'interface ou une énergie de fissuration interfaciale représentatives de l'adhérence. Pour que l'étude soit la plus complète possible les conditions d'élaboration les plus variées ont été envisagées. Elles concernent aussi bien les techniques de projection: i) projection à la flamme (FS), ii) par plasma sous vide (VPS), iii)) et par flamme à vitesse hypersonique (HVOF), que les matériaux projetés: i) métallique (NiCr 80-20), ii) céramique (Al_2O_3) et iii) composite (WC-Co-Cr). Les substrats: i) acier St 52-3, ii) acier austénitique chrome-nickel, iii) acier inoxydable X3CrNiMo13-4, iv) et alliage de titane TiAl-16V4. Ou encore les épaisseurs de revêtements visés ou la rugosité du substrat avant projection.

De cette façon il est espéré une grande variété de contraintes résiduelles et de propriétés mécaniques permettant une différentiation des influences des paramètres d'élaboration sur l'adhérence des revêtements et par suite, l'établissement d'un modèle pertinent de comportement.

Du point de vue méthodologique, quatre techniques d'essai ont été employées pour évaluer l'adhérence:

1. l'essai de traction selon la norme EN 582,
2. l'indentation interfaciale,
3. l'essai de cisaillement par traction axiale,
4. l'indentation Rockwell-C et modélisation par éléments finis.

Pour évaluer les contraintes résiduelles, trois méthodes très différentes ont été utilisées:

1. l'essai de courbure, associé à des modèles basés sur la théorie des poutres et du principe de superposition pour déterminer l'état et l'intensité de la contrainte résiduelle résultante dans le revêtement,

2. la méthode de perçage incrémentale basée sur l'analyse des déformations mesurées à l'aide d'une rosette de jauges de déformation permettant d'estimer le gradient des contraintes résiduelles à travers le revêtement et le substrat,
3. la méthode indirecte qui, à partir des résultats de l'indentation interfaciale, analyse en termes de contrainte les variations de la ténacité d'interface, en fonction de l'épaisseur du revêtement.

Les résultats les plus importants sont les suivants:

Quelle que soient les méthodes d'évaluation utilisées, elles aboutissent à une description de l'état des contraintes résiduelles en assez bon accord entre elles pour les tendances générales. Toutefois, on observe une différence significative pour l'intensité de contraintes résiduelles entre les valeurs calculées, mesurées et évaluées. Cette différence peut être attribuée à deux facteurs, i) différence d'hypothèses de calcul dans les modèles physiques utilisés, ii) différence de volume concerné par l'évaluation ; zone proche de l'interface pour l'indentation interfaciale, zone superficielle pour le perçage incrémental et volume total pour la méthode de courbure. Les mesures et estimations des contraintes résiduelles effectuées par les trois méthodes fournissent cependant une vision très utile pour la compréhension des phénomènes d'adhérence. La suivante (Figure 8-1) permet de comparer les valeurs des contraintes résiduelles obtenues par les trois techniques utilisées.

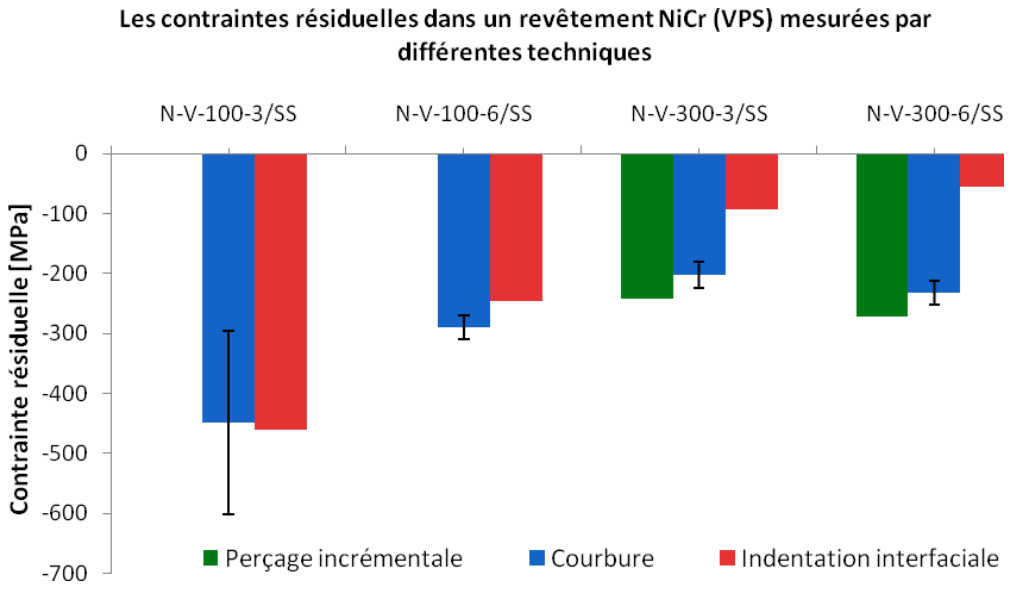

Figure 8-1: Les contraintes résiduelles dans un revêtement NiCr (VPS) mesurées par différentes techniques.

Les résultats obtenus par l'essai de traction (EN 582) n'ont jamais pu donner de résultats pertinents permettant d'estimer une valeur représentative de l'adhérence et par suite les résultats obtenus n'ont pas pu être corrélés aux résultats obtenus par les autres essais d'adhérence.

Les résultats obtenus par l'indentation de Rockwell-C ont abouti à très bonne concordance entre les résultats expérimentaux et les prévisions issues du calcul par éléments finis. Cependant cette méthode ne nous a pas permis d'évaluer l'adhérence pour tous les revêtements, car elle est ne donne de résultats que pour les revêtements fragiles et lorsque le délaminage du revêtement est assez grand.

Les méthodes d'adhérence effectuées dans la pratique courante n'ont pas d'autre ambition que de fournir des éléments de comparaison entre des méthodes testées simultanément. La plupart ne sont pas reproductibles et ne peuvent permettre le calcul d'une grandeur intrinsèque représentative du processus physique d'adhérence. Ici, nous avons montré que les méthodes d'indentation interfaciale et de cisaillement par traction offrent les meilleures perspectives du point de vue de la cohérence et de la fiabilité des grandeurs physiques obtenues. Par exemple, pour les revêtements métalliques, une corrélation quasi-linéaire entre les résultats

d'indentation interfaciale et de cisaillement par traction a été obtenue comme la montre les figures ci-dessous (Figure 8-2 et Figure 8-3):

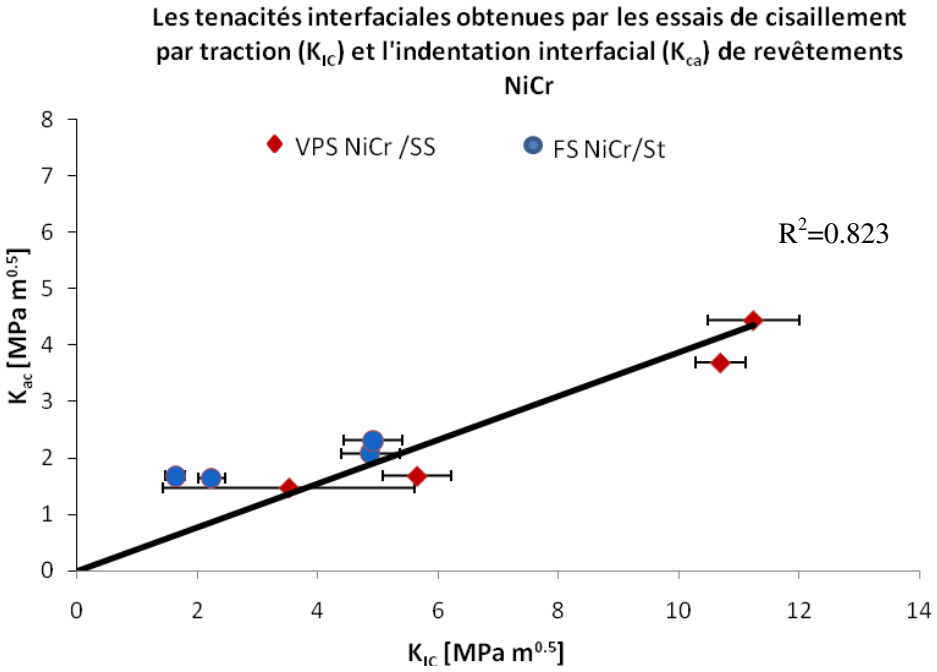

Figure 8-2 : une corrélation quasi-linéaire entre les ténacités interfaciales obtenues par l'indentation interfaciale et de cisaillement par traction

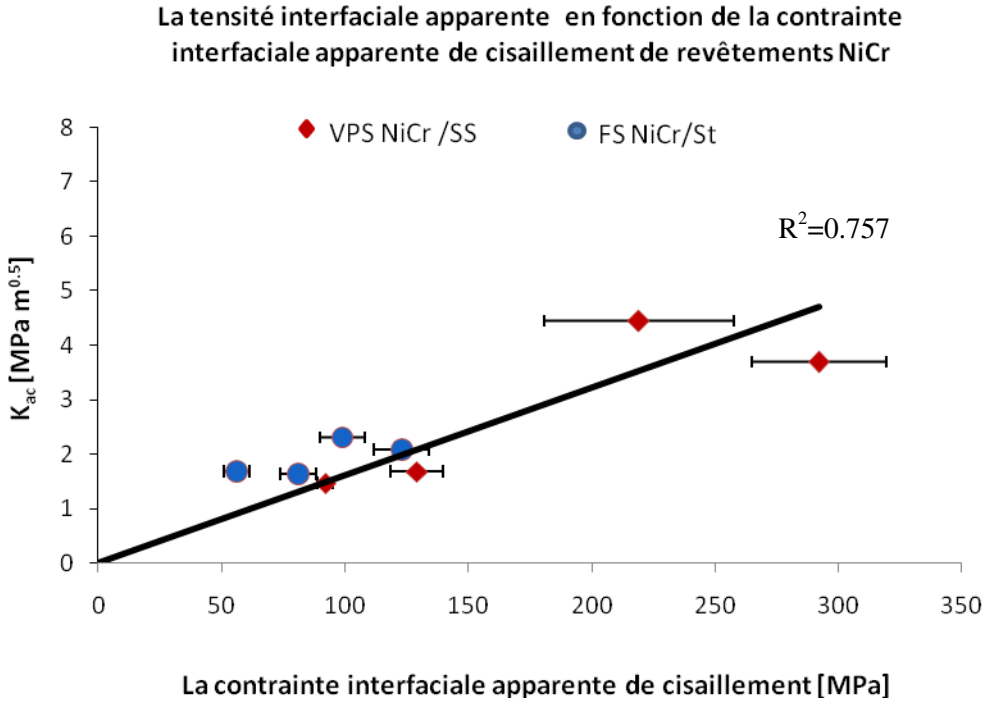

Figure 8-3 : une corrélation quasi-linéaire entre la ténacité interfaciale obtenue par l'indentation interfaciale et la contrainte interfaciale apparente de cisaillement de revêtements NiCr

Ce résultat est très nouveau est très important, car aucune comparaison entre ces deux tests n'avait jamais été faite. Le fait que les deux essais donnent des résultats parfaitement cohérents et fiables, montre leur pertinence pour évaluer l'adhérence. Cela n'était pas évident à priori, compte tenu de la nature même de ces essais effectués dans conditions de chargement de géométrie très différentes.

Enfin, le traitement de recuit, en permettant l'établissement d'un nouvel état de contraintes à l'intérieur du revêtement et du substrat a permis de quantifier leur influence sur l'adhérence.

CHAPTER 1 : INTRODUCTION AND OBJECTIVES

1. INTODUCTION

Thermal spraying is a widely used technique for the production of various protective coatings to improve or modify the engineering performances and/or increase component life, e.g. by thermal barrier, wear resistant, and corrosion resistant surface layers.

The applications field of these coatings are very large and can be found in aerospace, industrial gas turbines, the petrochemical, gas and automotive industries.

Coatings can be made from dissimilar materials (metals, ceramics or polymers) and be sprayed on to metallic or ceramic substrate.

The thermal spray process involves introduction of feedstock materials (powder, wire or rod) in to the flame. The molten or semimolten droplets impinge the substrate, flatten, cool down and rapidly solidify to form a thin “splat”. The deposit is built up by successive deposition and interbonding among the splats. Therefore, the resulted coating has properties quite different from bulk materials of the same composition, as consequence of porosity, anisotropy, oxides and residual stress. In spite of many advantages using thermal spray technique for surface modifications, (e.g. deposition wide range of materials, low processing cost, range of coating thickness from few 10 microns up to some millimetres, and minimal thermal degradation to substrate, etc.), the low adhesion strength, high porosity, anisotropic properties, and low loading capacity restrict its applications. However, the adhesion of a coating on its substrate is a crucial parameter determining the reliability and performance of a coating/substrate system. For evaluating the coating-substrate adhesion, many methods were developed. A significant number is based on the linear elastic fracture mechanics (LEFM)

approach [1-3]. Among the most widespread methods used are indentation tests [4, 5], shear tests, [6-9] tensile adhesive strength [10-12] and double cantilever beam (DCB) test [13]. The best test method for a given coating is often the one that simulates practical stress condition [14-16]. However, each method is related to a certain type of coating, loading condition and application of the coating. The experimentally determined adhesion values are thus not free from effects due to the measurement method used. Therefore it is unfortunately not always possible to compare measurements obtained by different methods [17]. The test that works with one coating system may not necessarily work with another [18-20]. Hence, there is no standard adhesion test for coating system which can fully fill all material requirements. Bearing in mind that coating adhesion is not a constant in practical applications, but rather a complicated property that depends on, apart of the process, loading conditions, on coating thickness [10] and on interface roughness [21-25]. Furthermore, another crucial parameter is the residual stress in the coating which can play a significant role on the service performance of mechanical parts, and can influence the coating adhesion [26-30].

The residual stresses in thermal spray technique are originated mainly from three sources:
i) quenching stress due to cooling of the splats impinging the substrate surface, ii) thermal stress caused by the mismatch of thermal expansion of coating and substrate during cooling the system to room temperature, iii) phase formation/transformation accompanied by volume change and/or chemical changes. These stresses are usually superimposed and it is very difficult to segregate the stress component. However, the resulted final residual stress can be evaluated using different methods [31]; each method its own limitations, stemming either from some simplifying assumptions or imprecise knowledge of relevant physical constants which vary significantly with processing parameters.

Evaluation of the residual stress state is very important, since it can affect the integrity and the performance of the coating-substrate system. It could have detrimental or beneficial effects, e.g. high tensile stress usually leads to cracking of coating [32, 33], whereas, compressive stress can suppress crack formation and

propagation and may therefore be beneficial increasing wear resistance and fatigue behavior.

The intensity and repartition of the stresses are also very important parameters. Giving only an approximate mean stress value, what is often quoted in industry, is meaningless, since the stress at the interface, which is one of the crucial stress parameter, can be very different from the mean stress in the coating. Therefore, it is primordial to increase the fundamental knowledge on residual stress, state, intensity and gradient in coating to optimize coating performance in service.

2. OBJECTIVES

The lack of systematic investigations on practical adhesion and on the effect of residual stress relief and particularly, the unreliability of the standard test methods in approaching intrinsic adhesion value of coating-substrate system have motivated the present work. The main objectives are the following:

1. to increase the fundamental understanding and identification of residual stress origin,
2. to enhance the knowledge of adhesion and on the main influencing parameters (apart of the process): e.g. coating thickness, interface roughness and, in particular, residual stresses relaxation.
3. to develop an analytical and experimental study on residual stress induced and on the practical adhesion of thermally sprayed coatings, as well as, to express these practical adhesion and residual stress in an accurate physical order in reliable method,
4. to evaluate the possible correlations between adhesion methods,
5. to study the annealing effect on the coatings, subsequently, quantifying the adhesion and residual stress relaxation.

PART A: LITERATURE SURVEY

CHAPTER 2 : OVERVIEW OF THERMALLY SPRAYED COATINGS

Thermal spray coatings are produced by melting and projecting a material in a stream of droplets impacting against a substrate and building up a surface coating with very wide range of coating thickness and substrate temperature (Figure 2-1). The earliest record of thermal spray processing is from the beginning of the 1900s, when a Swiss engineer, M. U. Schoop, presented patents for a system where lead and tin were melted in a welding torch by the energy of an acetylene/oxygen flame. He modified the arrangement to be able to spray powdered materials, and then patented, in 1909, the wire-arc spraying process (Figure 2-2). In the 1960s there was an expansion of the thermal spray techniques, due to the development of plasmas. These techniques were able to satisfy the increasing demand for thermal barrier and wear resistant coating systems. More recently, most developments have focused upon increasing particle velocities, thus allowing a decrease in the temperature of the sprayed particles, obtaining coatings with high adhesion strength, high density and lower oxide content [34-36]. This led to the development of processes such as cold spraying, where the particles are sprayed in a solid state at very high velocity. Today, thermal spraying includes a wide range of processes where coating

materials, in a wire or a powder form, are heated, with an electrical current, a plasma gas or a torch, and sprayed in particle form, which can be molten, partially molten or solid, with a carrier gas onto a substrate to form a coating.

Coatings can be made from dissimilar materials (metals, ceramics or polymers) and be sprayed on to metallic or ceramic substrate. The scope of coating deposition is to improve or modify the engineering performances (for instance resistance to wear, corrosion or high temperature) and/or increase component life. This process can be also applied for repairing the damaged part [37, 38]. The applications of these coatings are very wide and can be found in aerospace, industrial gas turbines, the petrochemical, gas and automotive industries.

Thermal spray methods offer a range of advantages over other coating techniques [39].

1. it can be deposited in wide range of materials,
2. low processing cost, since the deposition efficiency can vary from 1 to 45 kg/h,
3. wide range of coating thickness from few 10 microns up to some millimetres (Figure 2-3),
4. wide application range, e.g. wear resistance, thermal barrier coating, high temperature oxidation resistance, etc,
5. minimal thermal degradation to substrate.

Some of disadvantage of this process are:

1. low bond strength,
2. high porosity,
3. anisotropic properties,
4. low loading capacity, etc

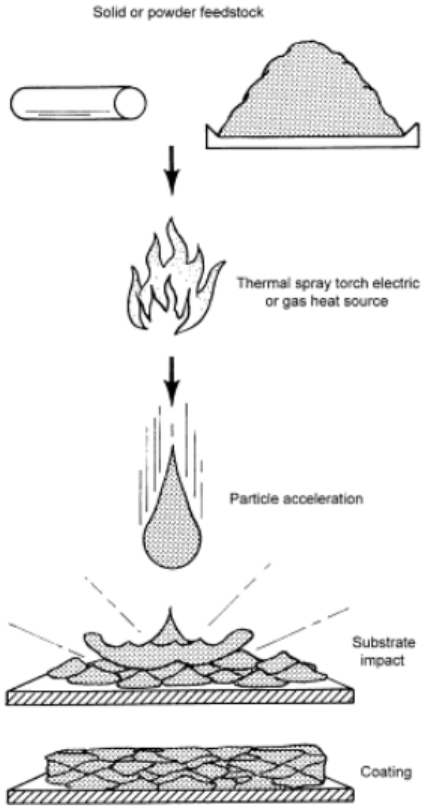

Figure 2-1: schematic presentation of thermal spray process.

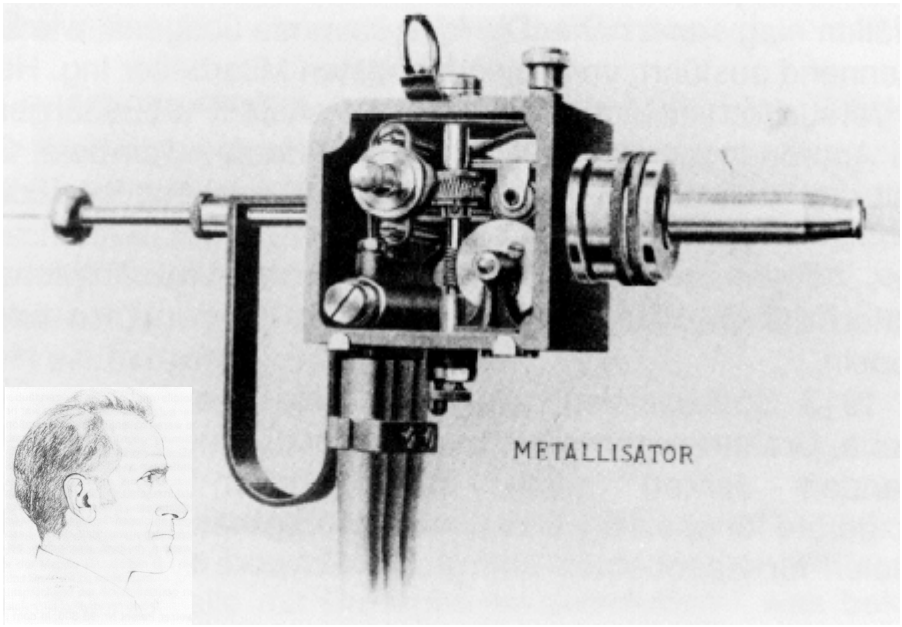

Figure 2-2: first gun on 1913 by Dr. M. Schoop.

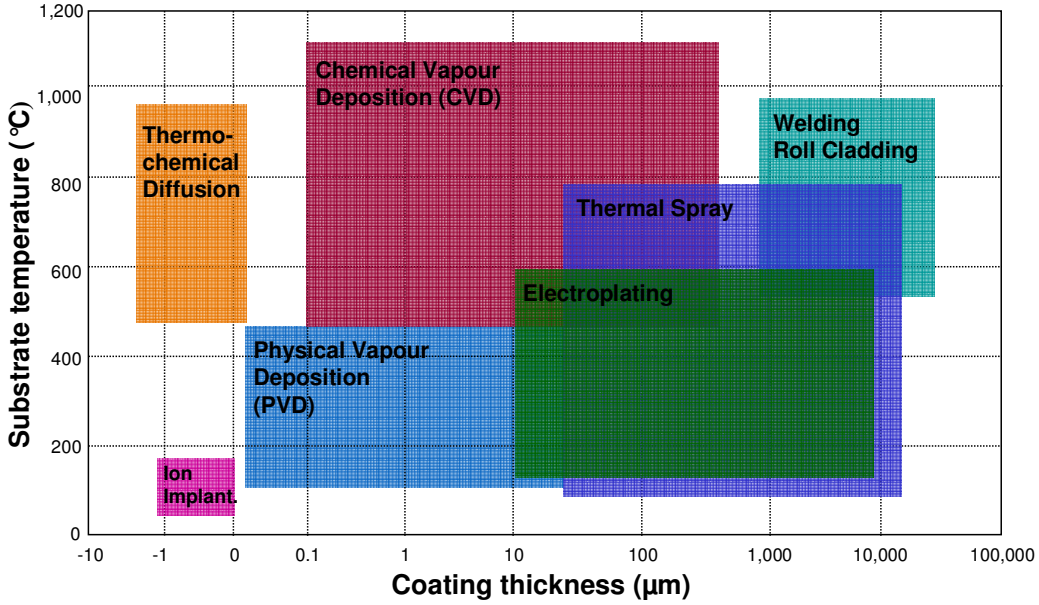

Figure 2-3: area map of typical coating thicknesses and substrate temperatures of different coating techniques [40].

1. THERMAL SPRAY PROCESSES

The fundamental principles of all thermal spraying processes are similar. Powder or wire consumable heated by oxy-fuel combustion (flame & HVOF) or electrically (arc & plasma) until molten or soft, and projected at speed onto a substrate to form a coating.

Thermal spraying processes have been widely used for many years throughout all the major engineering industry sectors for component protection and reclamation. Recent equipment and process developments have improved the quality and expanded the potential application range for thermally sprayed coatings. Therefore, thermal spraying is divided into four main categories:

1. Flame spraying.
2. High velocity oxyfuel (HVOF) spraying.
3. Plasma spraying.
4. Arc spraying.

Since plasma sprayed, flame, and HVOF coatings were the main focus of this study, this processing technique will be described first.

1.1 FLAME SPRAYING (FS)

Flame spraying is the oldest of the thermal spraying processes. The consumable (usually a powder or a wire) is heated and propelled onto a substrate to form a coating. A widespread of variety of materials can be deposited as coatings using this process and the vast majority of components are sprayed manually.

Flame spraying uses the heat from the combustion of a fuel gas (usually acetylene or propane) with oxygen to melt the coating material, which can be fed into the spraying gun as a powder, wire or rod.

The powder flame spraying process is shown in Figure 2-4. The powder is fed directly into the flame by a stream of compressed air or inert gas (argon or nitrogen). Alternatively, in some basic systems, powder is drawn into the flame using a venturi effect, which is sustained by the fuel gas flow. It is important that the powder is heated sufficiently as it passes through the flame. The carrier gas feeds powder into the centre of an annular combustion flame where it is heated. A second outer annular gas nozzle feeds a stream of compressed air around the combustion flame, which accelerates the spray particles towards the substrate and focuses the flame [41, 42].

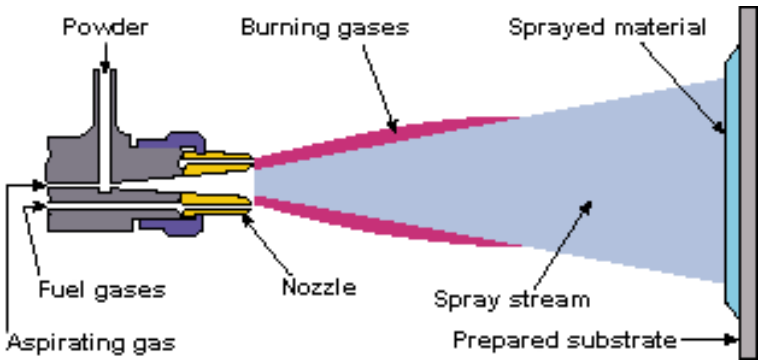

Figure 2-4: Schematic of the powder flame spray process[42].

1.2 PLASMA SPRAYING (PS)

The plasma spraying process involves the latent heat of ionized inert gas (plasma) being used to create the heat source. The most common gas used to create the plasma is argon; this is referred to as the primary gas.

The plasma torch consists of a cone shaped cathode and annular anode, which forms the nozzle (see Figure 2-5). An inert gas (usually argon, complemented with hydrogen or helium) is introduced into the chamber to form the plasma. Plasma is generated when a high-current pulse creates an arc between the electrodes. This causes ionization of the gas and the resulting plasma jet flows out the nozzle. Near the water –cooled walls of the anodes, there is a thin revolving layer of cooler, non-conductive gas that confines the plasma to the centre of the anode. This plasma can have velocities of several hundred m/s and temperature of the order of 15000 °C and above. Therefore, even high melting point refractory materials can be melt and sprayed. The feedstock material is introduced radially in general into the plasma jet through a feeding rube mounted near the nozzle; so that the hottest part of the jet is utilized. The plasma jet then melts the particles and propels them towards the substrate. Powder feeding is a critical step in the whole operation, determining the particle trajectory in the jet. For a successful coating deposition, the particles should be sufficiently heated to thoroughly melt without evaporation and should attain sufficient velocity to flatten and spread upon impact. Numerous studies, both theoretical and experimental were devoted to the problem of plasma-particle interaction [43-48], since a number of other factors influence the particle heating and acceleration e.g., torch and nozzle geometry, operation power, plasma heat content and velocity, size and density of the powder. There is many techniques based plasma spraying:

- APS : Atmospheric Plasma Spraying
- VPS : Vacuum Plasma Spraying
- RPS : Reactive Plasma Spraying (for example a N2 gas is used)
- IPS: Inert Plasma Spraying (for example, when the atmosphere is a neutral gas)
- HPPS: High Pressure Plasma Spraying

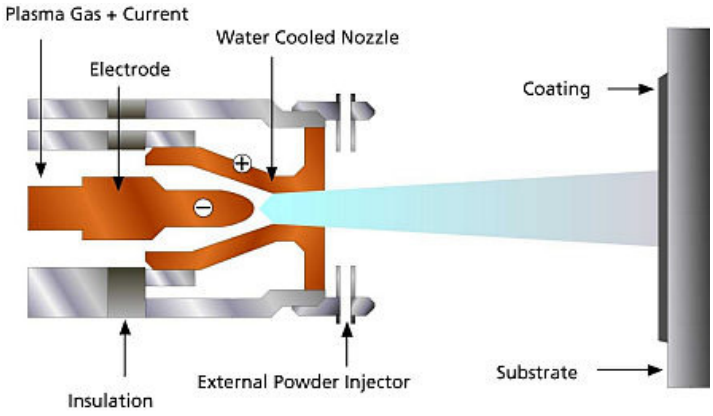

Figure 2-5: schematic presentation of plasma spray process.

1.3 HIGH VELOCITY OXY-FUEL SPRAYING (HVOF)

HVOF is a thermal spray process utilising the combustion of gases, such as Hydrogen or a liquid fuel such as kerosene. Fuel and oxygen mix and atomise within the combustion chamber under conditions that monitor the correct combustion mode and pressure. The process creates a high velocity which is used to propel the particles at near supersonic speeds before impact onto the substrate. One of the basic rules of spraying is that high combustion pressure = high gas velocity, high particle velocity and resulting high coating quality.

One of the key benefits of this system's high velocity is the extremely high coating density and low oxide content. The low oxides are due partly to the speed of the particles spending less time within the heat source and partly due to the lower flame temperature (around 3,000 °C) of the heat source compared with alternative processes.

Oxygen and fuel (kerosene, acetylene, propylene or hydrogen) mixture is introduced in the combustion chamber of the gun as shown in Figure 2-6 . It burns into a flame when ignited and the burnt gas acquires a very high temperature and escapes from the confinement of the small chamber at a high velocity while undergoing rapid expansion. From one end of the gun, powder is pushed into the center of the flame by a carrier gas. The particles melt and are immediately carried to the target by the hot gas through the nozzle of the gun at a high velocity [49, 50].

The HVOF process is one of the most popular thermal spraying technologies and has been widely adopted by many industries due to its flexibility and the superior quality of coatings produced. HVOF thermally sprayed coatings are used in a wide range of other applications such as the gas turbine, petroleum[51], chemical, paper/pulp [52], automotive [53] and manufacturing industries [54]. Tungsten carbide-cobalt (WC-Co) is the coating material under review in the report, has many applications in the above mentioned industries [55] , due to its impressive mechanical properties. The coating application of the WC-Co material is very popular; however the spray-forming of this material has not been widely documented [56-61]

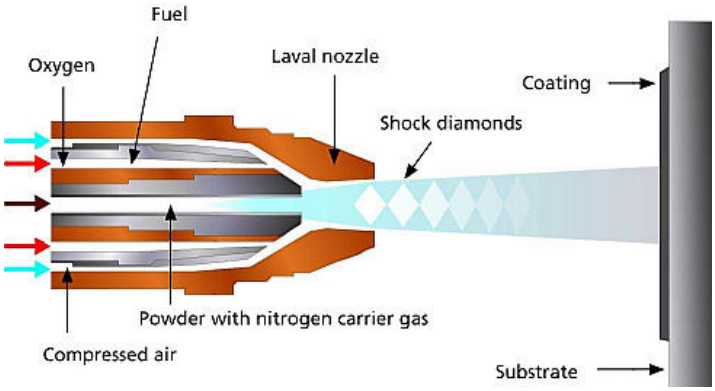

Figure 2-6: schematic presentation of High Velocity Oxy-Fuel spraying process.

2. COMPARISON BETWEEN THERMAL SPRAY PROCESSES

Figure 2-7 shows the different gas temperature in function of particle speed for the different processes in thermal spray coating. It is noticeable that HVOF provides a higher particle speed than that in VPS or FS. Gas temperature and particle speed are two important parameters and have a direct impact on the microstructure as shown in Figure 2-8 as a typical NiCr 80-20 sprayed by different techniques, where the difference in oxide content, porosity and morphology are well pronounced. However, these general properties of coatings are listed in Table 1.

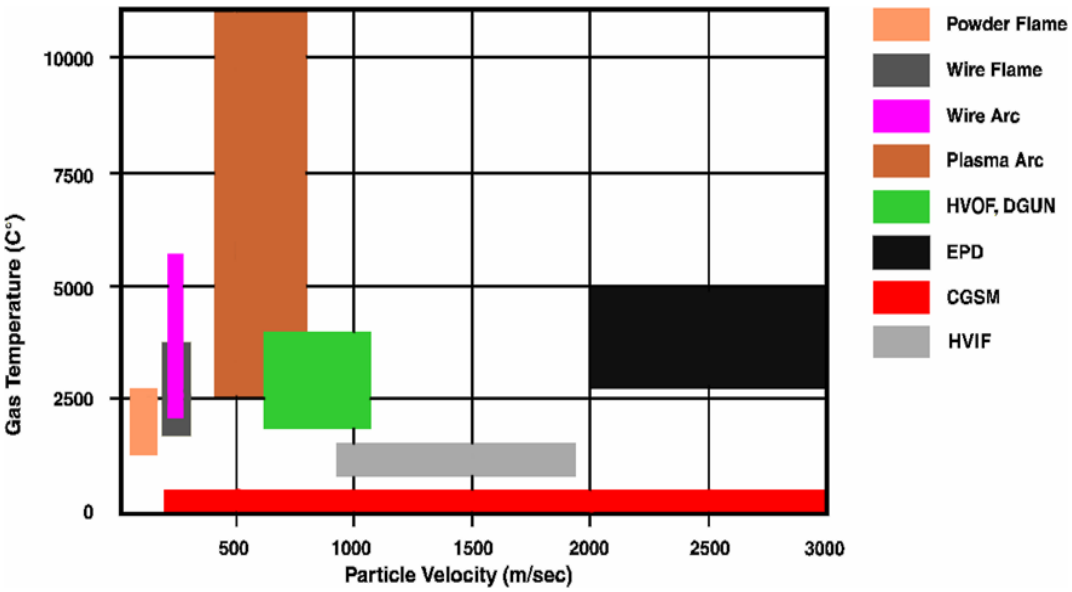

Figure 2-7: gas temperature in function of particle velocity for different thermal spray processes [40].

Where:

HVOF: High-velocity oxygen/fuel.

HVAF: High-velocity air/fuel.

HVIF: High-velocity impact forging [62].

CGSM: Cold Gas Spray Method [63] .

EPD: Electromagnetic Powder Deposition [64].

DGUN: Detonation- Gun spraying [36].

Table 1: A comparison of thermal spraying process and coating characteristics [42]

	Particle Velocity $m.s^{-1}$	**Adhesion MPa**	**Oxide content %**	**Porosity %**	**Deposition rate $kg.hr^{-1}$**	**Typical deposit thickness mm**
Flame	40	10-40	2-5	5-15	1-10	0.2-10
Plasma	200-300	20-70	1-3	5-10	1-5	0.2-2
HVOF	600-1000	>70	1-2	1-2	1-5	0.2-2

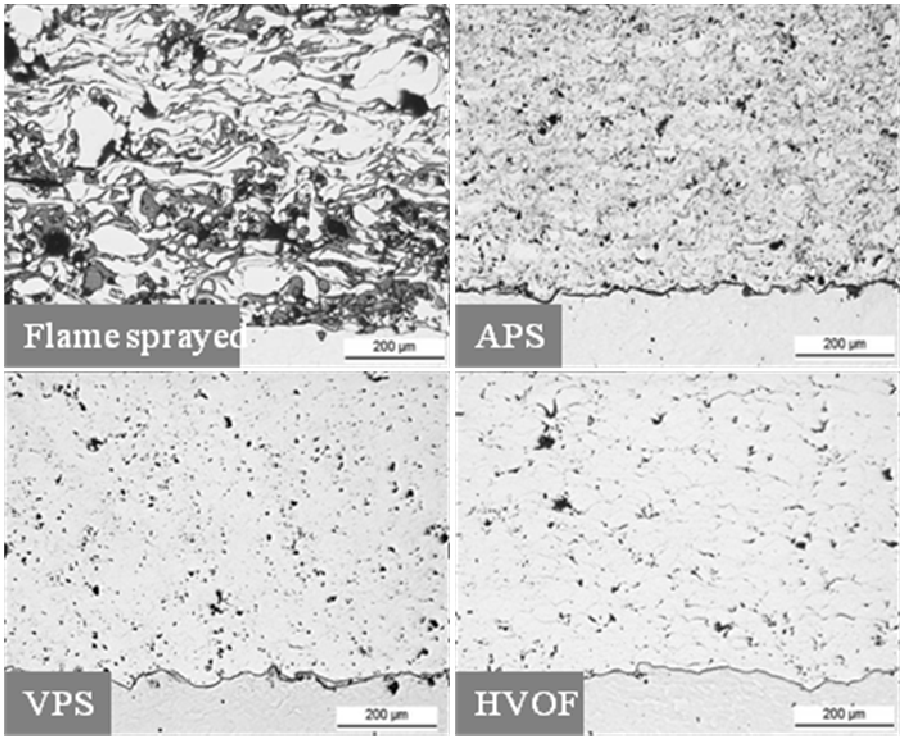

Figure 2-8: microstructure of different coatings process of the same powder of NiCr 80-20 and steel substrate.

3. COATING BUILD-UP, STRUCTURE AND PROPERTIES

Thermal spray coatings are built up by the accumulation of splats formed by the deposition of individual molten droplets (Figure 2-9) to form splats. Coating characteristics such as porosity, adhesion strength, and roughness depend on the shape of these splats and how they bond with each other and with the substrate (Figure 2-10). The form that splats assume after solidification is a function of process parameters such as particle size distribution, velocity, temperature, and degree of solidification, and substrate material and temperature [65]. Splat morphology has been widely investigated [65-71] since it has very important effect on coating adhesion. Sakakibara *et al.* [72] investigated yttria-stabilized zirconia particles on a polished stainless steel surface and found the disk splat showed a significant increase in adhesion. However, as common feature of all thermal spray coatings is their lamellar grain structure resulting from the rapid solidification of small globules, flattened from striking a cold surface at high velocities as shown in Figure 2-9 and Figure 2-11 and. Between the lamellae, a numerous of voids are generated. This void structure has been widely studied [73-

77]. Such structural features e.g. voids, oxides and not melted particles give rise to anisotropic coating properties, both thermal and mechanical [78].

For instance, the proportion of true-contact and no-contact areas was found to have a significant influence on thermal conductivity, Young's modulus [79], adhesion and quenching stress [80].

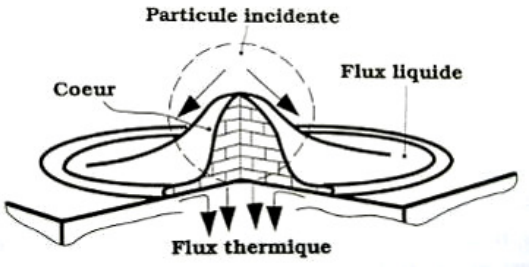

Figure 2-9 : melted particle splashing against the substrate [81].

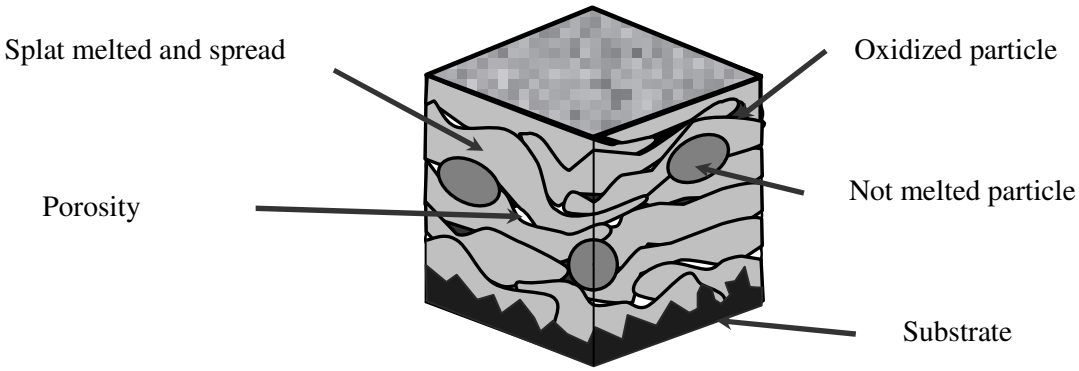

Figure 2-10: typical thermally sprayed coating morphology.

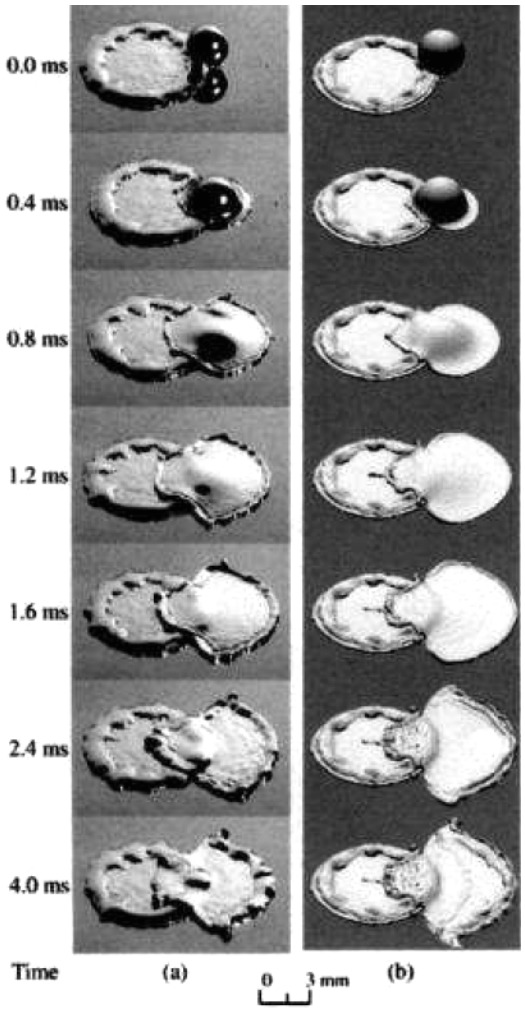

Figure 2-11 Comparison between experimental results (a) and numerical modelling (b) Obtained by Mostaghimi et al[82, 83].

On the other hand, when a molten particle strikes the surface, it interacts with the substrate in such manner that a weak or a strong bond is created. A strong bond maybe explained by the formation of metallurgical bond between the impinging particles and the surface. Localized diffusion between the melted substrate and particle have been proposed as the mechanism for this metallurgical bond [84, 85].

CHAPTER 3 : RESIDUAL STRESS IN THERMALLY SPRAYED COATINGS

1. DEFINITION AND ORIGIN OF RESIDUAL STRESS

The residual stresses can be defined as those stresses that remain in a material or body after manufacture and processing in the absence of external forces or thermal gradients [86]. Residual stress measurement techniques invariably measure strains rather than stresses, and the residual stresses are then deduced using the appropriate material parameters such as Young's modulus and Poisson's ratio. Within a measurement volume, in both, surface plane and through the depth, a single stress value is often considered which is a wrong consideration. However, Residual stresses are divided in three types:

1. type I: macro residual stresses that vary within the body of the component over a range much larger than the grain size,
2. type II: micro residual stresses that operate at the grain-size level, which result from differences within the microstructure and the presence of different phases or constituents in a material,
3. type III: are micro residuals stresses that exist within a grain, essentially as a result of the presence of dislocations and other crystalline defects. Types II and III are often grouped together as microstresses.

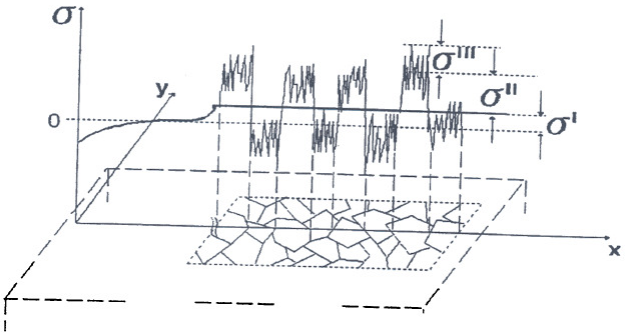

Figure 3-1: categorisation of residual stresses according to length scales [86].

Micro residual stresses often result from the presence of different phases or constituents in a material. They can change sign and/or magnitude over distances comparable to the grain size of the material under analysis.

The sources of stress generation in thermally sprayed coating are mainly quenching and thermal stresses [32]:

1.1 QUENCHING STRESS

When a droplet impinges on a substrate during spray deposition, it tends to spread to form a splat, which then quickly solidifies and cools. During this cooling, the thermal contraction of the splat will be inhibited by the underlying material, so that a tensile stress will be generated in the splat. Since splats are typically a few μm in thickness, it can always be assumed that they are on a massive substrate and the misfit strain associated with the contraction is entirely accommodated within the splat. The quenching stress is therefore given by the product of the misfit strain and the modulus of the deposit $\sigma_0 = \alpha_d \Delta T E_0$. The value of the quenching stress can vary over a wide range, but it is always in tensile. The tensile quenching stress level can theoretically achieve in the GPa range. But those values are normally well below such level: in fact, they usually range from a few MPa to a few hundred MPa. The main reason for this is the relaxation process during splat quenching e.g. microcracking, plastic flow, creep, interfacial sliding etc. (Figure 3-2)

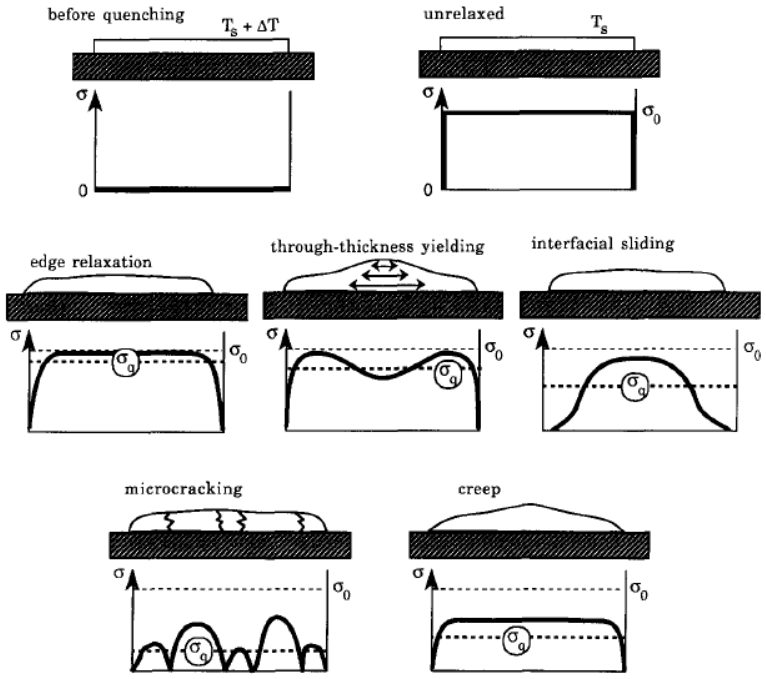

Figure 3-2: Schematic illustration of the stress distributions within a single splat before and after various stress relaxation phenomena have taken place [32].

The magnitude of quenching stress does not depend strongly on the substrate material, but varies significantly with the coating materials and the following spraying conditions:

- spraying distance due to the changes in intersplat bonding associated with increase in particle temperature and velocity,
- the deposition rate, determined by powder feed rate and torch traverse speed, as discussed in [87, 88],
- the substrate temperature T_s where its variation affects the final residual stress during spraying. as shown in Figure 3-3 [32].

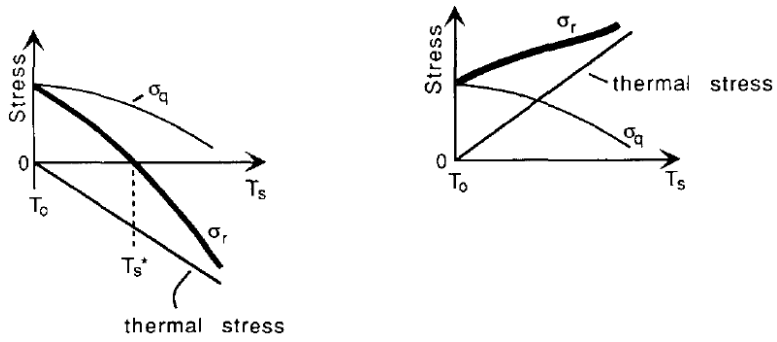

a) *b)*

Figure 3-3: schematic diagram of the variation of the final residual stress (σ_r) with substrate temperature T_s during spraying: a) $\alpha_c < \alpha_s$, b) $\alpha_c > \alpha_s$ [32], (σ_q=quenching stress).

Generally, metals have better wetting properties, better contact with the substrate and may be therefore able to retain higher stress than brittle ceramic, where the stress is largely reduced by cracking [89]. In metallic coatings, positive dependence of quenching stress on substrate temperature was observed in the lower temperature range, while a negative dependence found in the higher temperature range. Therefore, quenching stress increases with temperature due to improved intersplat bonding (since the Young modulus increased and decreased porosity were observed) up to a point where the intrinsic strength, decreasing with temperature, becomes a limiting factor [90]. This effect is more pronounced for metals than for ceramics, which has higher melting point and thus only the first mechanism plays a significant role in common deposition temperature range.

1.2 THERMAL STRESS

This is originated from the substrate-coating cool together, with or without thermal gradients. However this is a macroscopic because the sprayed coating can be considered as a continuous solid. This stress can be either tensile or compressive depending on the thermal expansion coefficients and thermal gradient and this can be expressed by:

$$\sigma_{th} = \frac{E_c}{1-\nu_c}(\alpha_c(T_a) - \alpha_s(T_a)) \cdot (T_d - T_c) \qquad 3\text{-}1$$

Where: T_d: *deposition temperature [K],*

T_a: *ambient temperature [K],*

α_s, α_c : coefficients of thermal expansion (CTE) of substrate and coating, resp. [K^{-1}],

E_c : Young modulus of substrate [MPa].

If $\alpha_c > \alpha_s$, the induced stresses during the secondary cooling will be tensile and the resulting residual stresses in the coating will always be tensile. If $\alpha_c < \alpha_s$, the resulting residual stresses in the coating may be either tensile or compressive, since the residual stresses which arise from the primary cooling (quenching) are always tensile. Therefore, the magnitude and the sign (+: tensile; -: compressive) of the resulting residual stress will depend on the balance between these sources. A summary of this model is given in Table 3-1.

Table 3-1: Induced stresses in the coating during thermal spraying [91]

Origin of stresses	$\alpha_c < \alpha_s$	$\alpha_c = \alpha_s$	$\alpha_c > \alpha_s$
Quenching stress	+	+	+
Thermal stress	-	0	+
Resulted residual stress	+ or -	+	+

+ ; tensile stress / - ; compressive stress

These stresses are superimposed on the ones already present from the deposition process. In addition to these two main sources, there are a various factors that can affect the stress, e.g. phase transformation accompanied by volume change, chemical changes (oxidation).

The residual stress can affect the integrity and the performance of the coating-substrate system. It could have detrimental or beneficial effects, e.g. high tensile stress usually leads to cracking of coating [32, 33], whereas, compressive stress can suppress crack formation and propagation, if it is in too high intensity, this can cause coating delamination from substrate [92, 93]. Other factor may be included is stress-induced phase transformation [94, 95]. This stress can be calculated from the following equation:

$$\sigma_{P.tranformation} = \frac{E_c(1-\rho'/\rho'')}{3.(2\nu - 1)} \qquad 3\text{-}2$$

In which ρ`and ρ``concern the densities of the coating material, prior to phase transformation, respectively. For example, a free standing alumina sample heated

to a temperature above 1373 K, a phase γ having a density of ρ`= 3.67 g/cm3 transforms to phase α of density ρ``= 3.98 g/cm3. It is noticeable that the resulted residual stress can be expressed as the sum of the all previous considered stresses:

$\sigma_{res} = \sigma_{quenching} + \sigma_{thermal} + \sigma_{P.\ transformation}$

2. THE INFLUENCE OF ANNEALING ON RESIDUAL STRESS

Residual stresses are often considered as unwanted and detrimental. However, as reviewed by Hurrell *et al* [96], there are many ways either to reduce potentially harmful residual stresses, or to introduce beneficial residual stresses to prolong life. At least two stress relief mechanisms are important:

1. plasticity caused by the reduced yield stress at elevated temperature which occurs essentially instantaneously as the temperature increases,
2. creep mechanisms which occur over a longer period of time.

It should be noted that because plastic strain generated from the misfit cannot be relieved by local plastic flow but requires larger scale rearrangement. However, the aim of post annealing of coating-substrate system is to reduce the residual stress intensity within the coating and at the interface. Depending on the temperature, annealing can mainly modify the distribution field of residual stress around the interface [97, 98]. However, Laribi [99] found a significant reduce of residual stress after annealing molybdenum coating on steel substrate and also found a chemical diffusion of a $\varepsilon(Fe_xMo_y)$ fragile intermediate phase at interface. Lesage [98] found the annealing treatment of NiCr coating at 600°C led to a considerable improvement of coating adhesion due to the reinforcement of the metallurgical bonding between the coating and the substrate which was attributed to inter diffusion of iron, nickel and chromium. Brossard [100] found in NiCr sprayed particles on the stainless steel substrates an inter-diffusion between both materials, and grains growing across the interface into both phases.

3. METHODS TO DETERMINE RESIDUAL STRESS

Residual stress measurements methods are divided in many categories:

1. analytical or numerical e.g. mathematical [101-103],
2. material removal techniques like hole drilling and layer removal [104-108],
3. mechanical methods like; curvature, displacement, or strain measurement [32, 109-111],
4. diffraction like X-ray or neutron methods [26, 112-114].

It is worthy to remind that X-ray is based on the deformation of the crystal lattice due to residual stresses. This method is also called "$\sin^2 \Psi$" method, and also practicable for another sources of radiation-neutrons.

The neutron diffraction method allows penetrating neutrons through-thickness stress profiling without any material removal whereas the X-ray diffraction is considered as a complementary technique; it can determine stress only in a thin surface layer. This "$\sin^2 \Psi$" method was used to measure stress in plasma sprayed coating and some limitations were found in absorption or radiation in a few μm for the X-rays and a few cm for neutrons, furthermore, it was difficult to determine for porous or graded coatings. However, such radiation methods are time consuming and expensive [31]. However, each technique has certain advantages and limitations. The incremental hole drilling method is becoming more and more important because of the in situ measurement in depth profile, the dependency of the component geometry, its quasi-nondestructive character since the small hole can be filled by different techniques e.g. welding or galvanic deposition, one of the disadvantage of this method is the residual stress required are measured in small volume and local [115-122].The advantage of the curvature method that allows determination of stresses in thick layers of graded or inhomogeneous composition, and is non-destructive and gives also a whole trend of residual stress for large volume [123-125]. A brief introduction of different analysis model based on beam theory curvature will be conducted using the following approaches:

3.1 STONEY APPROACH

The main assumption of Stoney equation [126] is the coating thickness is moderately thin compared to substrate ($h_c << h_s$), and the coating properties are closely resemble substrate. Therefore, he considered only the elastic modulus of substrate in his equation to give an average value of residual stress intensity.

$$\sigma_{Stoney} = \frac{\kappa E_s' \cdot h_s^2}{6h_c} \qquad 3\text{-}3$$

3.2 CLYNE APPROACH

Based on force momentum balance, the misfit strain $\Delta\varepsilon$ in the x-direction resulted from two plates bonded together arises during a change in temperature ($\Delta\varepsilon=\alpha\Delta T$) with stress distribution of $\sigma_x(y)$ and a curvature κ as shown in

Figure 3-4. The stress intensity $\sigma_x(y)$ and curvature κ can be evaluated from simple beam bending theory. The unbalanced momentum is resulted from the opposite forces ($-P$ and P). When the two plates are joined, an unbalanced moment M generates curvature κ of the composite plate. The momentum can be expressed by:

$$M = P \cdot (\frac{h_s + h_c}{2})$$

where h_c and h_s are the thicknesses of coating and substrate respectively.

The curvature of a beam κ is equal to the through-thickness gradient of strain, and can be expressed as:

$$\kappa = \frac{M}{\Sigma}$$

where Σ is the beam stiffness.

When the condition $h_c << h_s$ does not apply, then stresses and stress gradients are often significant in both constituents. Therefore, Clyne et al. [123, 127] have proposed mathematical expressions, which predict how axial residual stresses may change through coating thickness (y-axis) as shown in

Figure 3-4. These axial stresses depend on the coating and substrate Young's moduli and also on the thermal expansion mismatch between them. Considering an imposed misfit strain $\Delta\varepsilon$, in the x-direction, such as would arise during a

change in temperature, the resultant stress distribution, $\sigma_{x(y)}$, and the curvature κ were obtained from the simple beam bending theory. A general expression for uniform misfit strain considering that $h_c << h_s$ was obtained:

$$\Delta\varepsilon = \kappa \cdot \frac{E_c^2 h_c^4 + 4E_c E_s h_c^3 h_s + 6E_c E_s h_c^2 h_s^2 + 4E_c E_s h_c h_s^3 + E_s^2 h_s^4}{6E_c E_s (h_c + h_s) h_c h_s} \qquad 3\text{-}4$$

Where E_s and E_c are the Young modulus of substrate and coating respectively, (h_s=H in our case) and h_c are the thickness of the substrate and the coating, respectively, ν_c is the coating Poisson ratio.

From

Figure 3-4, we should distinguish two of residual stress at the interface, one in the coating and one in the substrate. However, the gradient of residual stress can be calculated as the following equations:

$$\sigma_c(y=0) = -\Delta\varepsilon \cdot \frac{E_c' h_s E_s'}{h_c E_c' + h_s E_s'} - E_c' \kappa\delta \qquad 3\text{-}5$$

$$\sigma_c(y=h_c) = -\Delta\varepsilon \cdot \frac{E_c' h_s E_s'}{h_c E_c' + h_s E_s'} + E_c' \kappa(h_c - \delta) \qquad 3\text{-}6$$

$$\sigma_{res}(y=-hs) = -\Delta\varepsilon \cdot \frac{E_c' h_s E_s'}{h_c E_c' + h_s E_s'} - E_c' \kappa(h_s - \delta) \qquad 3\text{-}7$$

$$\sigma_s(y=0) = \Delta\varepsilon \cdot \frac{E_c' h_c E_s'}{h_c E_c' + h_s E_s'} - E_s' \kappa\delta \qquad 3\text{-}8$$

$$\delta = \frac{h_c^2 E_c - h_s^2 E_s}{2(h_c E_c - h_s E_s)} \qquad 3\text{-}9$$

Where the δ is the distance to the neutral axe which has by definition a constant axial length in spite of the deflection.

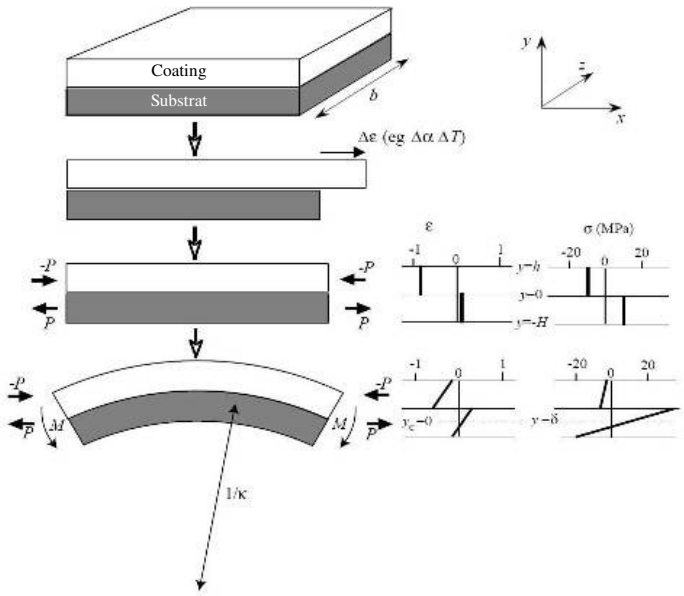

Figure 3-4: Schematic of the generation of curvature in a flat bi-materials plate [123].

3.3 CHIU APPROACH

Chiu [124] defined an average residual stress corresponding to the equilibrium stress in a real coated component as:

$$\sigma_{Chiu} = \kappa \cdot \frac{E_s h_s^3 + E_c h_c^3}{6(h_c + h_s)h_c} \qquad 3\text{-}10$$

This average residual stress in the coating σ_{Chiu} is equal to the arithmetic average between the residual stress at the surface in the coating and the residual stress at the interface in the coating. It is interesting to note that σ_{Chiu} converges to 0 when the hs/ hc ratio decreases. Therefore, this approach is limited to the coating thickness, since a thick coatings deposited on relatively thin substrates will often exhibit an average residual stress in the coating close to 0.

3.4 GODOY APPROACH

Godoy et al [125] defined an average in-plane normal stress at the interface in the coating and residual stress at the interface in the substrate, which is given as an average value of equations 3-5 and 3-8 by:

$$\sigma_{Godoy} = \frac{\sigma_c(y=0) + \sigma_s(y=0)}{2} \qquad 3\text{-}11$$

$$\sigma_c(y=0) = -\Delta\varepsilon \cdot \frac{E_c' h_s E_s'}{h_c E_c' + h_s E_s'} - E_c' \kappa\delta \qquad 3\text{-}12$$

$$\sigma_s(y=0) = \Delta\varepsilon \cdot \frac{E_c' h_c E_s'}{h_c E_c' + h_s E_s'} - E_s' \kappa\delta \qquad 3\text{-}13$$

CHAPTER 4 : ADHESION OF THERMALLY SPRAYED COATINGS

1. DIFINITION AND BASIC OF ADHESION

The word “adhesion” comes from the Latin verb “haerere” (to adhere, to stick to something). The prefix “ad” stands for “to”. So adhesion means sticking together of materials. Adhesion is the force of attraction between molecules of different substances while cohesion is the force of attraction between molecules of the same substance. However, the American Society for Testing and Materials (ASTM) (D907-70) defines adhesion as “the state in which two surfaces are held together by interfacial forces which may consist of valence forces or interlocking forces or both”. These bonding forces can be “Van der Waals” forces, electrostatic forces and/or chemical-bonding forces which are effective across the interface. An important distinction is made between basic adhesion, that is the maximum possible attainable value, and experimental or practical adhesion, which can be termed bond strength or adhesion strength [128, 129]. The relationship between the experimentally measured adhesion (EA) and the basic adhesion (BA) is given by:

EA = f(BA, other factors).

Such that EA < BA. However, in reality EA << BA owing to the effect of other factors on the test. These include residual stresses in the coating and the technique

used for measuring the bond strength (EA). Therefore, adhesion can be manifested in three different categories:

1.1 FUNDAMENTAL ADHESION

It is related to the nature and strength of the binding forces between two materials in contact with each other, such forces like; ionic, covalent, coordinate, metallic, hydrogen and Van der Waals. But this basic definition of adhesion is not very helpful as it is not possible either to calculate the contribution of each binding force or to measure adhesion forces in practical systems.

1.2 THERMODYNAMIC ADHESION

It is defined the change in free energy when an interface is formed (or separated) and is expressed as:

$W_A = \gamma_{s1} + \gamma_{s2} - \gamma_{s1,s2}$ *4-1*

In which $\gamma_{s1} + \gamma_{s2}$ represent, respectively, the specific surface free energies of material 1 (substrate), 2 (coating) and $\gamma_{s1,s2}$ represent the interfacial specific free energy. In case of liquid coatings, W_A can be easily determined by $W_A = \gamma_{LV}(1+\cos\phi)$ where γ_{LV} is the surface free energy of the liquid and ϕ is the contact angle of the liquid coating on the substrate.

1.3 PRACTICAL ADHESION

It signifies the forces or the work required to remove or detach a film or coating from the substrate. This includes the energy required to deform the coating and substrate as well as the energy dissipated as a heat or stored in the coating. The relationship between practical adhesion and fundamental one is expressed by:

Practical adhesion = f (fundamental adhesion, other factors) [130] *4-2*

The fundamental adhesion denotes the energy required to break chemical bonds at the weakest place in the coating-substrate system. The other factors can be residual stress in the coating, thickness, mechanical properties of coating and substrate, work consumed by plastic deformation, mode of failure, etc. The pertinent question is can one determine fundamental adhesion by making

practical adhesion measurement? It is very difficult, and maybe impossible to quantitatively determine the contribution due to the multitude of chemical factors. We can only hope to observe an increase in practical adhesion by improving the fundamental one.

2. METHODS OF ADHESION MEASUREMENT

Many methods have been developed for evaluating the coating-substrate adhesion. Among them, a significant number is based on the linear elastic fracture mechanics (LEFM) approach [1-3]. But, there are no universal tests for measuring coating's adhesion. Each method is related to a certain type of coating, loading condition, application of the coating etc. This can be explained by the variety of coating systems which represent different types of dissimilar material interfaces that are present in many industrial applications (metal/metal, metal/ceramic, polymer/metal, polymer/ceramic, etc). The tests that work with one coating system may not necessarily work with another [18-20]. Though, there is no standard adhesion test for coating system which can suite all materials. Among the most widespread methods used are indentation tests [4, 5], shear tests, [6-9] tensile adhesive strength like ASTM C633, ASTM F1147, ISO 14916, EN 582 [10-12] and double cantilever beam (DCB), where a large scatter of the results was observed and must be viewed quantitatively even the test system was very sensitive [13]. The best test method often becomes the one that simulates practical stress condition [14-16]. We should also note that adhesion is not a constant in practical applications, but rather a complicated property that depends on loading conditions on coating thickness [10] and on different parameters such as grit blasting to roughen the substrate surface [21-25]. Furthermore, the residual stresses due to the mismatch in thermal and mechanical properties between coatings and substrate are of importance [26-30]. However, Coating adhesion measurement methods can be divided in many categories as classified by Mittal [129]:

1. Qualitative and quantitative methods.
2. Destructive and non-destructive methods.
3. Mechanical and non-mechanical methods.
4. Fully developed, partly developed and the methods under development.

5. Practical methods and the methods of academic interest.
6. Routine and non-routine methods.

Further review of measurement methods was reported by Kharlamov [131], who summed up all applied methods in Figure 4-1.

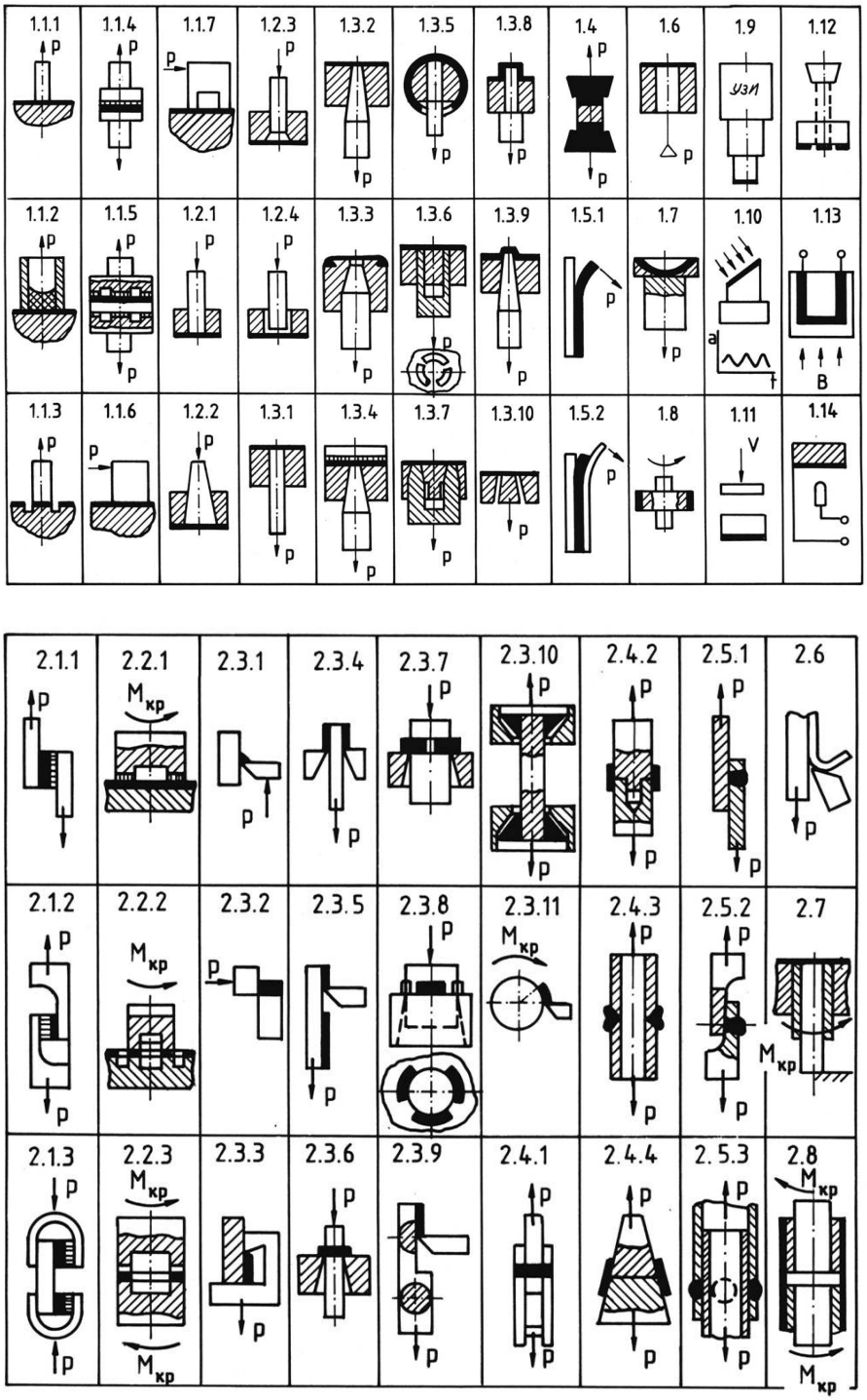

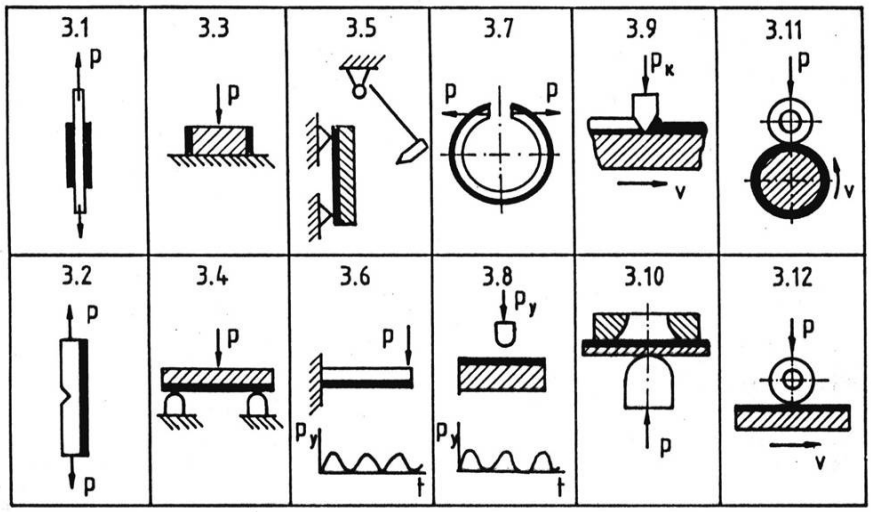

Figure 4-1: adhesion measurement methods reported by Kharlamov [131].

2.1 TENSILE ADHESION TEST (PULL –OFF)

The coatings are usually tested in a manner similar to that described by the DIN EN 582 [132] (ASTM Standard C633). This test consists of two cylindrical samples of 25 mm diameter, sprayed one and the counter body as shown in Figure 4-2. They are joined using an adhesive agent according to the standard test. Therefore, they are cured at elevated temperature. The adhesive strength is averaged from several tensile test results from the simple relation: $\sigma_{max} = F/A$, where F is the maximum force at failure, and A is the area of the cylinder surface.

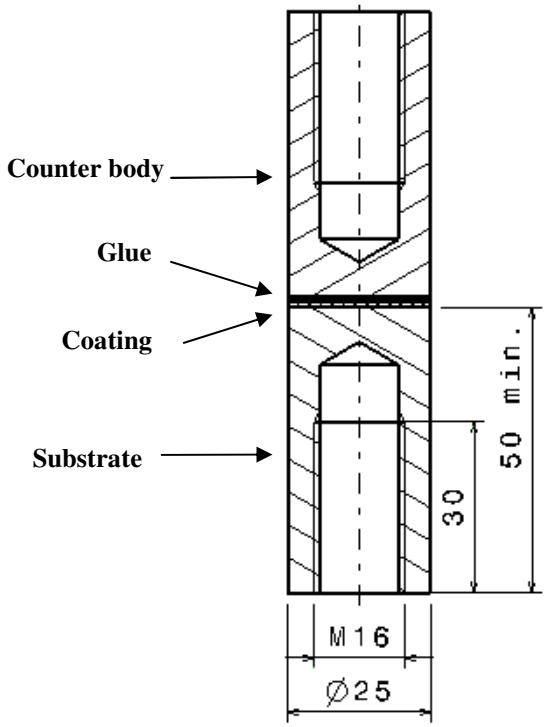

Figure 4-2: schematic presentation of tensile adhesion test according the standard configuration EN 582 [132].

Figure 4-3 shows the mode of coating failure and this can be described as either failure within adhesive (glue), adhesive, or cohesive. Adhesive failure takes place when the entire coating separates from the substrate whereas cohesive failure is occurs when failure takes place entirely within the coating. True adhesive failure (also termed interfacial failure) rarely occurs because of the rough nature of the substrate surface and adhesive failure in this case is defined as taking place near to the interface where the fracture surface exhibits areas devoid of the coating. Figure 4-4 shows an example of interfacial and adhesive mode failure.

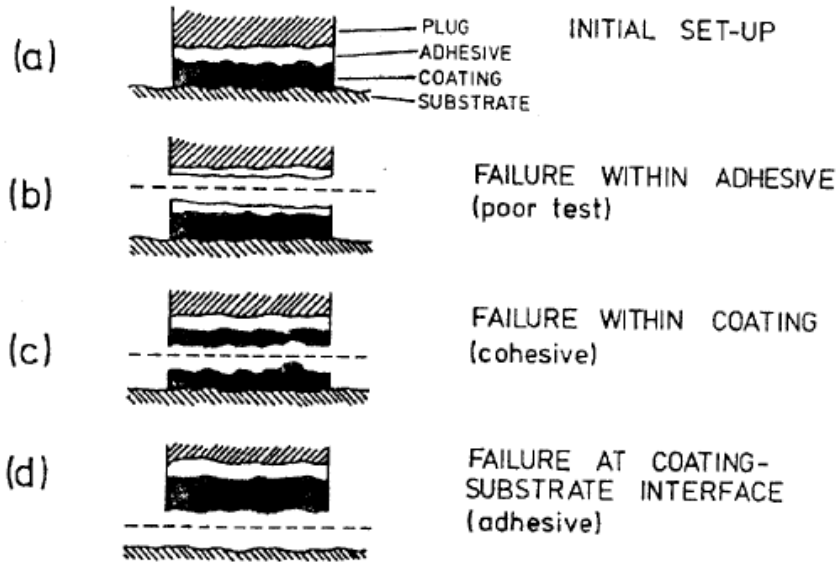

Figure 4-3: modes of coating failure [133].

a) b)

Figure 4-4: An example of failure analysis of Al_2O_3 coating showing a zone A (bright) on the counter part corresponds to the extent of the interfacial failure (between coating and substrate), and zone B (dark) showing an adhesive failure (between the coating and the glue) took place, a) counter body, b) coated body.

This test method suffers from the following difficulties:

1. simple tensile tests are difficult to perform, and very often the mixture applied force in tensile and shear lead to misinterpret the results [134],
2. the alignment must be perfect to insure uniform loading to the interface,
3. limitation by the strengths of available adhesive,
4. the possibility of adhesive penetrating within the coating,
5. stresses produced during setting of cement or adhesive,

6. non-uniform stress distributions or stress concentrations over the contact area during the pulling process [135].

In spite of all of these factors are sources to affect the adhesion strength measure, this test is still widely applied in industries.

2.2 INTERFACIAL INDENTATION

Some authors have used indentation tests searching to generate and propagate a crack at the interface in order to determine the adhesion between a coating and its substrate. Indentation may be performed at the surface of the sample perpendicularly to the coating [4, 136] or in a cross-section: either into the substrate near the interface [137] or directly at the interface between the substrate and the coating [138] as shown in Figure 4-5. The indentation is performed using a pyramidal Vickers indenter. Choulier [139, 140] showed that the generated cracks have a semi-circular shape and are localised in the interface plane crack radius (a) which can be measured by optical microscopy and he suggested the following equation for the cracking energy:

$$G_{Ic} = C\frac{P^2}{a^3} \qquad 4\text{-}3$$

This relation, which was deduced from empirical or theoretical considerations, involves a factor P^2/a^3 relating the indentation load P to the crack length a. Richard *et al* [141] suggested that an interface toughness would be strongly dependent on the Young modulus E and the coating hardness H as given by:

$$K_{1C} = C_{ste}\left(\frac{E}{H}\right)^{1/2} \times \frac{P}{a^{3/2}} \qquad 4\text{-}4$$

The previous formulations by Choulier and Richard do not fully represent well the behaviour experimentally observed for these materials. Therefore, further development to relate adhesion properties to the critical indentation load at the interface was carried out by Chicot and Lesage [142-144] who first used the critical point (P_c, a_c) characterized by crack length at interface a_c propagated when a critical load P_c is achieved. Based on that critical point, the authors defined the apparent interface toughness as a mechanical characteristic representing the adhesion of a thermal sprayed coating on its substrate:

$$K_{1C} = \frac{1}{\pi^{3/2} \times \tan\psi} \times \frac{P_c}{a_c^{3/2}} \qquad 4\text{-}5$$

Where ($\psi = 68°$) is the half angle of the indenter.

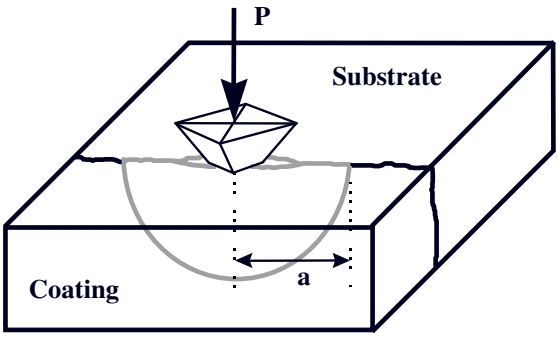

Figure 4-5 : Schematic representation of the interfacial indentation [145]

The research group of Lesage [142-144] represented the relation between crack length and indentation load using logarithmic scales (Figure 4-6).

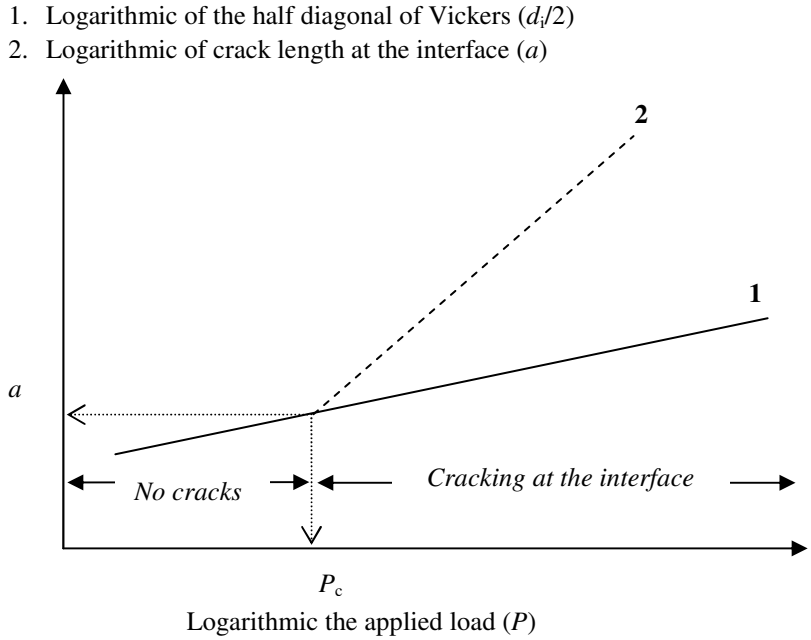

Figure 4-6: bilogarithmic presentation of load-crack length/Vickers imprint and the critical point (P_c,a_c)

This way Chicot and Lesage were able to develop further the model by considering the mechanical properties of a theoretical material representing the global behaviour of the interface:

$$K_{ca} = 0{,}015 \frac{P_c}{a_c^{3/2}} \cdot \left(\frac{E}{H} \right)_I^{1/2} \qquad 4\text{-}6$$

Where $(E/H)_I$ is the characteristic of mechanical properties of the interface. The methodology adopted to determine this characteristic is described here under.
From Figure 4-7, the geometrical condition of the coating - substrate should be considered to calculate the average diagonal of indenter imprint d_I as well as the plastic deformed zone radius of b_I at interface and they are expressed by:

$$d_I = \frac{d_R + d_S}{2} \qquad 4\text{-}7$$

$$b_I = \frac{b_R + b_S}{2} \qquad 4\text{-}8$$

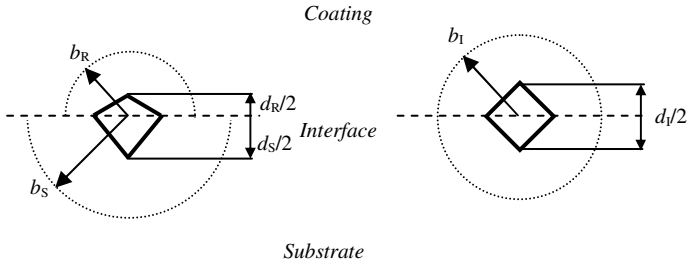

Figure 4-7: schematic presentation of the Vickers imprint and the plastic zone [142, 143]

The diagonal of Vickers hardness is defined by the general equation:

$$H = C \cdot \frac{P}{d^2} \qquad 4\text{-}9$$

Where H is the hardness and C is constant, P is the load and d is the diagonal of the imprint. The radius of the plastic zone is defined by the equation established by Lawn [146] including the mechanical property of materials:

$$b = \frac{d}{2} \sqrt{\frac{E}{H}} \cot^{1/3} \xi \qquad 4\text{-}10$$

Where ξ is the half angle between two lateral faces, for Vickers is $\xi = 74°$. Replacing 4-7 and 4-8 in 4-10 we obtain:

$$\left(\frac{E}{H}\right)_{\mathrm{I}}^{1/2} = \frac{2}{\cot^{1/3}\xi} \times \frac{b_{\mathrm{I}}}{d_{\mathrm{I}}} = \frac{2}{\cot^{1/3}\xi} \times \frac{b_{\mathrm{R}} + b_{\mathrm{S}}}{d_{\mathrm{R}} + d_{\mathrm{S}}} \qquad 4\text{-}11$$

In replacing the d_{R}, d_{S}, b_{R}, b_{S} in the equations defined in 4-9 and 4-10, we can obtain the expression:

$$\left(\frac{E}{H}\right)_{\mathrm{I}}^{1/2} = \frac{\left(\frac{E}{H}\right)_{\mathrm{S}}^{1/2}}{1+\left(\frac{H_{\mathrm{S}}}{H_{\mathrm{R}}}\right)^{1/2}} + \frac{\left(\frac{E}{H}\right)_{\mathrm{R}}^{1/2}}{1+\left(\frac{H_{\mathrm{R}}}{H_{\mathrm{S}}}\right)^{1/2}} \qquad 4\text{-}12$$

Recent work of Liu [147-149] revealed by his finite elements modelling that the stress intensity factor calculated prior to the interfacial indentation tests was in mode *I*, and this confirm the hypothesis of Chicot and Lesage.

2.3 IN-PLANE TENSILE TEST

The interpretation of the tensile test data to extract intrinsic fracture and interfacial properties of the coating – substrate system, like any other type of mechanical tests, is still non-trivial. Hu and Evans [150] obtained some analytical results on cracking and decohesion of thin film coatings on ductile substrates by assuming a sliding (yielding) interface and linearly elastic coating and substrate. Their results cannot be applicable to the cases when the substrate is undergoing fully plastic deformation [151-153]. Using the shear lag model, Aveston et al. [154] analyzed extensively the multiple fractures in brittle fibres embedded in unidirectional fibre reinforced composites and several researchers therefore applied the crack fragmentation test model based on Kelly and Tyson theory [155-160] of stress transfer of single fibre relating the critical fibre length to interfacial shear stress. Agrawal and Raj [151, 161] presented a theoretical analysis to estimate the ultimate shear strength of a metal–ceramic interface using the crack density or spacing data obtained from a tensile test (Figure 4-8). They also concluded that the maximum and minimum crack spacing between the cracks should differ by a factor of two. However, their analysis was based on the

assumption of a sinusoidal distribution of the interfacial shear stress and the validity of such an assumption has not been examined in detail.

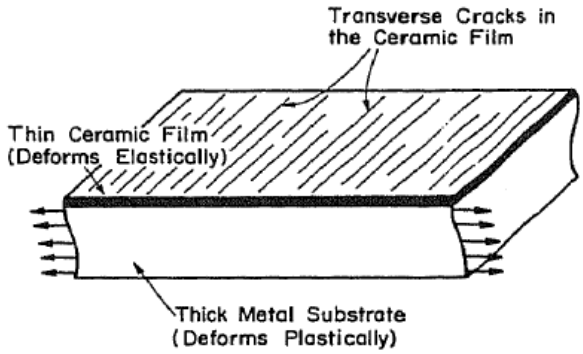

Figure 4-8: schematic presentation of shear lag proposed by Agrawal [151, 161].

Yang [162] also used the same approach of calculating the shear strength which is given by:

$$\tau = \frac{\pi.\sigma_c.h_c}{\delta_{\max}} \qquad 4\text{-}13$$

where, h_c is the coating thickness and δ_{max} is the maximum crack spacing at crack saturation level and $\sigma_c = E_c.\ \varepsilon_f$

The ultimate shear strength of the silica films on annealed 99.9% pure copper and nickel substrates was estimated to be 900 and 1400 MPa, respectively. However, these numbers are questionable as they greatly exceed the shear flow strength level for both metal substrates. Similarly, the ultimate shear strength of the NiO–Pt interfaces reported by Shieu et al. [163] to be as high as 4460 MPa for a Pt substrate with a tensile strength of 145 MPa is also rather doubtful. However, Chen [164, 165] adjusted the Agrawal approach as given by:

$$\tau = \frac{4.\sigma_c.h_c}{(\pi+4).\delta_{\max}} \qquad 4\text{-}14$$

He considered an elliptical configuration of shear stress distribution and non sinusoidal as Agrawal did. In addition, he took into account the residual stress in coating and obtained accurate results of TiN coating and AISI 304 substrate.

Cracking phenomenon is known to occur in composite materials consisting of brittle films adhering to high-elongation substrates, and a list of literature

concerning with the phenomenon is found in a monograph by Wojciechowski et al [166]. A shear lag model was adopted by Wojciechowski et al, who explained the mechanism how the stress piled up in segmented films of Ni-Fe alloy adhering to a polyimide substrate. However, their model did not take into account the residual strain which might have affected the fracture process considerably. Yanaka [167] suggested a crucial modification to the shear lag model for the multiple cracking of thin films in order to take into account the residual strain. However, the obtained results were found over estimated in calculating the critical fracture strength which lay in between 200 and 300 MPa and more than twice larger than published values for bulk SiO2 glasses may this attributed to the complicated fracture using this modified shear lag, since tensile and bending are involved in this loading stress. Besides only relatively simple and inexpensive testing instrumentation is needed, a tensile test produces in a well-controlled manner a large array of parallel cracks over the nominally homogenously deformed ductile substrate and it allows also in situ observation of cracking and decohesion of the coating via various microscopy tools.

2.4 ROCKWELL INDENTATION

Drory and *Hutchinson* 1996 [136] proposed using the indention perpendicular to the coating surface to determine the interfacial toughness of coating- substrate (Figure 4-9). This test method is quite attractive since a small volume is needed to perform such test. The objective of this test is to produce a local delamination. The driving force of the delamination is considered to be the elastic-plastic deformations of the substrate [5]. Important information required to determine the interfacial fracture toughness is the radial surface displacement of the indented material, around the indenter.

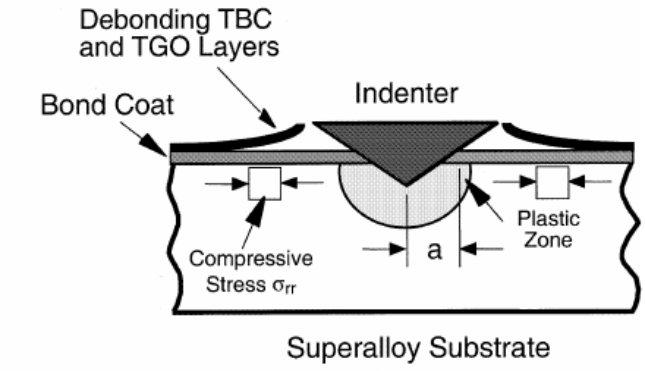

Figure 4-9 Schematic representation of the indentation perpendicular to the coating surface pprinciple of Rockwell indentation test [136].

Under loading, the plastic deformation of the substrate is encouraged in this test. The measurement involves loading by the diamond brale indenter (Figure 4-10). The coating delamination radius of coating resulted from indentation will be correlated to the later stress induced to calculate the interface toughness. Evaluation the interface toughness will be introduced in chapter 5.

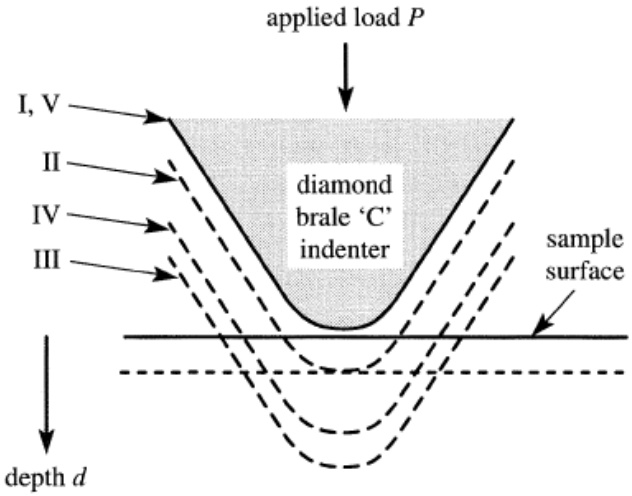

Figure 4-10: brale indentation test.

2.5 OTHER METHODS

The four-point bending test with notched symmetrical interfacial cracks (Figure 4-11) consists of a central notched bimaterial flexural beam [168, 169]. This method allows the measurement of the interfacial fracture toughness for a large range of stress factor mode mixity and for relatively equal normal and tangential stresses. The vertical displacement in the middle of the specimen is recorded

during the experiment by means of a displacement transducer. Even the simple geometry is simple, but the vertical cracking of coating made the evaluation of the interfacial toughness difficult [169, 170].

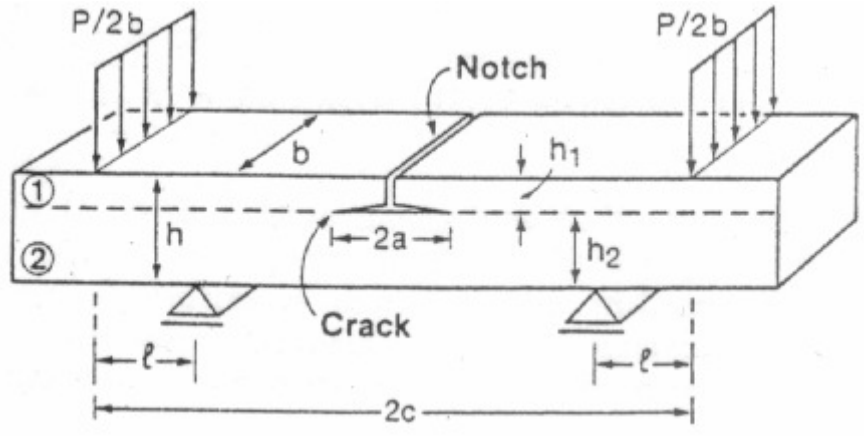

Figure 4-11: notched four points bending test with symmetrical crack at the interface.

The configuration of the double cantilever beam (DCB) specimen is shown in Figure 4-12. The coating layer is glued by an adhesive to the lower arm of the DCB specimen. The lower arm is manufactured from a material, which is stiffer than the adhesive. Both extremities of the specimens are loaded in tension in order to allow delamination between substrate and coating. This testing method is attractive because of the existence of a simple analytical solution to calculate the interfacial fracture toughness [171, 172]; as well as, the experimental observations show a more stable crack growth than those derived from other test methods [173]. However, one of the limitations in this test method is the bonding strength of the adhesive agent.

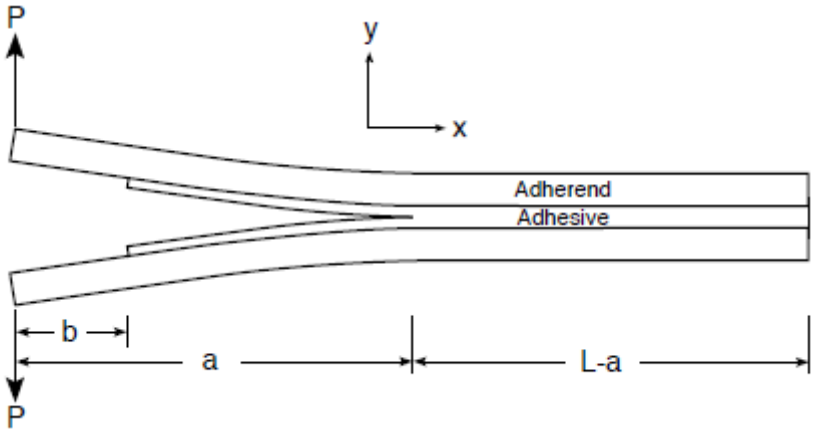

Figure 4-12: schematic presentation of a double cantilever beam specimen used to measure the mode I toughness of adhesive bonds [174].

The scratch test is a test method considered for qualitative evaluation of adhesion as suggested by Perry [175, 176] who studied the adhesion of of TiN and TiC CVD deposited coatings on steel. However, this test method is may be suitable for hard thin coatings (about 2-20 μm).

PART B: MATERIALS AND EXPERIMENTAL PROCEDURE

CHAPTER 5 : MATERIALS AND EXPERIMENTAL PROCEDURE

1. MATERIALS

1.1 SUBSTRATES

Four metallic materials were used as substrates. Their chemical compositions are summarized in Table 5-1.

1. Structural steel **St 52-3** (steel number 1.0570). This steel is often used in civil construction industry.
2. Austenitic chromium-Nickel steel **AISI 304** (steel number 1.4301). The main applications of this material are: marine equipment, nuclear vessels, paper industry, pressure vessels, chemical equipment and textile dyeing equipment. This steel exhibits good corrosion resistance, higher ductility, excellent formability and low carbon content when comparing to St 52-3.
3. Stainless steel **X3CrNiMo13-4** (steel number 1.4313) is mainly used in the heavy mechanical construction component such as water turbine wheel.
4. Titanium alloy **TiAl-16V4** (alloy number 3.7165). This alloy is used for the fabrication of biomedical implants for its good biocompatibility.

Table 5-1: chemical composition of substrates

Substrates	**Limit of chemical composition in wt %**							
St 52-3	**C**	**Si**	**Mn**	**P**	**S**	**Nb**	**Al**	**N**
	0.2	0.15- 0.5	1.6	0.035	0.035	0.02-0.04	0.02	0.009
AISI 304	**C**	**Si**	**Mn**	**P**	**S**	**Cr**	**Fe**	**Ni**
	0.08	1	2	0.045	0.03	18-20	74	8- 10.5
X3CrNiMo13-4	**C**	**Si**	**Mn**	**P**	**S**	**Cr**	**Mo**	**Ni**
	0..05	0.60	1.00	0.035	0.015	12.5 - 14	0.40 - 0.70	3.50 - 4.50
TiAl-16V4	**C**	**Ti**	**Al**	**V**	**O**	**Fe**	**Ni**	
	0.08	Rest	5.5- 6.75	3.5/4.5	0.2	0.4	0.05	

SUBSTRATE PREPARATION BEFORE COATING DEPOSITION

Substrate samples were:

- Degreased with acetone and alcohol with particular attention in handling the samples with gloves to avoid any surface contamination.
- Sand blasted with blocky alumina abrasive particles to produce surface roughness Ra 3 and 6 µm using grits of (F80) 0.150-0.212 mm and F24 with 0.600-0.850 mm diameter, respectively.
- Roughness measurements using an optical profilometer (Alti-Surf 500-Cotec-France) with maximum resolution of 10 nm in z axis, 0.5 µm in x,y lateral axes. The Ra value is averaged from five measurements.

1.2 COATINGS

The following powders have been considered in this work. They represent metallic, ceramic and cermet materials, respectively.

1. **NiCr 80-20** with grain size of 45-90 µm. This coating is widely used to protect the substrate against corrosion
2. **Al_2O_3** 99.5 wt% powder with grain size of 5-25 µm. Such coating is often used to protect the substrate against wear, chemical attack and sometimes as thermal barrier over a very wide range of temperatures.
3. **WC-Co-Cr** (81.1 wt%, C 5.3 wt%, Co 10wt% and Cr 3.6wt %). with the grain size of 20–50 µm. This coating is widely applied in industry as an excellent erosion wear resistant material, in particular, for water turbine blade.

Scanning electron microscopy (SEM) and Powder-shape® system based on a scanner [177, 178] have been used in order to characterize the grain morphology and statistical grain size distribution.

1.3 DEPOSITION PROCESSES

Three processes were used to deposit the powders: i) flame spraying (FS), ii) vacuum plasma spraying (VPS) and iii) high velocity oxy fuel (HVOF) spraying.

1.3.1 FLAME SPRAYING (FS)

Al_2O_3 and Ni-Cr 80-20 were deposited on two substrates: St 52-3 and TiAl-16V4, the parameters of deposition are summarized in Table 5-2.

Table 5-2: Parameters of flame spray process

Coatings	Al_2O_3	Ni-Cr 80-20
Air pressure [bar]	3	3
Acetylene pressure [bar]	0.7	1
O_2 pressure [bar]	4	1.4
Stand-off distance [mm]	150	250
Pre-heating T [°C]	250	375

1.3.2 VACUUM PLASMA SPRAYING (VPS)

Ni-Cr 80-20 was also deposited by VPS to avoid oxidation during deposition and to achieve higher density than that obtained by flame spraying process. The deposition parameters are summarized in Table 5-3.

Table 5-3: Parameters of vacuum plasma spraying process

Parameters	Coating: Ni-Cr 80-20
Stand-off distance [mm]	275
Robot speed [mm/s]	300
Chamber pressure [mbar]	100
Preheating T_s [°C]	280
Gas plasma [l/min]	46 Ar, 6 H_2
Gas powder [l/min]	1 Ar
Courant plasma [A]	750
Tension plasma [V]	54.8
Energy plasma [kW]	43.1
Temperature of deposition T_d [°C]	480

1.3.3 HIGH VELOCITY OXY FUEL (HVOF) SPRAYING

WC-Co-Cr powder was HVOF sprayed on X3-CrNiMo 13-14 stainless steel substrate. Cermet based WC–Co–Cr thermally sprayed coating is considered to be potential wear resistant coating material, since the WC grains are very well bonded to the metallic matrix. The hard WC particles in the coatings lead to high coating hardness and high wear resistance, while the metal binder Co–Cr supplies the necessary coating toughness [179, 180]. The range of HVOF spraying parameters are summarized in Table 5-4 (the exact parameters cannot be communicated because of the confidentiality agreement between EMPA and the industrial partner)

Table 5-4: parameters of high velocity oxy fuel (HVOF) spraying process

Parameters	Coating: WC-Cr-Co
Spray gun	Top-Gun
Kerosene pressure [bar], flow rate [l/h]	21-23, 20-24
O_2 pressure [bar], flow rate [l/min]	20-21, 800-1000
N_2 pressure [bar], flow rate [l/min]	9-10, 15-17
Spraying distance [m]	0.3 - 0.5

The sandwich based cermet coatings (combinations from 26 to 29 in Table 5-5) consists of three layers: i) cermet outer layer, ii) interlayer and ii) cermet inner layer deposited to the steel substrate.

Different interlayers were deposited on the first HVOF sprayed cermet WC-Co-Cr coating, then a cermet coating was sprayed as the upper coating to form the multilayered structure as shown in Figure 5-1. Interlayer coatings such as NiCr 80-20 and Co-Cr were deposited by HVOF on the first cermet coating. Ni layer was electrochemically deposited on the cermet coating at 55 °C using optimized parameters, 1.3 A and 5 V for 7 minutes, to achieve an uniform and continuous coverage of the Ni layer. The thickness of the Ni layer was approximately 60 μm and the cermet coating surface exhibits a Ra = 5 μm of roughness. After having deposited the Ni layer, only the half of the Ni-electroplated samples were grit blasted to achieve a roughness of around Ra ~ 4.5 μm. This is termed as Ni-plating-X (combination 29 in Table 5-5). The other Ni-electroplated samples were not grit blasted (combination 28 in Table 5-5) as shown in the cross section in Figure 5-2. The final layer of the multilayer coating is constituted by cermet and it has been deposited using the spraying conditions shown in Table 5-4.

The justification of such sandwich structure is the following: the outer cermet layer exhibits high hardness to improve abrasion behavior whereas the ductile interlayer is to accommodate the impact shock of particle in erosion. This sandwich has potential improvement in life time of coated tools used in mining, drilling tunnels and grinding as well as in water turbine blades.

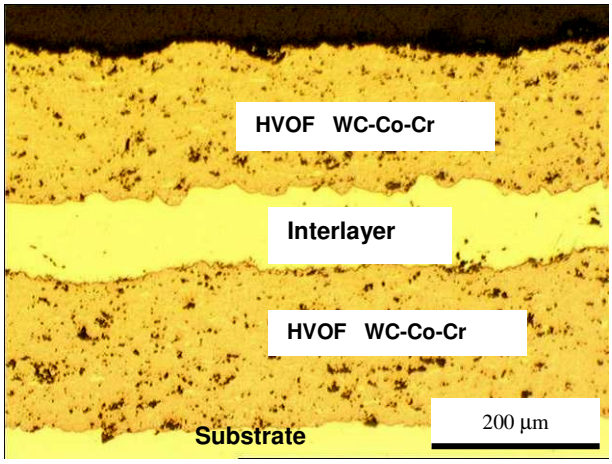

Figure 5-1: an example of sandwich structure based cermet coating.

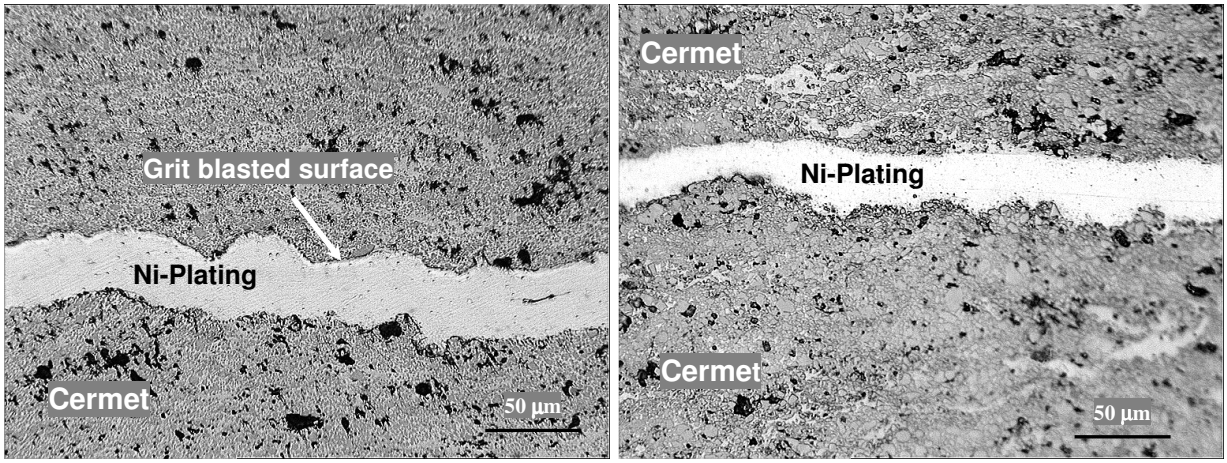

a) *b)*

Figure 5-2: micrographs of Ni-plating within cermet coatings, a) the grit blasted Ni-plating coating (combination 29), b) the Ni-plating coating as deposited without grit blasting (combination 28 in Table 5-5).

1.4 POST ANNEALING OF COATED SAMPLES

In order to investigate the influence of residual stress release on coating adhesion, some of VPS NiCr 80-20 coated samples were annealed in oven up to T_{an}=800°C for 75 minutes and cooled in air to room temperature.

1.5 NOMENCLATURE

The test matrix is divided in three main parts prior to deposition process as shown in Table 5-5, flame sprayed (FS), vacuum plasma sprayed (VPS) and high velocity oxy fuel sprayed (HVOF) coatings. The coating thickness value is

measured by an optical microscope in the cross sectioned samples and was averaged from 5 to 8 measurements. The grey highlighted combinations with nomenclature with the sign (*) stands for the samples annealed at 800°C.

Table 5-5: nomenclature of coating combinations

Process	Coating	Number	Coatings	Substrates	Coating thickness	Interface roughness	Nomenclature
					h_cµm	Ra µm	
FS	NiCr 80-20	1	NiCr 80-20	St 52-2	100 ± 23	3 ± 0.3	N-F-100-3/St
		2	NiCr 80-20	St 52-2	300± 32	3 ± 0.3	N-F-300-3/St
		3	NiCr 80-20	St 52-2	100± 23	6 ± 0.5	N-F-100-6/St
		4	NiCr 80-20	St 52-2	300± 32	6 ± 0.5	N-F-300-6/St
		5	NiCr 80-20	TiAl6V4	100± 23	3 ± 0.3	N-F-100-3/Ti
		6	NiCr 80-20	TiAl6V4	300± 32	3 ± 0.3	N-F-300-3/Ti
		7	NiCr 80-20	TiAl6V4	100± 23	6 ± 0.5	N-F-100-6/Ti
		8	NiCr 80-20	TiAl6V4	300± 32	6 ± 0.5	N-F-300-6/Ti
	Al_2O_3	9	Al_2O_3	St 52-2	100± 23	3 ± 0.3	Al-F-100-3/St
		10	Al_2O_3	St 52-2	300± 32	3 ± 0.3	Al-F-300-3/St
		11	Al_2O_3	St 52-2	100± 23	6 ± 0.5	Al-F-100-6/St
		12	Al_2O_3	St 52-2	300± 32	6 ± 0.5	Al-F-300-6/St
		13	Al_2O_3	TiAl6V4	100± 23	3 ± 0.3	Al-F-100-3/Ti
		14	Al_2O_3	TiAl6V4	300± 32	3 ± 0.3	Al-F-300-3/Ti
		15	Al_2O_3	TiAl6V4	100± 23	6 ± 0.5	Al-F-100-6/Ti
		16	Al_2O_3	TiAl6V4	300± 32	6 ± 0.5	Al-F-300-6/Ti
VPS	NiCr 80-20	17	NiCr 80-20	AISI 304	100± 21	3 ± 0.2	N-V-100-3/SS
		18	NiCr 80-20	AISI 304	100± 21	3 ± 0.2	N-V-100-3/SS*
		19	NiCr 80-20	AISI 304	300± 26	3 ± 0.3	N-V-300-3/SS
		20	NiCr 80-20	AISI 304	300± 26	3 ± 0.3	N-V-300-3/SS*
		21	NiCr 80-20	AISI 304	100± 21	6 ± 0.3	N-V-100-6/SS
		22	NiCr 80-20	AISI 304	100± 21	6 ± 0.3	N-V-100-6/SS*
		23	NiCr 80-20	AISI 304	300± 26	6 ± 0.3	N-V-300-6/SS
		24	NiCr 80-20	AISI 304	300± 26	6 ± 0.3	N-V-300-6/SS*
HVOF	Sandwich	25	WC-Co-Cr	X3CrNiMo13-4	500± 30	5 ± 0.6	Cer / steel
		26	WC-Co-Cr	NiCr 80-20	220± 20	5 ± 0.8	Cer /NiCr/ Cer
		27	WC-Co-Cr	CoCr	220± 20	5 ± 0.8	Cer /CoCr/ Cer
		28	WC-Co-Cr	Ni plating	220± 20	4.5 ± 0.5	Cer /Ni pl/ Cer
		29	WC-Co-Cr	Ni plating-X	220 ± 20	1 ± 0.1	Cer /Ni pl- x/ Cer

1.6 PHYSICAL PROPERTIES OF MATERIALS

The physical properties of coatings and substrates are presented in Table 5-6. Their hardness *Hv*, Young's modulus *E*, ultimate tensile strength (U.T.S) and yield strength (Y.S) have been measured by one of the two following methods; i) low-load indentation techniques [181, 182], ii) standard tensile tests according to ISO 6892 [183]. The hardness values were averaged from 10 measurements. The porosity of each coating was determined via image analysis by SEM. Assuming that resolution limits are considered, porosity within a microstructure can be easily detected by image analysis due to the high degree of contrast between the dark pores (voids) and the reflective coating material. Work by Fowler et al [184, 185] has shown that image analysis can reproducibly detect and measure microstructural features (pores, cracks, etc.) in thermal spray coatings. The reliability of these methods for specific experiments and metallographic conditions was statistically tested to give a 95% confidence level. The coefficient of thermal expansion (CTE) and ν Poisson ratio were taken from literature [186-189].

Table 5-6: physical properties of substrates and coatings

Materials	E GPa	Hv 0.1	ν	Porosity %	CTE µm/mK	Y.S MPa	U.T.S MPa
St 52-3	214	138 ± 16	0.3		12	471	568
AISI 304	202	248 ± 6	0.29		17.2	740	834
AISI 304/annealed	192	204 ± 7	0.29		17.2	537	716
X3CrNiMo13-4	210	260 ± 28	0.29		10.9	673	864
TiAl-16V4	151	354 ± 23	0.34		8.6	865	1034
NiCr 80-20 (FS)	98	195 ± 30	0.28	6.8	13		
NiCr 80-20 (VPS)	187	293 ± 13	0.26	4.2	12.5		
NiCr 80-20 (VPS) *	142	251 ±16	0.26	4	12.5		
Al_2O_3(FS)	49.5	286 ± 41	0.25	7	5.4		
WC-Co-Cr (HVOF)	266	1432 ± 141	0.26	2.1	5.8		
NiCr 80-20 (HVOF)	100	387 ± 42	0.29	3.2			
CoCr (HVOF)	144	697 ± 63	0.3	4.8			
Ni plating	243	516 ± 31	0.31	0.2			

** denoted for annealed samples*

1.7 MORPHOLOGY OF COATINGS

The morphology of each coating is shown in Figure 5-3. Flame sprayed NiCr 80-20 shows pronounced oxide layers between the splats and high porosity content, whereas the same coating deposited by VPS, is quasi oxide-free between the splats and has less porosity. Oxide interfaces between splats can be seen for the HVOF sprayed NiCr 80-20 with very low porosity.

Regarding the morphology of CoCr, some non-molten particles and very important oxide layers between splats can be seen. Distribution of WC phase can be seen in dark grey in the WC-Co-Cr coating. Investigation on the relation between microstructure features and wear mechanisms of materials subjected to solid particle erosion was previously reported by Hadad [190, 191] .

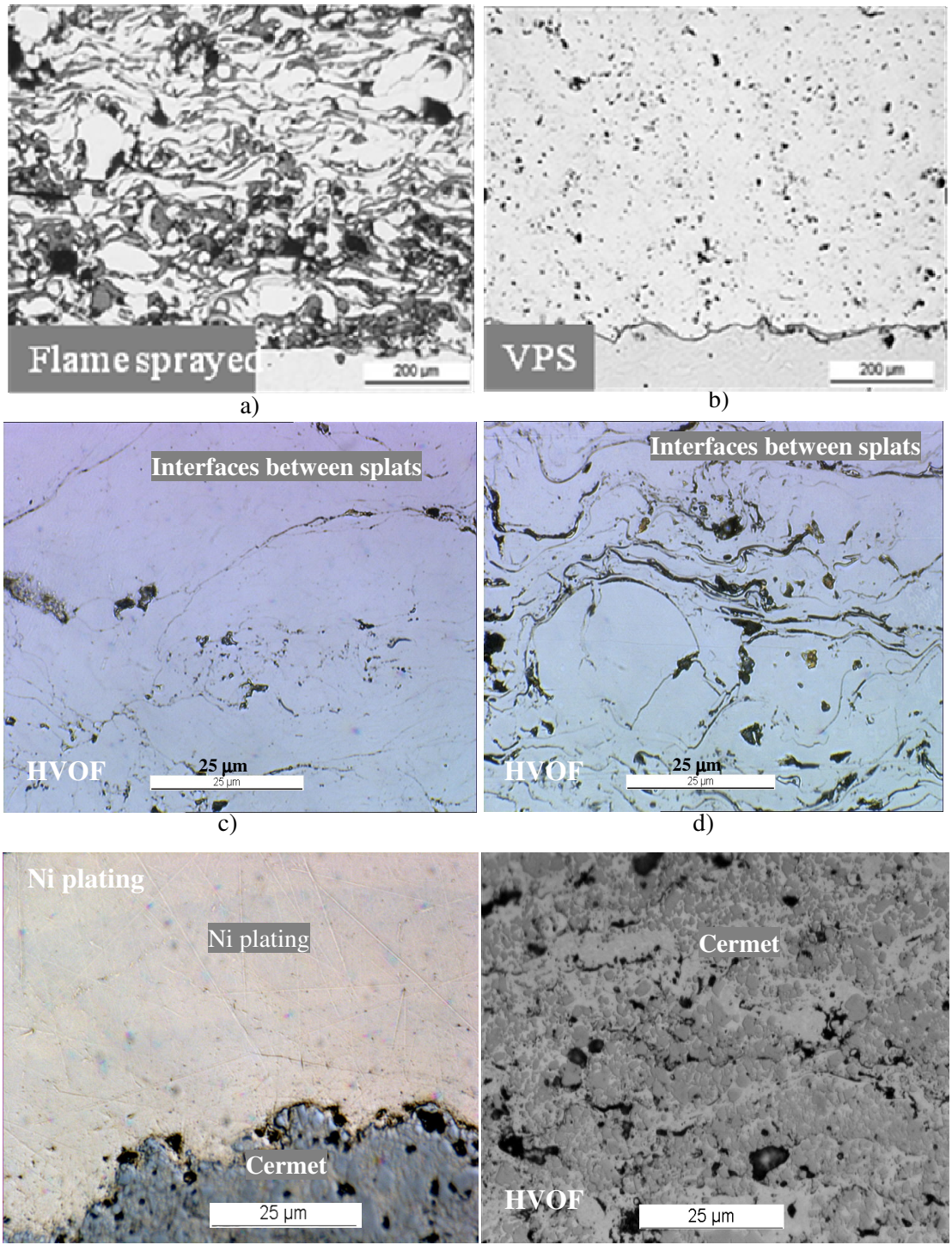

Figure 5-3, a) micrograph of FS NiCr 80-20, b) micrograph of VPS NiCr 80-20, c) micrograph of HVOF NiCr 80-20 sprayed as intermediate layer, d) micrograph of HVOF CoCr intermediate layer, e) micrograph of Ni plating morphology, e) HVOF WC-Co-Cr coating morphology.

2. EXPERIMENTAL PROCEDURE FOR RESIDUAL STRESS MEASUREMENTS

2.1 CURVATURE BENDING TEST

The dimensions of the testing samples were 150x40x8 mm. The profile length was 75 mm measured by mechanical profilometer UBM (Figure 5-4) with an acquisition rate of 20 measured points per 1 mm. The samples were measured in four steps;

i) substrate as received,
ii) grit blasted substrate,
iii) after spraying,
iv) after annealing at 800°C.

The residual stress was determined using different theoretical approaches. In all approaches, the deflection of samples *f* was calculated directly from the acquired data from the profilometer. Therefore, an arc radius configuration was assumed to calculate the curvature [192] :

$$r = \frac{1}{\kappa} = \frac{f}{2} + \frac{L_m^2}{8 \cdot f} \qquad 5\text{-}1$$

If the coating is in compression, the convex configuration can be observed, and if the coating is in tensile stress, a concave behavior will be observed (Figure 5-5). Other assumption is that the stress in z axes is negligible.

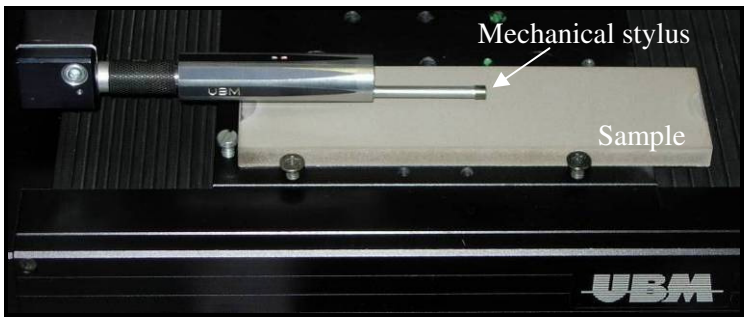

Figure 5-4: Mechanical profilometer UBM.

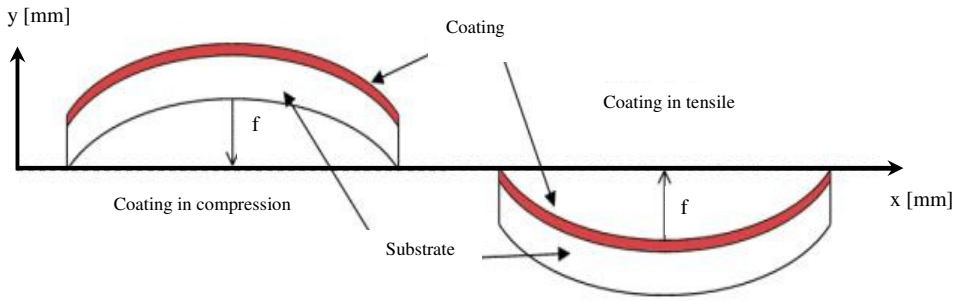

Figure 5-5 : Curvature configuration, convex and concave according to compression or traction stresses.

In chapter 3, different approaches were advanced for residual stress measurement based on curvature tests e.g. Stony, Clyne, Chiu and Godoy theories. Clyne and Godoy approach [125, 193] have been found attractive since the Godoy model calculates the average in-plane stress at the interface in the coating and residual stress at the interface in the substrate which is expressed in 5-2 to 5-5. Whereas, Clyne model provides an analytical solution for through coating thickness as described in chapter 3.

$$\sigma_c(y=0) = -\Delta\varepsilon \cdot \frac{E_c' h_s E_s'}{h_c E_c' + h_s E_s'} - E_c' \kappa \delta \qquad 5\text{-}2$$

$$\sigma_c(y=h_c) = -\Delta\varepsilon \cdot \frac{E_c' h_s E_s'}{h_c E_c' + h_s E_s'} + E_c' \kappa (h_c - \delta) \qquad 5\text{-}3$$

$$\sigma_{res}(y=-hs) = -\Delta\varepsilon \cdot \frac{E_c' h_s E_s'}{h_c E_c' + h_s E_s'} - E_c' \kappa (h_s - \delta) \qquad 5\text{-}4$$

$$\sigma_s(y=0) = \Delta\varepsilon \cdot \frac{E_c' h_c E_s'}{h_c E_c' + h_s E_s'} - E_s' \kappa \delta \qquad 5\text{-}5$$

$$\sigma_{Godoy} = \frac{\sigma_c(y=0) + \sigma_s(y=0)}{2} \qquad 5\text{-}6$$

$$\text{Where } \delta = \frac{h_c^2 E_c - h_s^2 E_s}{2(h_c E_c - h_s E_s)} \qquad 5\text{-}7$$

2.2 INCREMENTAL HOLE DRILLING TEST

This measurement technique consists of two stages:

1. Removal of the stressed material by drilling a small hole on the surface coating till substrate.
2. Measurement of the relaxation strains occurring around the hole by means of an extensometric rosette.

We used a HBM- RY 61 Drill-Hole Rosette illustrated in Figure 5-6 is fitted with a drilling bush which, together with an auxiliary device, ensures correct centring of the drill.

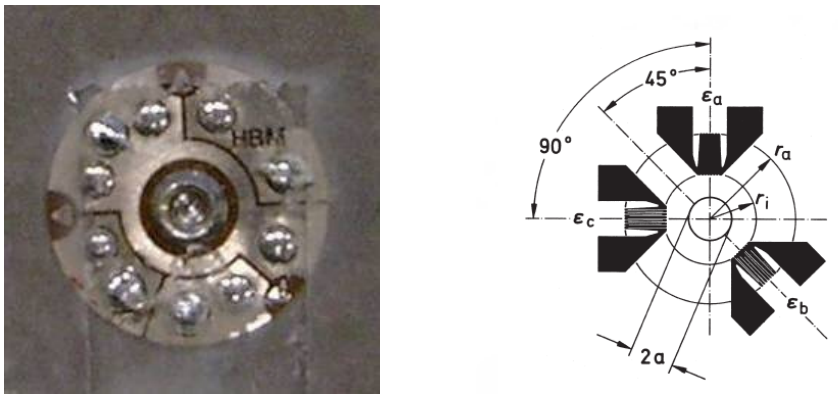

a) b)

Figure 5-6: a) drill- hole Rosette, b) configuration of RY 61 drill-hole Rosette.

The drilling kit was borrowed from HBM. The operating parameters of hole drilling are summarized in Table 5-7. The strain gauges were connected to the data acquisition system in Wheatstone half-bridge. Surface preparation has crucial importance in strain gauging, because it influences the quality of the adhesion between the test specimen and the strain gauge. The surface preparation was performed as the following:

i. surface degreasing using "HBM" cleaning solution, which is basically a mixture of acetone and isopropanol,
ii. manual abrasion of the specimen surface with abrasive paper N° 400 to reach a roughness value of Ra ~ 3 µm,
iii. cleaning with ethanol to remove the dust originated by the abrasion process,
iv. degreasing using "HBM" cleaning solution to assure a total removal of all the possible debris that may remain on the specimen surface.

The strain gauge is finally glued using "HBM X60" as an acrylic based adhesive. The ambient temperature was around 22 °C and the relative humidity was around 60%.

Table 5-7: Parameters of operating incremental hole drilling

Parameters	**Value**
Drill diameter d_0 [mm]	1.5
Rotational speed of drill [t/min]	2'800
Type of gauge	HBM 1-RY61-1.5/120
Number of incremental steps en z-axe (for h_c = 100 [µm])	10
Number of incremental steps en z-axe (for h_c = 300 [µm])	30

A comprehensive description of the method and the formulae for evaluation of the measurement results made in the 0°/45°/90° directions are given in the ref [194-196]. Amongst these, Hoffmann has used the same HBM- RY 61 Drill-Hole Rosette.

Once the microdeformations are measured for the three gauges a, b and c, one can determine the principle directions. The principle direction 1 makes an angle φ (equation 5-8) with the trigonometric direction prior to a, the principle direction 2 makes an angle of 90° with the principle direction 1.

Table 5-8 shows the principle of φ calculation between the principle axe and a direction of the rosette.

$$\varphi = \frac{1}{2}\arctan\left(\frac{\varepsilon_{in}^{a} + \varepsilon_{in}^{c} - 2\varepsilon_{in}^{b}}{\varepsilon_{in}^{c} - \varepsilon_{in}^{a}}\right) \qquad 5\text{-}8$$

Table 5-8: calculated φ between the principle axe and a direction of the rosett

Nominator	≥ 0	> 0	≤ 0	< 0
Denominator	> 0	≤ 0	< 0	≥ 0
φ	$\frac{1}{2}\arctan(\frac{nom}{denom})$	$\frac{\pi}{2} - \frac{1}{2}\arctan(\frac{nom}{denom})$	$\frac{\pi}{2} + \frac{1}{2}\arctan(\frac{nom}{denom})$	$\pi - \frac{1}{2}\arctan(\frac{nom}{denom})$
	$0 \leq \varphi < 45°$	$45° \leq \varphi < 90°$	$90° \leq \varphi < 135°$	$135° \leq \varphi < 180°$

When a strain gauge is bonded to the sample surface and a small hole is carefully drilled, a certain amount of deformation will occur as a result of removal of residual stress that initially existed in the specimen. Therefore, each measured

incremental strain change is the result not only of stresses in the drilled increment but are also influenced by stresses in previously drilled increments. In other word, the residual stress calculated release is $\sigma_{res}+\Delta\sigma_{res}$ where $\Delta\sigma_{res} = E.\ \Delta\varepsilon_{res}$. So that, it is of primary importance that the numerical values of the hole drilling calibration constants k_1 and k_2 should accurately represent the mechanics of the hole drilling process. The fundamental equation describing the relationship between the released strains measured during hole drilling and the underlying residual stresses has been established based on the principles of superposition of strain states [197-199].

$$\frac{d\varepsilon}{dz} = \frac{1}{E} K(z).\sigma(z) \qquad 5\text{-}9$$

The nominal measured strain ε_m can be calibrated in correlating them to K_1 and K_2 as the following [200]:

$$\Delta\varepsilon_{in}^{a} = K_1(z).\varepsilon_{m,a} + K_2(z).\upsilon.\varepsilon_{m,c} \qquad 5\text{-}10$$

$$\Delta\varepsilon_{in}^{b} = K_1(z).\varepsilon_{m,b} - K_2(z).\upsilon.\left[\varepsilon_{m,c} + \varepsilon_{m,a} - \varepsilon_{m,b}\right] \qquad 5\text{-}11$$

$$\Delta\varepsilon_{in}^{c} = K_1(z).\varepsilon_{m,c} - K_2(z).\upsilon.\varepsilon_{m,a} \qquad 5\text{-}12$$

Two-dimensional system here is considered, since the stress normal to a free surface can be neglected. It is possible to calculate the magnitude and direction of the maximum residual stress in the component by combining the principal residual stresses σ_1 and σ_2. The calculation is based on the experimental strain measured at each n^{th} increment of depth, ε^{a}_{in}, ε^{b}_{in} and ε^{c}_{in} and calibration coefficients K_1 and K_2.

The change in the hole geometry must also be taken into account. Each previously removed layer affects the total strain measured on the surface. So the strain measured on the surface due to the removed layer is expressed as follows [201, 202]

$\varepsilon_n{}^{j} = \varepsilon_{m,n}{}^{j} - \sum_{i=1}^{i=n-1} \varepsilon_{in}{}^{1}$ where j=a,b and c shown in Figure 5-6.

For example:

$$\varepsilon_3^a = \varepsilon_{m,3}{}^{a} - \sum_{i=1}^{2} \varepsilon_{i,3}^{a} = \varepsilon_{m,3}{}^{a} - (\Delta\varepsilon_{1,3}^{a} + \Delta\varepsilon_{2,3}^{a})$$

where ε^{j}_{mn} is the total strain measured on the surface when removing the n^{th} increment. ε^{j}_{in} corresponds to the part of the total strain related to layer *i* when the n^{th} increment is removed. The schematic drawing of the drilling process is shown in Figure 5-7.

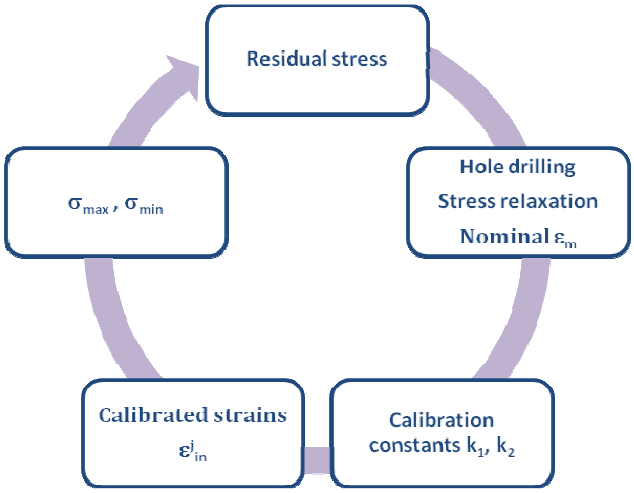

Figure 5-7: processing scheme for residual stress determination using the hole drilling method.

Once the strains ε^{a}_{in} , ε^{b}_{in} and ε^{c}_{in} are calibrated, the final principal stresses σ_{max} and σ_{min} are calculated according to the specifications of the Rosette HBM [196]

$$\sigma_{\max,\min} = -\frac{E_c}{4A}(\varepsilon^a_{in} + \varepsilon^b_{in}) \pm \frac{E_c}{4B}\sqrt{(\varepsilon^a_{in} + \varepsilon^c_{in} - 2\varepsilon^b_{in})^2 + (\varepsilon c^a_{in} - \varepsilon^a_{in})^2} \qquad 5\text{-}13$$

Where A and B are dimensionless calibration constants depending on the diameter and depth of the hole.

$$A = \frac{a^2.(1+\nu)}{2.r_a.r_i} \qquad B = \frac{2.a^2}{r_a.r_i}.\left[1 - \frac{a^2.(1+\nu).(r_a^2 + r_a.r_1 + r_i^2)}{2.r_a.r_i}\right] \qquad 5\text{-}14$$

ν = Poisson's ratio for the measurement object material,

r_a = external radius of the measurement grid,

r_i = internal radius of the measurement grid,

a = radius of the drill hole.

The directions of the principal stresses must be determined according to the schema given in section for the 0°/45°/90 ° rosettes.

Replacing the dimensional values of this specific rosette (RY 61) in (5-13): r_o=3.3 mm, r_i = 1.8 mm and a = 0.75 mm:

$$\sigma_{\max,\,\min} = \frac{-E_c \cdot (\varepsilon_{in}^a + \varepsilon_{in}^b)}{0{,}1894(1+\nu_c)} \pm \frac{-E_c \cdot \sqrt{(\varepsilon_{in}^a + \varepsilon_{in}^c - 2\varepsilon_{in}^b)^2 + (\varepsilon c_{in}^a - \varepsilon_{in}^a)^2}}{0{,}7576 - 0{,}0606 \cdot (1+\nu_c)} \qquad 5\text{-}15$$

The model used to determine the residual stress distribution is based on the hypotheses indicated below:

i. the stress determined is homogeneous in the removed layer,
ii. the material is elastic, isotropic and linear,
iii. the normal stress is negligible,
iv. the rosette geometry is perfect,
v. the residual stress determined is less than the elastic limit of the material,
vi. all displacements are continuous at the interface between the coating and the substrate.

The absolute equivalent stress can be determined using Von Mises equation:

$$\sigma_{VonMises} = \sqrt{\sigma_{\max}^2 + \sigma_{\min}^2 - \sigma_{\max}\sigma_{\min}} \qquad 5\text{-}16$$

2.3 RESIDUAL STRESS BY INTERFACIAL INDENTATION

The interfacial indentation test allows determining the residual stress in the coating. However, to avoid any misleading, the residual stress model will be introduced in (section 3.2) after introducing the indentation method.

3. EXPERIMENTAL PROCEDURE FOR ADHESION MEASUREMENTS

3.1 TENSILE ADHESION TEST (EN 582)

Testing samples of 25 mm diameter were joined with the cylindrical counter parts according to the standard test EN 582 [132] using an adhesive agent. The tensile load was applied with the Universal Epprecht-Multitest tensile machine. The mean adhesive strength values were avaraged from three to five tests performed under the same conditions and one as a blind test without coating in order to calculate the adhesive strength of the glue. The tensile adhesive strength was calculated by:

$$\sigma_{max} = F/A \qquad 5\text{-}17$$

Where F is the maximum load at rupture and A is the normal section of sample. The sample geometry is shown in Figure 5-8.

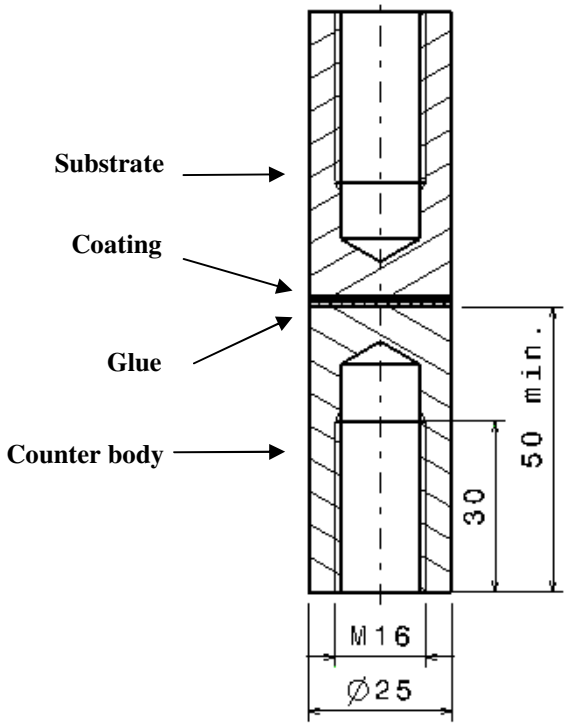

Figure 5-8: Schematic presentation of tensile adhesion test according the standard configuration EN 582 [132].

3.2 INTERFACE INDENTATION TEST

Coated samples were cross sectioned to have 40 mm width and 30 mm length as shown in Figure 5-9-a and polished up to 1 µm grit size. A conventional pyramidal Vickers micro indenter (Leitz Wetzler- Germany) with the angle of two opposite faces of 136° ± 0,3° with integrated optical microscope was used. The load at interface was maintained constant at least for 30 seconds in order to avoid the dynamic indentation. The lengths of diagonal imprint *d* and crack *a* were optically measured (100x of magnification) as shown in Figure 5-9-b.

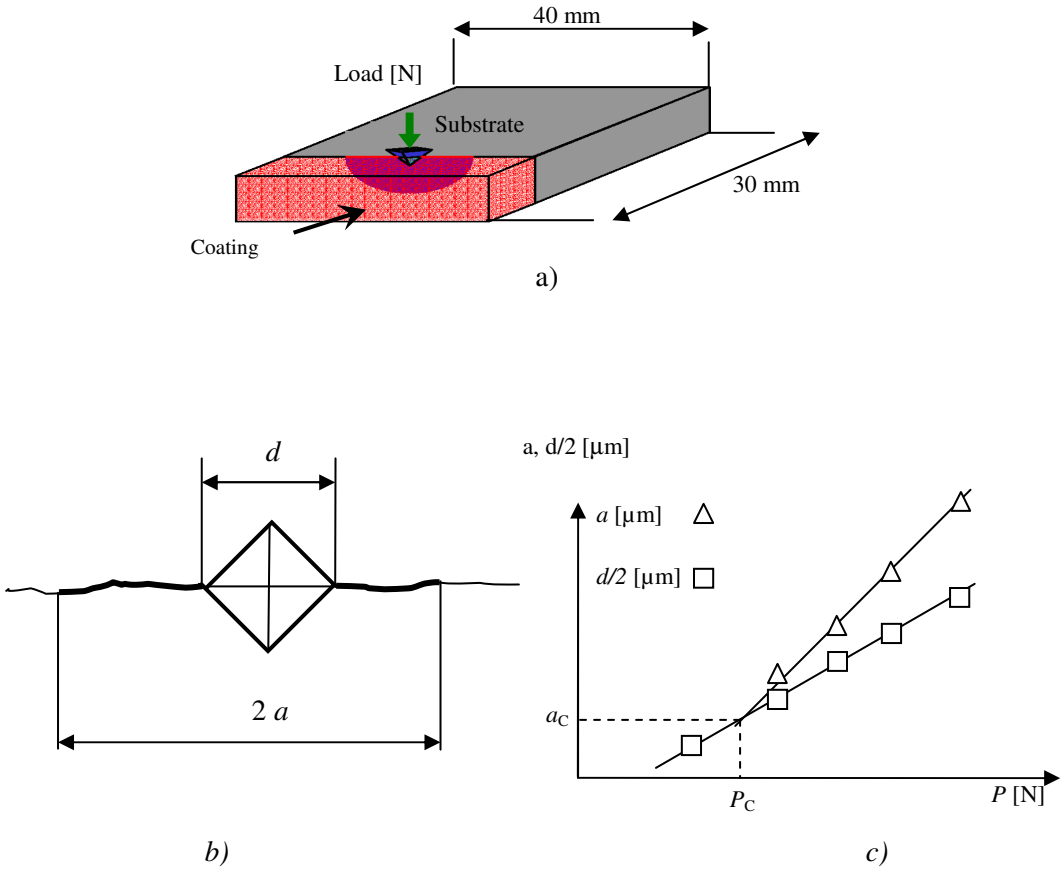

Figure 5-9: a) schematic 3D presentation of interface indentation on the cross section, b) crack measuring and diagonal hardness at the interface, c) bilogarithmic plot of two segments, diagonal of hardness and crack length.

The measured diagonals of the indent and associated crack length values can be plotted in a bilogarithmic diagram versus the indentation load. The two straight lines associated to these two measurements segments cross at the critical point (P_c, a_c) as shown in Figure 5-9-c. This point is very important since it represents

the resistance to crack initiation at the interface, i.e. a parameter related to the resistance to cracking of the interface. Knowing the critical point, the interface toughness can be calculated by the model proposed by Chicot and Lesage [145, 203-205] in the following equations:

$$K_{\mathrm{ca}} = 0{,}015\,\frac{P_{\mathrm{c}}}{a_{\mathrm{c}}^{3/2}} \cdot \left(\frac{E}{H}\right)_{\mathrm{I}}^{1/2} \qquad \textit{5-18}$$

Where the ratio $(E/H)_I$ representing the properties of the materials each part of the interface is given by the following equation:

$$\left(\frac{E}{H}\right)_{\mathrm{I}}^{1/2} = \frac{\left(\frac{E}{H}\right)_{\mathrm{S}}^{1/2}}{1+\left(\frac{H_{\mathrm{S}}}{H_{\mathrm{R}}}\right)^{1/2}} + \frac{\left(\frac{E}{H}\right)_{\mathrm{R}}^{1/2}}{1+\left(\frac{H_{\mathrm{R}}}{H_{\mathrm{S}}}\right)^{1/2}} \qquad \textit{5-19}$$

This method implies statistical calculation of cracks length induced by indentation. For example, the plot to determine the critical point contains averagely 10 to 15 points; each point is usually obtained from 6 to 10 indentation measurements.

Lesage and Chicot [97, 206] have shown that coating thickness has a large influence on interface toughness results. The residual stress effect on interface toughness is represented by a parameter *f*. This parameter is a function of the residual stress intensity and interfacial crack lengths. This influence can be expressed by:

$$K_{ca} = K_{ca0} + \frac{f(\sigma(h), a(h))}{t^2} \qquad \textit{5-20}$$

where K_{ca} is the interface toughness, K_{ca0} is the extrapolated toughness for an infinite thickness where the residual stresses are negligible as shown in

Figure 5-10, h is the coating thickness, $f[\sigma(h), a(h)]$ is a parameter depending on residual stresses and interfacial crack length. Lascar works [207], Lesage and Chicot [97, 206] define the hypothesis that the interface zone behaves as a brittle bulk material.

$$K_{ca} = K_{ca0} + \frac{2}{\sqrt{\pi}}.\sigma_{res}.\sqrt{a_{ca0}} \qquad \textit{5-21}$$

where σ_{res} is the residual stress intensity, $2 / \pi^{1/2}$ is a coefficient associated to the Vickers indent, and a_{ca0} is determined with the following system:

$$K_{ca0} = 0.015 \frac{P_{c0}}{a_{c0}^{3/2}} \cdot \left(\frac{E}{H} \right)_i^{1/2} \quad \text{(extrapolated value)} \qquad 5\text{-}22$$

$$\log(a_{ca0}) = \alpha + \beta . \log(P_{ca0}) \quad \text{(apparent hardness segment)} \qquad 5\text{-}23$$

Finally, from the precedents equations, the residual stress can be expressed by:

$$\sigma_{res} = \frac{(K_{ca} - K_{ca0}) * \sqrt{\pi}}{2.\sqrt{a_{ca0}}} \qquad 5\text{-}24$$

The σ_{res} of equation 5-24 can be calculated without any knowledge of how could be the intensity and repartition of the stress.

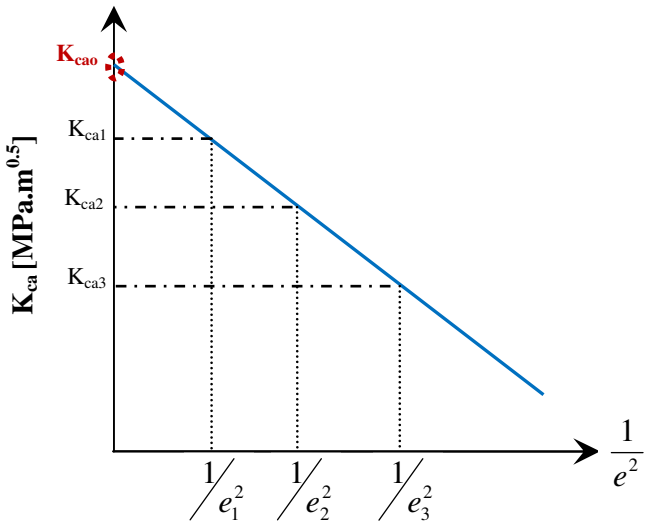

Figure 5-10: extrapolating K_{cao} from infinite thickness of coatings

3.3 IN-PLANE TENSILE TEST

The tensile tests were carried out on a micro-tensile stage (Kammrath & Weiss GmbH, Dortmund, Germany) which has been inserted under the light microscope (this can also be used inside a SEM). The whole geometry were defined according to the standard tests of ISO 6892 [183] as shown in Figure 5-11. Videos of the specimen surface were captured during tensile testing from frontal and upper sides. This was done on 1 to 24 in Table 5-5 samples, coated with one side and loaded along its longitudinal axis. The displacement rate was 64 µm/s

measured using an extensometer. The span of displacement measured was 20 mm. The Young modulus, yield strength and ultimate tensile strength were calculated from σ–ε curve with these tensile experiments.

Each combination of FS samples was tested only once, whereas, each combination of VPS samples was tested 3 times. Particular attention was paid to the evaluation of adhesion in this section. The theoretical approach will be discussed in details in chapter 7.

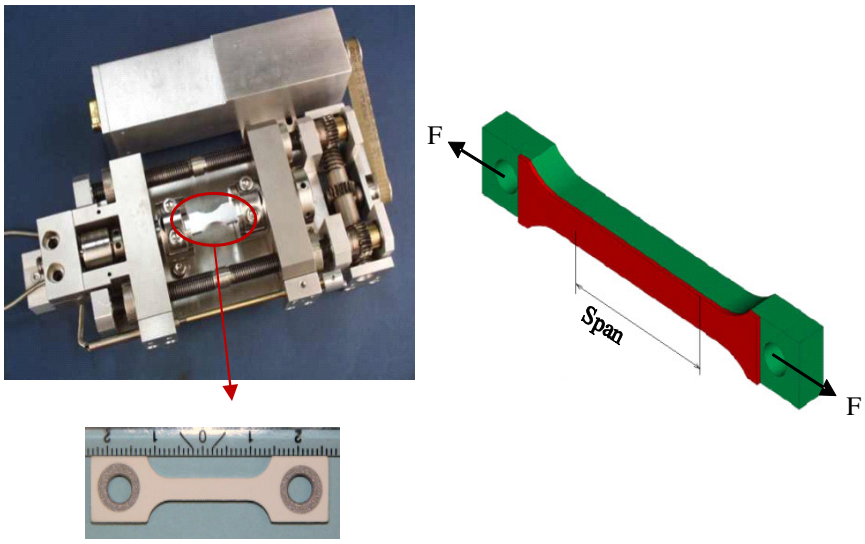

a) *b)*

Figure 5-11: a) micro-tensile stage (Kammrath & Weiss GmbH, Dortmund, Germany, b) sample configuration according to ISO 6892 [183] with one plane side coating.

3.4 ROCKWELL-C INDENTATION AND FINITE ELEMENTS SIMULATION

3.4.1 PRINCIPLE AND MEASUREMENTS

The method to determine the interface toughness has been proposed by Drory [136] for thin film deposited on a ductile substrate. This method has many advantages: i) low cost, ii) current widespread use in metallurgical laboratories.

The coated samples are placed in a Rockwell hardness tester using a conic brale C-indenter of 120° with a tip radius of 200 µm. 250 Kg of load (upper force limit of experimental setup) have been used as a method for assessing the adhesion of coating on ductile substrates. This requires the measurement of the radius of the

residual impression of the indented substrate and the coating delamination radius *D/d* or *R/a* as shown in Figure 5-12- a & b. A 3D topographic micrograph of a Rockwell-C indentation through the coating of Al_2O_3 on the substrate of TiAl6V4 is shown in Figure 5-12-c. *D* and *d* both values have been measured by an optical profilometer.

The indenter creates free edges in the coating at the radius *a* where it contacts the coating. From this edge, where the coating experiences the highest induced stresses, an interfacial crack between the coating and the substrate may be initiated, spreading outward radially to the point where the energy release rate available to drive the crack drops below the interface toughness. The interfacial delamination of the Al_2O_3 coating on the Ti alloy substrate is shown for example in Figure 5-12-c is accompanied by delamination and breaking-up the coating at a distance *R* to leave a narrow annular part of coating behind the interface crack tip. The coating in the example is well adherent and is partially detached around the indentation. The radius of the delamination around the hole stops growing as soon as the total strain energy in the layer locally equals the effective adhesion energy. The delamination radius is thus a measure of the adhesion. The deformation field around the indentation in the pure substrate can be simulated by finite elements modelling assuming the coating thickness is negligible to the indentation depth [5, 16, 136].

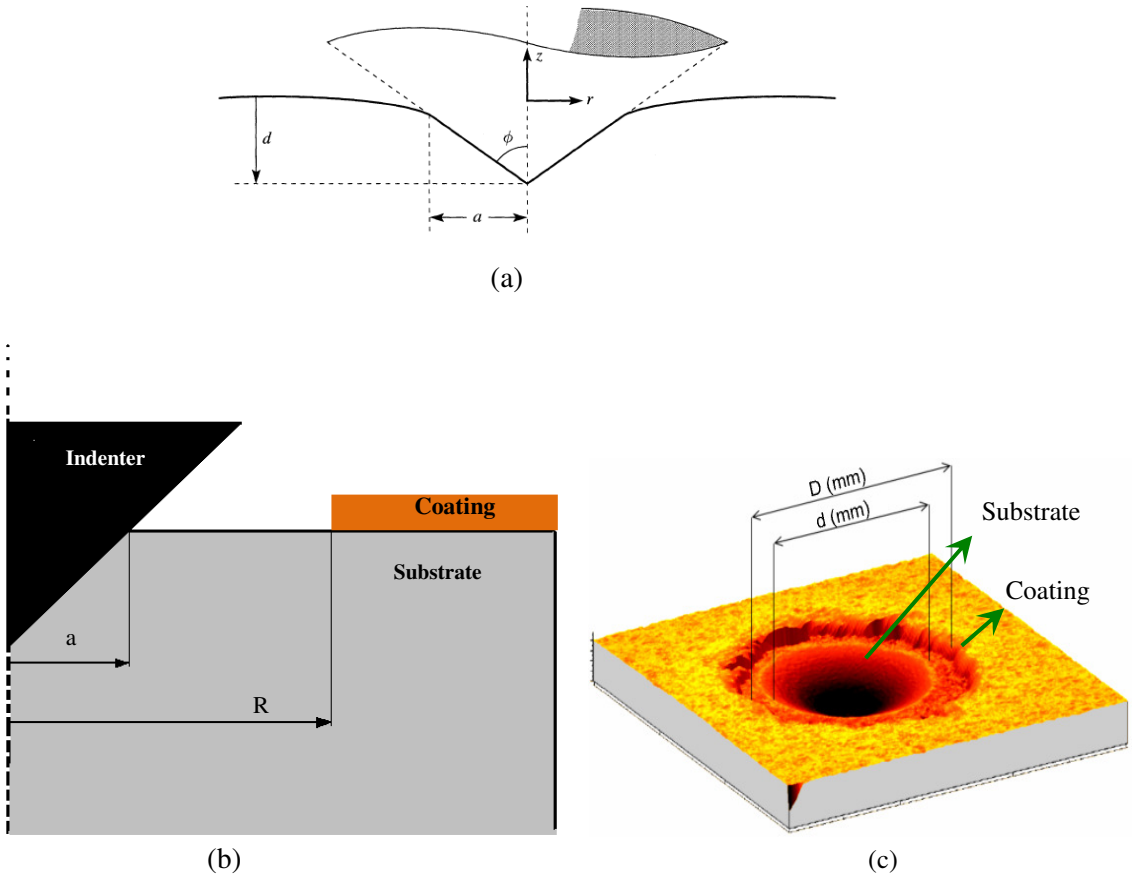

Figure 5-12,a) axisymmetric geometry of indentation experiment for mechanics analysis [136], b) schematic presentation of delamination radii R/a in the model, c) a topographic macrograph of the indentation and delamination.

3.4.2 NUMERICAL MODELLING BY FINITE ELEMENTS ANALYSIS

In this work, a finite element model has been established to simulate the indentation including effect which was not treated by Drory like friction coefficient of the indenter against the coating. The model contains a numerical simulation of the indentation combined with fracture mechanics analysis of the crack propagation at interface to allow the determination of interface toughness.

The axisymmetric model consists of 3270 fully integrated elements. Ideal elastic–plastic material behaviour for the substrates has been assumed. The finite elements mesh used is shown in Figure 5-13 with the assumption that the indenter is infinitely stiff. The displayed radial strain decreases at the surface with increasing distance from the indentation. The model takes into account several non-linearities like large deformations, plasticity and mechanical contact and

therefore a calculation takes several hours. Furthermore, 0.1 of frictional behaviour between indenter and counter-body has been assumed.

This model may suit mainly brittle coatings [208]. However, metallic and ceramic flame sprayed coatings samples were tested. Based on the model of Drory and Hutchinson [136], the radial stress, released rate energy and interface toughness can be calculated as the following:

$$\sigma_{rr,c} = \frac{E_C}{1-\upsilon^2_C}.((\varepsilon_{\mathrm{rr,sub}}(r)+\varepsilon_{\mathrm{res}})+\upsilon_C.(\varepsilon_{\varphi\varphi,\mathrm{sub}}(r)+\varepsilon_{\mathrm{res}})) \qquad 5\text{-}25$$

Where the residual strain is given by:

$$\varepsilon_{\mathrm{res}} = \frac{1-\upsilon_C}{E_C}\sigma_{res} \qquad 5\text{-}26$$

where $\sigma_{rr,\,c}$ is the radial stress generated by the indentation in the coating, from this stress components, the critical strain energy release rate G_c and the interface fracture toughness K_{IC} can be calculated [136, 208, 209]:

$$\mathrm{G_C} = \frac{(1-\nu_C^2).h_C}{2.E_C}.\sigma_{rr}(R)^2 \qquad 5\text{-}27$$

$$\mathrm{k_{IC}} = \sqrt{\frac{\mathrm{E_C}.\mathrm{G_C}}{(1-\upsilon_C{}^2)}} \qquad 5\text{-}28$$

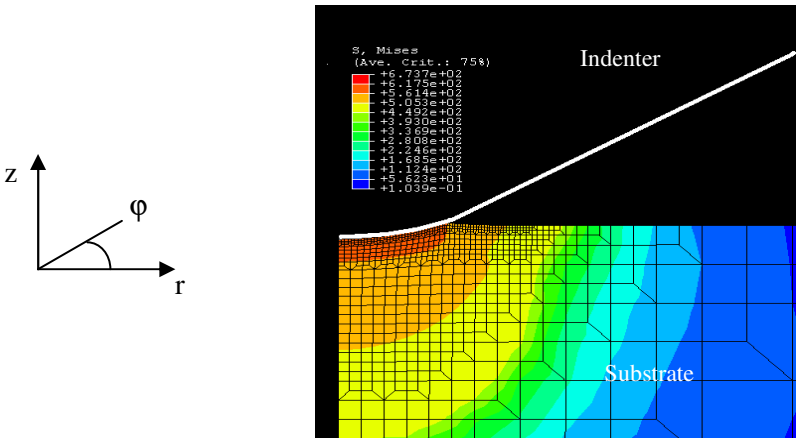

Figure 5-13: axisymmetric simulation by Abaqus in loading mode.

The boundary conditions such as the elasticity and plasticity of materials were acquired from the σ–ε curve obtained from the previous performed standard tensile test ISO 6892 [183] taking into account the true stress and true strain which are calculated from the following equations [210]:

$$\sigma_{True} = \sigma_{Nom}.(1+\varepsilon_{Nom}) \qquad 5\text{-}29$$

$$\varepsilon_{True} = Ln(1+\varepsilon_{Nom}) \qquad 5\text{-}30$$

4. SUMMARY

This chapter is a detailed account of the experimental procedures and protocol followed during the investigation. To start with, the substrate and powder materials have been introduced and the processes used to deposit the coatings have been stated. This is followed by an elaborate description of the strain measurement procedures to determine the residual stress using various approaches like curvature bending, hole drilling and interfacial indentation methods. However, to evaluate adhesion, pull-off, in-plane tensile, interfacial indentation and Rockwell indentation methods were described. Finally, the computational procedure to estimate stain and stress has been stated.

PART C: RESULTS AND DISCUSSION

CHAPTER 6 : RESULTS OF RESIDUAL STRESS

1. RESULTS OF CURVATURE BENDING TESTS

The average in-plane residual stress at the interface of a coating and its substrate was determined based on the beam theory using two approaches:

- Clyne [193] who developed an analytical solution for the stress induced through the whole coating section. Table 6-1 and Figure 6-1 show some results of residual stress distribution based on curvature bending.
- Godoy [125] whose methodology allows the estimation of the stress at and near the interface which is our zone of interest. Figure 6-2 shows the residual stress calculated for the as sprayed and annealed VPS NiCr-80-20 coatings.

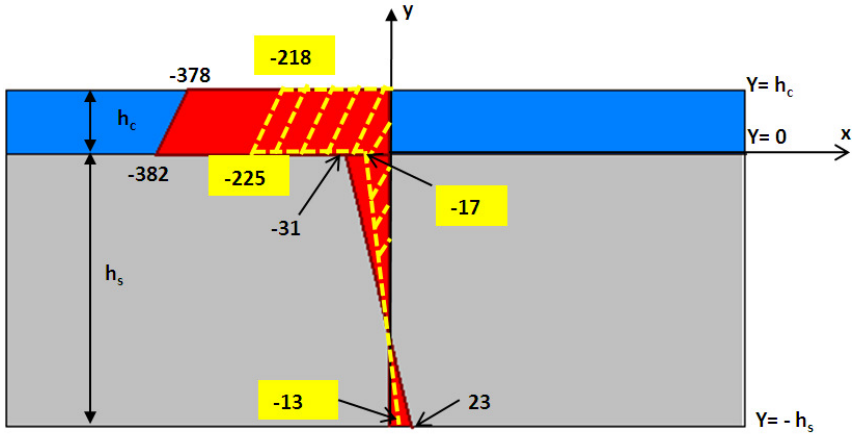

Figure 6-1: stress distribution in as sprayed N-V-300-3/SS and annealed coatings (in yellow) N-V-300-3/SS as highlighted in bold in Table 6-1*

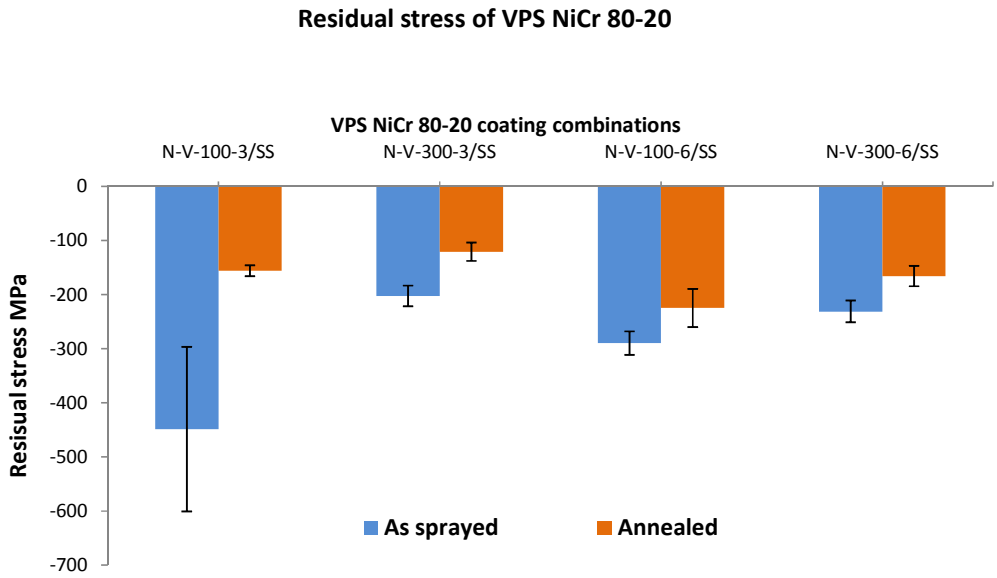

Figure 6-2: bending curvature residual stress of VPS NiCr 80-20 coatings measured and calculated using Godoy approach.

*Table 6-1: some of residual stress results calculated for one sample among three of each combination of as sprayed and annealed (denoted by *) VPS NiCr coatings obtained from bending curvature based on Clyne approach [127]*

Combinations	Residual stress distribution [MPa]			
	σ_c (y=h_c)	σ_c (y=0)	σ_s (y=0)	σ_s (y=-h_s)
N-V-100-3/SS	-531	-531	-16	13
N-V-100-3/SS*	-391	-297	-12	10
N-V-300-3/SS	**-378**	**-382**	**-31**	**23**
N-V-300-3/SS*	**-218**	**-225**	**-24**	**13**
N-V-100-6/SS	-567	-568	-17	14
N-V-100-6/SS*	-556	-423	-17	14
N-V-300-6/SS	-425	-429	-35	26
N-V-300-6/SS*	-372	-292	-39	23

The approaches of Clyne and Godoy gave different results, as it can be seen on Figure 6-2 and Figure 6-1. The analytical model of Clyne is mainly a stress distribution and the model takes only into account the induced stresses which arise from the secondary cooling (thermal stress), subsequently, residual stresses are always overestimated. However, Godoy considered the average stress in coating and the substrate at the interface zone, which represent our particular interest studied zone. Therefore, bending curvature analysis by Godoy approach will be considered in our study and will be compared to other measurements methods.

2. RESULTS OF INCREMENTAL HOLE DRILLING TESTS (IHD)

The residual stress state and gradients of as sprayed and annealed VPS NiCr 80-20 coatings were measured by the hole drilling method as previously described in chapter 5. Only coatings of thickness 300 µm were tested, because the method is known to give less precise results for coatings of a lower thickness such as 100 µm [211]. The negative stress values stand for compressive state, whereas the positive values stand for tensile one.

Figure 6-3 and Figure 6-4 show the incremental hole drilling results for two different coatings, VPS NiCr 80-20 as sprayed and annealed, with 300 µm of thickness with two levels of roughness, Ra=3 and Ra=6 µm. The theoretical interface location is placed on the graph, but may vary slightly prior the

interfacial roughness. Such location (highlighted in blue) is referred as "near interface" in the rest of the document.

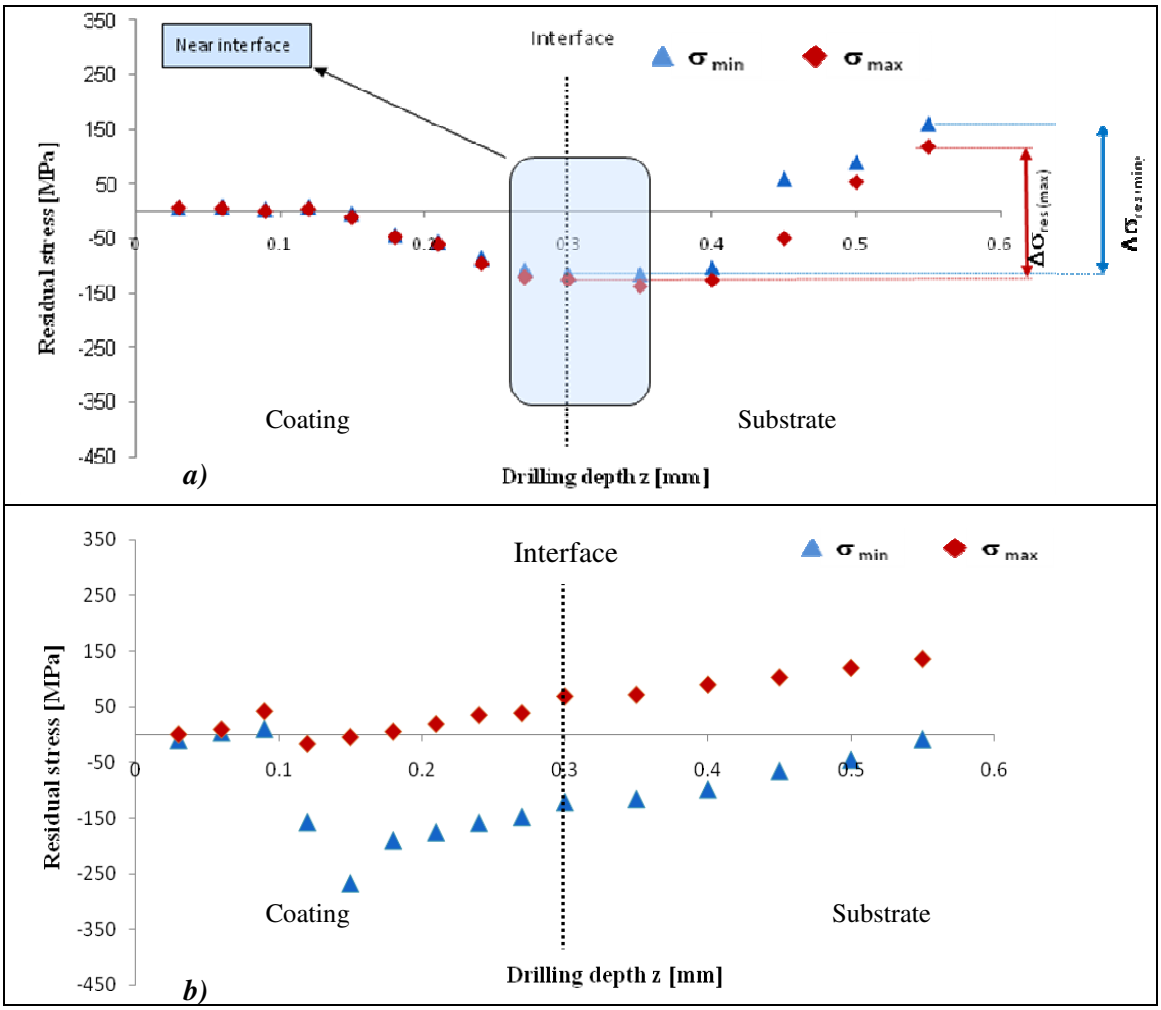

Figure 6-3: through-thickness residual stress of a) as sprayed VPS NiCr 80-20 with 3 µm of interface roughness (combination 19: N-V-300-3/SS) showing the gaps in residual stresses and b) the annealed sample (combination 20: N-V-300-3/SS).*

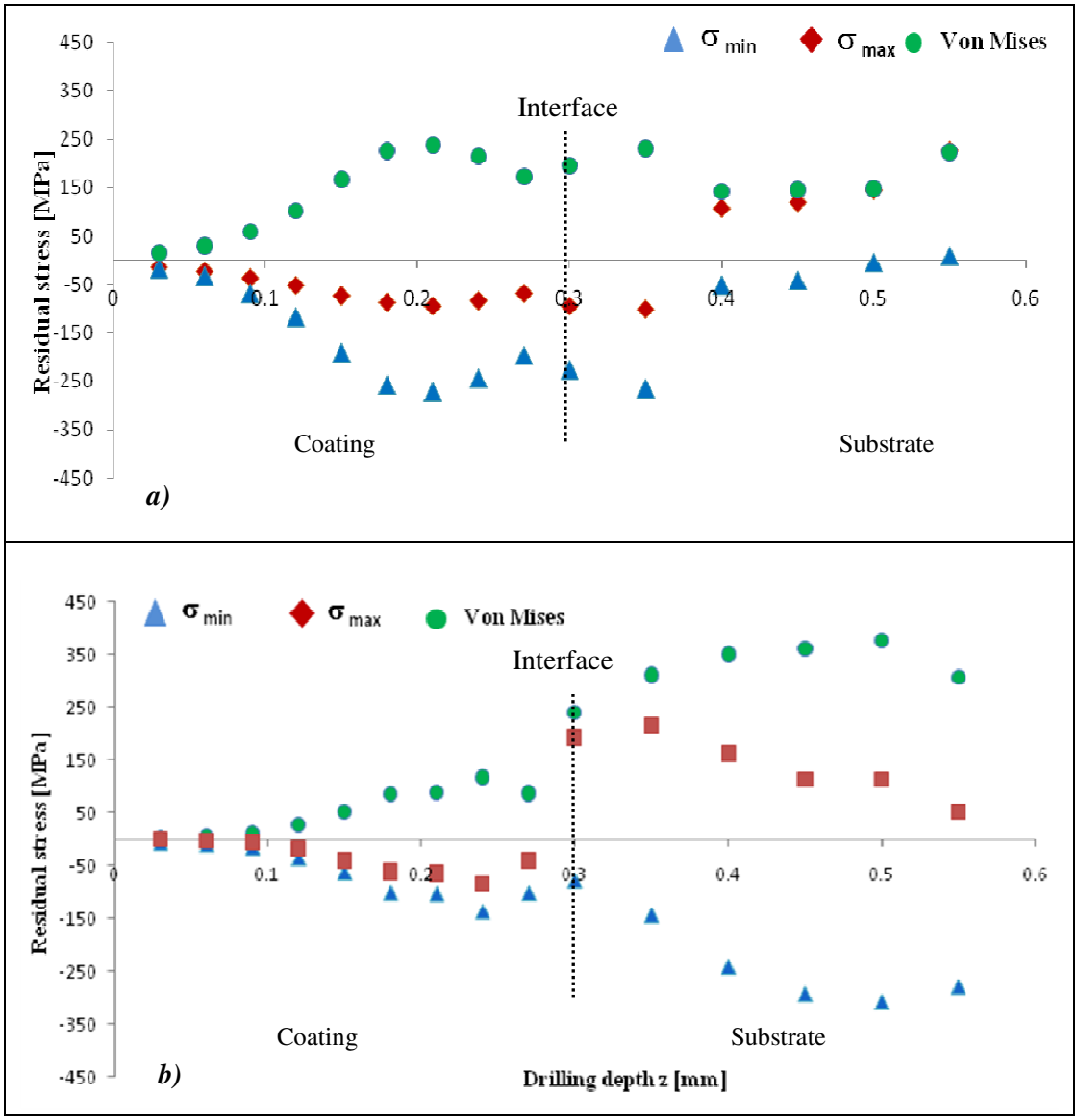

Figure 6-4: through-thickness residual stress of a) as sprayed VPS NiCr 80-20 with 6 µm of interface roughness (combination 23: N-V-300-6/SS) and b) the annealed sample (combination 24: N-V-300-6/SS).*

The principal stress components σ_{min} and σ_{max} through the as sprayed coating section are illustrated in Figure 6-3-a and Figure 6-4-a showing a compressive stress field along the whole coatings thickness, which become less compressive towards the coating surface. The variation in principal stresses is mainly due to the direction of plasma torch translation. Such variation of principal stresses was also observed in literature [107, 115, 212-215].

In order to express the through-coating stress profile in one magnitude order, one can distinguish different intensities:

i. The mean equivalent Von Mises stress near the interface zone (highlighted in blue Figure 6-3-a) was determined and presented in Figure 6-4 and Table 6-2. The order of magnitude is expressed in Figure 6-5 including the standard deviation to indicate the gradient of residual stress within three points near interface zone. The mean equivalent Von Mises stress is only an approximation upon the local stress intensity, but it did not provide any information about the stress distribution. The effect of annealing on residual stress will be discussed in the next section.

ii. The gap between residual stresses located at the interface and at the substrate are presented in Figure 6-3-a for the two principal directions and designed as $\Delta\sigma_{res\ (min)}$ and $\Delta\sigma_{res\ (max)}$. Figure 6-6 and Figure 6-7 show the absolute values of these gaps $\Delta\sigma_{res\ (max)}$ and $\Delta\sigma_{res\ (min)}$ respectively.

Table 6-2: Von Mises stresses near the interface of combinations and residual stress gap between interface and substrate in VPS NiCr 80-20 coating

Combinations	Von Mises v.s. depth MPa			Mean V.M$_{res}$	S.T	$\Delta\sigma_{res,max}$	$\Delta\sigma_{res,min}$
	0.27 mm	0.3 mm	0.35 mm	MPa	MPa	MPa	MPa
N-V-300-3/SS	115	121	128	121	7	274	243
N-V-300-3/SS*	170	166	163	166	4	67	113
N-V-300-6/SS	173	195	230	199	29	272	272
N-V-300-6/SS*	87	241	312	213	115	255	207

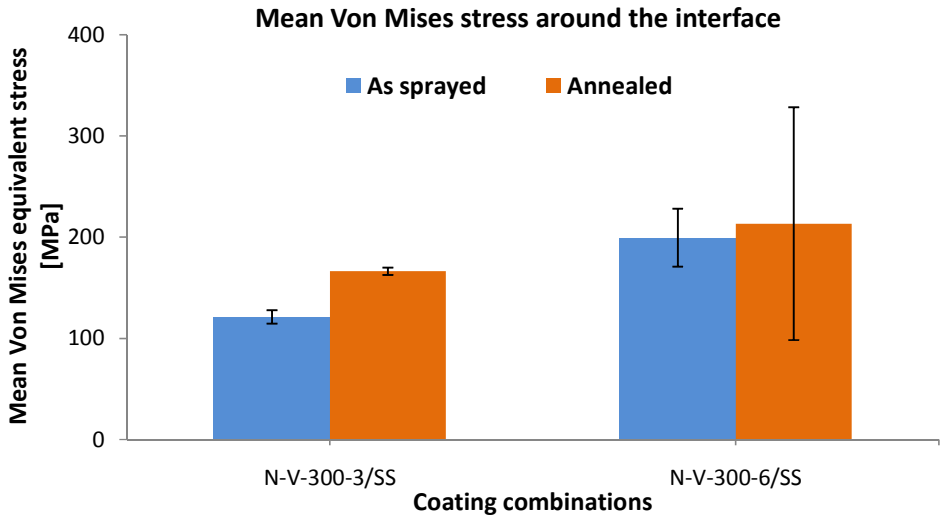

Figure 6-5: mean equivalent Von Mises stress within the near interface for the NiCr 80-20 as sprayed and annealed.

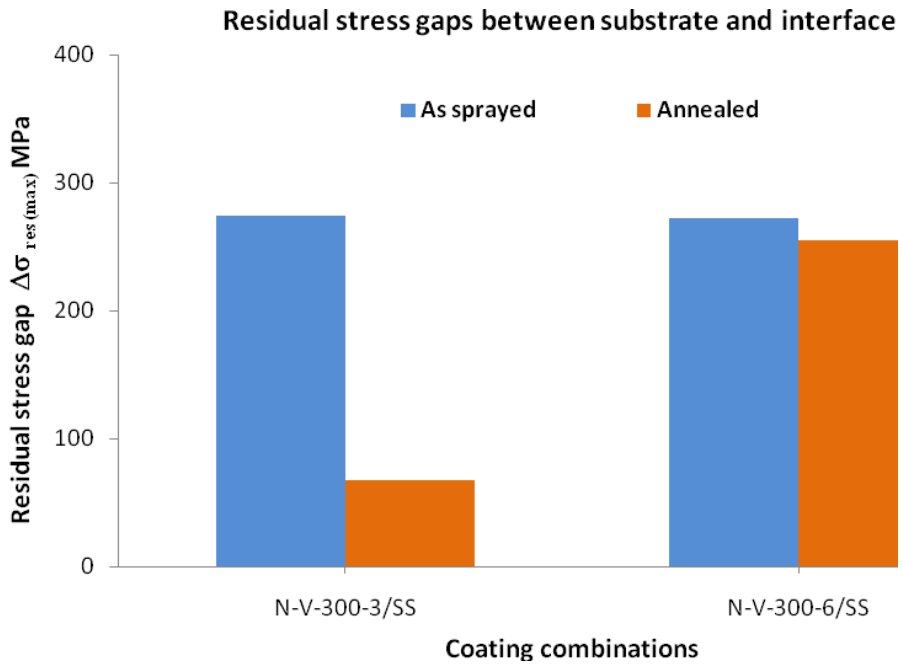

Figure 6-6: the gap $\Delta\sigma_{res\ max}$ in residual stress between interface and substrate for the NiCr 80-20 as sprayed and annealed.

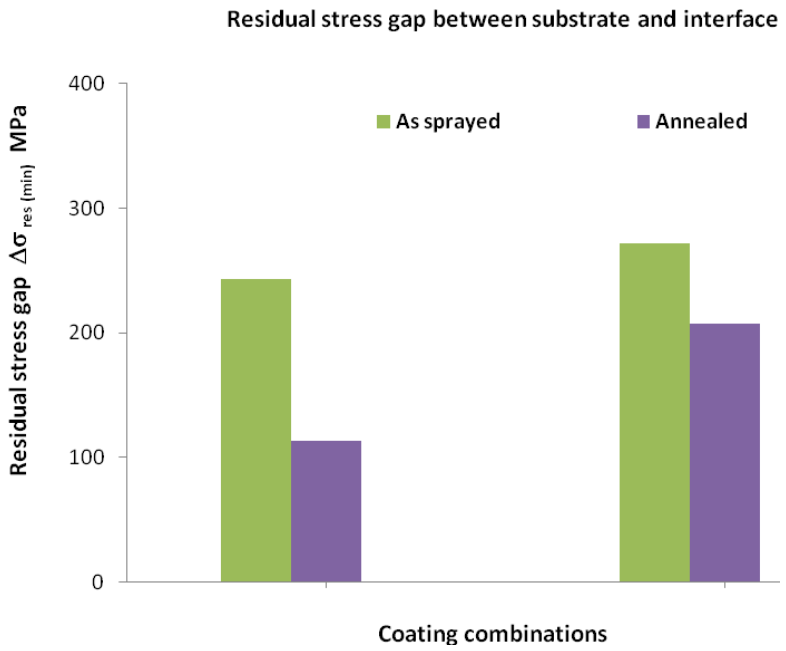

Figure 6-7: the gap $\Delta\sigma_{res\ min}$ in residual stress between interface and substrate for the NiCr 80-20 as sprayed and annealed.

It is acknowledged that if the stress/strain behavior is nonlinear due to yielding or other causes, the calculated residual stresses will be erroneous [215]. Localized yielding due to the drilling of the hole may occur if the initial residual stress is close to the yield strength of the material. Therefore the measurements are considered as valid only if the residual stresses are below 70% of the yield strength as it is recommended by Grant [215]. Even more cautious standard ASTM E 837-01 [216] states that this technique is only valid in situations where the residual stresses do not exceed 50% of the yield strength. In this work, the highest absolute value of residual stress was found to be 271 MPa. The yield strength of NiCr is approximated to be three times the Vickers hardness value [217, 218], to give 293 x 3= 879 MPa. Subsequently, the highest residual stress value can present around 30% of yield strength.

Furthermore, it is well recognized that the hole drilling method is not accurate below (approximately) 50% of the hole diameter because the depth reached by the drill is too far from the surface where the strain gauges are placed and the variations of their deformation very difficult to measure [202]. In experimental studies, the hole diameter is 1.5 mm, the results therefore, are considered to be reasonably accurate for drilling depths up to 0.6 mm.

Some other problems can also influence the precision of the measurement. For example, Sasaki et al [219] have shown in a recent work that the eccentricity of the hole is also an important experimental parameter to consider. When there is no measurable eccentricity, the hole drilling method allows to determine the stress with an error of not more than 3% of the actual value. When there is a noticeable eccentricity, the error can be of 20% - 30% of the true value. Oettel [220] also estimated the uncertainty of the gauge itself at 3% of the highest level of strain. Schajer [221], Grant [215] and Valente [212, 222] also pointed out various sources of error, but the operator skill has been identified as probably the most important parameter in achieving a reliable and quality measurement.

3. RESULTS OF RESIDUAL STRESS BY INTERFACIAL INDENTATION

Table 6-3 summarized the residual stresses results obtained by interfacial indentation (methodology explained in 3.2 chapter 5). Tensile stresses were obtained for all coatings on Ti alloy substrate while the other combinations were in compressive stress, the reason of these different states in residual stress will discussed in the next section.

Table 6-3: summary of residual stress results determined by interfacial indentation

Process	Coatings	Number	Combinations	h_c	Ra	K_{ca}	a_0	K_{ca0}	σ_{res}
				µm	µm	MPa. $m^{0.5}$	µm	MPa. $m^{0.5}$	MPa
FS	NiCr 80-20	1	N-F-100-3/St	100	3	1.68	23.9	2.39	-159
		2	N-F-300-3/St	300	3	2.31	8.00	2.39	-24
		3	N-F-100-6/St	100	6	1.64	35.80	2.14	-90
		4	N-F-300-6/St	300	6	2.08	13.0	2.14	-14
		5	N-F-100-3/Ti	100	3	1.42	1.12	0.78	386
		6	N-F-300-3/Ti	300	3	1.41	3.94	0.78	62
		7	N-F-100-6/Ti	100	6	3.18	0.58	0.74	646
		8	N-F-300-6/Ti	300	6	1.01	0.32	0.74	525
	Al_2O_3	9	Al-F-100-3/St	100	3	1.34	2.62	1.62	-60
		10	Al-F-300-3/St	300	3	1.59	2.83	1.62	-14
		11	Al-F-100-6/St	100	6	1.86	1.78	0.59	-60
		12	Al-F-300-6/St	300	6	0.73	1.87	0.59	-80
		13	Al-F-100-3/Ti	100	3	3.01	0.77	1.41	28
		14	Al-F-300-3/Ti	300	3	1.02	5.30	1.41	14
		15	Al-F-100-6/Ti	100	6	3.94	0.58	0.74	646
		16	Al-F-300-6/Ti	300	6	0.77	0.32	0.74	525
VPS	NiCr 80-20	17	N-V-100-3/SS	100	3	1.47	41.0	4.81	-462
		18	N-V-100-3/SS*	100	3	2.19	24.0	3.92	-309
		19	N-V-300-3/SS	300	3	4.44	12.5	7.81	-92
		20	N-V-300-3/SS*	300	3	3.81	20.8	3.92	-21
		21	N-V-100-6/SS	100	6	1.68	66.1	3.94	-246
		22	N-V-100-6/SS*	100	6	2.91	15.9	2.51	91
		23	N-V-300-6/SS	300	6	3.69	16.0	3.94	-56
		24	N-V-300-6/SS*	300	6	2.55	12.4	2.51	12

* highlighted combinations are denoted for annealed samples

4. DISCUSSION

Results of residual stress obtained from bending curvature, incremental hole drilling and interface indentation all revealed a compression stress field achieved in the as sprayed NiCr coatings on the steel substrates. These results can be therefore explained by the physical properties of coating-substrate systems as previously stated in table 5-6 chapter 5. For example, the as sprayed VPS

NiCr/AISI304 system has (α_c = 12.5 < α_s= 17.2 µm/mK) and the resulting induced stresses are dependent on the magnitude of the stresses which arise from the secondary cooling (thermal stress), bearing in mind that the induced stresses due to the primary cooling (quenching) are always tensile. Because the $\Delta\alpha$ =4.7 µm/mK value in this coating –substrate system is quite significant (even at high temperature as observed by Ishida [223]. Figure 6-8 shows the increase of the CTE of both, coating and substrate and the droop of E modulus accordingly) for the stresses induced by thermal shrinkage when the specimen is cooled down from the process temperature to room temperature (ΔT *is around* 730 K). Therefore, the compressive stresses associated to the secondary cooling process are dominant.

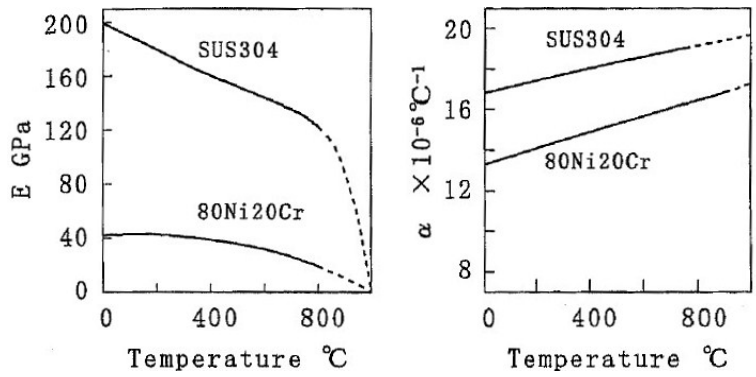

Figure 6-8: Young modulus and thermal expansion coefficient of NiCr 80-20 plasma sprayed coating on SUS 304 substrate [223].

The results from interfacial indentation shown in Table 6-3 revealed that a tensile stresses were occurred in all coatings sprayed on Ti alloy substrate. This can be explained by the following points:

i. For the FS NiCr coatings on Ti alloy substrate, as this system characterized by α_c=14>α_s=8.6 µm/mK. Evidenced tensile residual stresses are resulted and this is in agreement with literature [224, 225] as well as with the predicted theoretical stress state as reported in Table 6-4.

Table 6-4: induced stresses in the coating during thermal spraying [91]

Origin of stresses	$\alpha_c < \alpha_s$	$\alpha_c = \alpha_s$	$\alpha_c > \alpha_s$
Quenching stress	+	+	+
Thermal stress	-	0	+
Resulted residual stress	+ or -	+	+

+ ; tensile stress / - ; compressive stress

ii. Regarding the Alumina coatings on Ti alloy substrate, where α_c=5.7<α_s=8.6 µm/mK (at room temperature), at the spraying conditions (melting temperature of alumina (bulk) is around 2000 °C and the substrate preheating up to ~250°C), the coefficients of thermal expansion are getting closer (α_c = 10 and α_s= 9.2 µm/mK, an approximative value is assumed taken from [226]), it means that the $\Delta\alpha$ value is maybe tending to be very small. Therefore, the tensile stresses associated to the primary cooling (quenching) process are dominant (quenching stress is always in tensile).

The stress distribution, its intensity and state (sign) in the coating, is strongly dependent on the specific spray process [227] and processing conditions [228]. Figure 6-9 gives a schematic presentation of the stresses that could be obtained using different temperature deposition, The final residual stress state through the whole coating/substrate system is the result of the superposition of stresses of different nature induced during the spray process: quenching, thermal mismatch, and peening stresses, together with the compressive stress state of the substrate induced during the grit blasting prior to spraying [229-231] (see Figure 6-10).
In addition to these stress sources, there are a various factors that can affect the stress, e.g. phase transformation accompanied by volume change and chemical changes like oxidation.

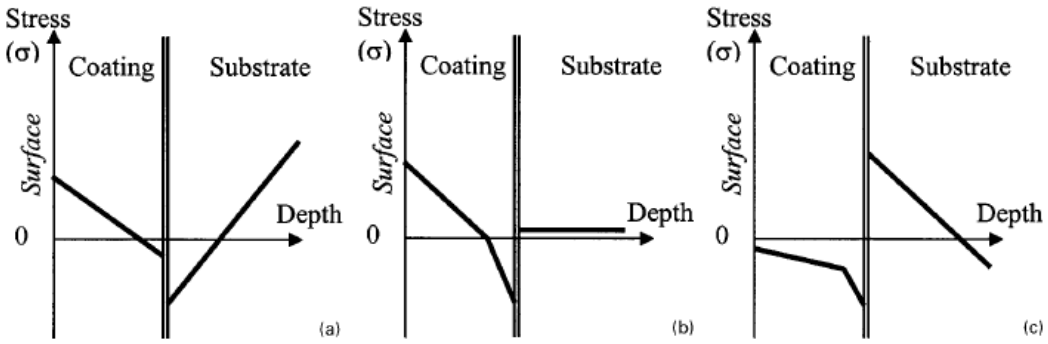

Figure 6-9: schematic profile of residual stress as function of temperature of deposition of molybdenum, a) a low T_d, b) middle T_d, c) high T_d [232].

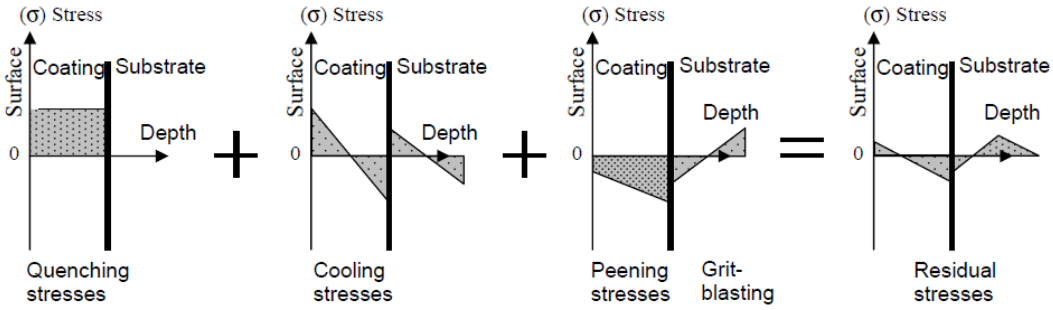

Figure 6-10: Schematic presentation of radial stress distribution in HVOF sprayed coating (Inconel 718 coatings on Inconel 718 substrates) [229].

Lyphout [229, 230] found compressive stress is achieved in both coating and in substrate at the interface, but the difference in stress amplitude at the interface $\Delta\sigma^{S;C}_{int}$ seems to significantly decrease when coating thickness is increased and this is in perfect agreement with our results illustrated in Figure 6-2.

Figure 6-11 shows a comparison results of VPS NiCr of residual stress obtained by bending curvature, interface indentation and incremental hole drilling (IHD) methods. However, two statements are to be considered:

i. for coatings with 100 µm thick; the residual stresses obtained by the bending curvature and interfacial indentation methods seem to be in a comparable order of magnitude. This agreement is not found at higher coating thickness e.g. 300 µm because residual stresses obtained by interfacial indentation are localized in a small volume circumscribed at the interface zone,

ii. for coatings with 300 µm thickness, the residual stresses obtained by bending curvature and incremental hole drilling show a comparable order of magnitude.

However, main residual stresses were found to decrease with the increase of coating thickness, and this was mainly attributed to possible annealing effects on the stress in previous layers caused by heat input from new layers.

The difference in residual strress intensities obtained by previous methods is possiibly attributed to the following factors:

i. the difference in the relevant measurement volume/area of the coatings-substrate system, for example, the hole drilling measurements are localized to a volume of the order to 1 mm^3, whereas, the interface indentation measurements are localized on loaded zone along the interface for important length of sample section (40 mm long), while the curvature measures the stress in coating of tenth of millimeters over a 7 cm of length.
ii. the difference in analytical model and assumptions of residual stress estimation.

This can be schematically illustrated in Figure 6-12 containing the three models of residual stress. The measured bending curvature is based on the beam theory using Godoy appoach as an average residual stress at the interface between substrate and coating and denoted by σ_{Godoy}. In the incremetnal hole drilling; the profiles obtained could be expressed in a single value such as the gap in radial stress between interface and substrate σ_{IHD}. The residual stresses obtained with interfacial indentation denoted by σ_{ind} were calculated starting from several (up to 100) indentation measurements while curvature residual stresses are averaged mainly from 3 measurements. It is very interesting to see every testing method of residual stress gives a unique value and has different characteristics, e.g. interface indentatation can provide a very coherent results at and around the interface, whereas the bending can give very general information about residual stress state and intensity of all the sample, lastly, the incrementatl hole drilling method can locally provide in a small volume, a through coating gradient of residual stress.

To conclued, the methods employed are complementary, and each can supply unique information.

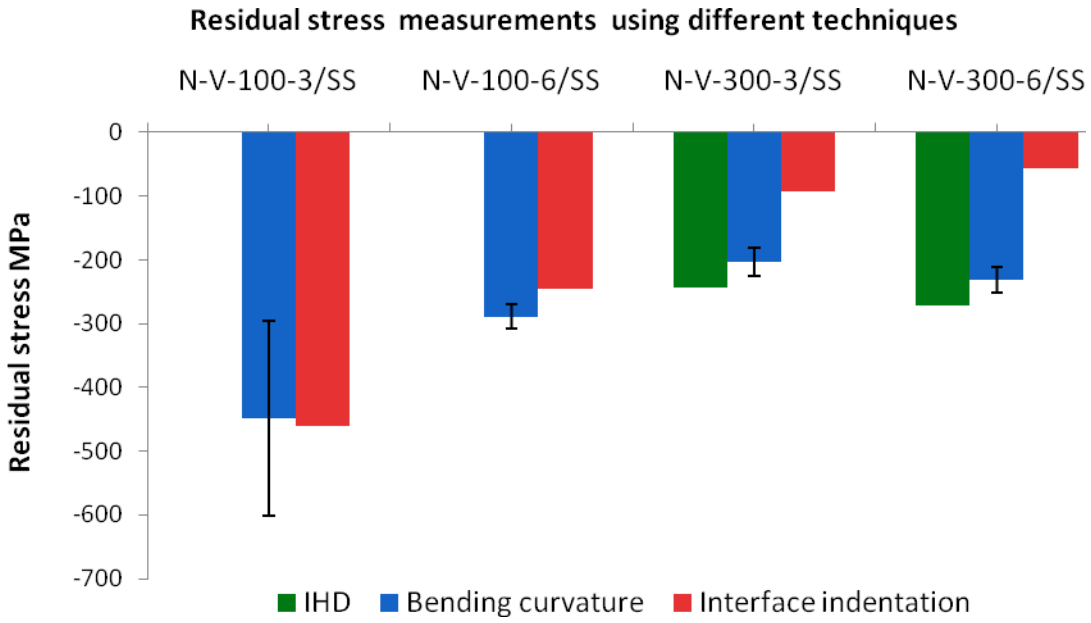

Figure 6-11: Residual stress of as sprayed VPS NiCr coating measured by different techniques.

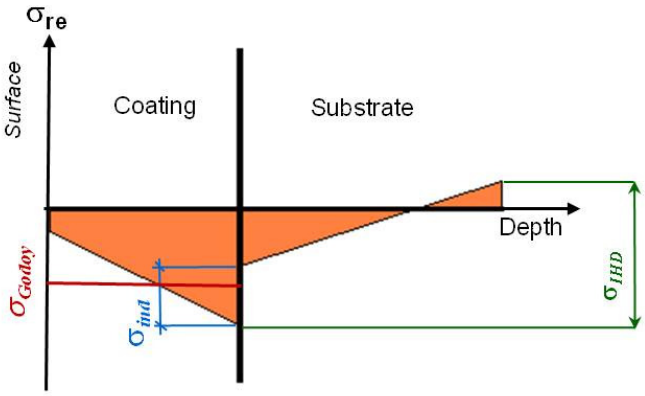

Figure 6-12: schematic presentation of different model of residual stress calculation.

4.1 EFFECT OF ANNEALING ON RESIDUAL STRESS

The annealing treatment up to 800°C for 75 min that has been carried out on the samples aiming to reduce the intensity of residual stress in the coating and at the interface. The general residual stress results obtained after annealing showed a partial release within the range of 20% down to 65%. These orders of reduction were also observed in the following references [98, 99].

Results obtained from bending curvature confirm an important residual stress relief was occurred as shown in

Figure 6-2. For coating with 300 µm thickness, the residual stress relief was measured in the range of 30% down to 40 %. For coating with 100 µm thick, two different orders of relief can be observed:

i. for coating with Ra= 3 µm of interface roughness, a decrease down to 65% was achieved,
ii. coating with Ra= 6 µm of interface roughness, only a 22% of residual stress relief was measured. This may be explained by the fact of a higher of mechanical interlocking (higher interfacial roughness) helped to retain more the residual stress.

Figure 6-3 and Figure 6-4 illustrate the principal stresses intensities σ_{min} and σ_{max} through the coating and show for the as sprayed samples a compressive stress field along the whole coatings thickness. The annealed profile can be distinguished by two components of principal stress, one is in compression and the other was developed after annealing to be in tensile, this stress conversion to tensile can be explained by two reasons:

i. the elastic stress relief and conversion prior to the direction of plasma torch translation,
ii. phase transformation or/and new phase formation after annealing which led to an important relief of residual stress and to a partially conversion to tensile stress state. This case will be analyzed and discussed later in chapter 7, where chromium segregation and chromium carbide have been observed within the coating and at the interface.

However, this residual stress conversion to tensile state was locally observed and was not the dominant stress field within the coating, because the bending curvature results did not show any tensile behavior in the annealed samples. However, Figure 6-5 shows higher Von Mises stress value for annealed specimen than for as sprayed ones. This can be explained by the calculation of Von Mises equivalent stress ($\sigma_{VonMises} = \sqrt{\sigma_{max}^2 + \sigma_{min}^2 - \sigma_{max}\sigma_{min}}$), as the difference between σ_{min} and σ_{max} components near interface zone in annealed samples is higher than that in as sprayed one, the Von Mises stresses subsequently are larger as illustrated in Figure 6-4. However, to avoid this misleading, an example can be given; the σ_{min} at the interface of as sprayed sample is -225 MPa whereas, the σ_{min} = -76 MPa at the interface of annealed sample.

Results obtained by interfacial indentation method shown in Table 6-3 indicate an important release in the residual stresses was achieved after annealing, in particular, combinations 22 and 24, a conversion in residual stress state from compression to tensile was occurred, for example, in combination 24, the residual stress converts from –56 to +91 MPa, it is very interesting results since this conversion has also been partially observed locally in incremental hole drilling results. This conversion in residual stress state is previously discussed in the previous paragraph.

After annealing, Weyant [233] observed a decrease of residual stress intensity in the thermal barrier coatings (consisting of a NiCoCrAlY bond coat and an yttria-stabilized zirconia (YSZ) topcoat) and a reduction of residual stress gap between the substrate and the coating. However, as reviewed by Hurrell *et al* [96], there are many ways either to reduce potentially harmful residual stresses, or to introduce beneficial residual stresses to prolong life. At least two stress relief mechanisms are important:

1. plasticity caused by the reduced yield stress at elevated temperature which occurs essentially instantaneously as the temperature increases,
2. creep mechanisms which occur over a longer period of time [234].

It should be noted that because plastic strain generated from the misfit cannot be relieved by local plastic flow but requires larger scale rearrangement. Depending on the temperature, annealing can mainly modify the distribution of residual

stress around the interface [97, 98]. Furthermore, annealing can affect significantly the microscopic residual stress type I and II as previously reported in chapter 3, and less the thermal stress issued from the mismatch of CTE of coating and substrate. For example, Laribi [99] found a significant reduction of residual stress after annealing molybdenum coating on steel substrate, where a chemical diffusion of a $\varepsilon(Fe_xMo_y)$ fragile intermediate phase at interface was observed. Lesage [98] found the annealing treatment of NiCr coating at 600°C led to a considerable improvement of coating adhesion due to the reinforcement of the metallurgical bonding between the coating and the substrate which was attributed to inter diffusion of iron, nickel and chromium. Brossard [100] found in NiCr sprayed particles on the stainless steel substrates an inter-diffusion between both materials, and grains growing across the interface into both phases.

5. SUMMARY

In this chapter, the results of residual stress measurements were reported using three methods; curvature bending, incremental hole drilling and interfacial indentation. The obtained results can be summarized in the following points:

1. the residual stress obtained using all methods were measured to be in compression state in NiCr coatings on the steel substrates. This was explained prior to the physical properties e.g. CTE, of coating-substrate systems,
2. tensile stress were obtained using interfacial indentation were occurred in all coatings sprayed on Ti alloy substrate. Evidenced tensile stress in the system FS NiCr coatings-Ti alloy substrate was achieved, since this system is characterized by $\alpha_c=14>\alpha_s=8.6$ µm/mK. On the other hand, the tensile stress achieved in the alumina coatings-Ti alloy substrate system was found to be mainly associated to the primary cooling (quenching) process,
3. comparing residual stress results of VPS NiCr obtained three previous methods. Two statements can be considered according to coating thickness:
    i. a comparable order of magnitude in residual stress was achieved in coatings with 100 µm thickness when comparing results of bending curvature to interfacial indentation methods,

ii. for coatings with 300 µm thickness, the residual stresses obtained by bending curvature and incremental hole drilling show a comparable order of magnitude.

Every testing method of residual stress has some characteristics and advanges, e.g. interface indentatation can provide very coherent results at and around the interface, whereas the bending can give very large information about residual stress state and intensity of all the sample, while, the incrementatl hole drilling method can locally provides residual stress through-coating profile. The difference in residual stress intensities obtained by the three methods is not only attributed to the difference in analytical model in residual stress estimation, but it is also related to the relevant measurement volume/areas of the coatings-substrate system, for example, the hole drilling measurements are localized to a volume of the order to 1 mm^3, whereas, the interface indentation measurements are localized on loaded zone along the interface for important length of sample section (40 mm long), while the bending curvature measures the strain in coating of tenth of millimeters over a 7 cm of length. However, the methods employed are complementary, and each can supply unique information.

4. The effect of annealing can be concluded in the following points:
   i. The general effect of annealing treatment up to 800°C for 75 min reduced the intensity of residual stress in the coating and at the interface. From bending results, coating with interface roughness of Ra= 3 µm showed a decrease in residual stress down to 65%, whereas, coating with interface roughness of Ra= 6 µm, only a 22% of a decrease was achieved. This may be explained by the fact of a higher of mechanical interlocking helped to retain better the residual stress within the coating.
   ii. IHD method showed a compressive stress components along the whole coatings thickness in the as sprayed samples, the profile of annealed sample showed one of principal stress component was in compression and the other was developed after annealing to be in tensile, this is mainly due to the elastic stress relief and conversion prior to the direction of plasma torch translation, and/or new phase formation after annealing. This case will be analyzed and discussed later in chapter 7, where chromium

segregation and chromium carbide have been observed within the coating and at the interface.

iii. Some of annealed results (e.g. combinations 22 and 24) obtained by interfacial indentation method revealed also a conversion in residual stress state to tensile for the same reasons explained above.

CHAPTER 7 : RESULTS OF ADHESION MEASUREMENTS

1. TENSILE ADHESION MEASUREMENTS (EN 582)

Tensile adhesion tests were carried out on combination samples 1-16 and 25-29. The results including the standard deviation and fracture modes are summarized in Table 7-1.

Table 7-1: results of tensile adhesion tests according to the EN 582

Process	Coatings	Number	Combinations	$\sigma_{tensile}$ MPa	S.D MPa	Fracture mode
FS	NiCr 80-20	1	N-F-100-3/St	82	4	co
		2	N-F-300-3/St	54	17	co
		3	N-F-100-6/St	70	9	co
		4	N-F-300-6/St	51	5	co
		5	N-F-100-3/Ti	59	20	co
		6	N-F-300-3/Ti	40	6	co
		7	N-F-100-6/Ti	61	11	co
		8	N-F-300-6/Ti	48	6	co
	Al_2O_3	9	Al-F-100-3/St	90	7	co
		10	Al-F-300-3/St	42	10	ad/co
		11	Al-F-100-6/St	91	8	co
		12	Al-F-300-6/St	68	11	co
		13	Al-F-100-3/Ti	105	36	ad
		14	Al-F-300-3/Ti	41	23	ad
		15	Al-F-100-6/Ti	100	5	ad/co
		16	Al-F-300-6/Ti	78	10	ad
HVOF	Sandwich	25	Cer / steel	64	11	ad
		26	Cer /NiCr/ Cer	62	2	ad
		27	Cer /CoCr/ Cer	26	2	co
		28	Cer /Ni pl/ Cer	62	4	ad
		29	Cer /Ni pl- x/ Cer	64	4	ad

The denoted letters co and ad as fracture mode stand for adhesive failure (failure within the glue) and cohesive failure (failure within the coating), respectively.

Figure 7-1 and Figure 7-2 show the tensile adhesive strength values of metallic and ceramic coatings respectively. In both figures the tensile adhesive strength was observed to decrease with increasing the coatings thickness.

This can be explained by the glue used in the test that penetrates within the porous coating at the same level for the thick and thin coating, but the volume ratio of the strengthened layer (with the glue) to the volume of coating is different. Subsequently, the tensile adhesion may increase in the thin coating. As the flame sprayed coatings exhibit high porosity level up to 7 %. Therefore, the

penetration of the glue is an important parameter which can invalidate the physical properties of the coatings [235].

Tensile adhesive strength results for the sandwich based cermet coatings are shown in Figure 7-3. The failure of coatings was occurred adhesively between the glue and the substrate of counter body except for the combination 27 where the Co-Cr interlayer failed cohesively. This can be explained by the high concentration of oxide present within this coating that reduces the adhesion between the splats. Regarding the influence of interfacial roughness on adhesive strength, it is seen that both, ceramic and metallic coatings show a general tendency to increase with increasing Ra value until an optimum that depends on the substrate and coating materials. We have to precise that *Ra* is a topographic parameter, is only the representative of the average 2D roughness. Since it is unable to take into account the true area of contact between substrate and coating, it cannot explain accurately the effect of interface roughness on adhesion [25, 236, 237].

The effect of coating thickness on tensile adhesive strength was reported in ref [238]. Greving [10] found also the tensile adhesive strength of NiAl coating decreases with increasing coating thickness and he attributed this to the tensile residual stress distribution at the free-edges of coatings. Since the intensity of the free edge stress increases with the coating thickness, the tendency for debonding was more likely to appear in thicker coatings. Greving used layer-removal method to evaluate the in-plane residual stress within the coatings [10, 239]. The stress distribution along the z-axis has been assumed to follow a known pattern in this case. However, such assumption of residual stress in z-axis seems to be weak in our opinion, because the main influencing stresses are concerned with the stress in X-Y plane. Unger [240] also reported a similar decrease in bond strength for a plasma sprayed NiAl coating on Inconel 718 substrate. However, his findings illustrate the tendency for bond strength to decrease as coating thickness increases. Either of these two references did not elaborate on the type of failure, i.e., cohesive or adhesive that has taken place. Han [11, 241] simulated an axisymmetric crack at the interface edge between the coating and substrate for the same tensile test configuration to predict coating failure based on the energy

release rate. In spite of the fact that this crack extension was far away from real test conditions, the prediction of adhesive strength was in good agreement with experimental data.

Tensile adhesive tests involve a complex mixture of tensile and shear forces which render the interpretation of the results difficult [242]. Moreover, it has been discussed extensively in the literature [2, 18] that this test cannot be related to fracture mechanics indices like toughness, as the crack propagation is spontaneous and depends on the critical flaw size at the interface.

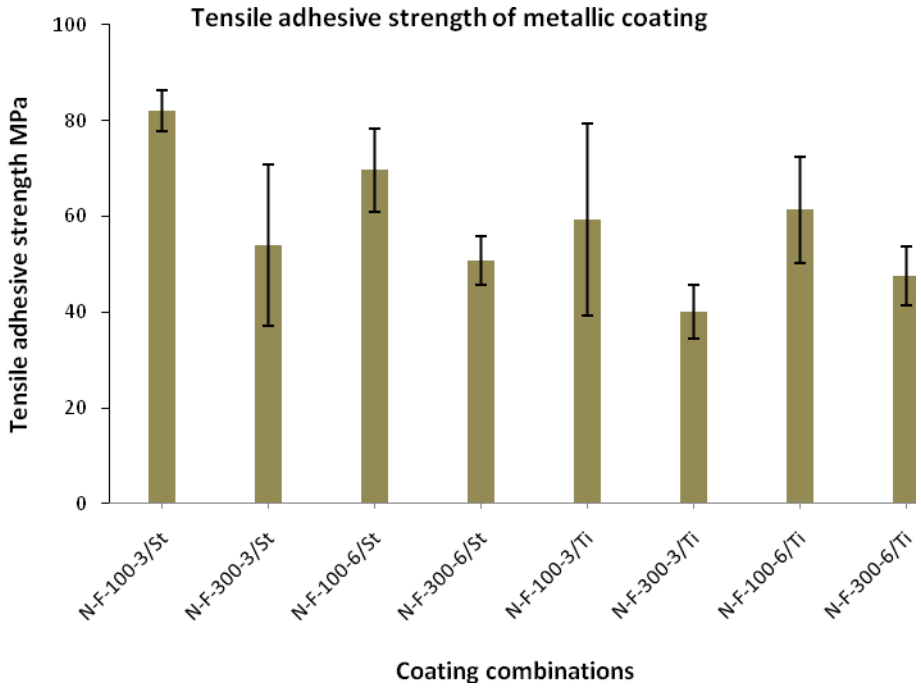

Figure 7-1: results of tensile adhesive strength test of metallic coatings according to EN 582.

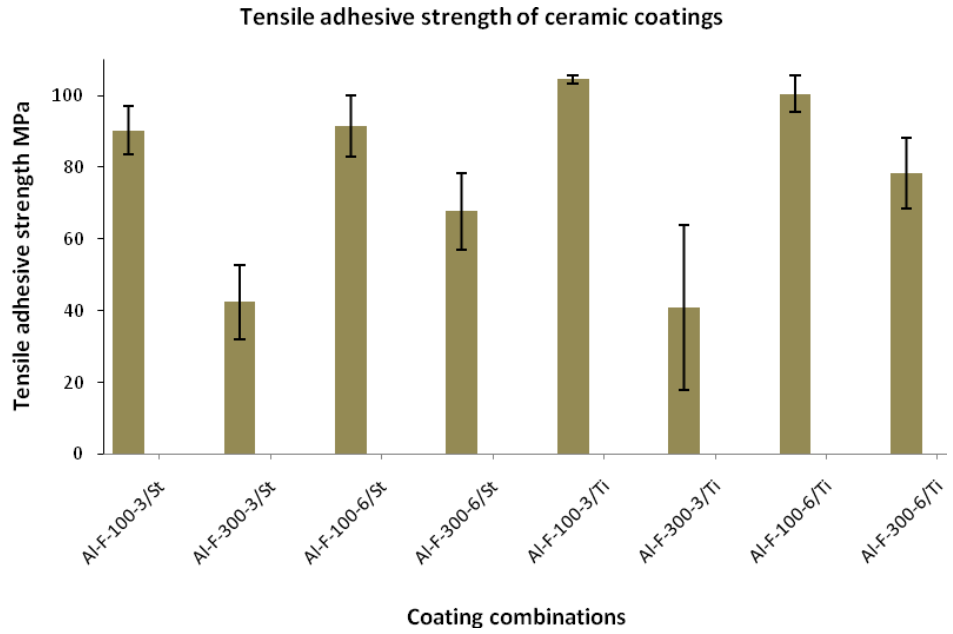

Figure 7-2: results of tensile adhesive strength test of ceramic coatings according to EN 582.

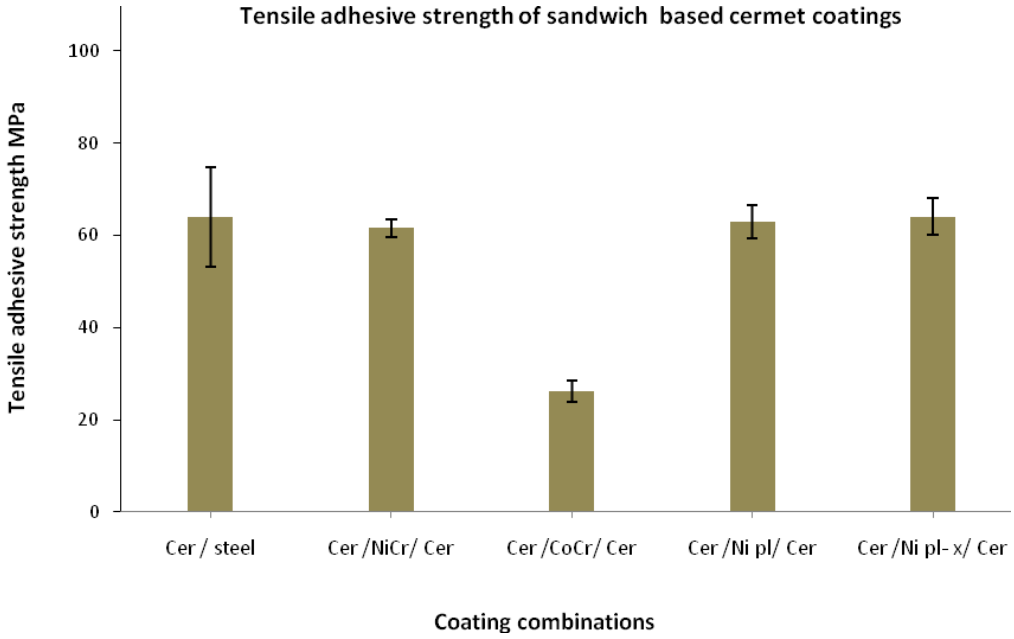

Figure 7-3: results of tensile adhesive strength test of sandwich combinations according to EN 582.

To conclude, such adhesive failure cannot yield to a physical value to quantify the adhesion and one can only assume that adhesion strength at the interface is stronger than those values obtained. The results that we obtained demonstrate that the tensile adhesive test might be no longer usable for the thermal spray coatings

that are routinely produced nowadays. Since the adhesion between these coatings and their substrate exceeds the resistance of the glue, fracture appears in majority cohesively in the coating or "adhesively" in the glue. Allowing the fact that the test is very time consuming, costly and gave very poor information on the adhesion properties of the materials and it is probably going to be abandoned in the near future in profit of more powerful tests. Some of them are described and used in the following.

2. INTERFACIAL INDENTATIONS

Table 7-2 shows the results of the interfacial indentations of the whole coating combinations as well as the critical load P_c and the critical crack length a_c. The sandwich based cermet coating combinations were tested by the indentations performed at the interface between the cermet coating and interlayer as shown in Figure 7-4. This interface was investigated, since a previous study showed that this location where the failure took place under tensile adhesion and shear tests.

Table 7-2: results of apparent interfacial toughness of coating combinations

Process	Coating	Number	Combinations	h_c	Ra	a_c	P_c	$(E/H)^{0.5}$	K_{ca}
				µm	µm	µm	N	-	MPa. $m^{0.5}$
FS	NiCr 80-20	1	N-F-100-3/St	100	3	5.21	0.13	8.34	1.68
		2	N-F-300-3/St	300	3	6.10	0.26	8.34	2.31
		3	N-F-100-6/St	100	6	14.03	0.16	8.34	1.64
		4	N-F-300-6/St	300	6	11.93	0.66	8.34	2.08
		5	N-F-100-3/Ti	100	3	0.84	0.01	7.12	1.42
		6	N-F-300-3/Ti	300	3	5.35	0.19	7.12	1.41
		7	N-F-100-6/Ti	100	6	3.51	0.09	7.12	3.18
		8	N-F-300-6/Ti	300	6	1.34	0.02	7.12	1.01
	Al_2O_3	9	Al-F-100-3/St	100	3	1.55	0.02	8.93	1.34
		10	Al-F-300-3/St	300	3	2.61	0.05	8.93	1.59
		11	Al-F-100-6/St	100	6	4.95	0.12	8.93	1.86
		12	Al-F-300-6/St	300	6	2.95	0.03	8.93	0.73
		13	Al-F-100-3/Ti	100	3	3.01	0.06	7.25	3.01
		14	Al-F-300-3/Ti	300	3	4.80	0.09	7.25	1.02
		15	Al-F-100-6/Ti	100	6	2.57	0.06	7.25	3.94
		16	Al-F-300-6/Ti	300	6	4.01	0.05	7.25	0.77
VPS	NiCr 80-20	17	N-V-100-3/SS	100	3	0.16	5.82	8.61	1.47
		18	N-V-100-3/SS*	100	3	0.13	4.01	8.75	2.19
		19	N-V-300-3/SS	300	3	1.46	12.17	8.61	4.44
		20	N-V-300-3/SS*	300	3	3.46	24.21	8.75	3.81
		21	N-V-100-6/SS	100	6	0.04	1.96	8.61	1.68
		22	N-V-100-6/SS*	100	6	0.01	0.74	8.75	2.91
		23	N-V-300-6/SS	300	6	0.21	3.84	8.61	3.69
		24	N-V-300-6/SS*	300	6	0.07	2.33	8.75	2.55
HVOF	Sandwich	25	Cer / steel	500	6	35.49	13.44	7.67	7.32
		26	Cer /NiCr/ Cer	250	6	6.51	0.35	4.87	1.53
		27	Cer /CoCr/ Cer	250	6	3.67	0.11	4.49	1.04
		28	Cer /Ni pl/ Cer	250	6	8.54	1.01	5.96	3.62
		29	Cer /Ni pl- x/ Cer	250	1	18.41	6.15	5.96	6.97

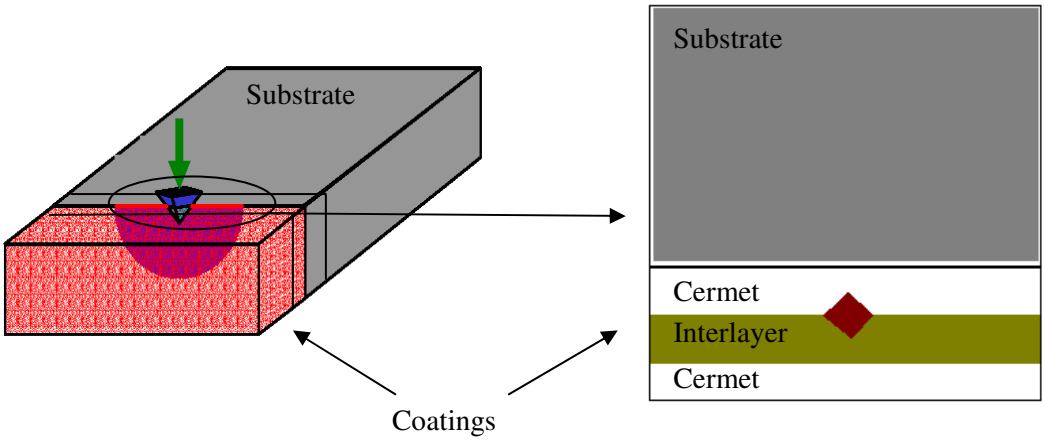

(a)

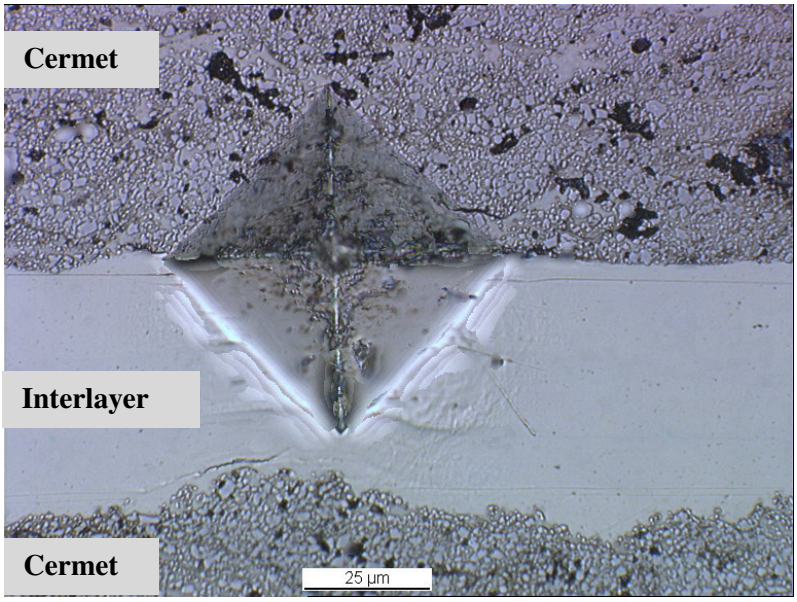

(b)

Figure 7-4: (a, b) schematic presentation of interfacial indentation on sandwich based cermet coatings, b): interfacial indentation on sandwich structure (combination 29).

Concerning the coatings on Ti alloy, the effect of coating thickness on the apparent interfacial toughness is exactly the same whatever the nature of the coating as shown in Figure 7-5 and Figure 7-6, i.e. a decrease of the K_{ca} with coating thickness (except for h_c = 100 µm NiCr where K_{ca} is almost the same than for h_c = 300 µm) was observed. This is because the state of residual stress at the interface is in tensile and this has been previously determined in Table 6-3 using the relation $K_{ca} = f(1/ h_c^{\ 2})$ and was in agreement with physical properties of matarials.

For the steel substrate it seems to be an inverse behaviour, i.e. the apparent interface toughness generally increases with coating thickness (except h_c= 300 for combination Al-F-300-6/st) and the relation $K_{ca}= f(1/ h_c^{\ 2})$ suggests a state of compressive stress at the interface (Figure 7-7 and Figure 7-8). This is in perfect accordance with the residual stresses calculated using the curvature methodology which gave smaller compressive stress values for higher thickness.

However, Steel and Ti alloy substrates have different thermal expansion coefficients. After spraying and cooling, this could lead to a very different state of residual stress either tensile or compressive in the coating even for identical spraying conditions. The difference in materials is a known to affect the state of stress in an important extent and possibly the sign of the stress [91, 243].

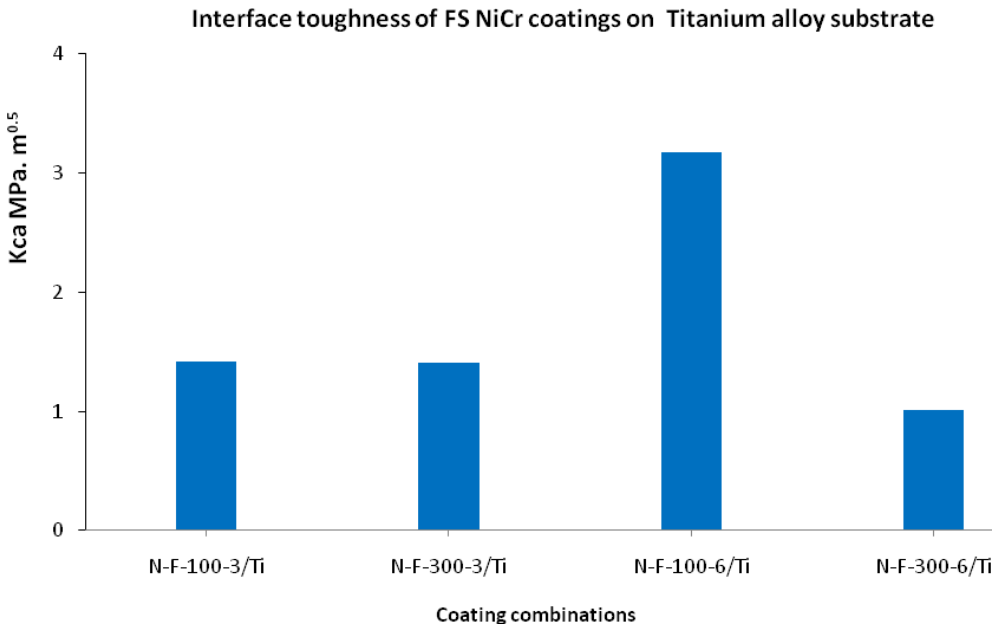

Figure 7-5: apparent interface toughness of NiCr coatings on titanium alloy substrate.

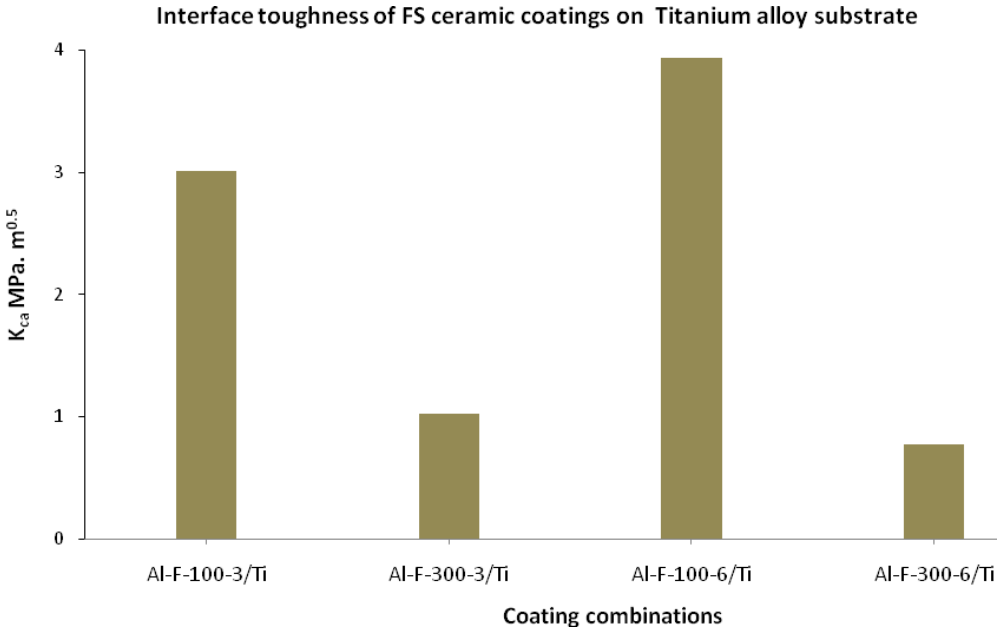

Figure 7-6: apparent interface toughness of Al_2O_3 coatings on titanium alloy substrate.

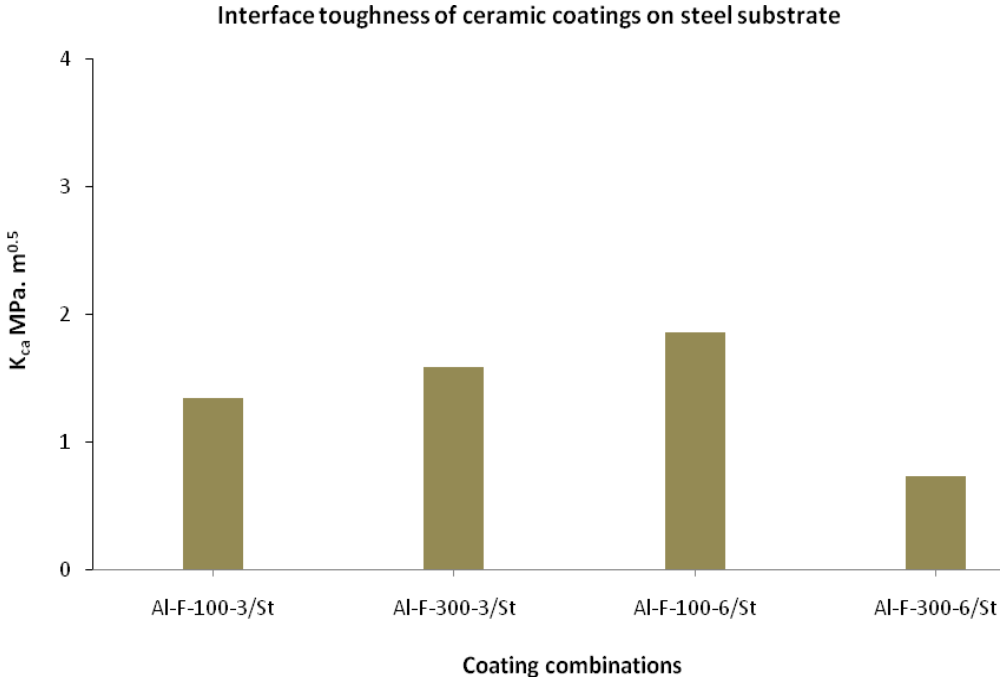

Figure 7-7: apparent interface toughness of Al_2O_3 coatings on steel substrate.

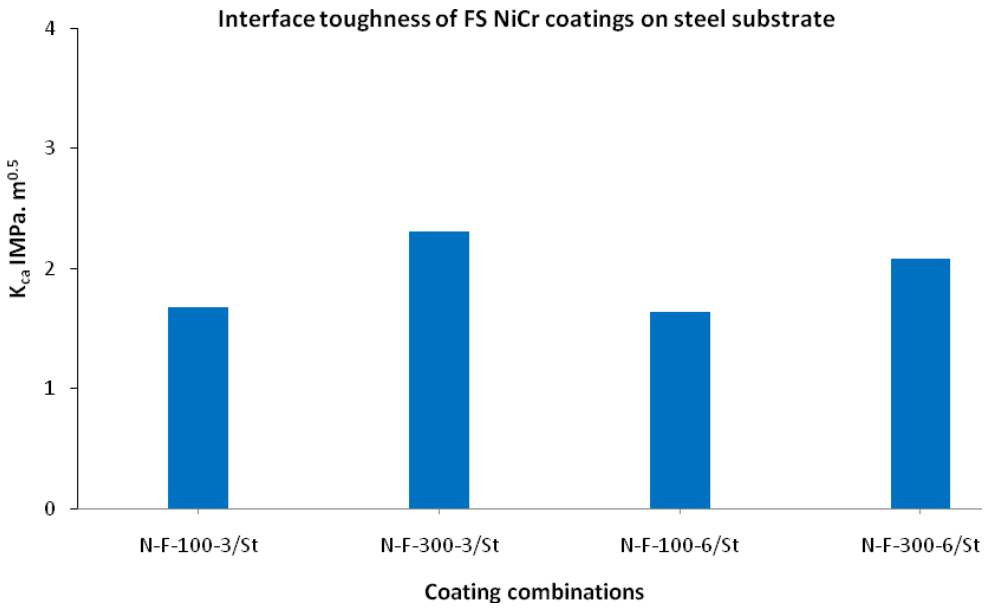

Figure 7-8: apparent interface toughness of FS NiCr coatings on steel substrate.

From Figure 7-9, the apparent interfacial toughness of Cer /Ni pl- x/ Cer shows higher than that of Cer /Ni pl/ Cer, because in the interfacial indention, the loading and stress intensity at the interface by interfacial indentation could drive the crack easily in the smooth interface than that roughened one. The combination Cer /NiCr/ Cer shows a low interfacial toughness value comparing to Ni plating interlayer and this was related to the microstructure features and mechanical properties of the inner layers, since the thermal spray technique provides different microstructure of coatings than that obtained by electrochemical deposition, e.g. interfaces between splats and in some cases oxides and these can facilitate crack propagation. On the other hand, Ni plating showed to have better mechanical properties than the other inner layers (Table 5-6). Combination 29 with Ni-plating-X interlayer shows a dense and strong interface to cermet coating in Figure 5-3 and Figure 7-10-a, whereas, the combination 27 with Co-Cr as interlayer exhibit lots of oxide layer are many microcracks propagated through the coating during indentation as shown in Figure 7-10-b. However, other adhesion test e.g. impact test was carried out on such sandwich combinations, fracture analysis was detailed. Results of sandwich adhesion were previously reported by Hadad [190, 191].

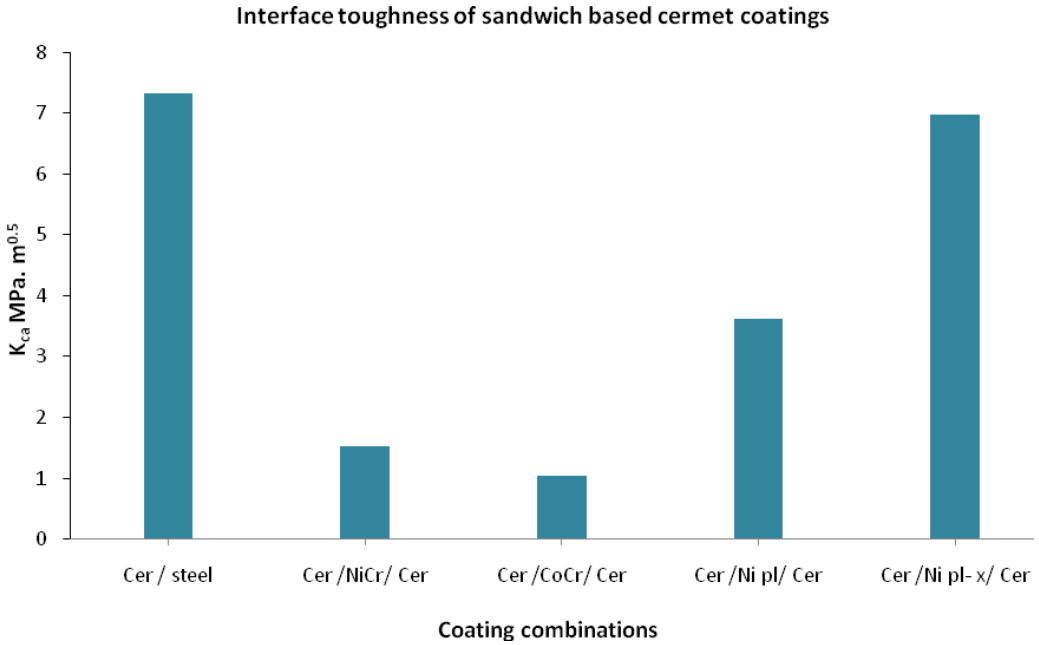

Figure 7-9: apparent interface toughness of sandwich based cermet coatings.

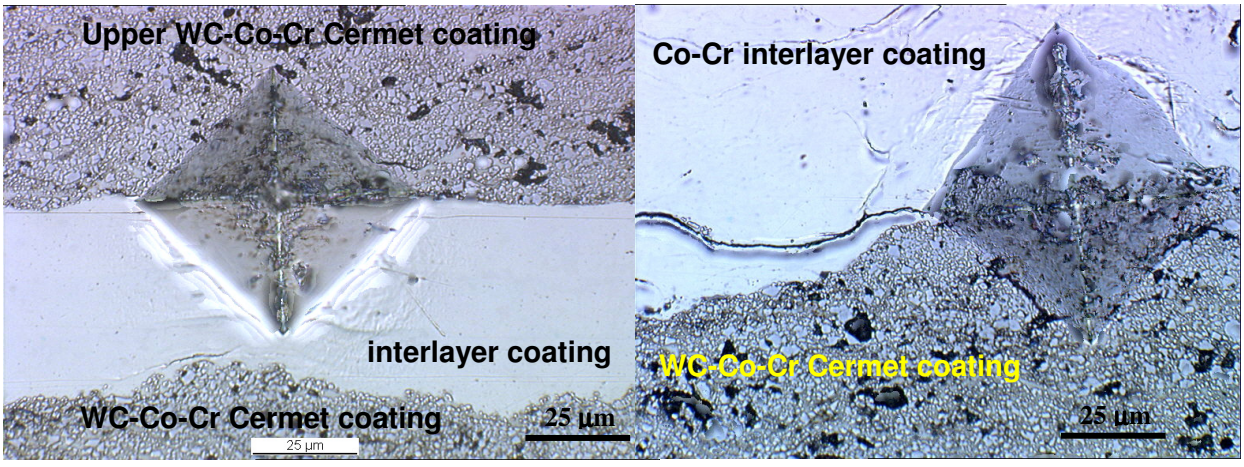

a) b)

Figure 7-10: micrograph of indentation at the interface between interlayer and cermet coating, a) combination 29- Cermet/Ni Plating-X /Cermet, b) interfacial indentation and cracks propagation through the Co-Cr inner coating in combination 27 Cer /CoCr/ Cer [190, 191].

The effect of residual stress relief on interfacial toughness can be seen in Figure 7-11 and this will be discussed in section 5-2 in this chapter, after having anlysed the annealed samples. However, Figure 7-12 and Figure 7-13 illustrate an example of as sprayed and annealed coatings in bilogarithmic graphs inlcluding error bars (cannot be seen, they are very small) to determine the critical point p_c and a_c, subsequently, the interface toughness.

To conclude, such test method did not give only a physical order of adhesion, but also, this method could be applied for a wide range of dissimilar coatings and substrates. In our case, metallic, ceramic and composite coating materials were all tested, the coherence of results gave a meaningful physical order of adhesion.

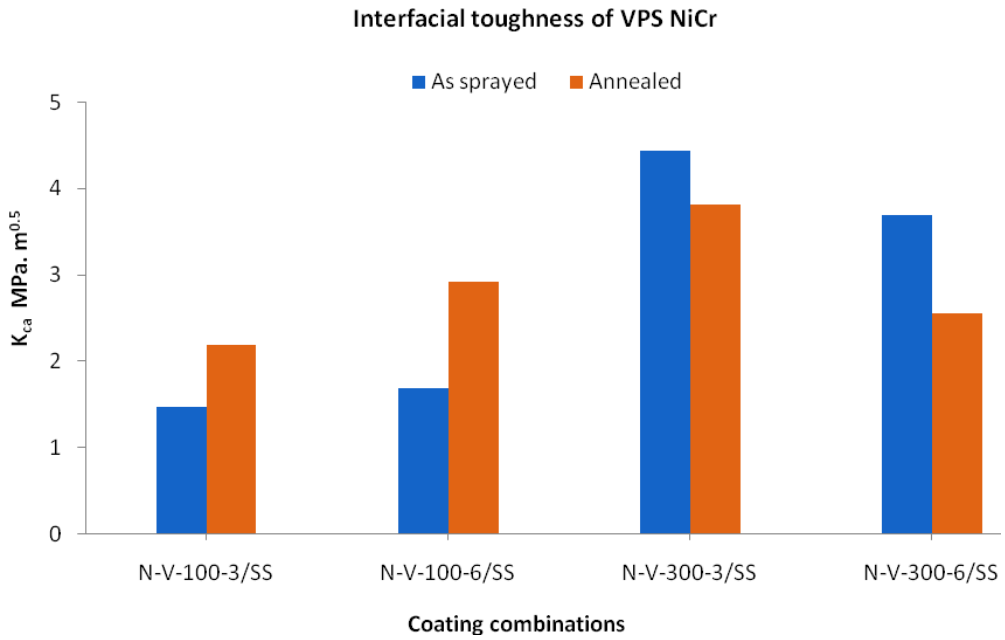

Figure 7-11: apparent interfacial toughness of VPS NiCr as sprayed and annealed coatings.

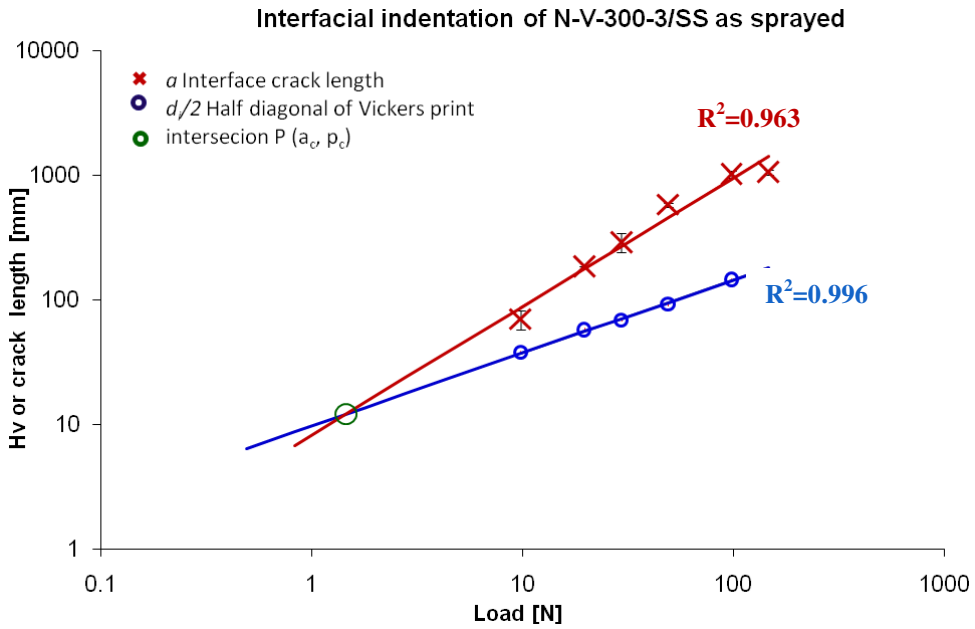

Figure 7-12: bilogarithmic plot of two segments, diagonal of hardness and crack length of VPS NiCr as sprayed coating.

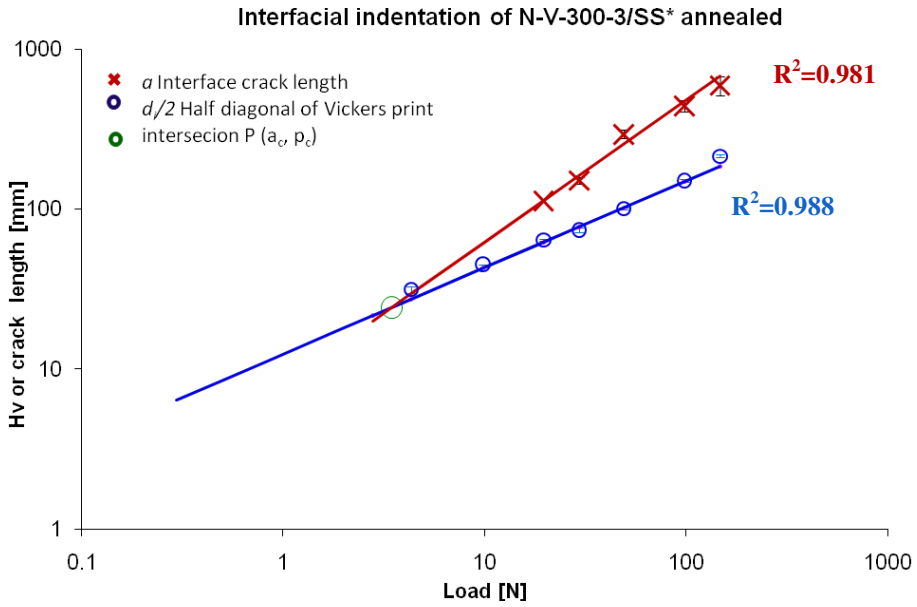

Figure 7-13: bilogarithmic plot of two segments, diagonal of hardness and crack length of VPS NiCr annealed coating.

3. IN-PLANE TENSILE TEST

The aim of this study is to apply the fragmentation technique via in-plane tensile test for thermally sprayed coating to drive expressions for interface coating toughness at critical strain and for the interfacial shear strength at the crack saturation level from simple stress transfer analysis.

Two cases in our analysis are considered:

i. ductile coating on ductile substrate (NiCr coating),

ii. brittle coating on ductile substrate (Al_2O_3 coating),

In the first case, the coating failure was dominated by cracks population as shown in Figure 7-14-a &b. In the second case, is involving brittle coating on ductile substrate: the critical strain is reached when the first crack appears and propagates through the interface and leads to coating decohesion as shown in Figure 7-14-c & d. Therefore, based in a theoretical model, the energy release rate and the corresponding interface toughness will be calculated.

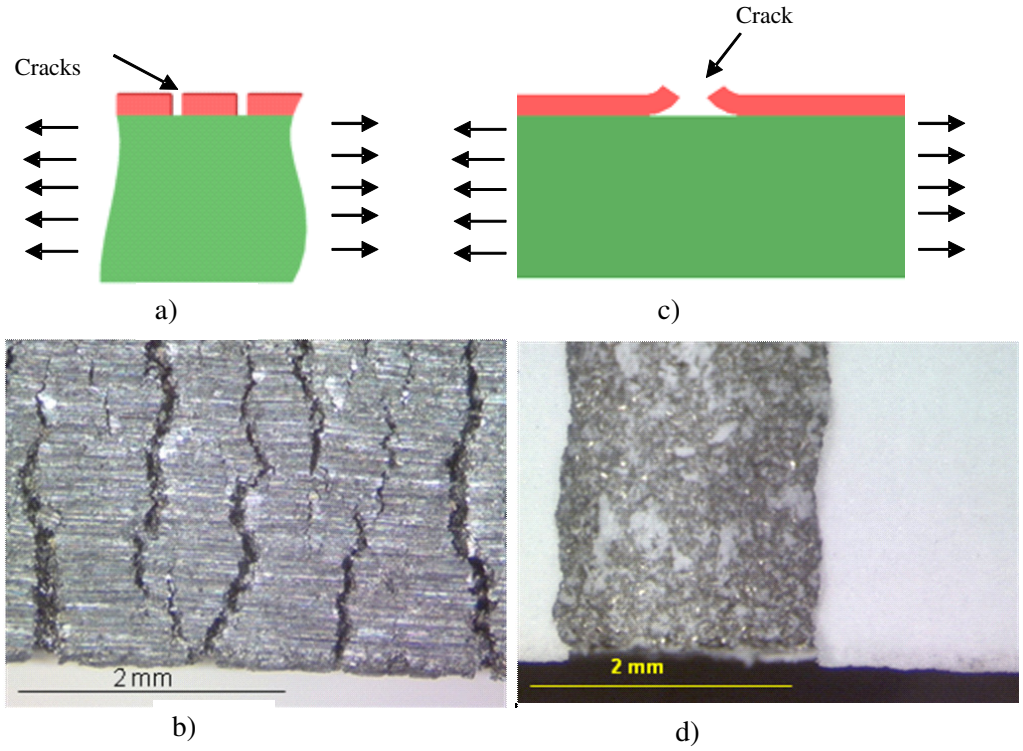

Figure 7-14: a) schematic side view of coating with crack fragmentation, b) upper view micrograph of coating governed by cracks fragmentation, c) schematic side view of coating failure with crack propagated through the coating then to the interface, d) upper view micrograph of coating failure by crack propagation in the coating and through the interface.

3.1 THEORETICAL MODEL OF STRESS TRANSFER ANALYSIS

The origin of the elastic stress transfer is based on the theory of fibre composite, where the interface transfers the stress from matrix to the fibre. Kelly et al. [244] first assumed that for reinforcement with discontinuous fibres, the applied load must be transferred to the fibres by means of shear forces at the fibre/matrix interface. If the matrix is a metal, the plastic flow will occur there first. It is further assumed that the whole of the matrix yield plastically and flows past the fibre which is stretched by the shear forces acting at the interface.

Kelly and Tyson [244] defined the critical length at the saturation stage under tension loading as the largest fragment which cannot break. So a fragment of length $l_c\ (1+\varepsilon)$ always breaks whereas one of length $l_c\ (1-\varepsilon)$ does not. Owing to this definition, all the fragments are uniformly distributed and will have a final crack spacing of between $l_c/2$ and l_c. Therefore, the critical fragment length is defined as:

$$l_C = 2.r.\frac{\sigma_{\max}}{\tau} \quad [245] \qquad 7\text{-}1$$

where σ_{max} is the tensile stress in fibre at the distance l_c from the end of the fibre, τ is the shear stress at interface and r is the fibre diameter (Figure 7-15).

In composite materials, several researchers therefore applied the crack fragmentation test model based on Kelly and Tyson theory [155-160] of stress transfer of single fibre relating the critical fibre length to interfacial shear stress. Figure 7-15 illustrates a simple single fibre model [245].

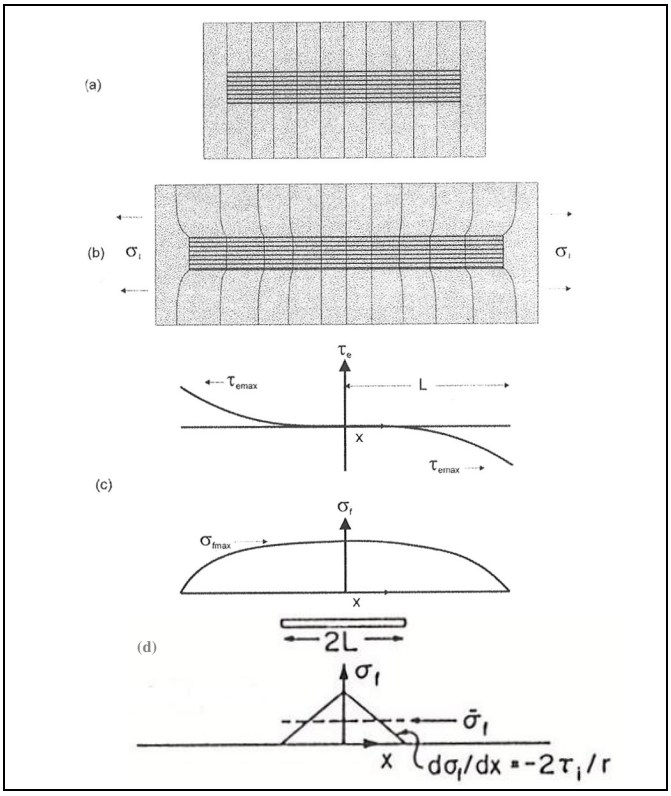

Figure 7-15: single fibre composite element: a) unstressed and b) stressed, c) shows the fibre -matrix interfacial stress and fibre internal stress transfer, d) shows the fibre length equal to the critical value [245].

Calculating the mean crack spacing is by analogy of car parking system is used, the minimum average spacing between cars of length parked at random in a given space. The average crack spacing in a length of composite has been quoted by Kimber and Aveston et al, [154, 155] to be (1,36 l_c/2) and this was theoretically and experimentally proved by Beeby [246, 247] who also found an average crack spacing of the same value. The critical crack spacing l_c has also been experimentally determined and modelled in several situations [6, 248] and was related using a stochastic failure approach to the average fragment length at saturation; the exact calculation of $\bar{l}$ as the mean crack spacing when an increase in strain does not lead to further fragmentation of the coating is $\bar{l} = 0{,}67.l_c$.

Fraser et al. [248] originally described the fibre fragmentation test and they are based on coupling of statistical fibre strength model with a computer simulated stochastic model. The test results were found in a good agreement with the theoretical models of critical crack spacing. The fibre composite test has become

one of the key methods to study failure mechanisms in fibre-reinforced composites, and most of the theoretical treatments of the fragmentation test can be found in the corresponding literature [249-258].

3.2 DETERMINATION OF INTERFACIAL SHEAR STRENGTH VIA CRACK FRAGMENTATION TECHNIQUE

In our case of study; a coating/substrate system is considered. The applied shear stress is being transferred from substrate to the coating and it generates progressive transversal crack fragmentations of coatings till cracks density reaches the saturation level. Therefore, cracks spacing can be calculated on the strained coatings.

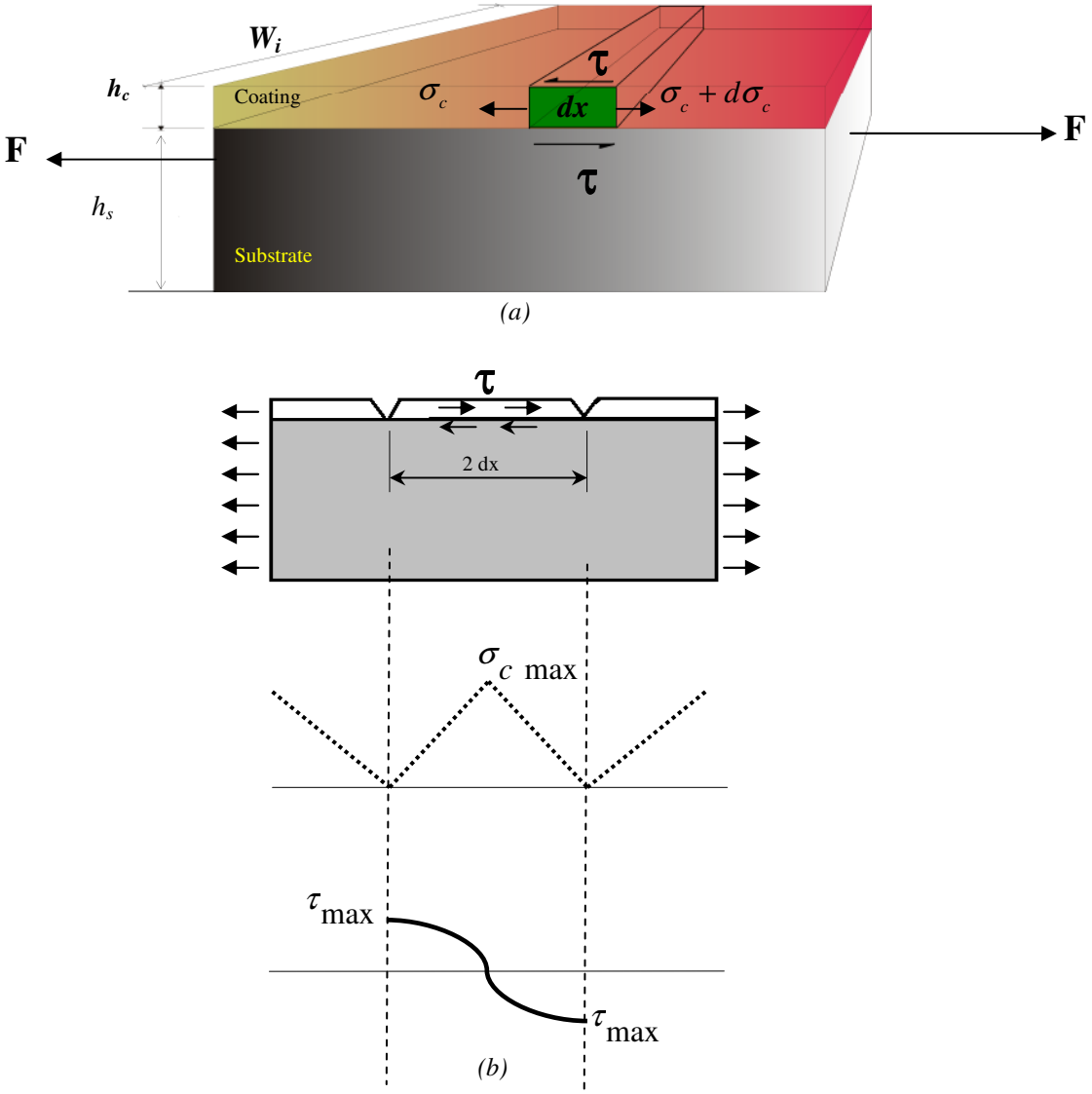

Figure 7-16: a): equilibrium of infinitesimal of coating dx length and h_c thickness along the loading direction, b) shear stress distribution on membrane.

The shear stress at the interface τ can be calculated from the equilibrium of infinitesimal of coating of *dx* length, thickness h_c and width W_i under tensile stress σ_c parallel to the interface as shown in Figure 7-16.

$$W_i.h_C.\sigma_c + W_i.dx.\tau = W_i.h_C.(\sigma_c + d\sigma_c) \qquad 7\text{-}2$$

$$\frac{d\sigma_c}{dx} = \frac{\tau}{h_c} \qquad 7\text{-}3$$

According to the previous analysis, the equation (7-3) was integrated with similar approach to that found in composite relating the critical length to shear stress [154, 155, 245]. Where the critical crack spacing in our case l_c is defined as

the minimum length for which the generated tensile stress $\sigma_{max,\ c}$ reaches a critical value to nucleate a crack and lead to breaking of the coating [245, 259]:

$$l_c = 2.h_c.\frac{\sigma_{\max,\ c}}{\tau} \qquad 7\text{-}4$$

If we consider $\bar{l} = 0{,}67.l_c$, the equation (7.4) becomes:

$$\tau = 1{,}34.h_c.\frac{\sigma_{\max,\ c}}{\bar{l}} \qquad 7\text{-}5$$

Figure 7-17 shows, the fragment length l_i, the mean crack spacing $\bar{l}$ can be calculated at increasing strain levels ε in terms of the inverse of crack density "CD" when i the cracks number are transversally propagated within the coating experimentally counted in L length unite:

$$CD = \frac{i}{L} = \frac{1}{\bar{l}} \qquad 7\text{-}6$$

Replacing (7-6) in (7-5), we can express the interfacial shear strength versus crack density:

$$\tau = 1{,}34.h_C\ .\sigma_{max,\ c}.\frac{i}{L} \qquad 7\text{-}7$$

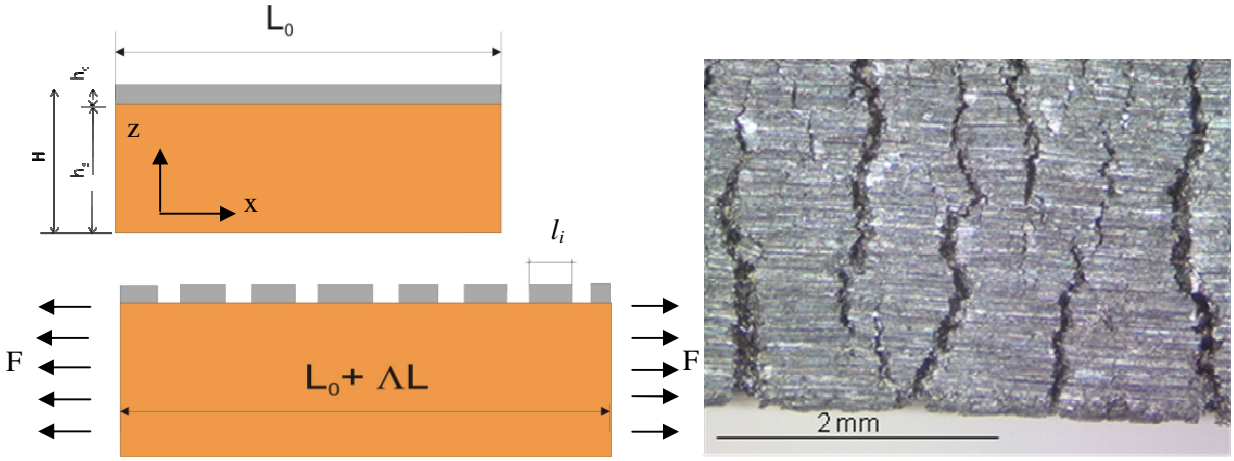

(a) (b)

Figure 7-17: a) schematic presentation of side-view of bi-layer system loaded in tensile stress, b) example of upper view of crack fragmentation in NiCr 80-20 thermally sprayed coating on a Steel substrate.

Figure 7-19 shows a cross sectioned FS NiCr coating on a steel substrate with different magnifications after substrate rupture. The substrate is completely strained up to 19%. The cracks within the coating are at the last stage of saturation level of fragmentations. In spite of crack bifurcation in some case through the interface (point C in the bottom of the micrograph), it is very interesting to observe a strong adhesion and an intact interface in the middle of the fragmented coating.

In tensile loading, the crack fragmentation process can be divided mainly in three stages as shown in Figure 7-18.

In the first stage "A", the tensile loading increases with time till cracks randomly take place within the coating, where the tensile strength of coating attaints his highest value $\sigma_{max,\,c}$. In ductile coatings, the first crack appears in coating within the plastic deformation stage. In the second stage "B" which corresponds to a semi-linear increase of crack density where new cracks nucleate and crack spacing increases accordingly. In the last stage "C", nor further cracks initiate, the fragmentation rate virtually stops and reaches the saturation stage and this can be accompanied with some coating delamination.

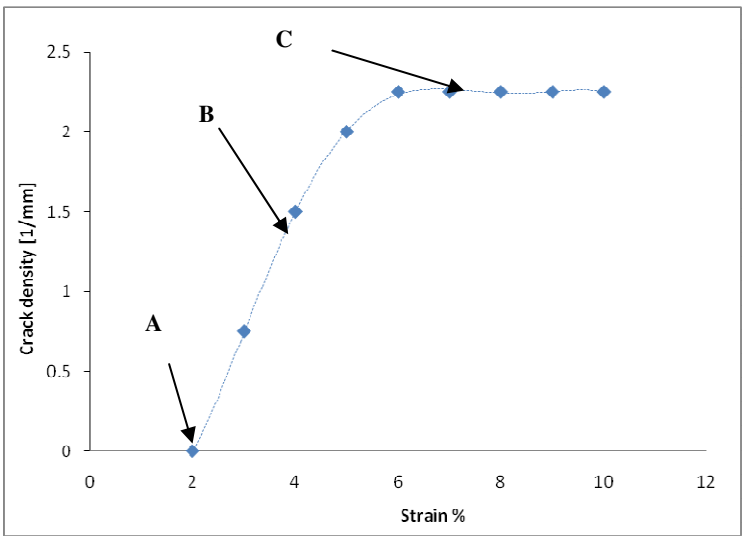

Figure 7-18: the three main stages of coating fragmentation (example of combination 3, N-F-100-6/St).

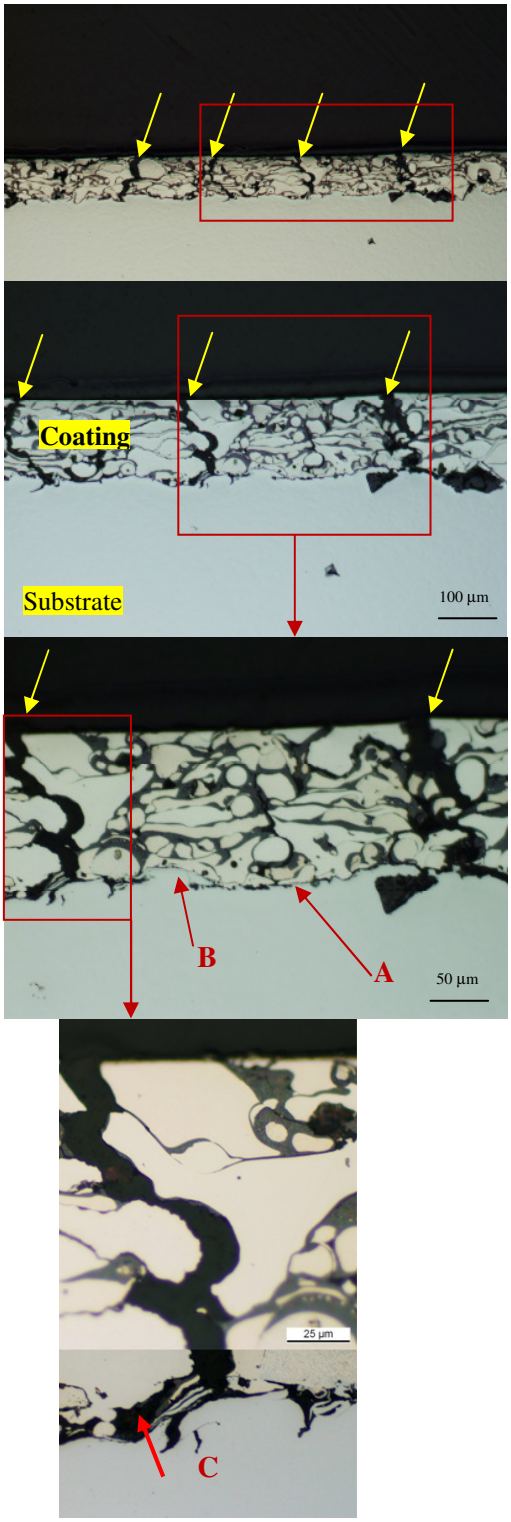

Figure 7-19: cross sectioned FS NiCr 80-20 thermally sprayed coating on a Steel substrate showing transversal cracks with yellow arrays perpendicular to the interface and crack bifurcation through the interface.

3.3 RESIDUAL STRESS RELAXATION

The equation (7-7) presents only the apparent interfacial shear strength, since the residual stresses are not explicitly accounted for. Therefore, interfacial shear strength is a value of practical adhesion and not an intrinsic property of coating/substrate system. This τ is a sum of an intrinsic term τ_{int}, and residual stress term τ_{res}.

The formation of cracks in the coating produces a relaxation in the macroscopic stresses in the coating and at the interface coating-substrate, subsequently, will result in a proportional change in apparent interfacial shear strength [260]. Therefore, the apparent interfacial shear strength is linearly dependent on the residual stress. The magnitude of the stress relaxation $\Delta\sigma_{res}$ is proportional to the residual stress exhibits in the coating σ_{res}. In elasticity theory, the stress relaxation mechanism at the coating/substrate interface was found to be inversely proportional to the radial distance from the crack [261-263]. Grosskreutz and McNeil [262] assumed that the stress is elastic, and then the relaxation field will be over the fragment length characteristic. In fragmentation, the average stress in fragment decreases with decreasing fragment size till the saturation stage is reached. At the saturation crack fragmentation, $\bar{l} = 0.67.l_c$ as previously reported. Therefore, the average residual stress at the saturation ($\sigma_{res,c}$) can, with the assumption of constant shear stress, yield

$$\sigma_{res,c} = 0{,}67.\sigma_{res} \qquad 7\text{-}8$$

Therefore, the apparent tensile strength $\sigma_{max,c}$ can be expressed:

$$\sigma_{max,c} = \sigma_{int}(l_c) + 0{,}67.\sigma_{res} \qquad 7\text{-}9$$

The term $\sigma_{int}(l_c)$ presents the intrinsic tensile strength of the coating $\sigma_{int}(l_c)=\sigma_{max,c}- 0{,}67.\sigma_{res}$ and $\sigma_{max,\,c}$ is the apparent tensile coating strength that can be measured experimentally when first crack appears in the fragmentation stage. Considering τ as the sum of an intrinsic term τ_{int}, and residual term $\tau_{res.}$ This τ can be expressed by replacing (7-9) in (7-4), and in (7-5):

$$\tau = \tau_{int} + \tau_{res} = 2.h_c.\frac{\sigma_{int}(l_c) + 0{,}67.\sigma_{res}}{l_c} = 1{,}34.h_c.\frac{\sigma_{int}(l_c) + 0{,}67.\sigma_{res}}{\bar{l}} \qquad 7\text{-}10$$

However, any change in residual stress level will result in a proportional change in apparent interface shear strength $\Delta\tau = 1.34.h_c.\frac{\Delta\sigma_{res}}{\bar{l}}$.

Replacing the equation (7-10) in (7-7), we can finally express the ***apparent*** interfacial shear strength (AISS) versus the crack density:

$$\tau = 1{,}34.h_C\,\sigma_{\max c}.\frac{i}{L} = 1{,}34.h_C.(\sigma_{\text{int}}(l_c) + 0{,}67.\sigma_{res})\frac{i}{L} \qquad 7\text{-}11$$

Whereas the ***intrinsic*** interfacial shear strength (IISS) versus the crack density can be given by:

$$\tau_{\text{int}} = 1{,}34.h_c.\sigma_{\text{int}}(l_c)\frac{i}{L} = 1{,}34.h_c.(\sigma_{\max c} - 0.67.\sigma_{res})\frac{i}{L} \qquad 7\text{-}12$$

3.4 DETERMINATION OF THE APPARENT COATING STRENGTH

The membrane stresses (we call it membrane to differentiate it to the bending one) in homogenous plate are distributed uniformly in the whole cross section. In plates with surface layers (perpendicular to loading axes) with different properties, the stresses will be different in each layer.

The tensile force externally applied can be a sum of two forces using the cross sectional approach, the equilibrium of diagram forces can be expressed as the following:

$$F = F_c + F_s \qquad 7\text{-}13$$

Considering the plane strain tensile modulus:

$$E'_{c,s} = \frac{E_{c,s}}{1-\nu^2_{c,s}} \qquad 7\text{-}14$$

$$\sigma.H = \sigma_c.h_c + \sigma_s.h_s \qquad 7\text{-}15$$

$$\sigma = \sigma_C.\frac{h_C}{H} + \sigma_S.\frac{h_S}{H} \qquad 7\text{-}16$$

c and s are denoted for coating and substrate respectively, H is the whole thickness of bi-layer sample (Figure 7-17), h is the thickness of substrate or coating, σ is the tensile stress and ν is the Poisson's ratio.

Considering the bi-layer strains are equal before first crack occurs in the elastic domain:

$\varepsilon_s = \varepsilon_s = \frac{\sigma_s}{E'_s} = \frac{\sigma_c}{E'_c}$, $\sigma_s = \sigma_c \frac{E'_s}{E'_c}$ replacing this in (7-16), this will give:

$$\sigma = \sigma_C . \left[\frac{h_c}{H} + . \frac{E'_s}{E'_c} . \frac{h_s}{H} \right] \qquad 7\text{-}17$$

$$\sigma . E'_c = \sigma_c . (E'_c . \frac{h_c}{H} + E'_s . \frac{h_s}{H}) \qquad 7\text{-}18$$

The stress distribution is schematically presented in Figure 7-20. σ_c reaches the maximum value of $\sigma_{max,c}$ when first crack channels within the coating. Replacing the effective elastic moduli (7-14) in equation (7-18) to obtain the apparent coating strength:

$$\sigma_c = \frac{\sigma . E_c . H}{E_c . h_c + \left(\frac{1 - \nu_c^{\,2}}{1 - \nu_s^{\,2}} \right) E_s . h_s} \qquad 7\text{-}19$$

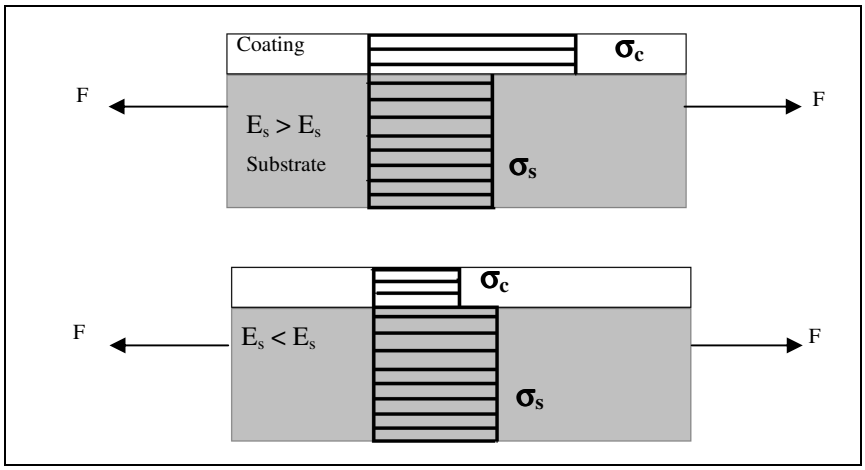

Figure 7-20: stress distribution in coating-substrate system loaded by uniaxial force.

3.5 DETERMINATION OF ENERGY RELEASE RATE

The amount of energy released by unit increment of fracture surface is referred to, as the strain energy release rate *G* with the principle of Griffith [264], the crack will propagate, if the energy release rate attains or exceeds a critical value.

$$G \geq G_c \qquad 7\text{-}20$$

The critical value G_c corresponds to the energy necessary for the creation of unit area fracture surface, and this can be supplied by loading forces and generally expressed as:

$$G = \frac{dW}{dA} - \frac{dU}{dA} \qquad 7\text{-}21$$

where dW is the work done by external forces during the increase of the crack by a surface of dA, and dU is the increment of the energy simultaneously in the body. However, the quantity G_c is the fracture energy which is considered to be a material property in bulk materials which is independent of the applied loads and the geometry of the body. The interface toughness was derived from the analysis of energy release rate G_c for crack channelling in the coating- substrate system [12, 136, 259, 265] taking into account the internal stress contribution. In this case the G_c is expressed by:

$$\boldsymbol{G_C} = \frac{\pi}{\boldsymbol{2}} \frac{(\sigma_{res} + \sigma_{\max,c})^2}{E'_C} . h_c . g(\alpha, \beta) \qquad 7\text{-}22$$

Where $\sigma_{max,c}$ is the apparent coating strength, can be calculated from equation (7-19), and $g(\alpha,\beta)$ are the non-dimensional mismatch Dundurs parameters [8, 265-268] since the elastic properties of materials can be characterized by two constants: elastic modulus and Poisson's ratio. Two materials thus need four constants. However, if these materials are strongly bonded together, the strains in the interface area depend only on two parameters α and β as these are given bellow:

$$\alpha = \frac{E'_c - E'_s}{E'_c + E'_s}, \beta = \frac{1}{2} \cdot \frac{\mu_c(1-2\nu_s) - \mu_s(1-2\nu_c)}{\mu_c(1-\nu_s) - \mu_s(1-\nu_c)} \qquad 7\text{-}23$$

Where: $\mu_{c,s} = \frac{E_{c,s}}{2(1-\nu_{c,s})}$ and $E'_{c,s} = \frac{E_{c,s}}{1-\nu_{c,s}}$ *7-24*

The parameters α and β both vanish when dissimilarity between elastic properties of the materials is absent. α and β change signs when the materials are switched. It is clear from (7-23) that α can vary from -1 to +1. In Addition, the physical admissible range of β with respect to α can be obtained by restricting μ (the shear modulus) to be positive and requiring $0 \leq \nu \leq 0.5$ such that $|\alpha\text{-}4\beta| \leq 1$. The Dundurs α and β parameters were calculated prior to the mechanical properties of

materials, g (α, β) was depicted from the detailed study performed by Beuth as shown in Figure 7-21 [8]. The summarized Table 7-3 presents all these parameters.

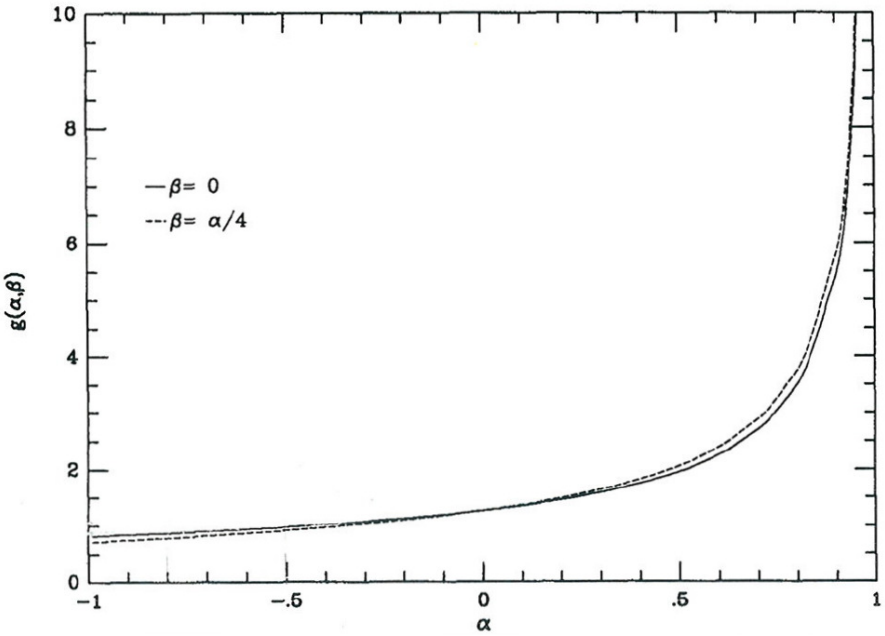

Figure 7-21: plot of g(a, b) for a fully cracked film problem [8].

Table 7-3: summary of Dundurs parameters α, β and g prior to coating combinations

	NiCr FS/steel N° 1-4	NiCr FS/Ti alloy N° 5-8	Al Fs/ Steel N° 9-12	Al FS/ Ti N°13-16	NiCr VPS / SS As sprayed	NiCr VPS / SS Annealed
E_c [MPa]	97500	97500	47500	47500	187653	14235
v_c [-]	0.265	0.265	0.25	0.25	0.265	0.265
E'_c [MPa]	104864	104864	50667	50667	201826	15310
μ_c [MPa]	38538	38538	19000	19000	74171	5626
E_s [MPa]	214000	151000	214000	151000	202088	192000
v_s [-]	0.29	0.29	0.29	0.29	0.29	0.29
E_s' [MPa]	233650	164865	233650	164865	220644	209630
μ_s [MPa]	82946	58527	82946	58527	78329	74419
α	-0.38	-0.22	-0.64	-0.53	-0.04	-0.86
β	-0.13	-0.08	-0.22	-0.19	-0.03	-0.28
g	0.9	1.2	0.93	0.9	1.25	1.18

In the tensile experiments of brittle coating and ductile coating, the strained coating follow the substrate deformation till first crack occurred transversally within the coating parallel to the interface. Therefore, this energy release rate

approach stands for calculating the fracture energy to channel crack at interface as shown in equation (7-22).

The crack of brittle Al_2O_3 coating propagates within the coating and extends though the interface as presented in Figure 7-22.

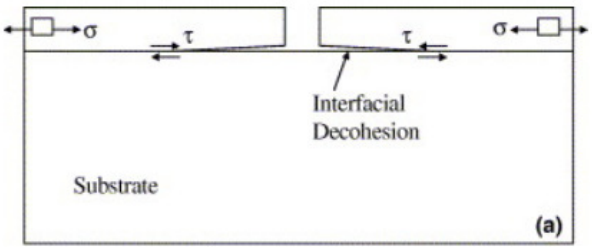

Figure 7-22: interfacial decohesion of Al_2O_3 coating.

If the substrate or coating has lower toughness compared to the interface, cracking may occur in the substrate or in the coating [268], but that possibility is not considered here. The fundamental approach to evaluate the interface coating toughness of brittle film was investigated by Thouless [269-272]. The energy release rate for the plane strain interface crack under axial tension was studied by Mincek and Henrik [12, 273, 274] and can be expressed by:

$$G_c = \frac{1-\nu^2}{E_c}(k_I^2 + k_{II}^2) = 0.5\,\frac{1-\nu^2}{Ec}.(\sigma_{max,\,c} + \sigma_{res})^2.h_C \qquad 7\text{-}25$$

Where K_I and K_{II} are the stress intensity factors. The interface toughness fracture can be expressed by [12, 208]:

$$K_{IC} = \sqrt{\frac{E_c.G_c}{(1-\upsilon_c^2)}} \qquad 7\text{-}26$$

3.6 RESULTS AND DISCUSSION

In-plane tensile tests were carried out on coating combinations from 1 to 24. The results can be divided in three tables prior to the deposition technique. The interface coating toughness, apparent intrinsic interfacial shear strengths are tabulated in Table 7-4, Table 7-5 and Table 7-6.

Table 7-4: apparent interfacial shear strength and interface coating toughness of FS NiCr coatings

Coating	Number	Nomenclature	$\sigma_{max,c}$ MPa	σ_{res} * MPa	i Crack number	Apparent/ intrinsic τ [MPa]	G_c (Eq. 7.22) $J.m^{0.5}$	K_{IC} (Eq. 7.26) MPa $m^{0.5}$
FS NiCr 80-20	1	N-F-100-3/St	239	-158	7	56/**31**	26	1.6
	2	N-F-300-3/St	247	-24	4	99/**93**	231	4.9
	3	N-F-100-6/St	241	-89	10	81/**61**	48	2.2
	4	N-F-300-6/St	244	-24	5	123/**115**	227	4.9
	5	N-F-100-3/Ti	759	386	10	254/**261**	1060	10.5
	6	N-F-300-3/Ti	713	62	3	215/**220**	2812	17.2
	7	N-F-100-6/Ti	754	646	16	404/**421**	1011	10.3
	8	N-F-300-6/Ti	736	525	4	296/**437**	856	9.5

*σ_{res} * the residual stress calculated from the interface indentation (Table 6-3)*

Table 7-5: interface toughness of FS Al_2O_3coatings

Coating	Number	Nomenclature	$\sigma_{max,c}$ MPa	G_c (Eq. 7.25) $J.m^{0.5}$	K_{IC} (Eq. 7.26) MPa $m^{0.5}$
FS Al_2O_3	9	Al-F-100-3/St	368	90	2.1
	10	Al-F-300-3/St	349	312	4.0
	11	Al-F-100-6/St	358	89	2.1
	12	Al-F-300-6/St	368	273	3.7
	13	Al-F-100-3/Ti	679	261	3.6
	14	Al-F-300-3/Ti	576	844	6.5
	15	Al-F-100-6/Ti	709	497	5.0
	16	Al-F-300-6/Ti	596	600	5.5

Table 7-6: results of VPS NiCr as sprayed and annealed coatings

Coating	Number	Nomenclature	$\sigma_{max,c}$ MPa		σ_{res} MPa		Crack N°		Apparent/ intrinsic τ MPa		K_{IC} (Eq. 7.26) MPa $m^{0.5}$	
			Mean	S.T	Mean	S.T	Mean	S.T	Mean	S.T	Mean	S.T
VPS NiCr 80-20	17	N-V-100-3/SS	700	6	-449	152	20	1	92/**52**	3/**11**	3.5	2.1
	18	N-V-100-3/SS*	521	8	-156	10	18	1	61/**48**	3/**1**	5.7	0.1
	19	N-V-300-3/SS	666	20	-203	19	16	3	219/**174**	38/**30**	11.2	0.8
	20	N-V-300-3/SS*	503	2	-121	17	13	1	126/**106**	8/**9**	10.3	0.5
	21	N-V-100-6/SS	693	20	-290	22	28	2	129/**92**	11/**11**	5.7	0.6
	22	N-V-100-6/SS*	504	15	-225	35	21	1	69/**49**	5/**1**	4.4	0.3
	23	N-V-300-6/SS	672	3	-231	20	22	2	292/**225**	27/22	10.7	0.4
	24	N-V-300-6/SS*	510	6	-166	19	13	1	128/**100**	9/**10**	9.3	0.7

When a ductile coating on ductile substrates subjected to uniaxial tension, the coating undergoes elastic deformation while the metal substrate undergoes elastic–plastic deformation. As the continuity between the coating and the substrate must be maintained at their interface before failure, this gives rise to interfacial shear stress when the coating inhibits deformation of the substrate. As a result of the interfacial shear stress, force is transferred from the substrate to the coating. As the substrate deformation increases, this tensile stress will accumulate and eventually reach the fracture strength of the coating. Parallel long cracks then show up on the surface of the substrate with the coating in a direction perpendicular to the tensile loading axis. Once the first array of multiple channel cracks are formed throughout the once continuous coating, the stresses within the cracked coating segments are relaxed and modified by the free edges of cracks. The first crack was occurred within the coating after 1.5-3% true strain of substrate-coating system, the energy release rate therefore was determined based on this stress-strain value. The interfacial shear values were measured after reaching the fragmentation saturation level and were determined at 8-10% true strain of coating-substrate system.

The maximum reached value of interfacial shear strength τ_{max} should be lower than or equal to the maximum shear flow stress of the substrate (i.e. the maximum shear stress can be exerted through the ductile substrate undergoing elasto- plastic deformation). These maximum values were found to be 123, 437 and 292 MPa of

coatings on St 52-3, Titanium alloy and AISI 304 substrates respectively as shown Table 7-4 and Table 7-6. One can estimate the shear flow stress of materials assuming the Von Mises isotropic plasticity, the shear stress is only $1/\sqrt{3}$ of the tensile yield strength as reported in Table 5-6.

For example; the yield strength of Ti alloy substrate is 865 MPa, according to Von Mises, the shear strength will be 499 MPa. (The coating yield strength was approximated to be three times the Vickers hardness value [217, 218]). To sum up, the obtained apparent interfacial shear strength (AISS) values were compared to shear flow stress of materials and we found that the AISS did not (in all the cases) exceed the shear strength of substrates. In addition, the maximum error bar (standard deviation) of AISS presented in such test was measured to be within 10% of the mean AISS value.

Figure 7-23 and Figure 7-24 show the apparent and intrinsic interfacial shear strength (AISS and IISS) of all coatings. The IISS is lower in magnitude than the AISS only for all coatings deposited on steel substrate, and this is due to the compressive residual stresses exhibited in the coating. The inverse behavior was observed for coatings on Ti alloy substrate, and this was mainly attributed to the tensile residual stress exhibits in the coating. These both behaviours, in tension and compression residual stress are in perfect harmony with the previsous investigation of residual stress in chapter 6.

Figure 7-25 shows the apparent interfacial shear strength (AISS) in a perfect accordance in general trend to the interface fracture toughness of FS NiCr coating on steel substrate. The (AISS) increased with the increase the coating thickness and roughness.

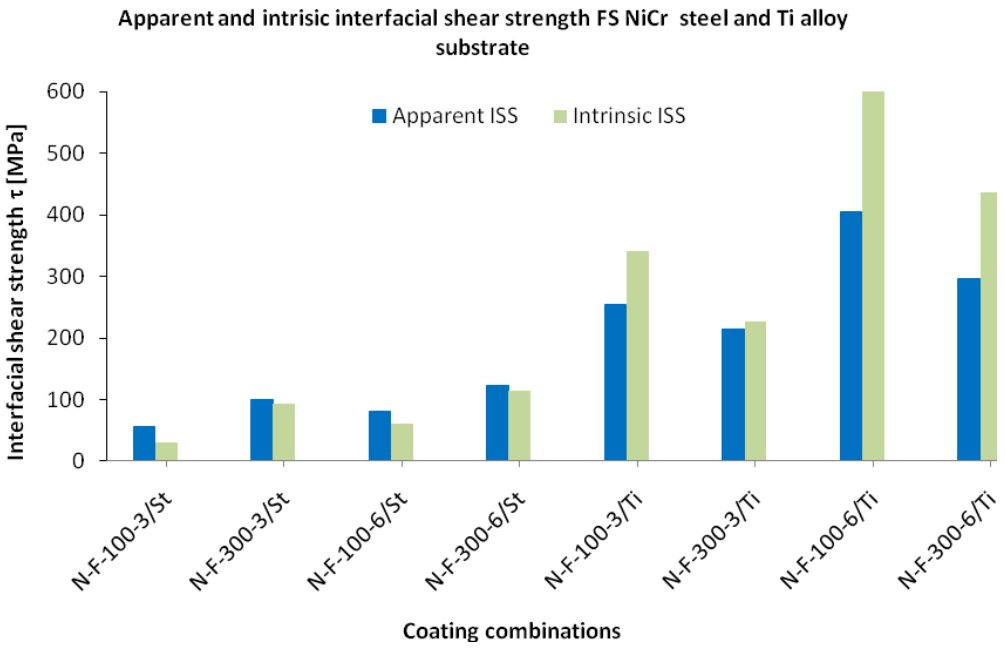

Figure 7-23: apparent and intrinsic interfacial shear strength of FS NiCr and Al_2O_3 coatings

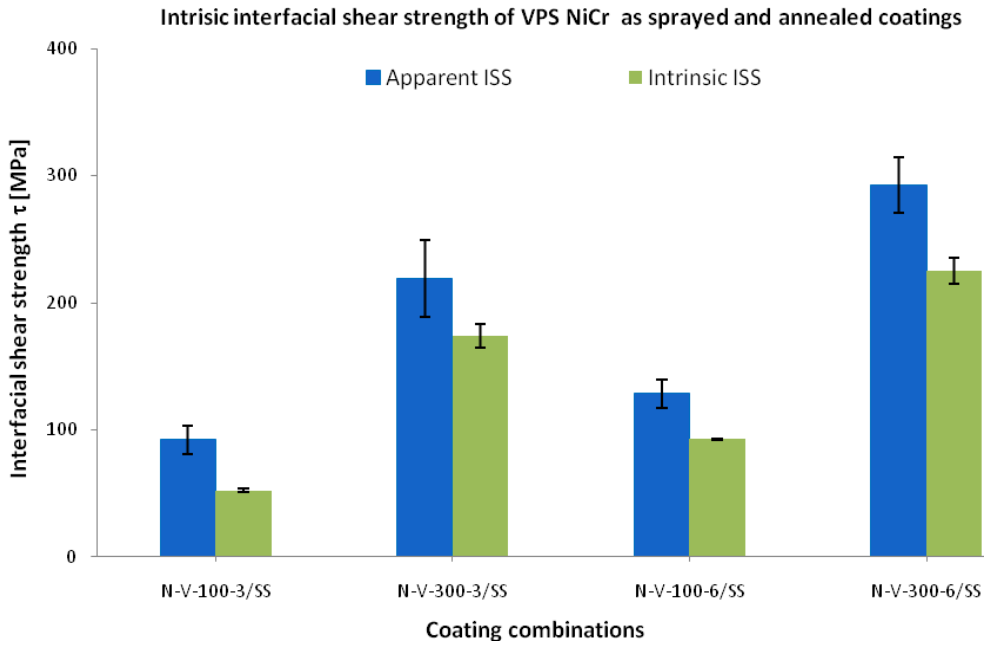

Figure 7-24: apparent and intrinsic interfacial shear strength of VPS NiCr coatings

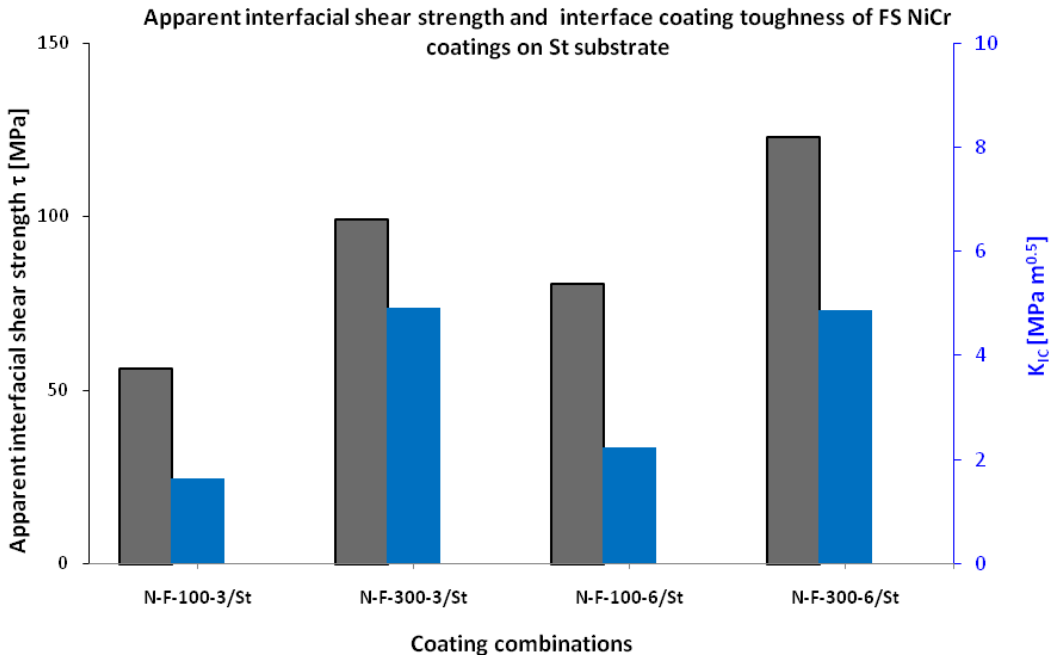

Figure 7-25: apparent interfacial shear strength and toughness of FS NiCr coatings on steel substrate (coloured bars are accorded to the vertical axes).

The results of metallic coatings on Ti alloy substrate are presented in Figure 7-26, an inverse behavior was observed to that of steel substrate, and this opposite behavior was mainly attributed to the residual stress state (in tensile) as previously observed and reported in chapter 6. The ceramic coating results presented in Figure 7-27 shows the AISS increased with coating thickness increasing and less sensitive to interface roughness.

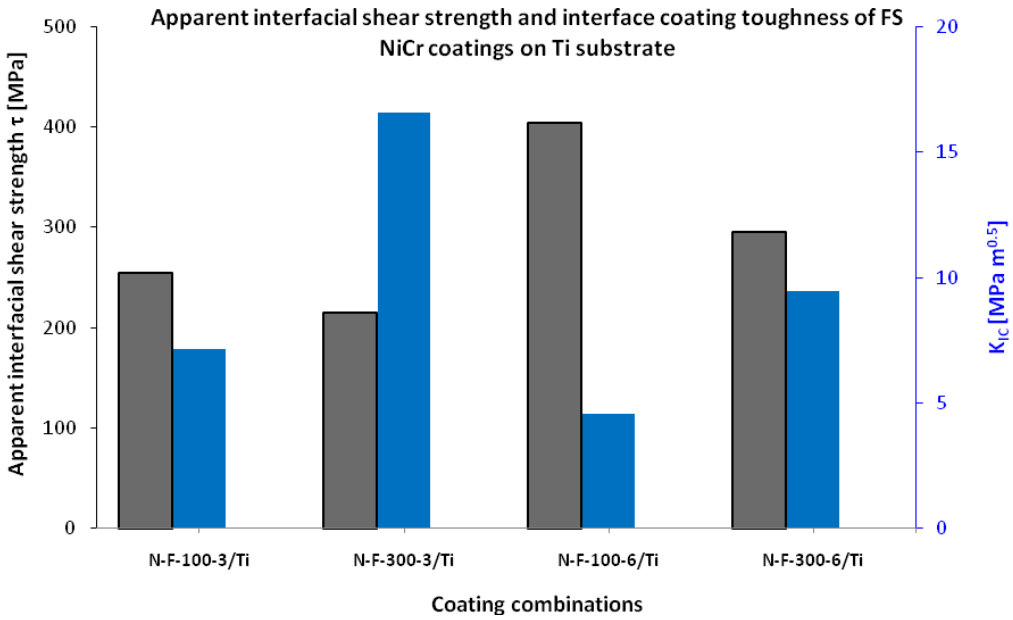

Figure 7-26: apparent interfacial shear strength and toughness of FS NiCr coatings on Ti alloy substrate (blue bar values are belonging to the right axe).

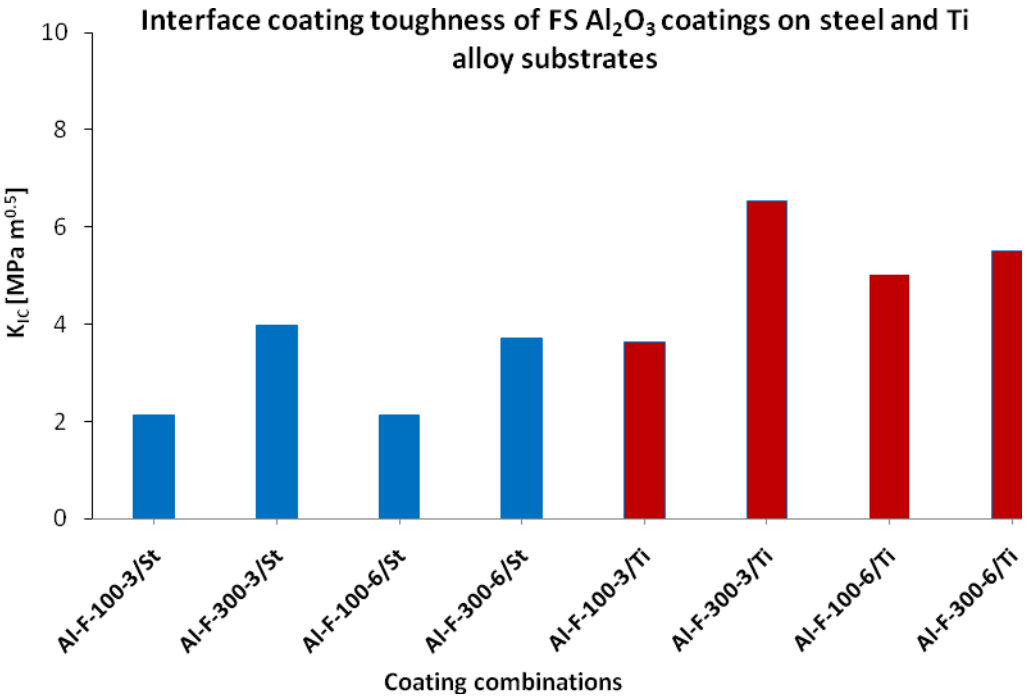

Figure 7-27: interface coating toughness of flame sprayed alumina coatings on both substrates, steel (blue bars) and Ti alloy (red bars)

The annealing effect will be discussed later. However, an important decrease of AISS can be observed due to annealing (Figure 7-28). The interfacial shear strength and the interface coating toughness of VPS NiCr as sprayed coating revealed interesting accordance between these both orders of adhesion presented

in Figure 7-29 showing a very good agreement with the apparent interfacial shear strength AISS prior to the increase in coating thickness and roughness. Annealing led also to decrease in interface coating toughness as presented in Figure 7-30 (except annealed samples of N-V-100-3-SS was higher than that of as sprayed one, this was mainly due to $\Delta\sigma=[\sigma_{max,c}+ (-\sigma_{res})]$ calculated in the energy release rate $G_c = 0.5 \frac{1-\nu^2}{Ec} .(\sigma_{max,\ c} + \sigma_{res})^2 .h_c$, because the residual stress relaxed in very large extent in the as sprayed sample and $\Delta\sigma$ therefore was smaller to that in the annealed one, subsequently, the energy release rate was greater). The high scatter in the K_{IC} of N-V-100-3/SS observed in Figure 7-30 was mainly attributed to the variation of residual stresses measured by bending curvature.

The shear stress distribution along the interface (Figure 7-16) of a cracked coating segment obtained in this work is not sinusoidal at all as previously suggested by Agrawal and Raj [151, 161]. Consequently, their method of measuring the interfacial shear strength of a metal–ceramic interface may be quite inaccurate. The ultimate shear strength of the silica films on annealed 99.9% pure copper and nickel substrates was estimated to be 900 and 1400 MPa, respectively. However, these numbers are questionable as they greatly exceed the shear flow strength level for both metal substrates. Similarly, the ultimate shear strength of the NiO–Pt interfaces reported by Shieu et al. [163] to be as high as 4460 MPa for a Pt substrate with a tensile strength of 145 MPa is also rather doubtful. Chen et al. [165] obtained the interfacial shear strength of a TiN coating on a steel substrate to be 650 MPa, which is also clearly higher than the shear flow strength of the steel (450 MPa). Zhang [275] obtained interfacial shear strength of hydroxyapatite coatings on Ti6Al4V substrates 392 to 571 MPa based on the Agrwal theory, where the interfacial shear strength τ_{max} in Agrwal model is derived on the assumption of zero residual stress. In his experimentation, when the tensile residual stress was taken into account, the shear strength increased from 393 to 573 MPa, it is very questionable results, since tensile residual stress helps crack propagation at the interface, subsequently, a decrease of shear strength should be expected rather than an increased one.

To sum up, we do believe such measurement seems to be coherent since no value acceded the yield strength of substrate or/and of coatings. However, the obtained interface fracture toughness deduced from fragmentation tests can be later compared to that by other methods.

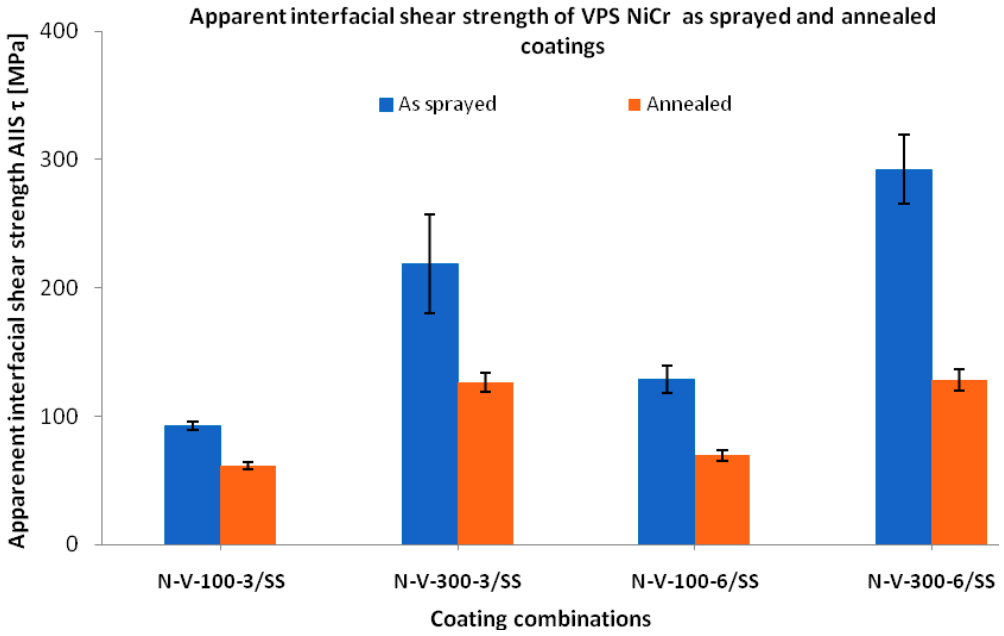

Figure 7-28: apparent interfacial shear strength of VPS NiCr 80-20 as sprayed and annealed coatings.

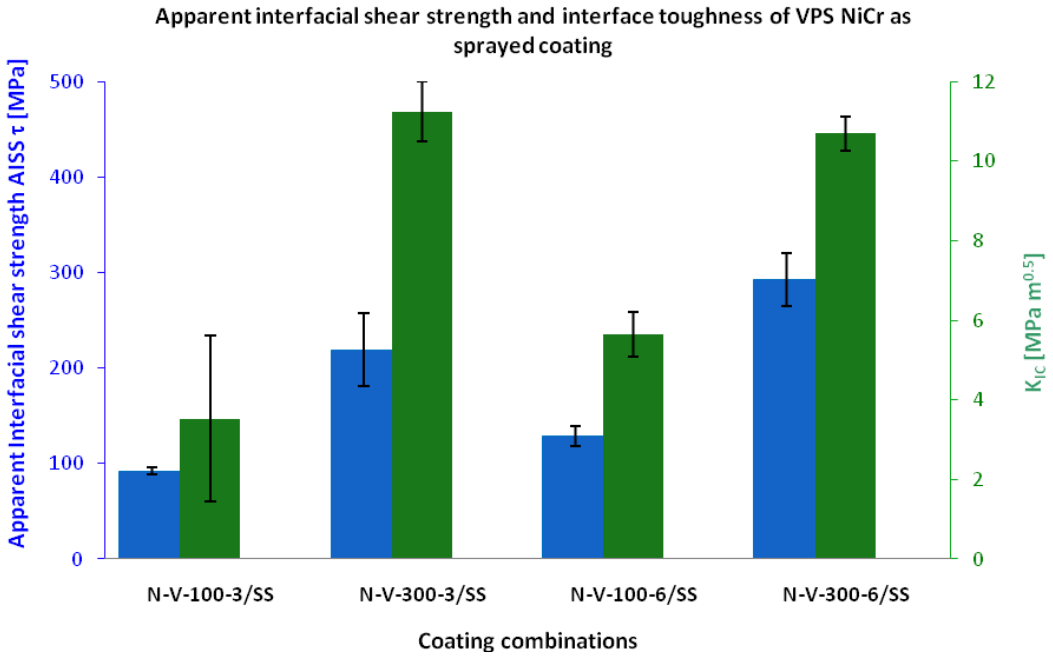

Figure 7-29: apparent interfacial shear strength AISS and toughness of VPS NiCr 80-20 as sprayed coatings (coloured bars are accorded to the corresponding vertical axes).

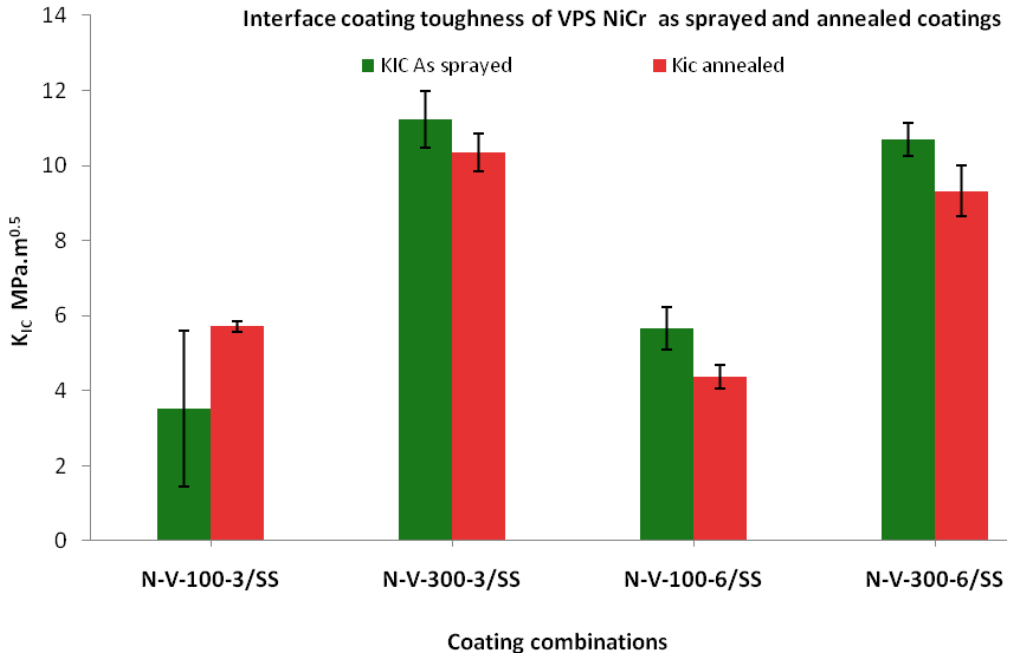

Figure 7-30: fracture toughness of VPS NiCr 80-20 as sprayed and annealed coatings.

In this study, interface fracture toughness and interfacial shear strength of ductile and brittle thermally sprayed coatings on ductile substrates were investigated using in-plane tensile test. This test method provides in a well controlled manner a large array of parallel cracks over the somewhat homogenously deformed ductile substrate and allows in situ observation of crack development in the coating with various microscopy tools. Additionally, the experimental set up is simple and inexpensive to build.

4. ROCKWELL INDENTATION AND FINITE ELEMENTS SIMULATION

The delamination radii were measured by an optical profilometer (Alti-surf 500-Cotec-France) and reported in Table 7-7. Furthermore, an example of 3D topographic measurement is presented in Figure 7-31. Figure 7-32 shows the finite elements calculations for C- Rockwell indentation into coatings on the Ti alloy substrate at maximum load. Three steps were applied on our model, Pre-loading in 50 N, Loading with 2452 N (corresponding to 250 Kg what experimentally performed), then unloading as shown in the example.

The displayed radial strain decreases at the surface with increasing distance from the indentation. The total strain deformations (elastic and plastic) vs.

delamination ratio are shown in Figure 7-33 and Figure 7-34 for the coatings deposited on steel and Ti alloy substrates, respectively. An example of the radial stress in function of delamiantion rate for brittle coating was calculated from the equation 7-27 and shown in Figure 7-35.

$$\sigma_{rr,Coating} = \frac{E_C}{1-\upsilon^2_C}.((\varepsilon_{\mathrm{rr,\,sub}}(r)+\varepsilon_{\mathrm{res}})+\upsilon_C.(\varepsilon_{\varphi\varphi,\,\mathrm{sub}}(r)+\varepsilon_{\mathrm{res}})) \qquad 7\text{-}27$$

Table 7-7: delamination ratio R/a of combinations

Process	Coatings	Number	Combinations	Delamination ratio R/a
FS	NiCr 80-20	1	N-F-100-3/St	1.20
		2	N-F-300-3/St	1.25
		3	N-F-100-6/St	1.03
		4	N-F-300-6/St	1.15
		5	N-F-100-3/Ti	1.27
		6	N-F-300-3/Ti	1.3
		7	N-F-100-6/Ti	1.04
		8	N-F-300-6/Ti	1.15
	Al_2O_3	9	Al-F-100-3/St	1.63
		10	Al-F-300-3/St	1.24
		11	Al-F-100-6/St	1.49
		12	Al-F-300-6/St	1.79
		13	Al-F-100-3/Ti	1.99
		14	Al-F-300-3/Ti	1.48
		15	Al-F-100-6/Ti	2.05
		16	Al-F-300-6/Ti	2.36

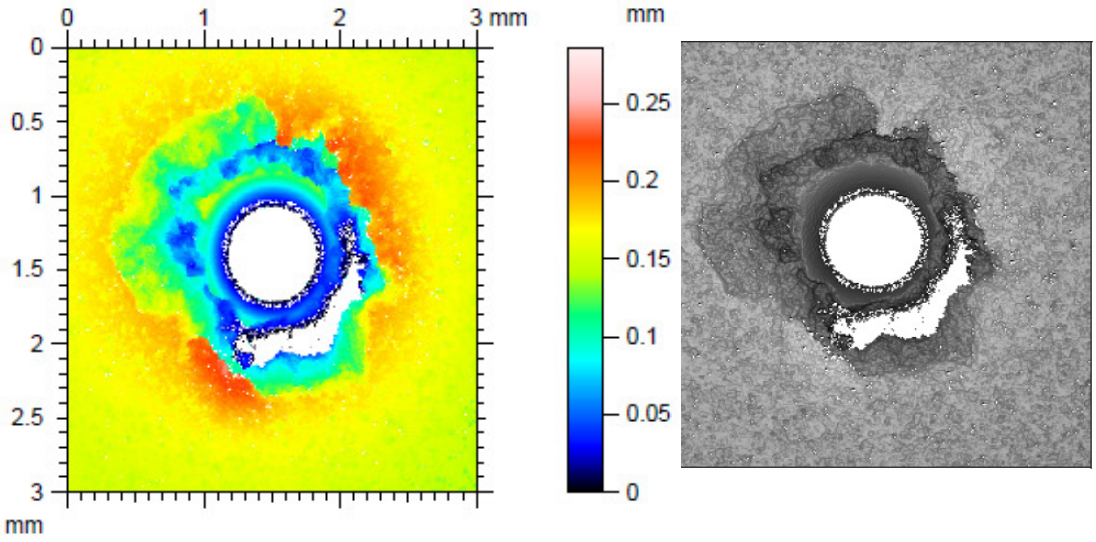

Figure 7-31: 3D topographic presentation of a Rockwell-C indentation into alumina coating on Ti alloy substrate (example of combination Al-F-300-6/Ti with delamination ratio of 2.36).

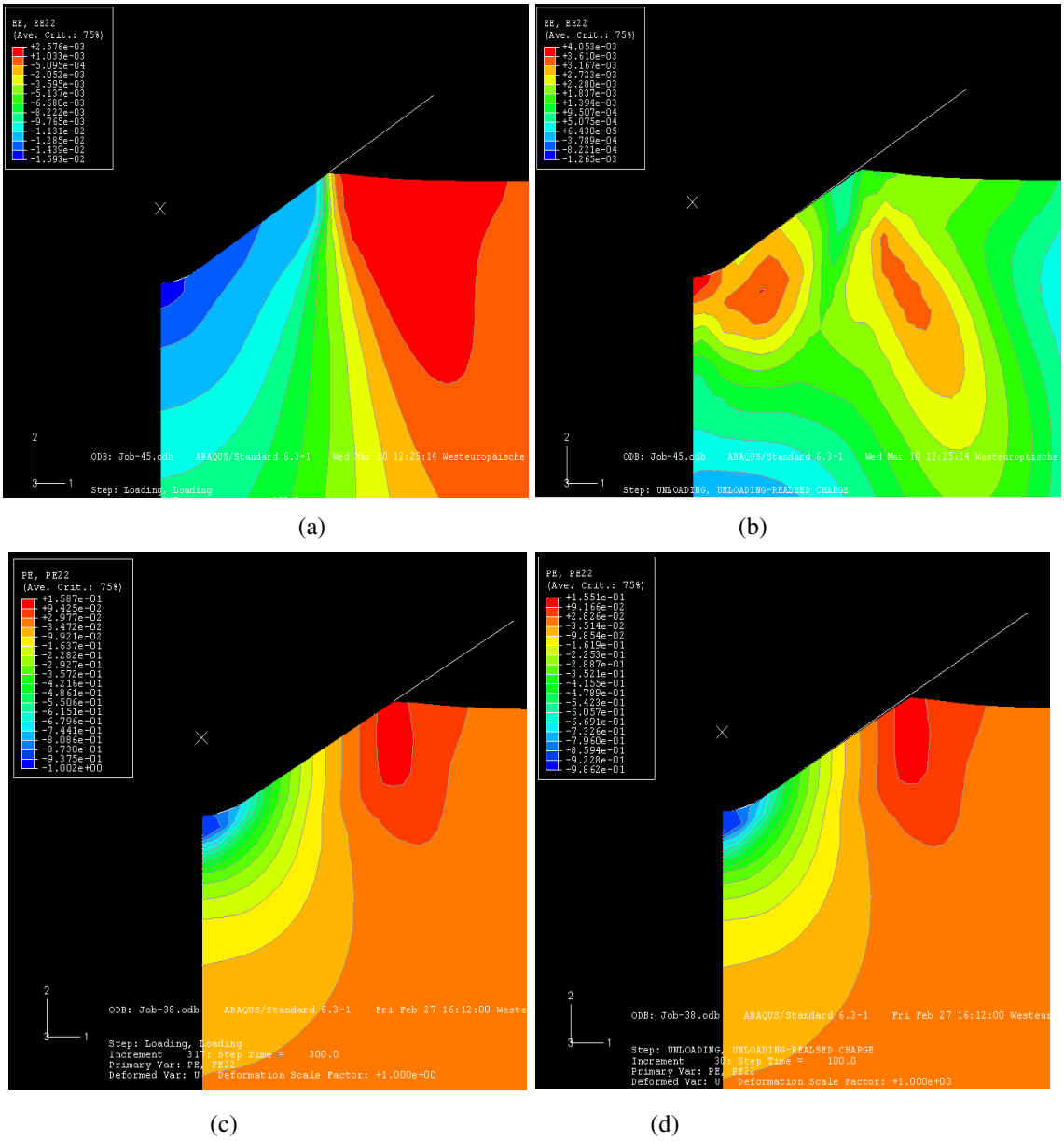

Figure 7-32: an example of elastic strain deformation of coatings on Ti alloy substrate a) loading, b) unlading, c) plastic strain deformation of coatings on Ti alloy substrate in loading mode, d) unloading.

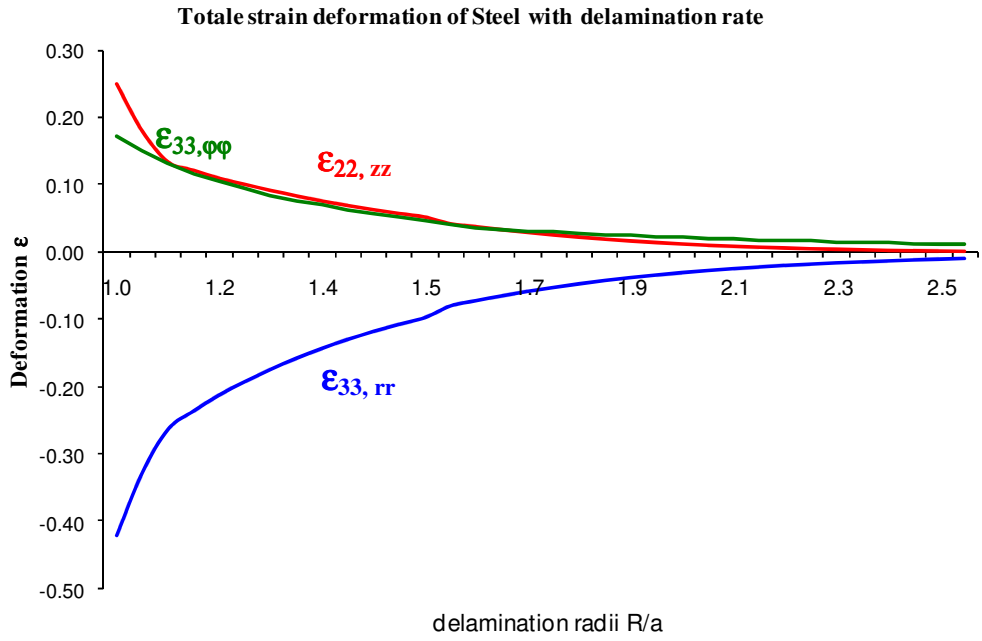

Figure 7-33: the total (elastic and plastic) deformation in function of delamination radii (Al_2O_3/Steel).

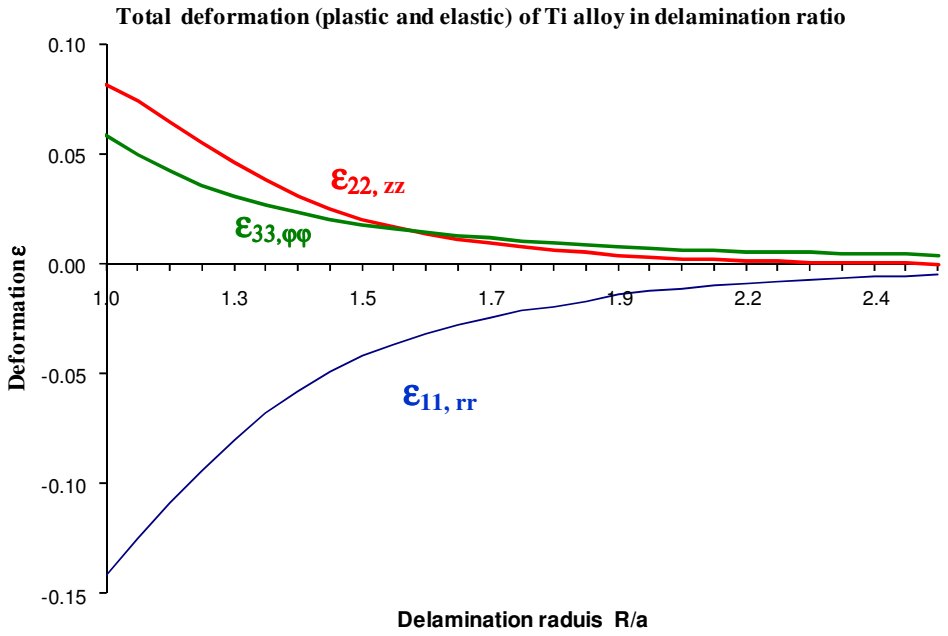

Figure 7-34: the total (elastic and plastic) deformation in function of delamination radii (NiCr/ TiAl6V4).

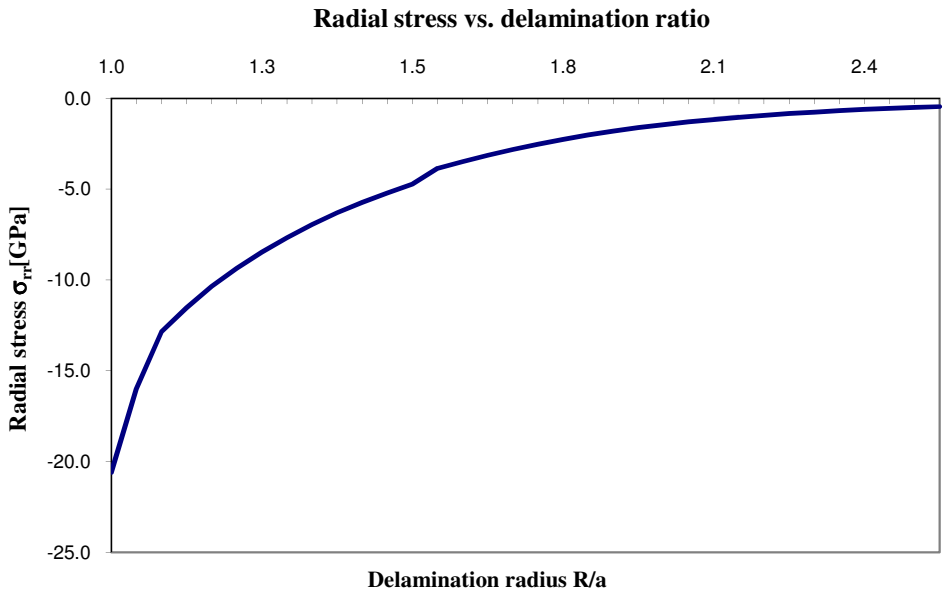

Figure 7-35: radial stress for brittle coating on steel substrate versus the delamination ratio.

In order to verify the simulated model, the experimentally measured indentation depth (after the unloading) of coatings deposited on both, steel and TiAl6V4 substrates were compared to the simulated spatial displacement of the indenter. The simulation results were approximately within 10% of the experimentally measured values as shown in Table 7-8.

Table 7-8: topographical measurements and spatial displacement

Materials	Experimentally measured indentation depth (displacement in z)	Finite element simulation (Displacement in z)
	µm (UBM)	µm (Abaqus)
TiAl6V4	172 ± 8	200
Steel	267± 6	290

The results of energy release rate (equation 5-27) and interfacial toughness (equation 5-28) were calculated versus the delamination radii R/a, when R/a < 2, incoherent results were found. Therefore, only Al_2O_3 coating on Ti alloy was in the reasonable order to magnitude of interfacial toughness as shown in Table 7-2 and Table 7-9.

Table 7-9: the summary results of finite elements simulation by Abaqus

Rockwell Indentation			
Nomenclature	Delamination radii R/r	Energy release rate G_c J/m^2	Interfacial toughness MPa. m $^{0.5}$
Al-F-100-3/Ti	1.99	247	3.7
Al-F-100-6/Ti	2.05	147	2.8
Al-F-300-6/Ti	2.36	60	1.8

The difference in indentation depth between experimental and simulating values was mainly attributed to three factors:

1. the friction coefficient introduced between indenter and substrate in our case was 0.1. Vasinonta [5] showed that friction coefficient used in modelling can considerably affect the numerical results,
2. second, it was assumed in the simulation that the indenter has an infinite rigidity, whereas, the tip deformation has to be considered in calculation [276].
3. the mechanical stiffness of the layer in the calculation was neglected.

In particular, the last assumption may introduce large errors, especially if the coatings are thick. In order to have a good fit between experimental and model simulation results, authors [5, 136, 277] shown that the delamination ratio should be $2 \leq R/a \leq 5$. In our case, in effect, when the delamination ratio was higher or near 2 we found a good agreement between experimental and modelled values. The energy release rate and the corresponding interfacial toughness values were found in the range of magnitude of the values published in literature [18, 193, 278, 279]. Unfortunately, the delamination ratio R/a was found less than 2 for the majority of the combinations that we studied and gave incoherent energy release rates.

The thicker coating did not show higher interface toughness, even the energy is proportional to layer thickness. Furthermore, in the cases where it can be assumed that the layer thickness is negligible compared to the indentation depth a thin film simulation, as the one proposed by Michler [277], can be validly used.

To sum up, we observed that some of the results showed coherent order of interface toughness and fitted well the simulated values when delamination ratio was more and near two. The other results with delamination ratio less than two were excluded from our results since this yield to very large errors and out of the applicability range of this model.

5. DISCUSSION

5.1 EXAMINATIONS OF ANNEALED COATING

As concluded in chapter 6, annealing helped to reduce the residual stress intensity in the coating and around the interface. However, it is primordial to understand the influence of residual stress on adhesion. Therefore, metallographic analyses of the annealed samples were carried out.

Cross sections of both as-sprayed and annealed VPS NiCr coatings have been observed under a High Resolution Scanning Electron Microscope (HRSEM Hitachi 4800 equipped with Energy-Dispersive X-Ray Spectroscopy (EDS) available at EMPA-Thun-CH). Images have been obtained using a backscattered electron detector (BSED). In addition, some elemental analyses were performed using Electron Probe Micro Analyser (EPMA) integrated inside the SEM with the added capability of elemental analysis using wavelength dispersive spectrometry (WDS). The EPMA measurements were performed at ENSCL -École Nationale Supérieure de Chimie de Lille in France, in the Cameca SX-100 facility employing the following conditions; Kα and Lα wavelengths, acceleration voltage 20 kV and current 200 nA.

The primary characteristic of an EPMA is the ability to acquire precise, quantitative elemental analyses at very small "spot" sizes (as little as 1-2 microns). The wavelength-dispersive (WD) spectrometers have significantly higher spectral resolution and enhanced quantitative potential as compared to energy dispersive spectroscopy (EDS). Further details on EPMA principle are available in ref [280]. However, back scattered electron (BSE) images were obtained. Low and high magnification images were taken in various parts of the samples in order to have representative micrographs.

Figure 7-36 shows the micrographs of as-sprayed and annealed VPS NiCr coatings in cross section with different magnifications. Dark phases were observed at the coating-substrate interface as shown Figure 7-37 in the BSE micrograph obtained from HRSEM. These dark points (numbered in yellow) were investigated using the EDS where the semi-quantitative results revealed the carbon presence in atomic percent of the three spots 1, 2 and 3 were found to be 18 %, 30% and 24% respectively.

From Figure 7-38, at the substrate/coating interface of the annealed sample, the X-ray mappings illustrate an accumulation of Fe which could be attributed to diffusion across the interface. Furthermore, a segregation of Cr was also observed within the annealed coating and mainly located at the interfaces between splats. The chromium enrichment at the interfaces between splats might be attributed to the high chemical affinity of chromium towards the carbon which is present in the ambient atmosphere and in the substrate. This segregation is maybe enhanced by the insolubility of nickel in chromium carbide [281].

Based on the previous EDS and EPMA results, it can be stated that most of the chromium carbide phases were formed during the annealing at 800°C. This is very probable since the ratio of Ni to chromium decreases within the grains and increases at the interfaces of splats. This also can explain the decrease of coating hardness from 293 ± 13 Hv (as sprayed) down to 251 ±16 Hv (annealed). The stoichiometry of the carbide compound in question (e.g. $Cr_{23}C_6$, Cr_7C_3 or Cr_3C_2) is not known at present. For such investigation, an X-ray diffraction or/ and EBSD (Electron Backscatter Diffraction) analysis could be useful. The formation of carbides at surfaces of various materials is an important process with regard to modifying their mechanical and tribological properties. However, Wang [282] studied the Cr_3C_2-25%NiCr coating and shows that all these carbides could be present and this was confirmed by Richert [283] having TEM analysis indicated that phases such as Cr_3C2, Cr_7C_3 and $Cr_{23}C_6$ were found in the coating. Regarding the temperature of carbide formation, Salaita [284] found that carbides form slowly below 300°C and rapidly between 300 and 600°C, and using the X-ray diffraction, he found the formation of a Cr_7C_3 bulk phase above 600°C and a

$Cr_{23}C_6$ bulk phase above 700°C were occurred and this agglomeration or precipitation of the carbides results in reduction of the coating hardness. This is in agreement with our analysis results upon the carbide phases and the hardness decrease of annealed coating.

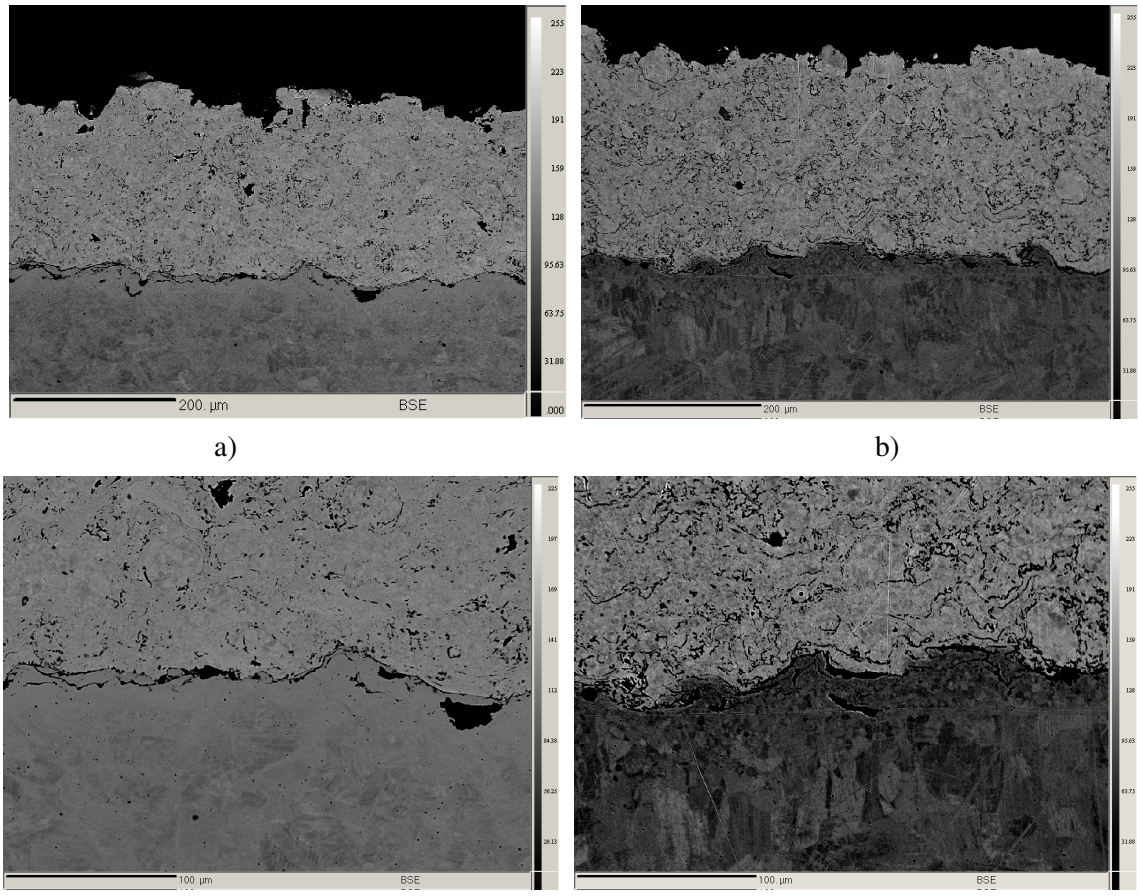

Figure 7-36: BSE micrographs of cross sectioned VPS NiCr coatings; a &c) as sprayed coating, b &d) annealed coating.

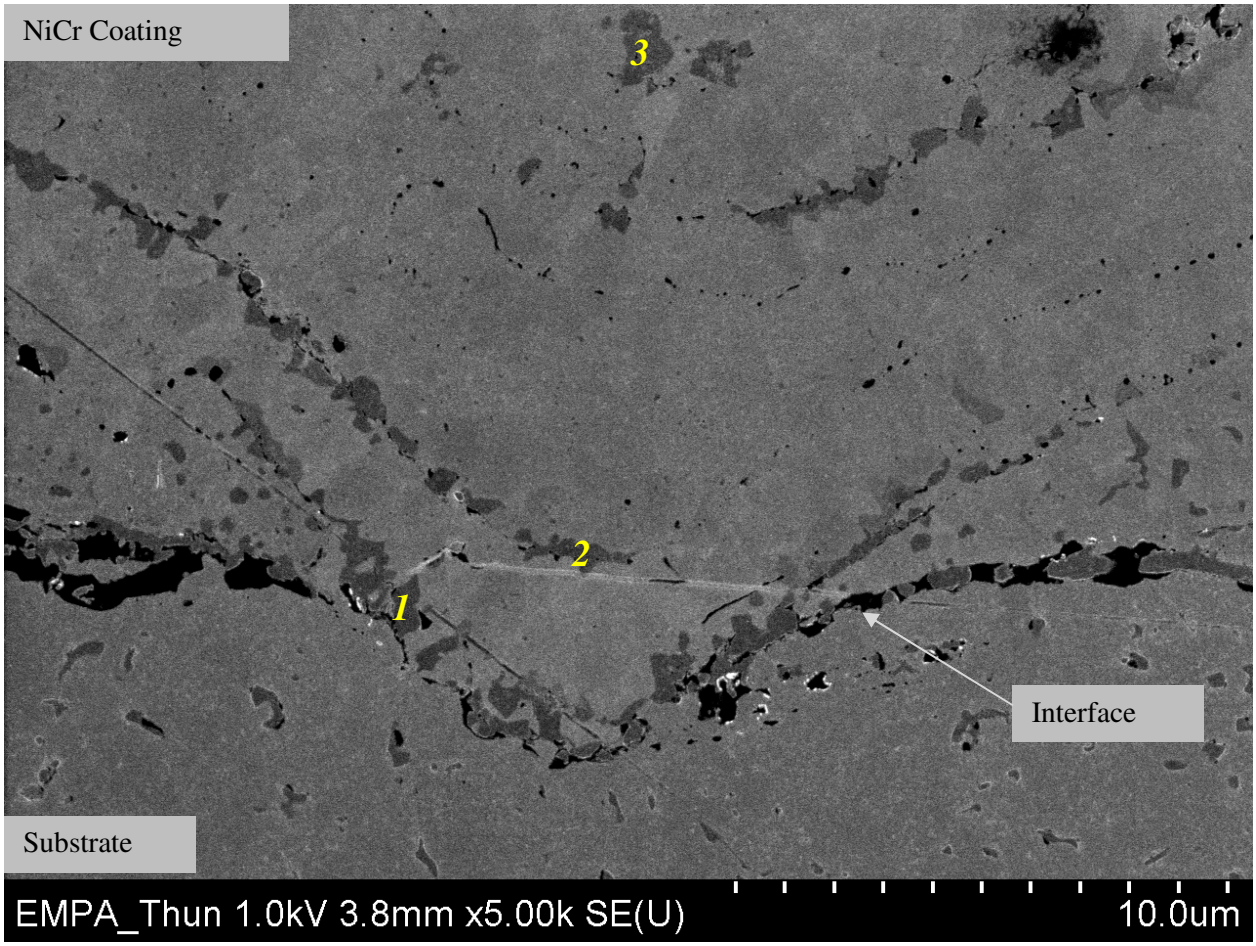

a)

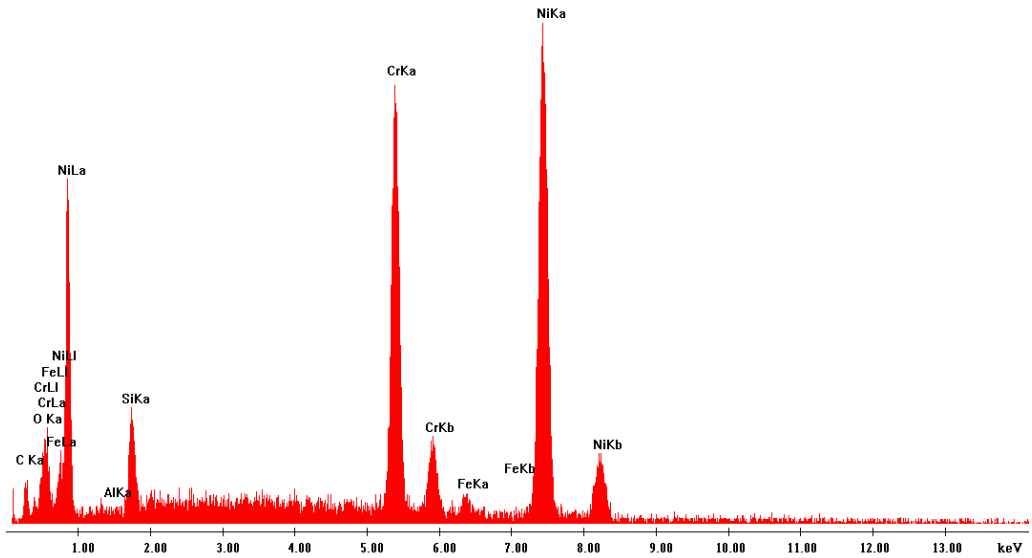

b)

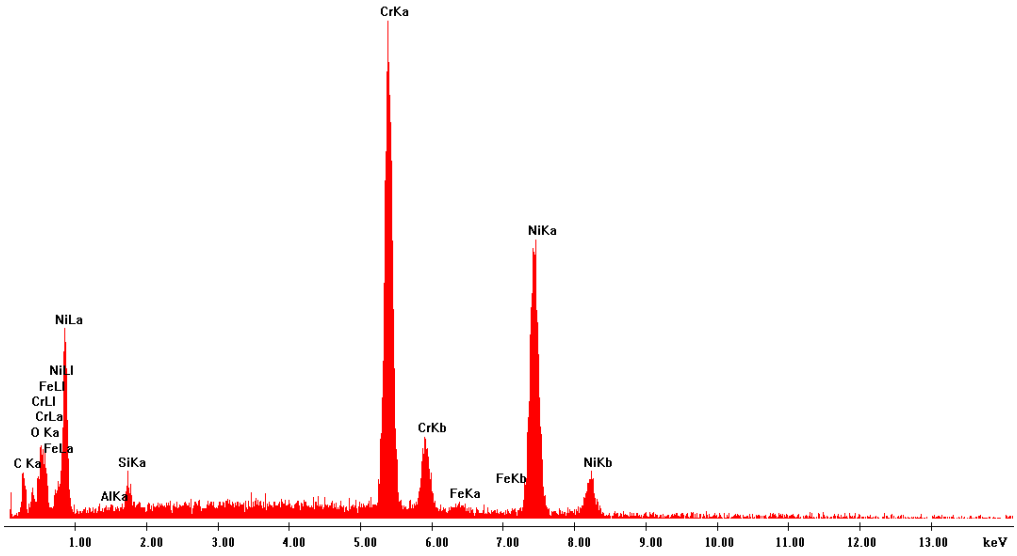

c)

Figure 7-37: BSE micrographs of cross sectioned VPS NiCr annealed coating with the yellow corresponding EDS measurements, a & b) are the EDS analysis of the points 1 and 2, respectively.

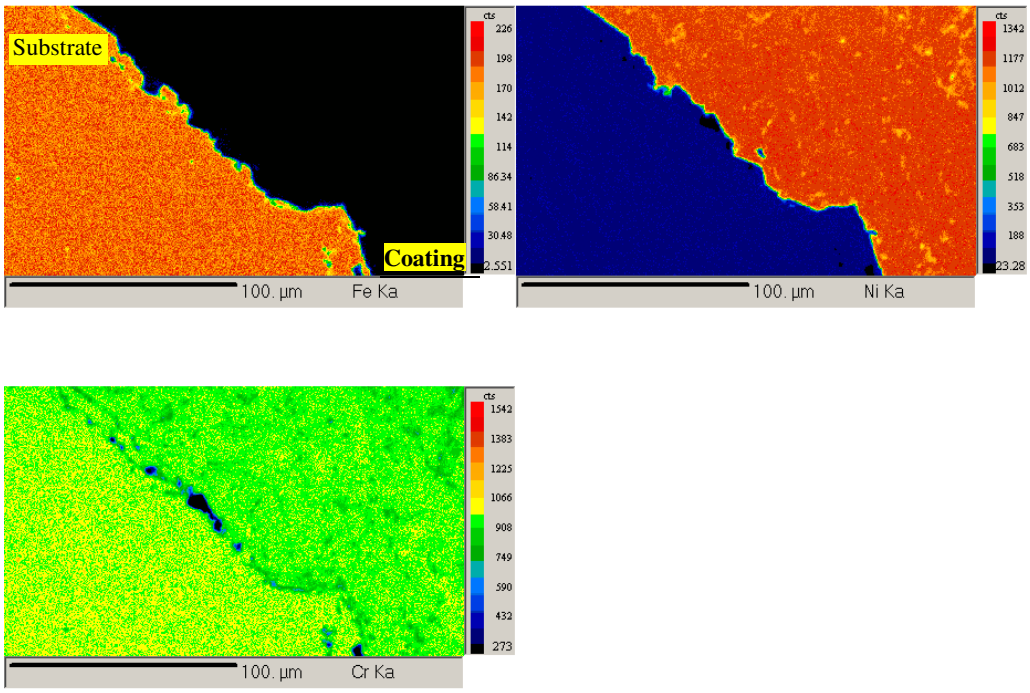

a)

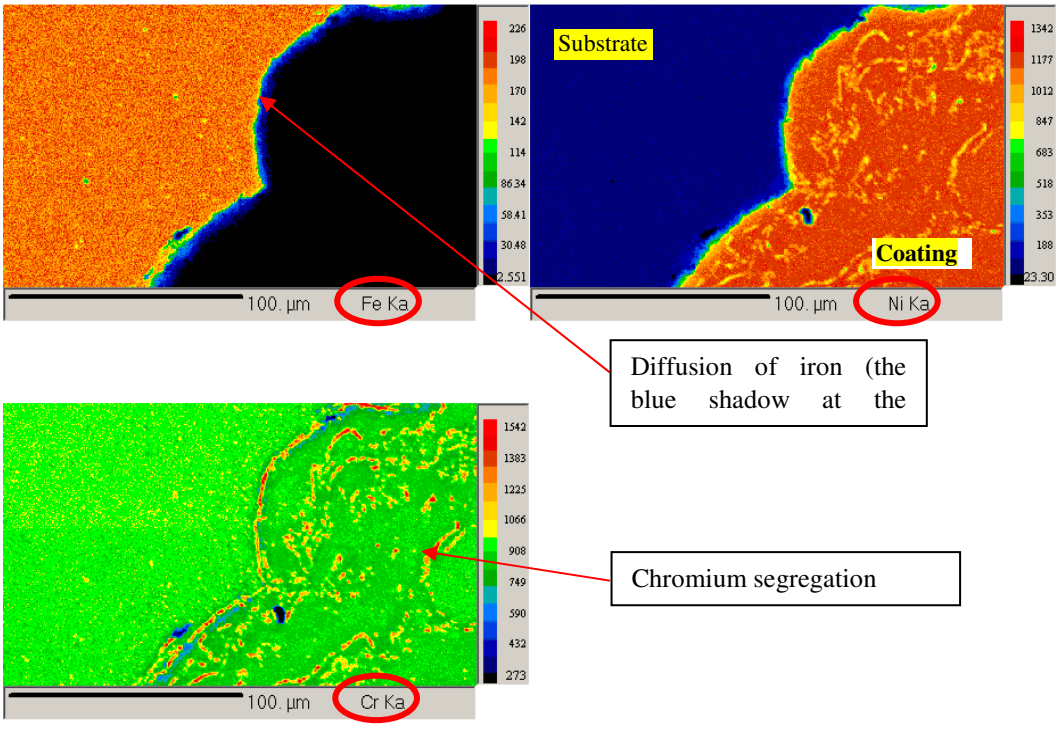

b)

Figure 7-38: EPMA mappings of Fe, Ni and Cr at the coating–substrate interface of VPS NiCr coatings, mappings are color coded: red = high concentration in the element, black = low concentration in the element. a) as sprayed, b) annealed.

5.2 THE EFFECT OF ANNEALING ON ADHESION

Figure 7-28 showed the apparent interfacial shear strength of as sprayed and annealed samples. The residual stress relief contributes to reduce adhesion order in the range from 30% down to 60%. This can be explained by the state of residual stress being in compression which opposites to the crack channeling at the interface. The higher compressive stress in the coating-substrate system helped to increase adhesion. Similar trend can be also observed in interface toughness shown in Figure 7-30.

However, the interface indentation method is more sensitive to residual stress at the interface. Figure 7-11 showed the interfacial toughness results of as sprayed and annealed coatings from which we can distinguish two different behaviors:

i. for the VPS NiCr coating with 100 μm of thickness, annealing led to an increase in the interface toughness.
ii. inversely, for the coating with 300 μm of thickness, the annealing treatment led to a decrease of interface toughness.

Such behaviors can be explained by three different parameters that play very important role to influence the interface toughness, (the most predominant parameter is still not known at the present):

1. the effect of compositional gradient: after annealing, a formation of different phases were occurred, e.g. *Fe* diffusion though the interface and toward the coating has been stated, in addition to that, the *Cr* segregation within the coating was also observed. Subsequently, these might lead to an important change of interface behaviour when subjected to indentation. However, the effect of compositional gradient thickness of coating on residual stress has been conducted by Zhang [285-287] and he showed that the compressive radial stress developed at the interface is changed to tensile when increasing the coating thickness as shown in Figure 7-39.

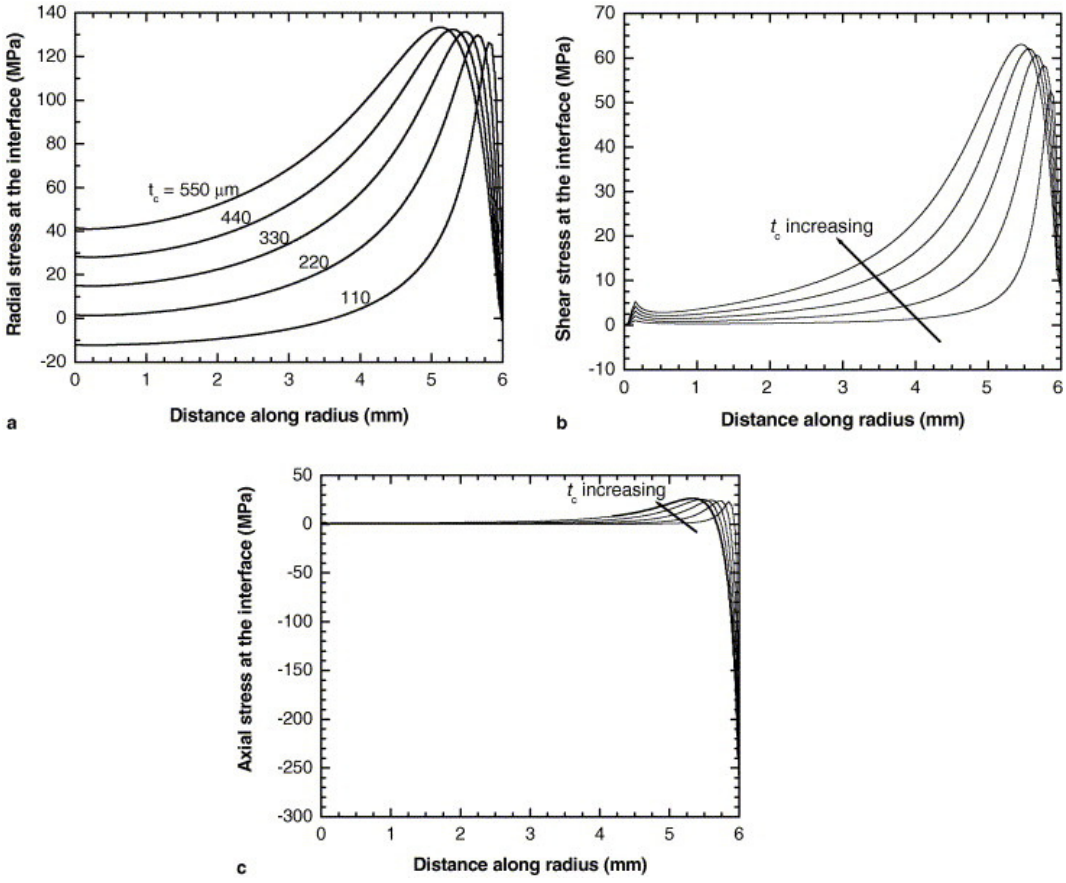

Figure 7-39: effect of coating thickness on the residual stresses at the coating/substrate interface: (a) radial stress, (b) shear stress, and (c) axial stress [285].

2. the residual stress gradient in the coating: the residual stresses act in different ways at the surface and at the interface and, depending on the thickness of the coating, one or the other could be predominant. As a consequence, the $\Delta\sigma$ parameters introduced below could explain this behavior. Figure 7-40 shows the increase in bond strength when $\Delta\sigma_{int}^{S;C} > \Delta\sigma_{int}^{surf}$ and a decrease when $\Delta\sigma_{int}^{S;C} < \Delta\sigma_{int}^{surf}$, respectively. In our experimental study, although the residual stress gradient measured by the hole drilling corresponds to the state where $\Delta\sigma_{int}^{S;C} < \Delta\sigma_{int}^{surf}$, the interface toughness was, surprisingly, found to decrease with coating thickness increasing. Therefore, this parameter might be not the main dominant one that can influence the interface toughness. However, in the interfacial indentation test, it has been shown in ref [97, 206, 288, 289] that the difference between the stresses located around both sides of the interface has a large influence and the residual stress generated in the coating

was found to decrease with the increase of coating thickness. This is because they considered the amplitude factor of residual stress at the interface as shown in Figure 7-40.

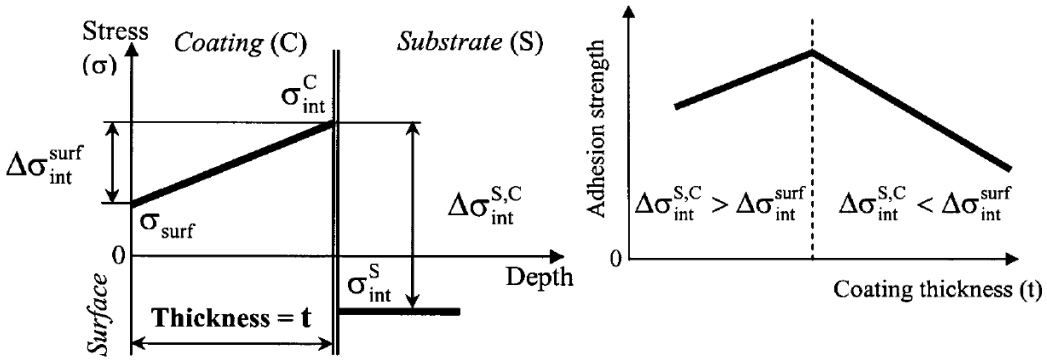

Figure 7-40: Residual stresses parameters for thermal sprayed coating studies [288].

3. the influence of coating thickness on interface indentation toughness: this was previously studied on NiCr coatings [206, 290]. The toughness increase with thickness can be explained by the schematic presentation in Figure 7-41. When applying a load *P* on different coating thicknesses, opening a crack in mode *I* type would be easier for a thinner coating.

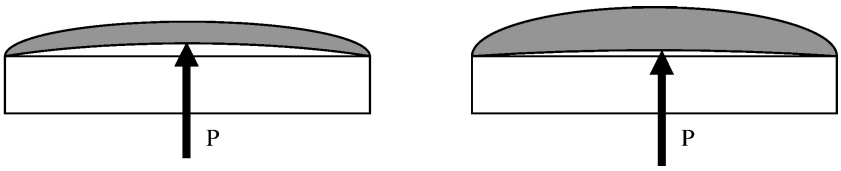

Figure 7-41: Effect of coating thickness on adhesion [291].

The contribution of each parameter among the three mentioned above, to the interface toughness might be hardly quantified, since they can be associated, but however, these points deserve a detailed study.

Lesage [98] using the energy-dispersive X-ray analysis performed on as received sample and annealed sample . It is seen that inter diffusion takes place during annealing since the composition line of iron, nickel and chromium decrease in a 4-µm zone of thickness instead of being 2-µm of thickness for the as received sample (Figure 7-42).

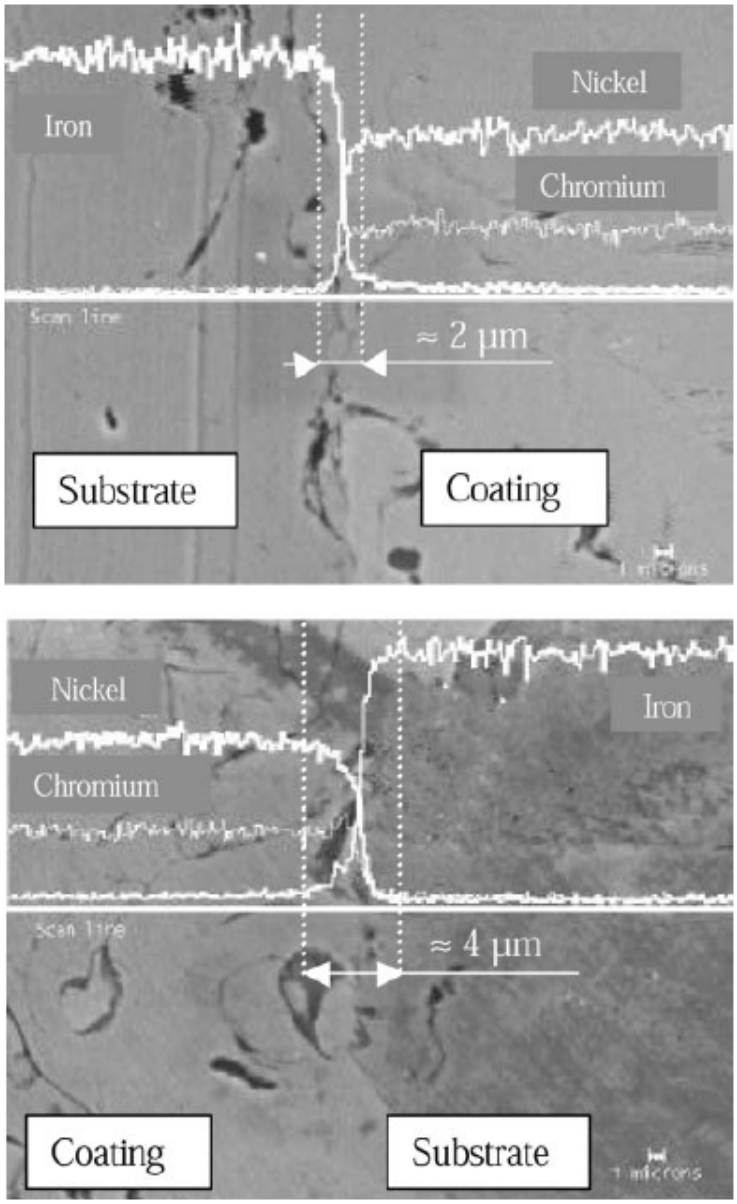

Figure 7-42: energy-dispersive X-ray analysis of a) as received sample and b) annealed sample [98].

Brossard [100] found in NiCr sprayed particles on the stainless steel substrates that both materials have the same crystalline structure (f.c.c.) with similar lattice parameters. Moreover, examination of the Fe-Ni binary phase diagram shows that at high temperatures these elements are intersoluble [292]. As a result, a continuous structure often forms across the splat-substrate interface, with, usually, inter-diffusion between both materials, and grains growing across the interface into both phases.

Khan [293] investigated the Zirconia thermal barrier coating with CoNiCrAlY bond coatings deposited onto Hastelloy-X nickel based super alloy substrate. Annealing at 650°C, he found the residual stresses profile measured by hole drilling, turned from tensile to compressive state at the ceramic surface, in the bond coat the residual stress intensity was higher in compression and for the substrate side, the residual stress intensity was lowered.

When annealing at 650°C and 1050 °C, the adhesion determined by interface indentation (bond coat-substrate interface) was observed to be subsequently increased as shown in Figure 7-43. One of conclusion of Khan was that the interface indentation test seems to be more sensitive to residual stress state compared to the standard tensile adhesion test. But the annealing do not improve adhesion in all the situations, for example, Laribi [99] observed a decrease of adhesion after the annealing treatment conducted on molybdenum coatings on 35CrM04 steel substrate. He attributed this decrease to the formation, as a results of chemical diffusion of a $\varepsilon(Fe_xMo_y)$ fragile intermediate phase at interface, which facilitated the coating decohesion.

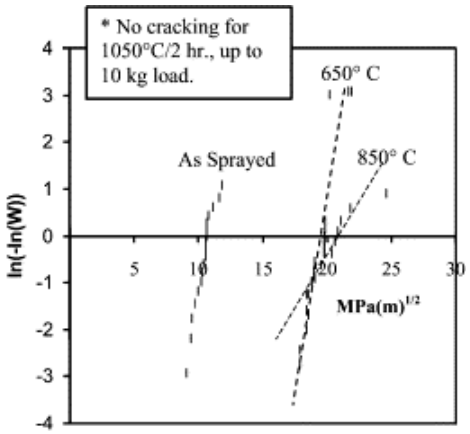

Figure 7-43: heat treatment effect over the interface indentation toughness of the substrate–bond coat interface [293]

Chicot [97] and Khan [293] found that the annealing treatment of NiCr coating at 600°C led to a considerable increase of the coating adhesion, and they attributed this to the improvement of metallurgical bond observed. Godoy [125] studied the NiCrAl on different steel substrates and found that the post annealing can improve the adhesion for system possessing $\alpha_c < \alpha_s$. He showed that the thickest

coatings displayed the lowest adhesion strength represented in Figure 7-44. Such results indicate a possible correlation between residual stresses at the interface and coating/substrate adhesion strength. Conversely, the average residual stress in the coating decreases as the coating thickness increases, suggesting an inverse correlation between both variables. However, in the paper [125], the ASTM standard tensile adhesion test was used and unfortunately, the coating fracture was not at all explained in this paper to validate such observations.

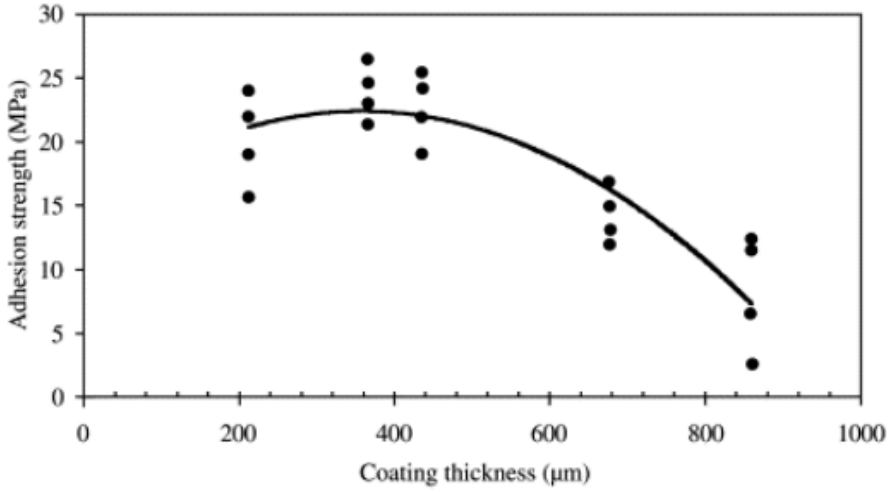

Figure 7-44: adhesion strength of NiCrAl coatings deposited at different thicknesses on AISI 1020 substrates, experimental results obtained from tensile tests [125].

5.3 COMPARISON BETWEEN ADHESION TESTS

As a confirmation of its lack of pertinence we could not correlate the tensile adhesion (EN 582) results to those obtained with any other test, since the failure was not localized at the interface. As a result, non physical order of adhesion could be extracted from this test.

For ceramic alumina coatings, no evident correlation was found between in-plane and interfacial indentation results. This might be attributed to:

i. the brittle behaviour of crack channelling through the interface in uncontrolled manner,
ii. the difference in loading conditions, one is directly applied in compression at interface whereas the other is indirectly applied in tension,

iii. the difference in stress intensity factor, in indentation was found to be in mode *I* [149, 294] and in mode II for the in-pane tensile test [269-272].

For metallic coatings, in general, a perfect accordance between in-plane and interfacial indentation results was found concerning the effects of coating thickness and roughness. Figure 7-45 shows a quasi-linear correlation between interface toughness values obtained by interfacial indentation and in-plane tensile methods including the standard deviation. However, the K_{IC} obtained by in-plane tensile test was found in higher order to that determined by interfacial indentation. This difference can be mainly attributed to the following factors:

1. The coating fracture toughness for the in-plane tensile test was calculated on the base of the estimated energy release rate due to crack channelling. Dundurs parameters were used with the pre-existing crack tip in the theoretical model of calculation (equation 5-25), but in our case we don't know the crack tip dimensions and, subsequently, the results revealed a higher toughness values compared to interfacial toughness. However, the upper limit of energy release rate has been estimated.
2. The difference in sensitivity of testing method to the residual stress, since interface indentation showed very sensitive to residual stress in small volume close to the interface.
3. The difference in contribution of other factors in the equation:
   Practical adhesion = f (fundamental adhesion, other factors) (chapter 4)
   like mode and rate of loading necessary to initiate the cracking at the interface. As an example, Hull et al [17] compared different adhesion testing methods, and studied the effect of thickness of gold film (up to 500 nm) on silicon substrate by peeling, pulling of and scratch tests. The three tests gave completely different results, because different parameters of tests were involved and the contribution of "other factors" are different, subsequently different practical adhesion values.

Figure 7-46 shows also a quasi linear correlation between the apparent interfacial toughness (by interfacial indentation) and the apparent interfacial shear strength (AISS by in-plane tensile).

The FS and VPS coating can be differentiated by their adhesion /cohesion behaviour since they exhibit different microstructure, porosity and residual stress level. However, both methods yield very coherent physical values of adhesion.

In spite of the few results obtained by Rockwell-C indentation, a comparable order of interface toughness was achieved (Table 7-9) when comparing to that obtained by interface indentation. The slight difference in magnitude order is mainly due to loading process and the fracture mode, since the interface indentation is dominated by mode *I* [294] whereas the Rockwell-C indentation is dominated by a mixed mode, *I* and *II* [5].

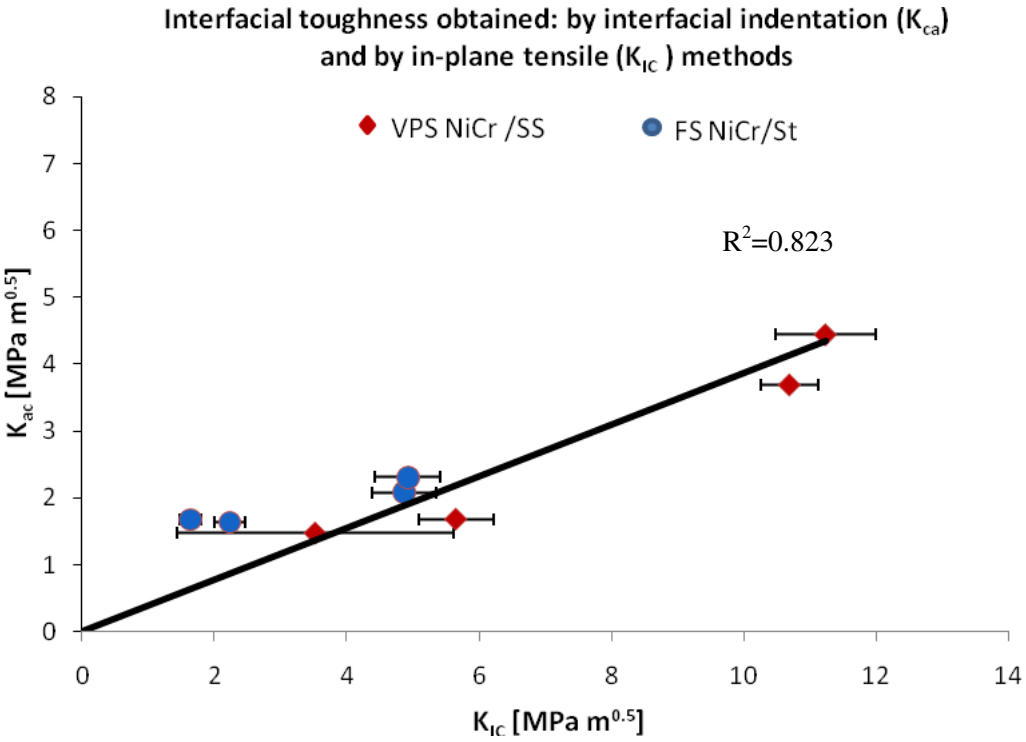

Figure 7-45: apparent interfacial toughness (by interfacial indentation) versus the interface coating toughness (by in-plane tensile test) of VPS and FS NiCr 80-20 coatings.

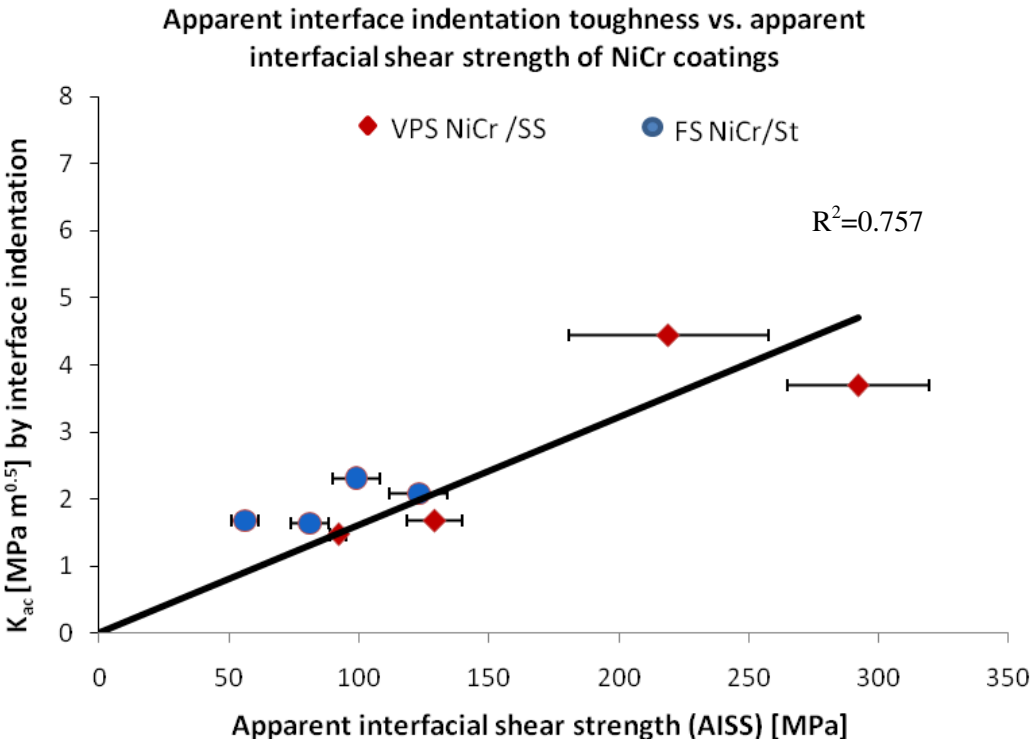

Figure 7-46: apparent interface toughness (by interfacial indentation) versus the apparent interfacial shear strength (by in-plane tensile test) of VPS and FS NiCr 80-20 coatings

6. SUMMARY

In this chapter, four adhesion methods were carried out; tensile adhesion, interface indentation, in-plane tensile and Rockwell-C indentation (assisted by finite elements simulation). The main results can be summarized in the following points:

1. Regarding the tensile adhesive tests (EN 582), the coating failure could not yield a physical value to quantify the adhesion and one can only assume that adhesion strength at the interface is stronger than those values obtained. Those obtained results demonstrate that such test is no longer usable for the thermal spray coatings that are routinely produced nowadays. Since the adhesion between these coatings and their substrate exceeds the resistance of the glue, and fracture in majority was occurred cohesively in the coating or "adhesively" in the glue. Allowing the fact that the test is very time consuming, costly and give very poor information on the adhesion properties of the materials and it is probably going to be

abandoned in the near future in profit of more meaningful tests. Therefore, we could not correlate this tensile adhesion test to other tests.

2. The interfacial indentation showed very reliable and coherent results through all the coatings, the physical values of adhesion were expressed by the interface toughness. The influence of coating thickness and coating roughness on adhesion was conducted. The results of interface indentation of sandwich based cermet coatings shown that combination Cer /Ni pl-x/ Cer revealed the highest adhesion value among others and this was mainly attributed to the microstrucutre of Ni inner layer and its mechanical properties. Fracture analysis of other combinations were detailed in Hadad [190, 191].

3. The in-plane tensile method relies on the development of transverse crack patterns in a brittle coating when the relatively ductile supporting substrate is plastically deformed under an applied uniaxial load. This crack behaviour has been adequately described by a shear-lag analysis that directly relates crack density to the load transfer capabilities of the interface. This shear lag theory allows the establishment of a steady state of constant crack density observed at relatively high strain levels. The crack fragmentation method employed in this study could offer two order of adhesion: the energy release rate and the apparent interfacial shear strength. The interface fracture toughness was calculated based on the estimated energy release rate due to crack channelling using Dundurs parameters.

   The apparent interfacial shear strength AISS revealed very good accordance to the increase in coating thickness and roughness. Such measurement seems to be coherent since no value was acceding the yield strength of substrate or/and of coatings. The in-plane tensile method provides in a well controlled manner a large array of parallel cracks over the nominally homogenously deformed ductile substrate and allows in situ observation of cracking of coating via various microscopy tools. It is additionally simple and inexpensive testing instrument.

4. Results obtained by Rockwell-C indentation showed coherent interface toughness values and fit simulation well when delamination ratio was more and/or around two. The other results with the delamination ratio less than two were excluded from our results since this yielded a very large error and out of the applicability range of this model. However, this test method could be mainly applied for brittle coatings on a ductile substrate

5. Elemental analysis of annealed samples up to 800°C revealed different mechanism; e.g. a diffusion of *Fe* through the interface and chromium carbide formation at the interfaces of splats. Annealing helped reducing the magnitude order of residual stresses in the coatings. Subsequently, a reduction in adhesion order was observed in different manner. However, the apparent interfacial shear strength was decreased after annealing in the range from 30% to 60%, depending on the interface roughness; the higher adhesion reduction was achieved in the lower interface roughness, since the higher mechanical interlocking at the interface help to retain better the compressive residual stress. The interfacial indentation was found to be more sensitive to stress variation, since the effect of annealing on adhesion was found dependent on the coating thickness, different reasons for such behavior were discussed.

6. The interface indentation and the in-plane tensile test results were compared. Metallic coatings showed quasi-linear correlation between results obtained by both techniques. This is a novel finding, and very important since no comparison between these two tests was ever made, the fact that the two tests gave perfectly coherent and reliable results demonstrate their pertinence to evaluate adhesion since they are based on very different geometric and loading conditions.

CHAPTER 8 : FINAL CONCLUSIONS AND FUTURE SCOPE

8.1 FINAL CONCLUSIONS

The objectives of this thesis and the importance of investigating the adhesion of thermally sprayed coating to its substrate as well as the residual stress induced have been described in chapter 1. A review of thermally sprayed coating, deposition processes, structures, main properties and coating build-up have been conducted in chapter 2. Fundamental understanding on residual stresses in thermally sprayed coating, their origins, methods and approaches of residual stress evaluation and annealing effect has been gained in chapter 3. Chapter 4 provided an overview of adhesion, such as; definition and characteristics, methods mainly used in laboratories and in industries to evaluate adhesion. Principal advantages and disadvantages of each method were discussed.

Chapter 5 dealt with experimental procedures and protocol followed during the investigations. The substrate and powder materials have been introduced and the processes used to deposit the coatings have been stated. To summarize that, three processes were used in our study, FS, VPS, and HVOF to deposit; metallic NiCr 80-20, ceramic Al_2O_3 and WC-Co-Cr composite coating materials on different metallic substrates; St 52-3, AISI 304, X3CrNiMo13-4, TiAl-16V4. This was followed by an elaborate description of the strain measurement procedures to determine the residual stress using various approaches like curvature bending,

incremental hole drilling (IHD) and interfacial indentation methods. Experimental procedure of adhesion measurement and data evaluation were described for procedures like pull-off, in-plane tensile, interfacial indentation and Rockwell indentation (assisted by finite elements simulation) methods.

In chapter 6, the residual stresses were measured using; curvature bending, incremental hole drilling and interfacial indentation methods. The obtained results can be summarized in the following points:

1. Residual stress obtained using all methods revealed a compression stress field achieved in NiCr coatings on the steel substrates. This was explained according to the thermal expansion coefficients of coating-substrate systems.
2. The residual stress results of VPS NiCr obtained from three previous methods were compared according to the coating thickness:
    i. a comparable order of magnitude in residual stress was achieved in coatings with 100 µm of thickness when comparing results from bending curvature and interfacial indentation methods,
    ii. for coatings with 300µm thick, the residual stresses obtained by bending curvature and incremental hole drilling show a comparable order of magnitude.

    The residual stress measurements performed by all methods provide a large insight to its gradient, intensity and state, and each can supply unique information, hence, they are complementary to each other. The difference in magnitude order of residual stress intensities obtained by the three methods is not only attributed to the difference in analytical model in residual stress estimation, but it is also related to the relevant measurement volume/areas of the coatings-substrate system, for example, the hole drilling measurements are localized to a volume of the order to ~1 mm^3, whereas, the interface indentation measurements are spread on loaded zone along the interface for an important length of sample section (40 mm of length), while the bending curvature measures the strain in coating of tenth of millimeters over a few cm of length.

3. The effect of annealing treatment up to 800°C for 75 min on residual stress can be summarized as follows:
   i. Annealing helped to reduce the intensity of residual stress in the coating and at the interface. Curvature bending results showed a decrease in residual stress for the coating with Ra= 3 µm down to ~ 65%, whereas, for the coating with Ra= 6 µm, only a decrease of ~22% was measured. This is attributed to mechanical interlocking at the coating –substrate interface which retain residual stress within the coating.
   ii. The residual stress gradient obtained by IHD method on the annealed coating showed one of principal stress was in compression and the other developed after annealing to be in tensile. This was explained by the new phase formation: where *Fe* diffusion through the interface, chromium segregation and a chromium carbide phase formation have been observed within the coating and at the interface.
   iii. Some of annealed results (e.g. combinations 22 and 24) obtained by interfacial indentation method also revealed a conversion in residual stress state to tensile for the same reasons explained above. While comparing methods to measure residual stress, it is observed that the interfacial indentation test used for residual stress determination, at the interface, shows more sensitivity to stress variations.

In chapter 7, results of adhesion obtatined by; tensile adhesion, interface indentation, in-plane tensile and Rockwell-C indentation methods were discussed. The main conclusions are:

1. Results of tensile adhesive test did not yield a physical value to quantify the adhesion since the coating fracture was not occurred at the interface. This test was found to be very time consuming, costly and yielded very little information on the adhesive properties of the materials. Subsequently, we could not correlate this tensile adhesion to other tests.
2. The interfacial indentation testing method could be applied for all types of coatings on the ductile substrates and yielded to very reliable and coherent results expressed by the interface toughness (K_{ca}) as physical values of

adhesion. The influencing parameters like, coating thickness, interface roughness and residual stress were discussed.

3. Particular attention was paid to conduct the model and data evaluation of the in-plane tensile testing method. This crack fragmentation method could provide two orders of adhesion:
   i. the interface fracture toughness (K_{IC}) was determined based on the energy release rate,
   ii. secondly, at the crack saturation stage, the apparent interfacial shear strength (AISS) was determined. In addition, the residual stress intensity induced in the coating allowed us to estimate the intrinsic interfacial shear strength.

   The influence of interface roughness and coating thickness on the adhesion has been discussed. The obtained values of interfacial shear strength were found to be very coherent and none exceeded the yield strength of substrate or/and of coating.

   This test method was found to provide in a well controlled manner a large array of parallel cracks over the deformed ductile substrate and allows in situ observation of cracking of the coating via various microscopy tools. It is additionally simple and inexpensive testing instrument.

4. The Rockwell-C indentation results were found to be in very good agreement with the finite elements simulation. In addition, these results were also in agreement with those of the interfacial indentation test. The obtained interface toughness values fitted simulation well when delamination ratio was more and/or around two. The other results with the delamination ratio less than two were excluded since these were associated with a large error and out of the applicability range of this theoretical model. However, this test method could be mainly applied for brittle coatings on a ductile substrate.

5. Elemental analysis of annealed samples up to 800°C revealed different mechanism; e.g. a diffusion of *Fe* through the coating-substrate interface was occurred, and chromium carbide formation at the interfaces of splats was

observed. Annealing helped reducing the magnitude order of residual stresses in coatings and at the interface.

6. The effect of residual stress relief, achieved by annealing, on adhesion was found to reduce adhesion order in different manner; e.g. the apparent interfacial shear strength (AISS) was decreased in the range from 30% to 60%, depending on the interface roughness; the higher adhesion reduction was achieved in the lower interface roughness, since the higher mechanical interlocking at the interface help to retain better the compressive residual stress. On the other hand, the interfacial indentation was found to be more sensitive to stress variation, and mainly dependent to the coating thickness, for example, the VPS NiCr coating with 100 μm of thickness, annealing led to an increase of up to ~70% in the interface toughness, whereas, for the coating with 300 μm, annealing led to a decrease down to ~30% in interface toughness. This opposite behavior was discussed.

7. The interface indentation and the in-plane tensile results were compared. Metallic coating showed quasi-linear correlation between results obtained by both techniques. This is a novel finding, and very important since no comparison between these two tests was ever made, the fact that the two tests gave perfectly coherent and reliable results demonstrate their pertinence to evaluate adhesion since they are based on very different geometric and loading conditions.

To conclude, the residual stress measurements performed by three methods provide a large insight to its gradient, intensity and state, and they are therefore complementary one to the other. The performed adhesion methods measured mainly what is termed the practical adhesion. It seems that interface indentation and in-plane tensile methods provide the best prospects of relating practical levels of adhesion to the performance of real engineering components in service. Therefore, it is expected that the results in this thesis, and the future publications which can stem from it, are of value to those working in the thermal spray community.

8.2 FUTURE SCOPE

As reported in chapter 4, the relationship between practical and fundamental adhesion was expressed by:

Practical adhesion = f (fundamental adhesion, other factors)

Therefore, a pertinent question has been dressed; can one determine fundamental adhesion by making practical adhesion measurement? This is still an open question for further future study. Therefore, we decided to fundamentally understand the adhesion at first level of thermal spray coating. Consequently, we carried out a recent attempt [295] to quantify the adhesion of alumina single splat sprayed on a polished steel substrate using indentation experiments inside a scanning electron microscope. Based on energy release rate of interfacial crack, the stress intensity factor was found to be $K_{II} = 4.43 \pm 1.0$ MPa $m^{1/2}$ which is possibly overestimated since the tensile residual stress has not been taken into account. However, in spite of the high scatter, such order of magnitude might be comparable to interfacial coating toughness found in our study (ranged from 2.1 to 4.0 MPa $m^{1/2}$).

Our first approach to quantify adhesion of one single splat might be an improper approach to study the fundamental adhesion, because of two reasons:

i. in spite of steel substrate is considered one of the most used in the field of thermal spray application, the surface chemistry is still not enough known. Recent investigations were carried out by Brossard [70, 100, 296-302] revealed complex phenomena resulted at interface when spraying NiCr splat on polished stainless steel substrate as shown in Figure 8-1 with the following marked points: (1) columnar grains (≤ 1 μm in diameter) (see region marked 1), (2) the apparent good contact between the splat and the substrate and alignment of grains suggests that melting of the substrate may have then occurred locally in this zone. (3) some voids at the splat-surface (4) curling up of the splat rim at its periphery, which occurs because of the surface tension effect during spreading, the poor adhesion of the splat under the rim and the shrinking of the splat to accommodate the stress arisen from the solidification and cooling down. (5) phase was identified by TEM to be NiO.

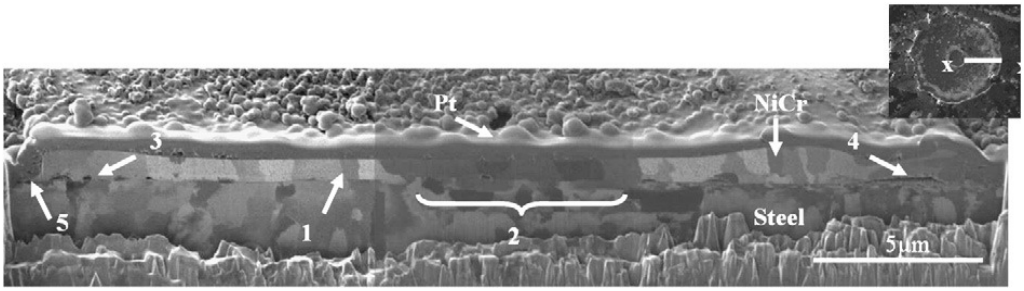

Figure 8-1: FIB cross-section of a disc-shaped NiCr splat on steel substrate [302].

ii. The deposited splats are too different in shape, thickness, thermodynamic history and size as shown in Figure 8-2. This occurs since, the splats while contacting the substrate, possesses a wide range of temperature, size and velocity. Therefore, numerous processing parameters can play a major role to influence splat adhesion, such as, preheating temperature, particle size, shape, velocity, temperature, deposition distance, etc. Even if those parameters are optimised to obtain disc adherent splat as some authors did [65, 71, 303-313], lots of statistical adhesion measurements should be involved.

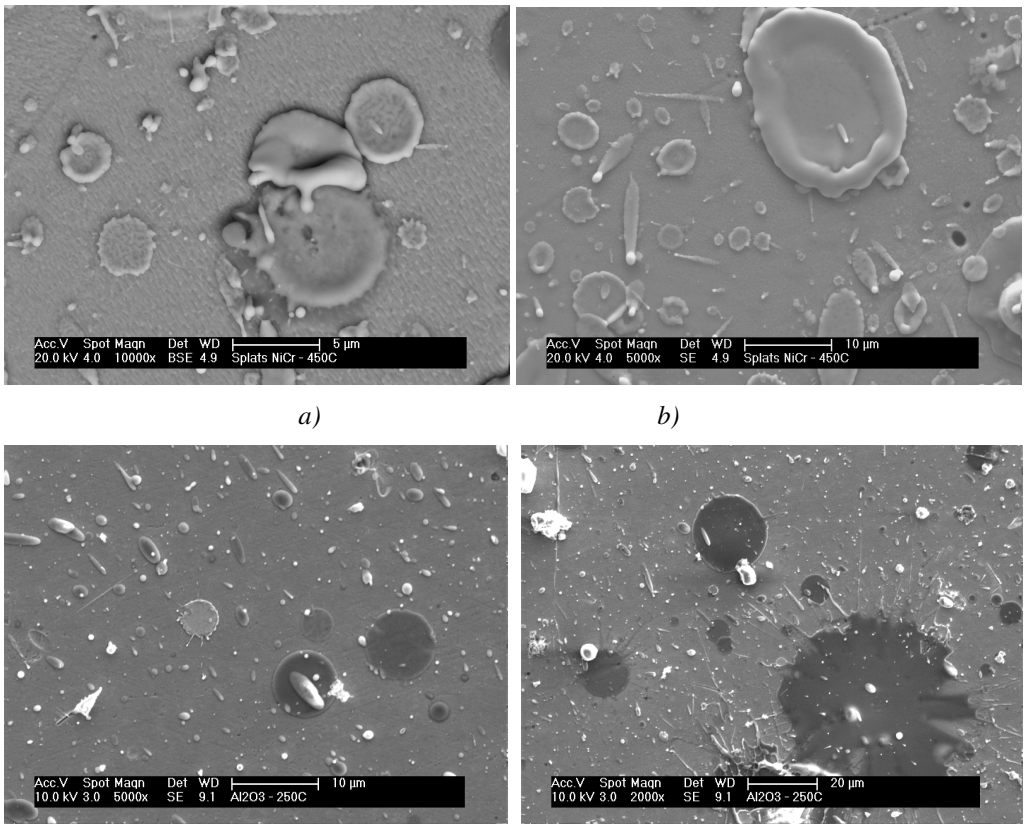

Figure 8-2: a & b) splats of Ni Cr 80-20 at preheated substrate to 450 °C, c & d) splats of Al_2O_3 at preheated substrate 250°C.

For the reasons mentioned above, we decided to spray a thin alumina coating on a polished sapphire (single crystal) substrate in order to study the fundamental adhesion. This alumina-sapphire presents a very interesting system to investigate, since the CTE of both materials are similar and this might be beneficial for reduction in thermal stress, where the tensile quenching residual stress can dominate. In addition, the interface chemistry might be less complicated than that of steel, since the saturation of oxidation is already achieved in this sapphire/alumina interface.

First preliminary results revealed FS alumina spraying on a polished sapphire (single crystal) was not successful and only few splat where adhered as shown in Figure 8-3.

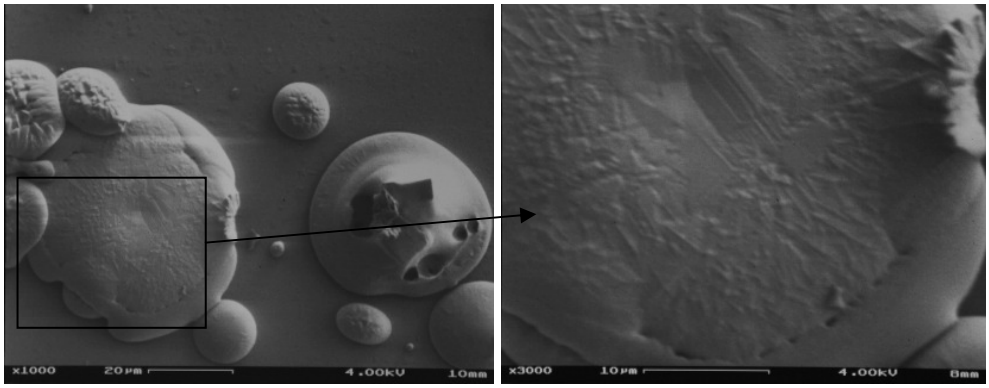

Figure 8-3: FS splat of Al_2O_3 on Sapphire (Single crystal) with sapphire surface roughness Ra: 0.001 µm.

The sapphire (single crystal) substrate was therefore grit blasted using alumina grits to have a roughness of Ra=1.1 µm and a FS alumina coating has been deposited on, having a 70 and 200 µm of coating thickness. The 200 µm of coating peeled off during cooling, this might be explained by the tensile stress gradient. The morphology of the background free standing coating is shown in Figure 8-4.

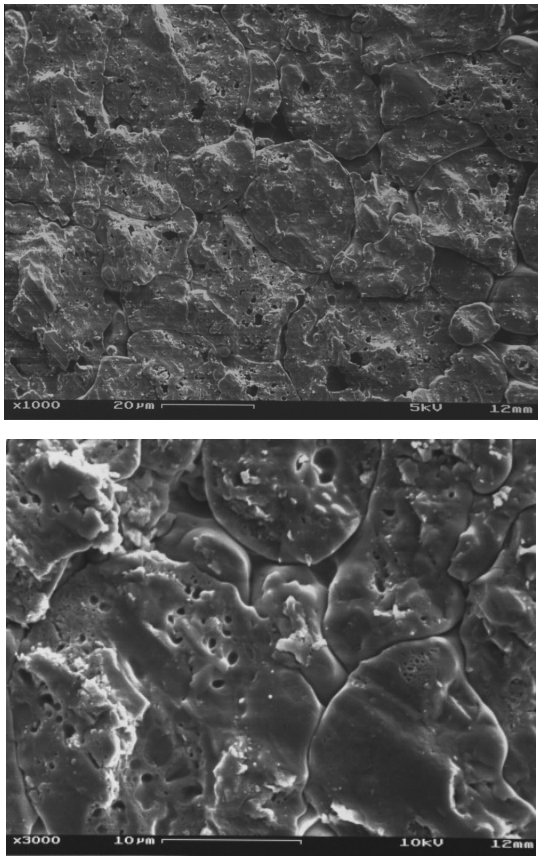

Figure 8-4: background of the free standing alumina coating on a polished sapphire substrate.

Last deposition of alumina on the grit blasted sapphire (single crystal) shows the importance of mechanical interlocking system where the splats can be accommodated. The critical surface roughness should be defined to guarantee the minimum of adhesion. Therefore, the proposed future work, as an extension of adhesion investigation, is to perform a gradient in surface roughness which is not only expressed by Ra value, but expressed in very fundamental and scientific manner, like mean spacing of holes/pillars, their shape, size, depth and distribution. This surface gradient of sapphire substrate could be achieved by laser for example.

Coating adhesion therefore can be investigated using scratch test along the topographic gradient interface. For fundamentally understanding the residual stress contribution to the adhesion mechanism, the residual stresses at the interface and underneath in substrate can be measured using high resolution X-Ray diffraction and/or Raman spectroscopy.

CURRICULUM VITAE

Name and date of birth:	Mousab HADAD 9th January 1974
Phone:	++41 79 316 89 88
E-mail:	mousab.hadad@empa.ch
Nationality:	Swiss

CURRENT OCCUPATION AND WORK EXPERIENCE

Current occupation: since 2002 as a scientist, projects leader in Coating Technology and Tribology in "Swiss Federal Laboratories for Materials Science and Technology" (EMPA) at Thun-Switzerland.

ACADEMIC SUPERVISION

2003 Supervision of diploma thesis of Yvers Martin (Etude de la résistance à l'usure de revêtements composites contenant différents types de carbures de tungstène) The University of Applied Sciences- HES EIVD Yverdon. Switzerland.

2004 Supervision of diploma thesis DEA -diplôme d'études approfondies- of Guillaume Marot (Détermination de la ténacité interfaciale des revêtements projetés thermiquement) University of Science & Technologies of Lille -France.

2004 Supervision of diploma thesis of Luca Bacciarini (La mise en service d'un équipement de projection plasma APS) The University of Applied Sciences- HES EIVD Yverdon. Switzerland.

2004 & 2005 Practical training of students; FSRM and Master degree courses (Master of Micro and Nanotechnology MNT Bodensee).

2004 & 2006 Highly involved in the supervision of PhD student's thesis upon "Investigation of different adhesion measurements of thermally sprayed coatings regarding the influence of residual stresses" Ecole des Hautes études d'ingénieur, Lille (France).

2004 & 2005 practical training of students; FSRM and Master degree courses (MNT Bodensee).

2007 Supervision of diploma thesis – Projectipn Plasma: Réalisation et caractérisation de revêtement, The University of Applied Sciences- HES EIVD Yverdon. Switzerland.

2007 Supervision of diploma work of Damian Frey & Simon Wüsst– New conception of tribometer under high temperature, The University of Applied Sciences Nordwestschweiz- Brugg. Switzerland.

2007 Lectures and practical training of students; University of Applied Sciences in FFHS Bachelor degree courses (FSB Dietikon).

EDUCATION

1998-2002	University of Applied Sciences. Mechanical Engineering Yverdon-Les- Bains. Switzerland.
2002-2003	Diploma thesis in tribology "**The tribological investigations of laminates composites and multi-layers"**

AWARDS AND HONOURS

January 2003	Vallorbe Metallurgy Price for best Diploma thesis.
October 2002	Best final exam's results at the University of Applied Sciences HES. EIVD Yverdon. Switzerland.
February 2006	Top 25 article of Journal downloads of Journal of American Ceramic Society "Fractography, Mechanical Properties, and Microstructure of Commercial Silicon Nitride–Titanium Nitride Composites-2005"

COURSES AND TRAINEES

1997	Italian Language- Perugia & Monza- Italy
1999	English solidification course in Ramsgate- UK
2001	Trainee in tribology - polytechnics of Bucharest –Romania
2002	Trainee in tissue replacement- Queen Mary University Biomedical Engineering London. UK.
2003	Intensive course of Electro-chemistry. EMPA Thun. Switzerland.
2006	Intensive course of Fundamental business and management, EMPA Academy. Switzerland
2007	Intensive course of Research Management, ETH Zurich. Switzerland

LANGUAGES

French:	Fluent (oral and written)
English:	Fluent (oral and written)
Italian:	Fluent (oral and written)
German:	Fluent (oral)

MEMBERSHIP

Executive member in Swiss tribology http://www.swisstribology.ch

Executive member in "Swiss engineering association" http://www.swissengineering.ch

Active Member in SGO-STT (Swiss association of surface treatments) http://www.sgo-sst.ch

Member in ASM international, http://www.asminternational.org

Executive member in ETSA, The European Thermal Spray Association

PUBLICATIONS AND CONFERENCES

1. Hadad M, Marot G, Démarécaux P, Lesage J, Michler J, Siegmann S. Adhesion tests for thermal spray coatings: Application range of tensile, shear and interfacial indentation methods. In: Lugscheider E, editor. ITSC 2005 Thermal Spray connects: Explore its surfacing potential! Basel, Switzerland: DVS-Verlag GmbH, 2005. p.759.
2. Hadad M, Blugan G, Kübler J, Rosset E, Rohr L, Michler J. Tribological behaviour of Si3N4 and Si3N4-%TiN based composites and multi-layer laminates Wear 2006;260:634.
3. Hadad M. Bürgler P, Hitzek R, Siegmann S, **Patent**: Verfahren zum Wiederherrichten von abgenutzten Oberflächen hartstoffbeschichteter Bauteile. CH, 2006. p.10.
4. Hadad M, Hitzek R, Buergler P, Rohr L, Siegmann S. Wear performance of sandwich structured WC-Co-Cr thermally sprayed coatings using different intermediate layers. Wear 2007;263:691.
5. Hadad M, Marot G, Demarecaux P, Chicot D, Lesage J, Rohr L, Siegmann S. Adhesion tests for thermal spray coatings: correlation of bond strength and interfacial toughness. Surf Eng 2007;23:279.
6. Hadad M, Hitzek R, Buergler P, Rohr L, Siegmann S. Wear performance of sandwich structured WC-Co-Cr thermally sprayed coatings using different intermediate layers. Wear 2007;263:691.
7. Hadad M, Hockauf M, Meyer LW, Marot G, Lesage J, Hitzek R, Siegmann S. Adhesion evaluation of multilayered based WC-Co-Cr thermally sprayed coatings. Surf Coat Tech 2008;202:4399.
8. Hadad M, Bandyopadhyay PP, Michler J, Lesage J. Tribological behaviour of thermally sprayed Ti-Cr-Si coatings. Wear 2009;267:1002.
9. Blugan G, Hadad M, Janczak-Rusch J, Kuebler J, Graule T. Fractography, mechanical properties, and microstructure of commercial silicon nitride-titanium nitride composites. J Am Ceram Soc 2005;88:926.
10. Derler S, Gerhardt LC, Lenz A, Bertaux E, Hadad M. Friction of human skin against smooth and rough glass as a function of the contact pressure. Tribology International 2009;42:1565.
11. Derler S, Huber R, Feuz H-P, Hadad M. Influence of surface microstructure on the sliding friction of plantar skin against hard substrates. Wear 2009;267:1281.
12. Balic EE, Hadad M, Bandyopadhyay PP, Michler J. Fundamentals of adhesion of thermal spray coatings: Adhesion of single splats. Acta Mater 2009;57:5921.
13. Bandyopadhyay PP, Hadad M, Jaeggi C, Siegmann S. Microstructural, tribological and corrosion aspects of thermally sprayed Ti-Cr-Si coatings. Surf Coat Tech 2008;203:35.
14. Marot G, Lesage J, Demareaux P, Hadad M, Siegmann S, Staia MH. Interfacial indentation and shear tests to determine the adhesion of thermal spray coatings. Surf Coat Tech 2006;201:2080.

15. Bandyopadhyay PP, Siegmann S. An investigation of the effect of processing conditions on the microstructure of vacuum plasma-sprayed Ti–Zr–Ni quasicrystal coatings. J. Coat. Technol. Res. 2008;5:379.
16. Marot G, Demarecaux P, Lesage J, Hadad A, Siegmann S, Staia MH. The interfacial indentation test to determine adhesion and residual stresses in NiCrVPS coatings. Surf Coat Tech 2008;202:4411.

CONFERENCES AND POSTERS

17. Marot G, Démarécaux P, Hadad M, Siegmann S, Staia MH, Lesage J. Internfacial indentation and shear tests to determine the adhesion of thermal spray coatings. Les Deuxièmes Rencontres Internationales sur la Projection Thermique. Lille. France, 2005.
18. Hadad M. L'évaluation de l'adhérence de WC-Co-Cr multi-couches déposés par projection thermique. Solothurn. Switzerland: SGO-SST, 2007.
19. Hadad M, Hitzek R, Buergler P, Rohr L, Siegmann S. Wear performance of sandwich structured WC-Co-Cr thermally sprayed coatings using different intermediate layers. In: Elsevier, editor. Wear of material (WOM). Montereal, Canada: Wear Journal, 2007.
20. Hadad M, Hockauf M, Meyer LW, Marot G, Lesage J, Hitzek R, Siegmann S. Adhesion evaluation and impact behaviour of sandwich structured based WC-Co-Cr thermally sprayed coatings. 3 RIPT 2007- Lille. France 2007.
21. Hadad M, Siegmann S, Rohr L, Hitzek R, Buergler P. Mechanical and tribological investigations of new WC-Co-Cr and locally refurbished coatings. International Thermal Spray Conference 2007. Beijing, People's Republic of China: ASM International, Materials Park, OH, USA, 2007.
22. Hadad M, Hitzek R, Michler J, Lesage J. Tribological behaviour of sandwich structured WC-CO-CR thermally sprayed coatings. In: Ciulli E, Piccigallo B, Bassani R, Franek F, Vižintin J, Crockett R, editors. 2nd European Confernence on Tribology. Pisa, Italy, 2009.
23. Marcano Z, Lesage J, Chicot D, Hadad M, Siegmann S, Mesmacque G, Puchi-Cabrera ES, Staia MH. Microstructure and adhesion of CrC-NiCr atmospheric plasma sprayed coatings. 3 RIPT 2007- Lille. France, 2007.
24. Marot G, Démarécaux P, Lesage J, Hadad M, Siegmann S, Staia MH. The Interfacial Indentation Test to Determine Adhesion and Residual Stresses in NiCr VPS Coatings. 3 RIPT 2007. - Lille France, 2007. p.11.
25. Bandyopadhyay PP, Siegmann S, Hadad M, Jaeggi C. Microstructural and Tribological Aspects of Thermally Sprayed Ti-Cr-Si Coatings. ITSC proceeding, Niederland, 2008.
26. Hadad M. Le comportement tribologique de composite Si3N4-TiN et ses structures multicouches laminées. Sixième rencontre romande interassociation Yverdon- Switzerland, 2005.
27. Hadad M. Adhesion tests for thermal spray coatings: Application range of tensile, shear and interfacial indentation methods. In: Lugscheider E, editor. ITSC 2005 Thermal Spray connects: Explore its surfacing potential! Basel, Switzerland: DVS-Verlag GmbH, 2005.
28. Hadad M. Adhesion tests for thermal spray coatings-tentative of correlation of bond strength and interfacial indentation. 18th international conference on surface modification technologies. Dijon- France: Ecole des Mines de Paris; Materials Modification Inc.; Université de Bourgogne, 2004.
29. Thermal Spray Conference 2007. Beijing, People's Republic of China: ASM International, Materials Park, OH, USA, 2007.
30. Hadad M, Hitzek R, Michler J, Lesage J. Tribological behaviour of sandwich structured WC-CO-CR thermally sprayed coatings. In: Ciulli E, Piccigallo B, Bassani R, Franek F, Vižintin J, Crockett R, editors. 2nd European Confernence on Tribology. Pisa, Italy, 2009.
31. Marcano Z, Lesage J, Chicot D, Hadad M, Siegmann S, Mesmacque G, Puchi-Cabrera ES, Staia MH. Microstructure and adhesion of CrC-NiCr atmospheric plasma sprayed coatings. 3 RIPT 2007- Lille. France, 2007.
32. Marot G, Démarécaux P, Lesage J, Hadad M, Siegmann S, Staia MH. The Interfacial Indentation Test to Determine Adhesion and Residual Stresses in NiCr VPS Coatings. 3 RIPT 2007. - Lille France, 2007. p.11.

33. Bandyopadhyay PP, Siegmann S, Hadad M, Jaeggi C. Microstructural and Tribological Aspects of Thermally Sprayed Ti-Cr-Si Coatings. ITSC proceeding, Niederland, 2008.
34. Hadad M. Le comportement tribologique de composite Si3N4-TiN et ses structures multicouches laminées. Sixième rencontre romande interassociation Yverdon- Switzerland, 2005.
35. Hadad M. Adhesion tests for thermal spray coatings: Application range of tensile, shear and interfacial indentation methods. In: Lugscheider E, editor. ITSC 2005 Thermal Spray connects: Explore its surfacing potential! Basel, Switzerland: DVS-Verlag GmbH, 2005.
36. Hadad M. Adhesion tests for thermal spray coatings-tentative of correlation of bond strength and interfacial indentation. 18th international conference on surface modification technologies. Dijon- France: Ecole des Mines de Paris; Materials Modification Inc.; Université de Bourgogne, 2004.

IN PREPARATION

1. Hadad M, Bandyopadhyay PP, Bellayer S, Chicot D, Lesage J, The effects of annealing on the residual stress and adhesion of NiCr 80-20 thermally sprayed coatings.
2. Hadad M, Lesage J, Crack fragmentation in-plane tensile test analysis of thermally spray coatings.
3. Hadad M, Lesage J, Measurements of residual stress of Ni-Cr 80-20 thermally sprayed coatings.
4. Hadad M, Bandyopadhyay PP, Bellayer S, Chicot D, Lesage J, Practical adhesion evaluations by: tensile adhesion, Rockwell-C indentations assisted by finite element simulation, and interface indentation.
5. Hadad M, Bandyopadhyay PP, Bellayer S, Chicot D, Lesage J, The role of residual stress relief on adhesion of thermally sprayed coatings.

REFERENCES

[1] Cheng Y-S, Douglas WH, Versluis A, Tantbirojn D. Analytical study on a new bond test method for measuring adhesion. Eng Fract Mech 1999;64:117.
[2] Menningen M, Weiss H. Application of fracture mechanics to the adhesion of metal coatings on CFRP. Surface and Coatings Technology 1995;76-77:835.
[3] Lai Y-H, Dillard DA. Using the fracture efficiency to compare adhesion tests. Int J Solids Struct 1997;34:509.
[4] Drory MD, Hutchinson JW. An indentation test for measuring adhesion toughness of thin films under high residual compression with application to diamond films. Materials Research Society 1995;383.
[5] Vasinonta A, Beuth JL. Measurement of interfacial toughness in thermal barrier coating systems by indentation. Eng Fract Mech 2001;68:843.
[6] Agrawal DC, Raj R. Measurement of the ultimate shear strength of a metal-ceramic interface. Acta metallurgica 1989;37:1265.
[7] Shieu FS, Shiao MH. Measurement of the interfacial mechanical properties of a thin ceramic coating on ductile substrates. Thin Solid Films 1997;306:124.
[8] Beuth JL. Cracking of thin bonded films in residual tension. Int J Solids Struct 1992;29:1657.
[9] Era H, Otsubo F, Uchida T, Fukuda S, Kishitake K. A Modified Shear Test for Adhesion Evaluation of Thermal Sprayed Coating. Materials Science and Engineering: A 1998;251:166.
[10] Greving DJ, Shadley JR, Rybicki EF. Effects of Coating Thickness and Residual Stresses on the Bond Strength of ASTM C633-79 Thermal Spray Coating Test Specimens. Journal of Thermal Spray Technology 1994;3:371.
[11] Han W, Rybicki EF, Shadley JR. Application of Fracture Mechanics to the Interpretation of Bond Strength Data from ASTM Standard C633-79. Journal of Thermal Spray Technology 1993;2:235.
[12] Mencík J. Mechanics of Components with Treated or Coated Sufaces: Kluwer Academic Publisher, P.O. Box17, 3300 AA Dordrecht, Netherlands, 1995.
[13] Sener J-Y, Ferracin T, Caussin L, Delannay F. On the precision of the wedge-opened double cantilever beam method for measuring the debonding toughness of adhesively bonded plates. International Journal of Adhesion and Adhesives 2002;22:129.
[14] Gan L, Ben-Nissan B, Ben-David A. Modelling and finite element analysis of ultra-microhardness indentation of thin films. Thin Solid Films 1996;290-291:362.
[15] Klingbeil NW, Beuth JL. Interfacial fracture testing of deposited metal layers under four-point bending. Eng Fract Mech 1997;56:113.
[16] Li HQ, Cai X, Cheng QL. Interfacial fracture property determination of coated systems: A finite element study. Journal of Materials Science Letters 2001;20:2167.
[17] Hull TR, Colligon JS, Hill AE. Measurement of Thin-Film Adhesion. Vacuum 1987;37:327.
[18] Berndt CC, Lin CK. Measurement of Adhesion for Thermally Sprayed Materials. Journal of Adhesion Science and Technology 1993;7:1235.
[19] Piggott MR. Why interface testing by single-fibre methods can be misleading. Compos Sci Technol 1997;57:965.
[20] Volinsky AA, Moody NR, Gerberich WW. Interfacial toughness measurements for thin films on substrates. Acta Mater 2002;50:441.
[21] Amada S, Hirose T. Influence of grit blasting pre-treatment on the adhesion strength of plasma sprayed coatings: fractal analysis of roughness. Surface and Coatings Technology 1998;102:132.

[22] Siegmann S. Investigations on the Substrate Surface Morphology for Thermal Sprayed Coatings. 17th International SAMPE Europe Conference: Success of Materials by Combination. Basel, CH: SAMPE Europe, 1996.
[23] Harris AF, Beewers A. The effects of grit-blasting on surface properties for adhesion. International Journal of Adhesion and Adhesives 1999;19:445.
[24] Siegmann S, Brown CA. Surface Texture Correlations with Tensile Adhesive Strength of Thermally Sprayed Coatings Using Area-Scale Fractal Analysis. In: Lugscheider E, Kammer PA, editors. 2nd United Thermal Spray Conference, vol. 1. Düsseldorf, D: DVS Verlag, Düsseldorf, 1999. p.355.
[25] Siegmann S. Scale-Sensitive Fractal Analysis for Understanding the Influence of Substrate Roughness in Thermal Spraying. In: Berndt CC, editor. 1st United Thermal Spray Conference. Indianapolis, Indiana: ASM International, Materials Park, OH 44073-0002, 1997.
[26] Keller T, Margadant N, Pirling T, Riegert-Escribano MJ, Wagner W. Residual stress determination in thermally sprayed metallic deposits by neutron diffraction. Materials Science and Engineering: A 2004;373:33.
[27] Ünal Ö, Sordelet DJ. In-Plane Tensile Strength and Residual Stress in Thick Al_2O_3 Coatings on Aluminum Alloy. Scripta Materialia 2000;42:631.
[28] Kesler O, Finot M, Suresh S, Sampath S. Determination of Processing-Induced Stresses and Properties of Layered and Graded Coatings: Experimental Method and Results for Plasma-Sprayed Ni-Al_2O_3. Acta Mater 1997;45:3123.
[29] Kesler O, Matejicek J, Sampath S, Suresh S, Gnaeupel-Herold T, Brand PC, Prask HJ. Measurement of Residual Stress in Plasma-Sprayed Metallic, Ceramic and Composite Coatings. Materials Science and Engineering: A 1998;257:215.
[30] Drory MD, Thouless MD, Evans AG. On the decohesion of residually stressed thin films. Acta metallurgica 1998;36:2019.
[31] Kesler O, Matejicek J, Sampath H, Suresh S, Gnaeupel-Herold T, Brand PC, Prask HJ. Measurement of residual stress in plasma-sprayed metallic, ceramic and composite coatings. Materials Science and Engineering A 1998;257:215.
[32] Kuroda S, Clyne TW. The Quenching Stress in Thermally Sprayed Coatings. Thin Solid Films 1991;200:49.
[33] Bengtsson P, Johannesson T. Characterization of Microstructural Defects in Plasma-Sprayed Thermal Barrier Coatings. Journal of Thermal Spray Technology 1995;4:245.
[34] Bunshah RF. Handbook of hard coatings deposition technologies, properties and applications. Park Ridge, New Jersey: Noyes Publications, 2001.
[35] H. Herman SS, R.C. McCune. hermal spray: current status and future
trends. MRS Bulletin 2000;25:17.
[36] Pawlowski L. <<The>> science and engineering of thermal spray coatings. Chichester: Wiley, 2008.
[37] Sahraoui T, Fenineche NE, Montavon G, Coddet C. Alternative to chromium: characteristics and wear behavior of HVOF coatings for gas turbine shafts repair (heavy-duty). Journal of Materials Processing Technology 2004;152:43.
[38] Sahraoui T, Fenineche NE, Montavon G, Coddet C. Structure and wear behaviour of HVOF sprayed Cr3C2-NiCr and WC-Co coatings. Materials & Design 2003;24:309.
[39] Davis JR. Handbook of Thermal Spray Technology: ASM International, 2004.
[40] Schneider KE, Belashchenko V, Dratwinski M, Siegmann S, Zagorski A. Thermal Spraying for Power Generation Components. Weinheim: Wiley-VCH Verlag GmbH & Co. KGaA, 2006.
[41] http://www.plasmacoat.co.uk.
[42] http://www.twi.co.uk.
[43] Westhoff R, Trapaga G, Szekely J. Plasma-Particle Interactions in Plasma Spraying Systems. Metall Trans B 1992;23:683.
[44] Hossain MM, Yao YC, Watanabe T. A Numerical Study of Plasma-Particle Heat Transfer Dynamics in Induction Thermal Plasmas for Glassification. Ieej T Electr Electr 2009;4:504.

[45] Dyshlovenko S, Pawlowski L, Pateyron B, Smurov I, Harding JH. Modelling of plasma particle interactions and coating growth for plasma spraying of hydroxyapatite. Surface & Coatings Technology 2006;200:3757.
[46] Gawne DT, Liu B, Bao Y, Zhang T. Modelling of plasma-particle two-phase flow using statistical techniques. Surface & Coatings Technology 2005;191:242.
[47] Bingham R, Tsytovich VN. The criteria for dust agglomeration in plasmas. Ieee T Plasma Sci 2001;29:158.
[48] Varacalle DJ, Castro RG. Analysis of the plasma-particle interaction during the plasma spraying of beryllium. J Nucl Mater 1996;230:242.
[49] Sobolev VV, Guilemany JM, Calero JA. Modelling of the formation of WC-Co coatings by HVOF spraying onto copper substrates. Revista De Metalurgia 1997;33:287.
[50] Sobolev VV, Guilemany JM, Miguel JR, Calero JA. Modeling of substrate-coating thermal interaction during high velocity oxy-fuel (HVOF) spraying of WC-Ni powder. Materials and Manufacturing Processes 1997;12:877.
[51] Moskowitz LN. Application of HVOF Thermal Spraying to Solve Corrosion Problems in the Petroleum Industry. In: Berndt CC, editor. 13th International Thermal Spray Conference - Thermal Spray: International Advances in Coatings Technology. Orlando, Florida USA: ASM International, Materials Park, OH 44073-0002, 1992. p.611.
[52] Matsubara Y, Tomiguchi A. Surface Texture and Adhesive Strength of High Velocity Oxy-Fuel Sprayed Coatings for Rolls of Steel Mills. In: Berndt CC, editor. 13th International Thermal Spray Conference - Thermal Spray: International Advances in Coatings Technology. Orlando, Florida USA: ASM International, Materials Park, OH 44073-0002, 1992. p.637.
[53] Fukutome H, Shimizu H, Yamashita N, Shimizu Y. The Application of Cerment Coating on Piston Ring by HVOF. In: Ohmori A, editor. 14th International Thermal Spray Conference: Thermal Spraying-Current Status and Future Trends, vol. 1. Kobe, Japan: High Temperature Society of Japan, 1995. p.21.
[54] Parker DS. Practical Application of Hvof Thermal Spray Technology for Navy Jet Engine Overhaul and Repairs. Plat Surf Finish 1995;82:20.
[55] Faga MG, Mattioda R, Settineri L. Microstructural and mechanical characteristics of recycled hard metals for cutting tools. Cirp Ann-Manuf Techn 2010;59:133.
[56] Sein H, Ahmed W, Rego C. Application of diamond coatings onto small dental tools. Diam Relat Mater 2002;11:731.
[57] Saito Y, Sato K, Matuda S, Koinuma H. Application of Diamond Films from Co-H2 Plasma to Tool Blade Coating. J Mater Sci 1991;26:2937.
[58] Sun FH, Zhang ZM, Chen M, Shen HS. Fabrication and application of high quality diamond-coated tools. Journal of Materials Processing Technology 2002;129:435.
[59] Sun FH, Zhang ZM, Shen HS, Chen M. Fabrication and application of smooth composite diamond films. Surface Engineering 2003;19:461.
[60] Kindermann P, Schlund P, Sockel HG, Herr M, Heinrich W, Gorting K, Schleinkofer U. High-temperature fatigue of cemented carbides under cyclic loads. Int J Refract Met H 1999;17:55.
[61] McHugh PE, Riedel H. A liquid phase sintering model: Application to Si3N4 and WC-Co. Acta Materialia 1997;45:2995.
[62] Chattopadhyay R. Advanced thermally assisted surface engineering processes. Boston, Mass.
[Online] New York: Kluwer Academic
Springer, 2004.
[63] Papyrin A. Cold spray technology. Oxford: Elsevier, 2007.
[64] Berndt CC, Deutscher Verband für Schweisstechnik, Thermal Spray Society. Thermal spray: a united forum for scientific and technological advances proceedings of the 1st United Thermal Spray Conference 15-18 September 1997, Indianapolis, Indiana. Materials Park, OH: ASM International, 1997.

[65] Vardelle M, Vardelle A, Leger AC, Fauchais P, Gobin D. Influence of Particle Parameters at Impact on Splat Formation and Solidification in Plasma Spraying Processes. Journal of Thermal Spray Technology 1995;4:50.
[66] Amada S, Haruyama M, Tomoyasu K. Splat Formation of Molten Tin, Copper, and Nickel Droplets. Surface and Coatings Technology 1997;96:176.
[67] Amada S, Imakawa I, Aoki S. Splat Profile of Impinging Droplets on Rough Substrates. In: Marple BR, Moreau C, editors. ITSC 2003 International Thermal Spray Conference - Advancing the Science and Applying the Technology, vol. 2. Orlando, FL: ASM International, 2003. p.857.
[68] Amada S, Tomoyasu K, Haruyama M. Splat formation of molten Sn, Cu and Ni droplets. Surf Coat Tech 1997;96:176.
[69] Brossard S, Munroe PR, Tran A, Hyland MM. Study of the Splat-Substrate Interface for a NiCr Coating Plasma Sprayed onto Polished Aluminum and Stainless Steel Substrates. Journal of Thermal Spray Technology 2010;19:24.
[70] Brossard S, Munroe PR, Tran A, Hyland MM. Study of the Splat-Substrate Interface for a NiCr Coating Plasma Sprayed onto Polished Aluminum and Stainless Steel Substrates. Journal of Thermal Spray Technology 2010;19:24.
[71] Fauchais P, Fukumoto M, Vardelle A, Vardelle M. Knowledge Concerning Splat Formation: An Invited Review. Journal of Thermal Spray Technology 2004;13:337.
[72] Sakakibara N, Tsukuda H, Notomi A. The Splat Morphology of Plasma Sprayed Particle and the Relation to Coating Property. In: Berndt CC, editor. 1st International Thermal Spray Conference - Thermal Spray: Surface Engineering via Applied Research, vol. 1. Montréal, Québec, Canada: ASM International, Materials Park, OH 44073-0002, 2000. p.753.
[73] Azarmi F, Coyle T, Mostaghimi J. Young's modulus measurement and study of the relationship between mechanical properties and microstructure of air plasma sprayed alloy 625. Surface & Coatings Technology 2009;203:1045.
[74] La Barbera-Sosa JG, Santana YY, Staia MH, Chicot D, Lesage J, Caro J, Mesmacque G, Puchi-Cabrera ES. Microstructural and mechanical characterization of Ni-base thermal spray coatings deposited by HVOF. Surface & Coatings Technology 2008;202:4552.
[75] Doherty R, Cai C, Kohler LKW. Modeling and microstructure development in spray forming. Int J Powder Metall 1997;33:50.
[76] Deshpande S, Kulkarni A, Sampath S, Herman H. Application of image analysis for characterization of porosity in thermal spray coatings and correlation with small angle neutron scattering. Surface & Coatings Technology 2004;187:6.
[77] Keller T, Wagner W, Allen A, Ilavsky J, Margadant N, Siegmann S, Kostorz G. Characterisation of thermally sprayed metallic NiCrAlY deposits by multiple small-angle scattering. Appl Phys a-Mater 2002;74:S975.
[78] Mcpherson R. A Review of Microstructure and Properties of Plasma Sprayed Ceramic Coatings. Surface & Coatings Technology 1989;39:173.
[79] Mcpherson R, Shafer BV. Interlamellar Contact within Plasma-Sprayed Coatings. Thin Solid Films 1982;97:201.
[80] Kuroda S, Dendo T, Kitahara S. Quenching Stress in Plasma-Sprayed Coatings and Its Correlation with the Deposit Microstructure. Journal of Thermal Spray Technology 1995;4:75.
[81] Haure T. Couches multifonctionnelles par procédé multitechnique. Laboratoire Sciences des Procédés Céramiques et de Traitement de Surface: Universite de Limoges, 2003.
[82] Mostaghimi J, Chandra S. Splat formation in plasma spray coating process. Pure Appl Chem 2002;74:441.
[83] Mostaghimi J, Pasandideh-Fard M, Chandra S. Dynamics of Splat Formation in Plasma Spray Coating Process. Plasma Chemistry and Plasma Processing 2002;22:59.
[84] Kitahara S, Hasui A. Study of Bonding Mechanism of Sprayed Coatings. Journal of Vacuum Science & Technology 1974;11:747.
[85] Longo FN. Metallurgy of Flame Sprayed Nickel Aluminide Coatings. Weld J 1966;45:S66.

[86] kandil FA, Lord, J. D. Fry, A. T, Grant, P. V. A review of residual stress measurement methods- a guide to technique selection. NPL Report MATC(A) 2001;04:34.
[87] Baradel N, Bianchi L, Blein F, Freslon A, Jeandin M. In Situ Measurement within Plasma-Sprayed Zirconia Coatings under Industrial Conditions. In: Coddet C, editor. 15th International Thermal Spray Conference - Thermal Spray: Meeting the Challenges of the 21st Century, vol. 1. Nice, France: ASM International, Materials Park, OH 44073-0002, 1998. p.563.
[88] Bianchi L, Lucchese P, Denoirjean A, Fauchais P, Kuroda S. Evolution of Quenching Stress during Ceramic Thermal Spraying with Respect to Plasma Parameters. In: Berndt CC, Sampath S, editors. 8th National Thermal Spray Conference - Advances in Thermal Spray Science and Technology. Houston, Texas, USA: ASM International, Materials Park, OH 44073-0002, 1995. p.267.
[89] Kuroda S, Fukushima T, Kitahara S. Significance of the Quenching Stress in the Cohesion and Adhesion of Thermally Sprayed Coatings. In: Berndt CC, editor. 13th International Thermal Spray Conference - Thermal Spray: International Advances in Coatings Technology. Orlando, Florida USA: ASM International, Materials Park, OH 44073-0002, 1992. p.903.
[90] Kuroda S, Dendo T, Kitahara S. Quenching Stress in Plasma Sprayed Coatings and its Correlation with the Deposit Microstructure. Journal of Thermal Spray Technology 1995;4:75.
[91] Takeuchi S, Ito M, Takeda K. Modeling of Residual-Stress in Plasma-Sprayed Coatings - Effect of Substrate-Temperature. Surf Coat Tech 1990;43-4:426.
[92] He MY, Evans AG, Hutchinson JW. Crack Deflection at an Interface between Dissimilar Elastic-Materials - Role of Residual-Stresses. International Journal of Solids and Structures 1994;31:3443.
[93] Bagchi A, Evans AG. The mechanics and physics of thin film decohesion and its measurement. Interface Sci 1996;3:169.
[94] Lee JD, Ra HY, Hong KT, Hur SK. The Effect of Residual-Stress on Martensitic-Transformation in Plasma-Sprayed Zro2 (8wt-Percent-Y2o3) Coatings. Surface & Coatings Technology 1992;54:64.
[95] Bowen HK, Uhlmann DR, Kingery WD. Introduction to ceramics. New York, N.Y.: Wiley, 1976.
[96] P. Hurrell TCW, D. Everett, Bate. Review of residual stress mitigation methods for application in nuclear power plant *Proc. PVP 2006 Vancouver, BC*, 2006.
[97] Chicot D, Marot G, Araujo P, Horny N, Tricoteaux A, Staia MH, Lesage J. Effect of some thermal treatments on interface adhesion toughness of various thick thermal spray coatings. Surf Eng 2006;22:390.
[98] Lesage J, Staia MH, Chicot D, Godoy C, De Miranda PEV. Effect of thermal treatments on adhesive properties of a NiCr thermal sprayed coating. Thin Solid Films 2000;377:681.
[99] Laribi M, Mesrati N, Vannes AB, Treheux D. Adhesion and residual stresses determination of thermally sprayed molybdenum on steel. Surf Coat Tech 2003;166:206.
[100] Brossard S, Munroe PR, Tran ATT, Hyland MM. Study of the microstructure of NiCr splats plasma sprayed on to stainless steel substrates by TEM. Surface & Coatings Technology 2010;204:1608.
[101] Gill SC, Clyne TW. Thermomechanical Modelling of the Development of Residual Stresses during Thermal Spraying. In: Blum-Sandmeier S, Eschnauer H, Huber P, Nicoll AR, editors. 2nd Plasma-Technik-Symposium, vol. 3. Lucerne, CH: Plasma-Technik AG, Wohlen, CH, 1991. p.227.
[102] Tsui YC, Clyne TW, Gill SC. Simulation of the Effect of Creep on Stress Fields during Vacuum Plasma Spraying onto Titanium Substrates. Surface and Coatings Technology 1994;64:61.
[103] Tsui YC, Gill SC, Clyne TW. The Effect of Substrate Creep on Residual Stress Development during Spraying of Boron Carbide on Titanium. In: Berndt CC, Sampath S,

editors. 6th National Thermal Spray Conference - Thermal Spray Industrial Applications. Boston, Massachusetts: ASM International, Materials Park, OH 44073-0002, 1994. p.669.
[104] Fry AT, Lord JD. Measuring the variation of residual stress with depth: A validation exercise for fine incremental hole drilling. Residual Stresses Vii 2006;524-525:531.
[105] Grant P, Lord J, Whitehead P, Fry T. Application of fine increment hole drilling for measuring machining-induced residual stresses. Advances in Experimental Mechanics IV 2005;3-4:105.
[106] Lord JD, Grant PV, Fry AT, Kandil FA. A UK residual stress intercomparison exercise - Development of measurement good practice for the XRD and hole drilling techniques. Ecrs 6: Proceedings of the 6th European Conference on Residual Stresses 2002;404-4:567.
[107] Rajendran R, Baksi P, Bhattacharya S, Basu S. Evaluation of nonunifrom residual stress using blind-hole drilling technique. EXPERIMENTAL TECHNIQUES 2008:58.
[108] Santana YY, La Barbera JG, Staia MH, Lesage J, Puchi Cabrera ES, Chicot D, Bemporad E. Measurement of residual stress in thermal spray coatings by the incremental hole drilling method. Les Deuxièmes Rencontres Internationales sur la Projection Thermique. Lille, 2005. p.348.
[109] Clyne TW, Tsui YC. The Effect of Intermediate Layers on Residual Stress Distributions and Debonding of Sprayed Thermal Barrier Coatings. In: Ilschner B, Cherradi N, editors. 3rd International Symposium on Structural and Functional Gradient Materials. Lausanne, Switzerland: Presses polytechniques et universitaires romandes, 1994. p.129.
[110] Gill SC, Clyne TW. Monitoring of Residual Stress Generation during Thermal Spraying by Curvature Measurements. In: Berndt CC, Sampath S, editors. 6th National Thermal Spray Conference - Thermal Spray Industrial Applications. Boston, Massachusetts: ASM International, Materials Park, OH 44073-0002, 1994. p.581.
[111] Gill SC, Clyne TW. Investigation of Residual Stress Generation during Thermal Spraying by Continuous Curvature Measurement. Thin Solid Films 1994;250:172.
[112] Martinelli AE, Drew RAL, Fancello EA, Rogge R, Root JH. Neutron Diffraction and Finite-Element Analysis of Thermal Residual Stresses on Diffusion-Bonded Silicon Carbide-Molybdenum Joints. J Am Ceram Soc 1999;82:1787.
[113] Matejicek J, Sampath S, Brand PC, Prask HJ. Neutron Diffraction Residual Stress Measurement on Thermally Sprayed Coatings. In: Berndt CC, editor. 1st United Thermal Spray Conference - Thermal Spray: A United Forum for Scientific and Technological Advances. Indianapolis, Indiana: ASM International, Materials Park, OH 44073-0002, 1997. p.861.
[114] Rogante M, Mikula P, Vrana M. Through-the-thickness residual stress analysis by neutron diffraction in inoxidizable martensitic steel samples with and without tungsten carbide coating. Surface & Coatings Technology 2009;204:650.
[115] Santana YY, Renault PO, Sebastiani M, La Barbera JG, Lesage J, Bemporad E, Le Bourhis E, Puchi-Cabrera ES, Staia MH. Characterization and residual stresses of WC-Co thermally sprayed coatings. Surface & Coatings Technology 2008;202:4560.
[116] Wenzelburger M, Lopez D, Gadow R. Methods and application of residual stress analysis on thermally sprayed coatings and layer composites. Surface & Coatings Technology 2006;201:1995.
[117] Santana YY, La Barbera-Sosa JG, Staia MH, Lesage J, Puchi-Cabrera ES, Chicot D, Bemporad E. Measurement of residual stress in thermal spray coatings by the incremental hole drilling method. Surface & Coatings Technology 2006;201:2092.
[118] Gadow R, Riegert-Escribano MJ, Buchmann M. Residual stress analysis in thermally sprayed layer composites, using the hole milling and drilling method. Journal of Thermal Spray Technology 2005;14:100.
[119] Montay G, Cherouat A, Nussair A, Lu J. Residual stresses in coating technology. J Mater Sci Technol 2004;20:81.
[120] Keller T, Margadant N, Pirling T, Riegert-Escribano MJ, Wagner W. Residual stress determination in thermally sprayed metallic deposits by neutron diffraction. Materials Science and Engineering a-Structural Materials Properties Microstructure and Processing 2004;373:33.

[121] Xiao JS, Liu CX, Zhao WH, Fu WB. Analysis and measurement of thermal residual stresses in ceramic/metal gradient thermal barrier coatings. Functionally Graded Materials Vii 2003;423-4:555.
[122] Koolloos MFJ, Houben JM. Residual stresses in As-sprayed and heat treated TBCs. Measurements and FEM calculations. Ecrs 5: Proceedings of the Fifth European Conference on Residual Stresses 2000;347-3:465.
[123] Clyne TW, Gill SC. Residual Stresses in Thermal Spray Coatings and Their Effect on Interfacial Adhesion: A Review of Recent Work. J Therm Spray Techn 1996;5:401.
[124] Chiu CC. Residual-Stresses in Ceramic Coatings as Determined from the Curvature of a Coated Strip. Mat Sci Eng a-Struct 1992;150:139.
[125] Godoy C, Souza EA, Lima MM, Batista JCA. Correlation between residual stresses and adhesion of plasma sprayed coatings: effects of a post-annealing treatment. Thin Solid Films 2002;420-421:438.
[126] Stoney GG. The Tension of Metallic Films Deposited by Electrolysis. Proceedings of the royale society, vol. Ser A 82. London, 1909. p.172.
[127] Clyne WT. *Residual stresses in thick and thin surface coating*. In: Withers P, editor. Encyclopaedia of Materials: Science and Technology, vol. 4. The Netherlands: Elsevier, 2001.
[128] Mittal KL. Adhesion and Adhesives - Comment. Journal of Adhesion 1974;6:377.
[129] Mittal KL. ADHESION MEASUREMENT OF THIN FILMS. Electrocomp Sci Tech 1976;3:21.
[130] Mittal KL. Adhesion Measurement of Films and Coatings. Tokyo: Utrecht, The netherlands, 1995.
[131] Kharlamov YA. Methods of Measurement of the Adhesion Strength of Coatings (Review). Industrial Laboratory 1987:453.
[132] DIN EN. Thermisches Spritzen; Ermittlung der Haftzugfestigkeit; Deutsche Fassung EN 582:1993. - Thermal spraying; determination of tensile adhesive strength; German version EN 582:1993 - Projection thermique; mesure de l'adherence par essais de traction; version allemande EN 582:1993. . EN 582 (1993-10), EQV; ISO 14916 (1999-08), EQV; ISO/FDIS 14916 (1999-04), EQV; SN EN 582 (1995), EQV; SNV DIN EN 582 (1994-01), EQV, 582.
[133] BERNDT CC. The adhesion of flame and plasma sprayed coatings Department of Materials Engineering. Clayton, Australia: Monash University, 1980.
[134] Jankowski AF. Adhesion of Physically Vapor-Deposited Titanium Coatings to Beryllium Substrates. Thin Solid Films 1987;154:183.
[135] Rickerby DG. A review of the methods for the measurement of coating-substrate adhesion Surface and Coatings Technology 1988;36 541
[136] Drory MD, Hutchinson JW. Measurement of the adhesion of a brittle film on a ductile substrate by indentation. Proc. R. Soc. Lond. A 1996;452:2319.
[137] Zhang H, Li DY. Application of a novel lateral force-sensing microindentation method for evaluation of the bond strength of thermal sprayed coatings. Surf Coat Tech 2005;197:137.
[138] Choulier D, Coddet C. Evaluation of the Adherence of Atmospheric Plasma Sprayed Coatings by the Use of Mechanical Tests, and Correlation with Coatings Microstructure. In: Bucklow IA, editor. 12th International Conference on Thermal Spraying, vol. 1. London, UK: Abington Publishing , Woodhead Publishing Ltd in association with the Welding Institute, 1989. p.77.
[139] Choulier D. Contribution à l'étude de l'adhérence de revêtements projetés à la torche à plasma : Modélisation et utilisation d'un test d'indentation à l'interface. vol. Thèse de doctorat: Université de Technologie de Compiègne. France, 1989.
[140] Choulier D, Fluzin P, Coddet C, Thauvin G. Characterization of the Substrate-Coating Interface Toughness by the Interfacial Indentation Test - Influence of Different Parameters on the Bond Strength. In: Eschnauer H, Huber P, Nicoll AR, Blum-Sandmeier S, editors. 1st Plasma-Technik-Symposium, vol. 2. Lucerne, CH: Plasma-Technik AG, Wohlen, CH, 1988. p.293.
[141] C. Richard JL, J-F. Flavenot, G. Béranger,. Revêtements NiCrAlY projetés par plasma: Effet des contraintes résiduelles sur la ténacité d'interface. CETIM Information 1991;120:67.

[142] Chicot D, Demarecaux P, Lesage J. Measurement of the apparent interface toughness by interfacial indentation tests. Revue De Metallurgie-Cahiers D Informations Techniques 1996;93:245.
[143] Chicot D, Demarecaux P, Lesage J. Apparent interface toughness of substrate and coating couples from indentation tests. Thin Solid Films 1996;283:151.
[144] Demarecaux P, Chicot D, Lesage J. Interface indentation test for the determination of adhesive properties of thermal sprayed coatings. Journal of Materials Science Letters 1996;15:1377.
[145] Chicot D, Démarécaux P, Lesage J. Apparent interface toughness of substrate and coating couples from indentation tests. Thin Solid Films 1996;283:151.
[146] Lawn BR, Evans AG, Marshall DB. Elastic-Plastic Indentation Damage in Ceramics - the Median-Radial Crack System. J Am Ceram Soc 1980;63:574.
[147] Liu G, Mouftiez A, Lesage J, Panier S. A Numerical fracture analysis of a stationary semicircular interface crack during interfacial indentation test. Les Deuxièmes Rencontres Internationales sur la Projection Thermique. Lille, 2005. p.335.
[148] Liu G, Mouftiez A, Robin C, Panier S, Lesage J. Evaluation of interfacial adhesive toughness by simulation of crack propagation in
interfacial indentation test. In: Lugscheider E, editor. ITSC 2005 Thermal Spray connects: Explore its surfacing potential! Basel, Switzerland: DVS-Verlag GmbH, 2005. p.139.
[149] LIU G. Modélisation de l'essai d'indentation interfaciale en vue de caractériser l'adhérence de revêtements projetés thermiquement. vol. Thèse de doctorat. Lille-France: Université des Sciences et Technologies de Lille,, 2005.
[150] Hu MS, Evans AG. The cracking and decohesion of thn films on ductile substrate. Acta metall 1989;37:917.
[151] Agrawal DC, Raj R. Measurement of the Ultimate Shear-Strength of a Metal Ceramic Interface. Acta Metallurgica 1989;37:1265.
[152] Jeong JH, Kwon D. Evaluation of the adhesion strength in DLC film-coated systems using the film-cracking technique. Journal of Adhesion Science and Technology 1998;12:29.
[153] Xie C, Li X, Tong W, Hector LG, Weiland H, Wieserman LF. Fracture of thin elastic films on a metal substrate. Proceedings of the Sem Ix International Congress on Experimental Mechanics 2000:846.
[154] Aveston J, Kelly A. Theory of Multiple Fracture of Fibrous Composites. J Mater Sci 1973;8:352.
[155] Kimber AC, Keer JG. On the Theoretical Average Crack Spacing in Brittle Matrix Composites Containing Continuous Aligned Fibers. JOURNAL OF MATERIALS SCIENCE LETTERS 1982;1:353.
[156] DiBenedetto AT. Evaluation of fiber surface treatments in composite materials. Pure & AppL Chem 1985; 57:1659.
[157] HANDGE UA. Analysis of a shear-lag model with nonlinear elastic stress transfer for sequential cracking, of polymer coatings. JOURNAL OF MATERIALS SCIENCE LETTERS 2002;37:4775
[158] Handge UA, Sokolov IM, Blumen A. Disorder and plasticity in the fragmentation of coatings. Physical Review E 2001;6401.
[159] Handge UA. Analysis of a shear-lag model with nonlinear elastic stress transfer for sequential cracking of polymer coatings. Journal of Materials Science 2002;37:4775.
[160] Frank S, Handge UA, Olliges S, Spolenak R. The relationship between thin film fragmentation and buckle formation: Synchrotron-based in situ studies and two-dimensional stress analysis. Acta Mater 2009;57:1442.
[161] Agrawal DC, Raj R. Ultimate Shear Strengths of Copper Silica and Nickel Silica Interfaces. Materials Science and Engineering a-Structural Materials Properties Microstructure and Processing 1990;126:125.
[162] Yang BQ, Zhang K, Chen GN, Luo GX, Xiao JH. Measurement of fracture toughness and interfacial shear strength of hard and brittle Cr coating on ductile steel substrate. Surf Eng 2008;24:332.

[163] Shieu FS, Raj R, Sass SL. Control of the Mechanical-Properties of Metal Ceramic Interfaces through Interfacial Reactions. Acta Metallurgica Et Materialia 1990;38:2215.
[164] Chen BF, Hwang J, Chen IF, Yu GP, Huang JH. A tensile-film-cracking model for evaluating interfacial shear strength of elastic film on ductile substrate. Surf Coat Tech 2000;126:91.
[165] Chen BF, Hwang J, Yu GP, Huang JH. In situ observation of the cracking behavior of TiN coating on 304 stainless steel subjected to tensile strain. Thin Solid Films 1999;352:173.
[166] Wojciechowski PH, Mendolia MS. On the Multiple Fracture of Low-Elongation Thin-Films Deposited on High-Elongation Substrates. Journal of Vacuum Science & Technology a-Vacuum Surfaces and Films 1989;7:1282.
[167] Yanaka M, Tsukahara Y, Nakaso N, Takeda N. Cracking phenomena of brittle films in nanostructure composites analysed by a modified shear lag model with residual strain. Journal of Materials Science 1998;33:2111.
[168] Howard SJ, Clyne TW. Interfacial Fracture-Toughness of Vacuum-Plasma-Sprayed Coatings. Surf Coat Tech 1991;45:333.
[169] Charalambides PG, Lund J, Evans AG, McMeeking RM. A test specimen for determining the fracture resistarim of bimaterial interfaces. Journal of Applied Mechanics-Transactions of the Asme 1989;56:77.
[170] Hofinger I, Oechsner M, Bahr HA, Swain MV. Modified four-point bending specimen for determining the interface fracture energy for thin, brittle layers. Int J Fracture 1998;92:213.
[171] Troczynski T, Camire J. On Use of Double Cantilever Beam for Coatings and Adhesion Tests. Eng Fract Mech 1995;51:327.
[172] Heintze GN, Mcpherson R. Fracture-Toughness of Plasma-Sprayed Zirconia Coatings. Surf Coat Tech 1988;34:15.
[173] Li Z. A new technique for determining fracture toughness K-IC and its confidence with single DCB specimen. Eng Fract Mech 1996;55:133.
[174] Nairn JA. Energy release rate analysis for adhesive and laminate double cantilever beam specimens emphasizing the effect of residual stresses. International Journal of Adhesion and Adhesives 2000;20:59.
[175] Perry AJ. Scratch Adhesion Testing of Hard Coatings. Thin Solid Films 1983;107:167.
[176] Perry AJ. The Adhesion of Chemically Vapour-Deposited Hard Coatings to Steel - the Scratch Test. Thin Solid Films 1981;78:77.
[177] Dvorak M, Schmid HG, Fischer F. Fast quality control of spray powders - Schnelle Pulverkorngrössenbestimmung zur Qualitätskontrolle. In: Lugscheider E, editor. ITSC 2002 International Thermal Spray Conference, vol. 1. Essen: DVS; TSS of ASM; IIW/IIS, 2002. p.580.
[178] Pons MN, Vivier H, Belaroui K, Bernard-Michel B, Cordier F, Oulhana D, Dodds JA. Particle morphology: from visualisation to measurement. Powder Technol 1999;103:44.
[179] Zhao L, Maurer M, Fischer F, Dicks R, Lugscheider E. Influence of spray parameters on the particle in-flight properties and the properties of HVOF coating of WC-CoCr. Wear 2003;257:41.
[180] Toma D, Brandl W, Marginean G. Wear and Corrosion Behaviour of Thermally Sprayed Cermet Coatings. Surface and Coatings Technology 2001;138:149.
[181] Ohmura T, Matsuoka S. Evaluation of mechanical properties of ceramic coatings on a metal substrate. Surface and Coatings Technology 2003;169-170:728.
[182] DIN EN ISO. Metallische Werkstoffe - Instrumentierte Eindringprüfung zur Bestimmung der Härte und anderer Werkstoffparameter - Teil 1: Prüfverfahren; Deutsche Fassung prEN ISO 14577-1:2000 / Metallic materials - Instrumented indentation test for hardness and materials parameters - Part 1: Test method; German version prEN ISO 14577-1:2000 / Matériaux métalliques - Essai d'indentation instrumenté pour l'essai de dureté et de paramètres de matériaux - Partie 1: Méthode d'essai; Version allemande prEN ISO 14577-1:2000. . EN ISO 14577-1 (2002-10), EQV; ISO 14577-1 (2002-10), EQV, 14577-1.
[183] EN. Metallische Werkstoffe - Zugversuch - Teil 1: Prüfverfahren bei Raumtemperatur / Metallic materials - Tensile testing - Part 1: Method of test at ambient temperature / Matériaux

métalliques - Essais de traction - Partie 1: Méthode d'essai à température ambiante. DIN EN 10002-1 (2001-12), EQV; BS EN 10002-1 (2001-09- 06), IDT; NF A03-001 (2001-10-01), IDT; SN EN 10002-1 (2001-09), EQV; OENORM EN 10002-1 (2002-01-01), IDT, 10002-1.
[184] Fowler DB, Riggs W, Russ JC. Image Analysis Applied to Thermal Sprayed Coatings. In: Bernecki TF, editor. 3rd National Thermal Spray Conference - Thermal Spray: Research and Applications. Long Beach, California, USA: ASM International, Materials Park, OH 44073-0002, 1990. p.303.
[185] D.B. Fowler WRaJCR. Inspecting thermal sprayed coatings. Adv. Mater. Process 1990;11:41.
[186] Dionnet B. Doctor Thesis, Influence des contraintes sur l'oxydation dans l'air à haute température d'alliages réfractaires. Limoges: University of Limoges, France, 1993.
[187] Huntz AM, Marechal L, Lesage B, Molins R. Thermal expansion coefficient of alumina films developed by oxidation of a FeCrAl alloy determined by a deflection technique. Appl Surf Sci 2006;252:7781.
[188] Dupeux M. Science des Matériaux, aide mémoire. Dunod, Paris 2004.
[189] www.matweb.com.
[190] Hadad M, Hockauf M, Meyer LW, Marot G, Lesage J, Hitzek R, Siegmann S. Adhesion evaluation of multilayered based WC-Co-Cr thermally sprayed coatings. Surf Coat Tech 2008;202:4399.
[191] Hadad M, Hitzek R, Buergler P, Rohr L, Siegmann S. Wear performance of sandwich structured WC-Co-Cr thermally sprayed coatings using different intermediate layers. Wear 2007;263:691.
[192] Gieck KR. Formulaire technique. Germering, 1997.
[193] Clyne TW. Residual Stresses in Thermal Spray Coatings and Their Effect on Interfacial Adhesion: A Review of Recent Work. Journal of Thermal Spray Technology 1996;5(4):401.
[194] Birkenfeld W. Messen von Eigenspannungen mittels Dehnungsmeßstreifen. Messtechnische Briefe, Hottinger Baldwin Messtechnik GmbH, Darmstadt (1968); 4:pp 37.
[195] Keil S. Zur Eigenspannungsermittlung mit DMS-Bohrlochrosetten. Messtechnische Briefe, Hottinger Baldwin Messtechnik GmbH, Darmstadt (1975); 11:pp 53.
[196] Hoffmann k. An Introduction to Measurements using Strain Gages. Darmstadt: Hottinger Baldwin Messtechnik GmbH, Darmstadt, 1989.
[197] Hwang BW, Suh CM, Kim SH. Finite element analysis of calibration factors for the modified incremental strain method. J Strain Anal Eng 2003;38:45.
[198] Wern H. Finite-Element Solutions for Mechanical Drilling Methods - a New Integral Formalism. J Comput Appl Math 1995;63:365.
[199] Flaman MT, Manning BH. Determination of Residual-Stress Variation with Depth by the Hole.Drilling Method. Exp Mech 1985:205.
[200] Escribano M, Gadow R, Buchmann M. Residual Stress Analysis in Thermally Sprayed Layer Composites, Using the Microhole Milling and Drilling Method. In: Marple BR, Moreau C, editors. ITSC 2003 International Thermal Spray Conference - Advancing the Science and Applying the Technology, vol. 2. Orlando, FL: ASM International, 2003. p.1297.
[201] Montay G, Cherouat A, Lu J, Baradel N, Bianchi L. Development of the high-precision incremental-step hole-drilling method for the study of residual stress in multi-layer materials: influence of temperature and substrate on ZrO2-Y2O3 8 wt.% coatings. Surf Coat Tech 2002;155:152.
[202] Valentini E, Beghini M, Bertini L, Santus C, Benedetti M. : Procedure to Perform a Validated Incremental Hole Drilling Measurement: Application to Shot Peening Residual Stresses.
[203] Demarecaux P, Lesage J, Chicot D, Mesmacque G. An Examination of the Validity of the Interface Indentation Test: Application to Thermal Sprayed Coatings. EURADH 94 Adhesion. Mulhouse, France: Société Français du Vide, 1994. p.524.
[204] Lesage J, Chicot D, Demarecaux P, Mesmacque G. Adhesion Properties of Thermal Sprayed Coatings, Deduced from the Interface Indentation Test. In: , editor. 49th International

Congress on the Technology of Metals and Materials, vol. 9. São Paulo, Brazil: Associaçao Brasileira et Metalurgia e Materials, 1994. p.475.
[205] Demarecaux P, Chicot D, Lesage J. Interface indentation test for the determination of adhesive properties of thermal sprayed coatings. Journal of Materials Science Letters 1996;15:1377.
[206] Lesage J, Chicot D. Role of residual stresses in interface toughness of thermally sprayed coatings. Thin Solid Films 2002;415:143.
[207] Lascar G-. Mesure des contraintes résiduelles dans des céreamiques par indentations VICKERS. J. Phys 1998;IV France:115.
[208] Michler J. Thesis: Diamond and diamond-like carbon films: Microstructure and assessment of mechanical properties. Material science. Lausanne: Ecole polytechnic Fédérale de Lausanne, Switzerland., 2000.
[209] Michler J, Mermoux M, von Kaenel Y, Haouni A, Lucazeau G, Blank E. Residual stress in diamond films: origins and modelling. Thin Solid Films 1999;357:189.
[210] Askeland DR, Phulé PP. The science and engineering of materials. Pacific Grove, Calif.: Thomson, 2003.
[211] Withers PJ, Bhadeshia HK. Residual stress Part 1 – Measurement techniques. Materials Science and Technology 2001;17:355.
[212] Valente T, Bartuli C, Sebastiani M, Loreto A. Implementation and Development of the Incremental Hole Drilling Method for the Measurement of Residual Stress in Thermal Spray Coatings. Journal of Thermal Spray Technology 2005;14:462.
[213] Moreira PMGP, De Matos PFP, Pinho ST, Pastrama SD, Camanho PP, De Castro PMST. The residual stress intensity factors for cold-worked cracked holes: a technical note. Fatigue Fract Eng M 2004;27:879.
[214] Lee HT, Rehbach WP, Hsu FC, Tai TY, Hsu E. The study of EDM hole-drilling method for measuring residual stress in SKD11 tool steel. J Mater Process Tech 2004;149:88.
[215] Grant PVL, J.D. and Whitehead, P.S. . The measurement of residual stress by Good Practice Guide No. 53. 2002.
[216] E837-01 A. Standard Test Method for Determining Residual Stresses by the Hole-Drilling Strain-Gage Method. 2001.
[217] Fischer-Cripps AC. Introduction to Contact Mechanics: Springer, 2007.
[218] Ashby. F. M JDRH. Engineering matarials 1. Butterworth Heinemann, 1996.
[219] K. Sasaki MKaTI. Accuracy of residual stress measurement by the hole-drilling method. Exp Mech 1997;37:250.
[220] Oettel R. The Determination of Uncertainties in Residual Stress Measurement_Manual of Codes of Practice for the Determination of Uncertainties in Mechanical Tests on Metallic Materials. Standards Measurement & Testing 2000:1.
[221] Schajer. GS AE. Stress calculation error analysis for incremental hole-drilling residual stress measurements. J Eng Mater Technol 1996;118:120.
[222] Valente T, Bartuli C, Sebastiani M, Casadei F. Finite element analysis of residual stress in plasma-sprayed ceramic coatings. Proceedings of the Institution of Mechanical Engineers Part L-Journal of Materials-Design and Applications 2004;218:321.
[223] Ishida. Tsuyoshi SK. Thermal stress and residual stress control of thermally sprayed 80Ni20Cr coating. JSME INternational Journal 1999;42:119.
[224] Widjaja S, Limarga AM, Yip TH. Modeling of residual stresses in a plasma-sprayed zirconia/alumina functionally graded-thermal barrier coating. Thin Solid Films 2003;434:216.
[225] Kraus I, Ganev N, Gosmanova G, Tietz HD, Pfeiffer L, Bohm S. Residual stresses in plasma-sprayed coatings Al2O3. Advanced Performance Materials 1997;4:63.
[226] Huntz AM, Maréchal L, Lesage B, Molins R. Thermal expansion coefficient of alumina films developed by oxidation of a FeCrAl alloy determined by a deflection technique. Applied Surface Science 2006;252:7781.
[227] Sampath S, Jiang XY, Matejicek J, Prchlik L, Kulkarni A, Vaidya A. Role of thermal spray processing method on the microstructure, residual stress and properties of coatings: an

integrated study for Ni–5 wt.%Al bond coats. Materials Science and Engineering: A 2004;364:216.
[228] Matejicek J, Sampath H, Gilmore D, Neiser R. In situ measurement of residual stresses and elastic moduli in thermal sprayed coatings: Part 2: processing effects on properties of Mo coatings. Acta Mater 2003;51:873.
[229] Lyphout C, Nylen P, Manescu A, Pirling T. Residual Stresses Distribution through Thick HVOF Sprayed Inconel 718 Coatings. Journal of Thermal Spray Technology 2008;17:915.
[230] Lyphout C, Nylén P, Wigren J. Characterization of Adhesion Strength and Residual Stresses of HVOF sprayed Inconel 718 for Aerospace Repair Applications. In: Marple BR, Hyland MM, Lau Y-C, Li C-J, Lima RS, Montavon G, editors. International Thermal Spray Conference 2007. Beijing, People's Republic of China: ASM International, Materials Park, OH, USA, 2007. p.588.
[231] Pina J, Dias A, Lebrun JL. Study by X-ray diffraction and mechanical analysis of the residual stress generation during thermal spraying. Materials Science and Engineering: A 2003;347:21.
[232] Sampath S, Jiang XY, Matejicek J, Prchlik L, Kulkarni A, Vaidya A. Role of thermal spray processing method on the microstructure, residual stress and properties of coatings: an integrated study for Ni-5 wt.%Al bond coats. Materials Science and Engineering a-Structural Materials Properties Microstructure and Processing 2004;364:216.
[233] Weyant CM, Almer J, Faber KT. Through-thickness determination of phase composition and residual stresses in thermal barrier coatings using high-energy X-rays. Acta Materialia 2010;58:943.
[234] Kuroda S, CLYNE TW. The quenching stress in thermally sprayed coatings Thin Solid Films 1991;200:49.
[235] Yang CY, Wang BC, Chang E, Wu BC. Bond Degradation at the Plasma-Sprayed Ha Coating/Ti6al-4v Alloy Interface - an in-Vitro Study. J Mater Sci-Mater M 1995;6:258.
[236] Brown CA, Siegmann S. Fundamental scales of adhesion and area–scale fractal analysis. International Journal of Machine Tools and Manufacture 2001;41:1927.
[237] Siegmann SD. Investigation of Substrate Roughness in Thermal Spraying by a Scale-Sensitive 3-D Fractal Analysis Method. 15th International Thermal Spray Conference - Thermal Spray: Meeting the Challenges of the 21st Century. Nice, France: ASM International, Materials Park, OH 44073-0002, 1998.
[238] Hadad M. Adhesion tests for thermal spray coatings: Application range of tensile, shear and interfacial indentation methods. In: Lugscheider E, editor. ITSC 2005 Thermal Spray connects: Explore its surfacing potential! Basel, Switzerland: DVS-Verlag GmbH, 2005.
[239] Greving DJ, Rybicki EF, Shadley JR. Through-Thickness Residual Stress Evaluations for Several Industrial Thermal Spray Coatings Using a Modified Layer-Removal Method. Journal of Thermal Spray Technology 1994;3:379.
[240] Unger RH. Comparison of Thermal Spray Bond Coats. In: Houck DL, editor. 1st National Thermal Spray Conference - Thermal Spray: Advances in Coatings Technology. Orlando, Florida: ASM International, Materials Park, OH 44073-0002, 1987. p.365.
[241] Han W, Rybicki EF, Shadley JR. An Improved Specimen Geometry for ASTM Standard C633-79 to Estimate Bond Strengths of Thermal Spray Coatings. Journal of Thermal Spray Technology 1993;2:145.
[242] Staia M, Ramos E, Carrasquero A, Roman A. Effect of Substrate Roughness Induced by Grit Blasting upon Adhesion of WC-17% Co Thermal Sprayed Coatings. Thin Solid Films 2000;377-378:657.
[243] Gill SC, Clyne TW. Investigation of Residual-Stress Generation during Thermal Spraying by Continuous Curvature Measurement. Thin Solid Films 1994;250:172.
[244] Kelly. A, Tyson. Tensile properties of fibre-reinforced metals: copper/tungsten and copper/molybdenum. J. Mech. Phys. Solids 1965;13:329.
[245] Piggott MR. Load Bearing Fibre Composites. New York kluwer Academic Publisher, 2002.

[246] **Beeby AW**. *An investigation of cracking on the side faces of beams,* Technical report. Cement and concrete association **1971**;42:466.
[247] **Beeby AW**. *The prediction of crack widths in hardened concrete*. The structural engineer **1979**;57A:9.
[248] Fraser WA AF, DiBenedetto AT. A computer modelled, single filament technique for measuring coupling and sizing agent effects in fibre reinforced composites. 30th conf. SPI reinforced plastics division vol. 22: The Society of the Plastics Industry, 1975.
[249] Hild F, Feillard P. Ultimate strength properties of fiber-reinforced composites. Reliab Eng Syst Safe 1997;56:225.
[250] Feillard P, Rouby D, Desarmot G, Favre JP. Limits of Conventional Micromechanical Analysis of Interface Properties in Glass Epoxy Model Composites. Mat Sci Eng a-Struct 1994;188:159.
[251] Feillard P, Desarmot G, Favre JP. Theoretical Aspects of the Fragmentation Test. Compos Sci Technol 1994;50:265.
[252] Feillard P, Desarmot G, Favre JP. A Critical-Assessment of the Fragmentation Test for Glass Epoxy Systems. Compos Sci Technol 1993;49:109.
[253] Hui CY, Phoenix SL, Kogan L. Analysis of fragmentation in the single filament composite: Roles of fiber strength distributions and exclusion zone models. J Mech Phys Solids 1996;44:1715.
[254] Andersons J, Leterrier Y. Coating fragmentation by branching cracks at large biaxial strain. Probabilistic Engineering Mechanics 2007;22:285.
[255] Andersons J, Leterrier Y, Tornare G, Dumont P, Manson JAE. Evaluation of interfacial stress transfer efficiency by coating fragmentation test. Mechanics of Materials 2007;39:834.
[256] Yarysheva LM, Panchuk DA, Bol'shakova AV, Volynskii AL, Bakeev NF. Fragmentation of a metallic coating during tensile drawing of a polymer support below its glass transition temperature. Polymer Science Series A 2005;47:968.
[257] Andersons J, Leterrier Y. The effect of defect location on coating fragmentation patterns under biaxial tension. Probabilistic Engineering Mechanics 2005;20:103.
[258] Andersons J, Leterrier Y. Advanced fragmentation stage of oxide coating on polymer substrate under biaxial tension. Thin Solid Films 2005;471:209.
[259] Hu MS, Evans AG. The cracking and decohesion of thin films on ductile substrates. Acta Metall 1989;37
[260] Thouless M, Jensen H, editors. In: Mittal KL, editor, Adhesion measurement of films and coatings: VSP, 1995.
[261] Timoshenko S, Goodier JN. Theory of Elasticity .New York: McGraw-Hill Book Co, 1951.
[262] Grosskreutz JC, McNeil MB. The fracture of surface coatings on a strained substrate. J. Appl. Phys 1969;40:355.
[263] Malzbender J, With Gd. Cracking and residual stress in hybrid coatings on float glass. Thin Solid Films 2000;2-359:210:214.
[264] Griffith AA. The phenomena of rupture and flow in solids. Phil. Trans. Roy. Soc 1920;**221**:163.
[265] Rochat G, Leterrier.Y, Fayet P, J.-A.E Mn. Stress controlled gas-barrier oxide coatings on semi-crystalline polymers. Thin Solid Films 2005;484:94.
[266] Dundurs J. Elastic interaction of dislocations with inhomogeneities, Mathematical Theory of Dislocations. 1969:7:115.
[267] S. Schmauder, Meyer M. Dundurs' Parameters and Elastic Constants. Zeitschrift für Metallkunde 1992;7:524:527.
[268] Hutchinson JW. Mixed Mode Fracture Mechanics of Interfaces in Metal-Ceramic Interfaces. *Acta-Scripta Metallurgica* 1990;*4* 295:306.
[269] Thouless MD, Evans AG, Ashby MF, Hutchinson JW. The Edge Cracking and Spalling of Brittle Plates. Acta metallurgica 1987;35:1333.
[270] Thouless MD, Evans AG. Comment on the Spalling and Edge-Cracking of Plates. Scripta Metall Mater 1990;24:1507.

[271] Thouless MD. Fracture mechanics for thin-film adhesion. IBM Journal of Research and Development 1994;34:367.
[272] Thouless MD. Some mechanics for the adhesion of thin films. Thin Solid Films 1989;181:397.
[273] H. Jesnsen. M JWH, K. Kim. Decohesion of a cut prestressed film on a substrate. Int. J. Solids Structures 1990;21:1099.
[274] M. Henrik WH, K. Kim. Decohesion of a cut prestressed film on a substrate. Int. J. Solids Structures 1990;26:1099.
[275] Zhang S, Wang YS, Zeng XT, Cheng K, Qian M, Sun DE, Weng WJ, Chia WY. Evaluation of interfacial shear strength and residual stress of sol-gel derived fluoridated hydroxyapatite coatings on Ti6Al4V substrates. Eng Fract Mech 2007;74:1884.
[276] He JL, Veprek S. Finite element modeling of indentation into superhard coatings. Surface and Coatings Technology 2003;163-164:374.
[277] Michler J, Tobler M, Blank E. Thermal annealing behaviour of alloyed DLC films on steel: Determination and modelling of mechanical properties. Diamond and Related Materials 1999;8:510.
[278] Zhou YC, Tonomori T, Yoshida A, Liu L, Bignall G, Hashida T. Fracture characteristics of thermal barrier coatings after tensile and bending tests. Surface and Coatings Technology 2002;157:118.
[279] Shaw LL, Barber B, Gell M, Jordan EH. Measurements of the Interfacial Fracture Energy of Thermal Barrier Coatings. Scripta Materialia 1998;39:1427.
[280] Goldstein JI, Newbury, D. E, Echlin, P, Joy, D.C, Lyman, C. E, Lifshin, E, Sawyer, L. C, and Michael, J.R,. Scanning Electron Microscopy and X-Ray Microanalysis: Plenum Press, 2003.
[281] Hanusovszky A, Koltai M, Trifonov I. Investigation of the Segregation Phenomenon in Ni-Cr Layers with Different Compositions. Thin Solid Films 1981;85:335.
[282] Wang CM, Sun HF, Song Q. Microstructure and performance analysis of Cr3C2-25%NiCr coating prepared by plasma spraying process. Surface Engineering (Icse 2007) 2008;373-374:47.
[283] M. Richert MK, B. Leszczyńska-Madej, I. Nejman, R. Grzelka, P. Pałka. The Cr3C2 thermal spray coating on Al-Si substrate. J. of achievements in materials and manufacturing engineering 2010;38.
[284] Salaita GN, Hoflund GB. Dynamic SIMS study of Cr3C2, Cr7C3 and Cr23C6. Applied Surface Science 1998;134:194.
[285] Zhang XC, Xu BS, Wang HD, Wu YX, Jiang Y. Effects of compositional gradient and thickness of coating on the residual stresses within the graded coating. Materials & Design 2007;28:1192.
[286] Zhang XC, Gong JM, Tu SD. Effect of spraying condition and material properties on the residual stress in plasma spraying. Journal of Materials Science & Technology 2004;20:149.
[287] Zhang XC, Xu BS, Wang HD, Wu YX. Effects of oxide thickness, Al2O3 interlayer and interface asperity on residual stresses in thermal barrier coatings. Materials & Design 2006;27:989.
[288] Araujo P, Chicot D, Staia M, Lesage J. Residual stresses and adhesion of thermal spray coatings. Surf Eng 2005;21:35.
[289] Marot G, Lesage J, Démarécaux P, Hadad M, Siegmann S, Staia MH. Interfacial indentation and shear tests to determine the adhesion of thermal spray coatings. Surface and Coatings Technology 2006;201:2080.
[290] Marot G, Démarécaux PH, Lesage J, Hadad M, Siegmann S, Staia MH. The interfacial indentation test to determine adhesion and residual stresses in NiCr VPS coatings. Surf Coat Tech 2008;202:4411.
[291] Marot G, Demarecaux P, Lesage J, Hadad A, Siegmann S, Staia MH. The interfacial indentation test to determine adhesion and residual stresses in NiCrVPS coatings. Surf Coat Tech 2008;202:4411.

[292] Massalski TB, Okamoto H. Binary alloy phase diagrams. Materials Park, Ohio: ASM International, 2001.
[293] Khan AN, Lu J, Liao H. Effect of residual stresses on air plasma sprayed thermal barrier coatings. Surf Coat Tech 2003;168:291.
[294] Liu G. Modélisation de l`essai d`indentation inlerfaciale en vue de caractérser làdhérence de revétemets projetés t`hermiquent. Lille: De Lille, 2005. p.1.
[295] Balic EE, Hadad M, Bandyopadhyay PP, Michler J. Fundamentals of adhesion of thermal spray coatings: Adhesion of single splats. Acta Mater 2009;57:5921.
[296] Brossard S, Munroe PR, Hyland MM. Study of the Splat Formation for HVOF Sprayed NiCr on Stainless Steel Substrates and the Effects of Heating and Boiling Pre-Treatments. Journal of Thermal Spray Technology 2010;19:990.
[297] Brossard S, Munroe PR, Hyland MM. Microstructural Study of Splat Formation for HVOF Sprayed NiCr on Pre-Treated Aluminum Substrates. Journal of Thermal Spray Technology 2010;19:1001.
[298] Brossard S, Munroe PR, Tran AT, Hyland MM. Study of the Splat Microstructure and the Effects of Substrate Heating on the Splat Formation for Ni-Cr Particles Plasma Sprayed onto Stainless Steel Substrates. Journal of Thermal Spray Technology 2010;19:1100.
[299] Brossard S, Munroe PR, Tran ATT, Hyland MM. Study of the Splat Microstructure, Splat-Substrate Interface, and the Effects of Substrate Heating on the Splat Formation for Ni-Cr Particles Plasma Sprayed on to Aluminum Substrates. Journal of Thermal Spray Technology 2010;19:1115.
[300] Brossard S, Munroe PR, Tran ATT, Hyland MM. Effects of Substrate Roughness on Splat Formation for Ni-Cr Particles Plasma Sprayed onto Aluminum Substrates. Journal of Thermal Spray Technology 2010;19:1131.
[301] Brossard S, Munroe PR, Tran ATT, Hyland MM. Study of the splat formation for plasma sprayed NiCr on aluminum substrate as a function of substrate condition. Surf Coat Tech 2010;204:2647.
[302] Brossard S, Munroe PR, Tran ATT, Hyland MM. Study of the effects of surface chemistry on splat formation for plasma sprayed NiCr onto stainless steel substrates. Surf Coat Tech 2010;204:1599.
[303] Fukumoto M, Huang Y. Flattening Mechanism in Thermal Sprayed Particle Impinging on Flat Substrate. In: Coddet C, editor. 15th International Thermal Spray Conference - Thermal Spray: Meeting the Challenges of the 21st Century, vol. 1. Nice, France: ASM International, Materials Park, OH 44073-0002, 1998. p.401.
[304] Fukumoto M, Huang Y. Flattening Mechanism in Thermal Sprayed Particle Impinging on Flat Substrate Surface. Journal of Thermal Spray Technology 1999;8:427.
[305] Fukumoto M, Katoh S, Okane I. Splat Behavior of Plasma Sprayed Particles on Flat Substrate Surface. In: Ohmori A, editor. 14th International Thermal Spray Conference: Thermal Spraying-Current Status and Future Trends, vol. 1. Kobe, Japan: High Temperature Society of Japan, 1995. p.353.
[306] Fukumoto M, Nishioka E, Matsubara T. Effect of Interface Wetting on Flattening of Freely Fallen Metal Droplet onto Flat Substrate Surface. Journal of Thermal Spray Technology 2002;11:96.
[307] Fukumoto M, Yamaguchi T, Yamada M, Yasui T. Splash Splat to Disk Splat Transition Behavior in Plasma-Sprayed Metallic Materials. Journal of Thermal Spray Technology 2007;16:905.
[308] Bianchi L, Blein F, Lucchese P, Vardelle M, Vardelle A, Fauchais P. Effect of Particle Velocity and Substrate Temperature on Alumina and Zirconia Splat Formation. In: Berndt CC, Sampath S, editors. 6th National Thermal Spray Conference - Thermal Spray Industrial Applications. Boston, Massachusetts: ASM International, Materials Park, OH 44073-0002, 1994. p.569.
[309] Cedelle J, Vardelle M, Fauchais P, Tanaka Y. Effect of Substrate Surface Topography and Temperature, on Millimeter and Micrometer Sized Splat Formation and on Thermal Contact Resistance. In: Marple BR, Moreau C, editors. Thermal Spray 2006: Science,

Innovation and Application. Seattle, Washington, USA: ASM International, Materials Park, OH, USA, 2006.
[310] Sampath S, Jiang XY, Matejicek J, Leger AC, Vardelle A. Substrate temperature effects on splat formation, microstructure development and properties of plasma sprayed coatings Part I: Case study for partially stabilized zirconia. Materials Science and Engineering: A 1999;272:181.
[311] Sampath S, Matejicek J, Berndt CC, Herman H, Léger AC, Vardelle M, Vardelle A, Fauchais P. Plasma Sprayed Zirconia: Relationships among Particle Parameters, Splat Formation, and Deposit Generation - Part II: Microstructure and Properties. In: Berndt CC, editor. 9th National Thermal Spray Conference - Thermal Spray: Practical Solutions for Engineering Problems. Cincinnati, Ohio: ASM International, Materials Park, OH 44073-0002, 1996. p.629.
[312] Vardelle A, Robert C, Wang GX, Sampath S. Analysis of Nucleation, Phase Selection and Rapid Solidification of an Alumina Splat. In: Berndt CC, editor. 1st United Thermal Spray Conference - Thermal Spray: A United Forum for Scientific and Technological Advances. Indianapolis, Indiana: ASM International, Materials Park, OH 44073-0002, 1997. p.635.
[313] Vardelle M, Vardelle A, Leger AC, Fauchais P. Dynamics of Splat Formation and Solidification in Thermal Spraying Processes. In: Berndt CC, Sampath S, editors. 6th National Thermal Spray Conference - Thermal Spray Industrial Applications. Boston, Massachusetts: ASM International, Materials Park, OH 44073-0002, 1994. p.555.

Mousab Hadad

UNIVERSITE DES SCIENCES ET TECHNOLOGIES DE LILLE
LABORATOIRE MECANIQUE DE LILLE-UMR CNRS 8107
VILLENEUVE D'ASCQ CEDEX- FRANCE

ADHESION AND RESIDUAL STRESS EVALUATION OF THERMALLY SPRAYED COATINGS

For thermal sprayed coatings that are characterized by thick coatings, the adhesion to the substrate and residual stresses are the main parameters determining their performance in service. Although many methods have been tried to assess adhesion, there is no test, nowadays, that satisfies all requirements, both technical and theoretical, necessary to properly represent the adhesion of a coating on its substrate. The essential idea here is to compare several test methods capable of delivering an interface toughness or interfacial fracture energy representative of the adhesion of coatings. Various conditions of spraying as well as different materials and substrates were used. Apart from the EN582 standard test, indentation interfacial, in-plane shear and C-Rockwell indentation associated with a finite element modelling were used. The residual stresses were estimated using the curvature bending, the incremental hole drilling and the indirect method based on the results of the interfacial indentation. We show that the methods of interfacial indentation and in-plane tensile tests provide the best prospects in terms of consistency and reliability of the physical quantities obtained. For example, for metallic coatings, a quasi-linear correlation was found between the results of the interface indentation and the in-plane tensile tests. This result is very important since both tests provide fully consistent and reliable results, thus demonstrating their relevance to assess adhesion. Finally, the annealing process, allowing the establishment of a new state of residual stress within the coating and substrate, was used to analyze the influence of residual stresses on adhesion.

Keywords: Adhesion, residual stress, interfacial indentation, in-plane tensile test, Rockwell C indentation, incremental hole drilling, bending curvature, and thermal spraying.

ÉVALUATION DE L'ADHERENCE ET DES CONTRAINTES RESIDUELLES DE REVETEMENTS OBTENUS PAR PROJECTION THERMIQUE

Pour les revêtements obtenus par projection thermique, c'est-à-dire entrant dans la catégorie des revêtements épais, l'adhérence sur le support et les contraintes résiduelles sont les paramètres principaux déterminant leur performance en service. Bien que de nombreuses méthodes aient été essayées pour évaluer l'adhérence, il n'existe pas de test satisfaisant toutes les exigences tant techniques que théoriques nécessaires pour représenter valablement l'adhérence d'un revêtement. L'idée essentielle est de comparer plusieurs méthodes d'essais capables d'aboutir à une ténacité d'interface ou une énergie de fissuration interfaciale représentatives de l'adhérence de revêtements préparés dans des conditions d'élaboration les plus variées possibles. En dehors de l'essai normalisé EN582, l'indentation interfaciale, l'essai de cisaillement et l'indentation Rockwell-C associée à une modélisation par éléments finis ont été utilisés. Les contraintes résiduelles ont été estimées par l'essai de courbure, le perçage incrémental et par une méthode indirecte à partir des résultats de l'indentation interfaciale. Pour les revêtements métalliques, on observe une corrélation quasi-linéaire entre les ténacités d'interface obtenues par indentation interfaciale et par cisaillement. Ce résultat, très nouveau, est très important, car le fait que les deux essais donnent des résultats parfaitement cohérents et fiables, montre leur pertinence pour évaluer l'adhérence. Enfin, le traitement de recuit, en permettant l'établissement d'un nouvel état de contraintes à l'intérieur du revêtement et du substrat, a permis de quantifier l'influence des contraintes résiduelles sur l'adhérence.

Mots clés : Adhérence, contraintes résiduelles, indentation interfaciale, cisaillement par traction, indentation par Rockwell-C, perçage incrémental, rayon de courbure, et projection thermique,